AN ABSTRACT OF THE THESIS OF

James Michael Eller for the degree of Master of Science in Civil Engineering presented on June 2, 2010.

Title: Predicting Pore Pressure Response in In-Situ Liquefaction Studies using Controlled Blasting

Abstract approved: _____

Scott A. Ashford

Originally used as a method to densify loose soils, controlled blasting has expanded its applicability to geotechnical engineering by becoming a research tool to physically generate liquefaction for full-scale in-situ tests, ranging from seismic performance of deep foundations to evaluating ground improvement techniques. Current methods used to design the blasting layout (i.e. charge weight, placement, etc.) rely upon empirical models that typically do not consider in-situ soil conditions in predicting pore pressure response. In addition, these empirical models were developed for single blasts whereas current blasting studies rely upon the use of multiple blasts in loading the soil.

Through the investigation of several controlled blasting case histories, a statistical analysis was performed on the recorded blasting results and in-situ soil data to observe if in-situ soil conditions significantly influence the generation of residual pore pressures for both single and multiple blasts. Based upon the study, it was found that the development of residual pore pressure during multiple blasts is highly influenced by the initial in-situ soil conditions and should be accounted for in predicting pore pressure response. Several multiple regression analyses were performed to identify which in-situ soil properties should be considered in an empirical model that predicts the blast-induced residual pore pressure. It was found that the best model was as a function of the blasting layout and the initial soil conditions represented by the SPT $(N_1)_{60}$ blow counts

and the effective overburden pressure, σ'_{v0}, expressed in kPa. The model was evaluated on case history data and it was found to be valid for blasting layouts that are relatively simple (i.e. square grid or circular array with less than 30 charges), but became unreliable for complex blasting layouts consisting of many charges (more than 30) or erratic blasting patterns. In addition, it was found that the model was statistically acceptable to be used for single blasts as well.

The new empirical model estimates the extent of liquefaction and residual pore pressure for both single and multiple blasts and can be used in design of future blasting studies. Although the empirical model has yet to be validated from experimental field tests, it is anticipated that this model could be a step in the development of energy-based design for assessing liquefaction potential and in performing ground improvement evaluations. As more blasting studies are being performed, the model is expected to be refined and improved with the increase in case history data.

PREDICTING PORE PRESSURE RESPONSE IN IN-SITU LIQUEFACTION STUDIES USING CONTROLLED BLASTING

by

James Michael Eller

A THESIS

submitted to

Oregon State University

in partial fulfillment of

the requirements for the

degree of

Master of Science

Presented June 2, 2010

Commencement June 2011

Master of Science thesis of James Michael Eller presented on June 2, 2010

APPROVED:

Major Professor, representing Civil Engineering

Head of the School of Civil and Construction Engineering

Dean of the Graduate School

I understand that my thesis will become part of the permanent collection of Oregon State University libraries. My signature below authorizes release of my thesis to any reader upon request.

James Michael Eller, Author

ACKNOWLEDGEMENTS

In the development and completion of this thesis, I would like to acknowledge the key players that made this task successful and enjoyable:

- My advisor, Professor Scott Ashford, who gave me the opportunity to work with him and take on this project
- The National Science Foundation (Award No. 0728120), that provided funding for the project.
- Dr. Yohskue Kawamata, who served as my "Rosetta Stone" in translating technical documents from Japanese to English.
- All the talented engineers and researchers that participated in the Ishikari Liquefaction Field Test with the Port and Airport Research Institute (PARI), Japan, and shared their research with me at the U.S/Japan Workshop on Controlled Blasting at Oregon State University in September 2009.
- The great group of Geotech faculty and graduate students here at Oregon State University of past and present that I had the opportunity to work with.
- The incredible support and encouragement from my family and friends.

TABLE OF CONTENTS

Page

1.0 Introduction 1

1.1 Seismic Design for Liquefaction 1
1.2 Statement of Objectives 4
1.3 Scope of Work 5

2.0 Literature Review 6

2.1 Controlled Blasting 6
2.1.1 History of Blasting in Civil Projects 6
2.2 Blast Design 7
2.2.1 Instrumentation 9
2.3 Pore Pressure Response During Blasting 10
2.3.1 Factors Affecting Pore Pressure Generation 14
2.4 Predicting Pore Pressure Response During Blasting 15
2.5 Motivation for Research 19

3.0 Materials and Methods 20

3.1 Introduction 20
3.2 Accounting for Multiple Blasts 21
3.2 Port of Ishikari, Japan 26
3.2.1 Site Conditions and Test Layout 27
3.2.2 Test Results 31
3.3 Vancouver, British Columbia, Canada, 2004 31
3.3.1 Site Conditions and Blasting Layout 32
3.3.2 Test Results 33
3.4 Maui, Hawaii, 2002 34
3.4.1 Site Conditions and Blasting Layout 35
3.4.2 Test Results 37

TABLE OF CONTENTS (Continued)

Page

3.5 Port of Tokachi, Hokkaido Island, Japan, 2001 38
3.5.1 Site Conditions and Blasting Layout 38
3.5.2 Test Results 41
3.6 Vancouver, British Columbia, Canada, 2000 44
3.6.1 Site Conditions and Blasting Layout 44
3.6.2 Test Results 46
3.7 San Francisco, California, 1998 47
3.7.1 Site Conditions and Blasting Layout 47
3.7.2 Test Results 49
3.8 Fort McMurray, Alberta, Canada, 1997 50
3.8.1 Site Conditions and Blasting Layout 50
3.8.2 Test Results 52
3.9 South Platte River, Colorado, 1987 54
3.9.1 Site Conditions and Blasting Layout 55
3.9.2 Test Results 57

4.0 Results 59

4.1 Pore Pressure Results From Case Histories 59
4.2 Evaluation of Existing Empirical Models 61
4.2.1 Single Blast Comparison to Empirical Model 62
4.2.2 Comparison of Multiple Blasts to Empirical Model 63
4.3 Development of a New Empirical Model 65
4.3.1 Pore Pressure Effect due to Relative Density 65
4.3.2 Multiple Regression Analysis 68
4.4.1 Empirical Model for Multiple Blasts 70
4.4.2 Empirical Model for Single Blasts 74

5.0 Discussion 76

5.1 Validating Empirical Models 76
5.2 Evaluation of Empirical Model for Multiple Blasts 76

TABLE OF CONTENTS (Continued)

Page

5.2.1 Maui Comparison 76
5.2.2 Vancouver Comparison 79
5.2.3 Tokachi Comparison 82
5.2.4 Ishikari Comparison 85
5.2.5 Overall Evaluation of Empirical Model for Multiple Blasts 88
5.3 Evaluation of Empirical Model for Single Blasts 89
5.4 Multiple Blast Model and Single Blast Model Comparison 91
5.5 Design Example 94
5.6 Limitations and Considerations 97

6.0 Summary and Conclusions 99

6.1 Summary of Work Performed 99
6.2 Summary of Results and Lessons Learned 100
6.3 Future Work and Research 101

Bibliography 102

Appendices 108

Appendix A – Site & Test Information for Case Histories 109

A.1 Port of Ishikari, Hokkaido Island, Japan 110
A.2 Vancouver, British Columbia, Canada, 2004 125
A.3 Maui, Hawaii, 2004 126
A.4 Port of Tokachi, Hokkaido Island, Japan 127
A.5 Treasure Island, San Francisco, California 135

Appendix B – Blasting and In-Situ Data 146

B.1 Multiple Blasts 147
B.2 Single Blasts 157

TABLE OF CONTENTS (Continued)

Page

Appendix C – Statistical Regression Analysis 158

C.1 Multiple Blasts: Logarithmic-Based Multiple Regression Analysis 159

C.2 Multiple Blasts: Power-Based Multiple Regression Analysis 168

C.3 Single Blasts: Logarithmic-Based Multiple Regression Analysis 177

C.4 Single Blasts: Power-Based Multiple Regression Analysis 180

LIST OF FIGURES

Figure Page

Figure 2-1 Generalized Wave Paths from an Explosion 11

Figure 2-2 Pore pressure response stages during blasting 13

Figure 2-3 Sand Boil due to liquefaction during Tokachi blasting study 14

Figure 2-4 Studer and Kok (1980) empirical model 16

Figure 2-5 Empirical models for predicting *Ru* for single blasts (assuming an initial effective vertical stress of 50 kPa) 17

Figure 2-6 Empirical Models predicting *Ru* for single blasts (Studer & Kok 1980) and multiple blasts (Rollins et al. 2004) 18

Figure 3-1 Blasting layout from example blasting study 23

Figure 3-2 Pore pressure time history from example blasting study 24

Figure 3-3 Residual pore pressure, *Ru*, vs. scaled distance for example blasting study 25

Figure 3-4 Typical Soil Profile for Ishikari Blasting Study 27

Figure 3-5 Blasting Layout for Ishikari Pilot Study 28

Figure 3-6 Blasting Layout for Ishikari Full-Scale Blasting Study 30

Figure 3-7 Maximum Residual Porewater Pressure Ratios from Ishikari Pilot Study P2 and Full-Scale Study 31

Figure 3-8 Typical Soil Profile for Vancouver, British Columbia Blasting Study 32

Figure 3-9 Blasting Layout for Pilot Study at Vancouver, British Columbia Test 33

Figure 3-10 Sequential Change in Residual Porewater Pressure Ratio, *Ru*, with respect to Scaled Distance from Vancouver Blasting Study 34

Figure 3-11 Typical Soil Profile for Maui Blasting Study 36

Figure 3-12 Blasting and Instrumentation Layout at Maui (distances in meters) 36

List of Figures (Continued)

Page

Figure 3-13 Residual Pore Pressure Response vs. Scaled Distance for Maui Blasting Study 38

Figure 3-14 Typical Soil Profile for Tokachi Blasting Study 39

Figure 3-15 Blasting Layout and Sequence during Tokachi Full-Scale Blast #1 40

Figure 3-16 Pore Pressure Transducer Layout during Tokachi Full-Scale Blast #1 41

Figure 3-17 Residual Pore Pressures vs. Scaled Distance during Tokachi Blasting Study, Pilot Test 42

Figure 3-18 Residual Pore Pressures vs. Scaled Distance during Tokachi Blasting Study, Full-Scale Test #1 43

Figure 3-19 Typical Soil Profile for Delta, British Columbia Blasting Study 45

Figure 3-20 Blasting and Instrumentation Layout at Delta, British Columbia Study 45

Figure 3-21 Maximum Residual Pore Pressure Ratio vs. Scaled Distance for Delta, British Columbia Blasting Study 46

Figure 3-22 Typical Soil Profile for Treasure Island, California Pilot Study 48

Figure 3-23 Blasting and Instrumentation Layout for Treasure Island Pilot Study 48

Figure 3-24 Maximum Pore Pressure Ratio vs. Scaled Distance for Treasure Island Pilot Study 49

Figure 3-25 Blasting Layout for CANLEX Blast Testing, Blast #2 ©Pathirage 2000 52

Figure 3-26 Blasting Layout for CANLEX Blast Testing, Blast #6 ©Pathirage 2000 52

Figure 3-27 Pore Pressure Ratio vs. Scaled Distance at CANLEX 54

Figure 3-28 Typical Soil Profile for South Platte River Study 55

Figure 3-29 Blasting and Instrumentation Layout for South Platte River Liquefaction Study (from Charlie et al. 1992) 56

Figure 3-30 Measured residual PPR vs. scaled distance in South Platte River blasting study 58

List of Figures (Continued)

Page

Figure 4-1 Pore Pressure Response vs. Scaled Distance for Multiple Blasts 59

Figure 4-2 Pore Pressure Response vs. Scaled Distance for Single Blasts 60

Figure 4-3 Studer & Kok (1980) and Rollins et al. (2004) empirical models compared with single and multiple blasts results 61

Figure 4-4 Residual Plot of Single Blasts Data to Studer and Kok (1980) model 62

Figure 4-5 Residual Plot of Single Blasts Data to Studer and Kok (1980) model 63

Figure 4-6 Multiple Blasts comparison to existing empirical models and observed trend lines 64

Figure 4-7 Residual Plot of Multiple Blasts Data to Studer and Kok (1980) model and Rollins et al. (2004) model 65

Figure 4-8 Pore pressure response for multiple blasts categorized by relative density .. 66

Figure 4-9 Pore pressure response from single blasts categorized by relative density ... 67

Figure 4-10 Log-based Empirical Model developed for Multiple Blasts (shown with 95% confidence limits) 71

Figure 4-11 Power-based Empirical Model developed for Multiple Blasts (shown with 95% confidence intervals) 72

Figure 4-12 Comparison of Logarithmic Model and Power Model for Multiple Blasts 73

Figure 4-13 Residual plot for log-based and power-based empirical models 74

Figure 4-14 Empirical Model for Single Blasts shown with 95% confidence intervals 75

Figure 5-1 Comparison of the Empirical Model to the Maui Blasting Study 77

Figure 5-2 Residual plot of Blast #1 and Blast #2 of Maui Blasting Study 78

Figure 5-3 Comparison of empirical model to Vancouver pilot study with incremental values shown 79

Figure 5-4 Residual plot from Vancouver Pilot Test compared to scaled distance 80

Figure 5-5 Residual plot from Vancouver Pilot Test compared to observed *Ru* 81

List of Figures (Continued)

Page

Figure 5-6 Comparison of the empirical model to the Tokachi pilot study 82

Figure 5-7 Residual plot of the Tokachi full-scale blast #1 compared to scaled distance (categorized by depth of pore pressure transducer)..... 83

Figure 5-8 Residual plot of the Tokachi full-scale blast #1 compared to observed *Ru* (categorized by depth of pore pressure transducer)..... 84

Figure 5-9 Comparison of empirical model to Ishikari pilot test..... 86

Figure 5-10 Residual plot of Ishikari pilot study and full-scale test to empirical model compared to scaled distance..... 87

Figure 5-11 Residual plot of Ishikari pilot study and full-scale test to empirical model compared to observed *Ru*..... 87

Figure 5-12 Comparison of empirical model for single blasts to existing models..... 90

Figure 5-13 Comparison of empirical model for single blasts with existing models with recorded case history data..... 90

Figure 5-14 Comparison of empirical model for single blasts with existing models with recorded case history data..... 91

Figure 5-15 Comparison of residual plot of empirical model for multiple blasts and Studer and Kok (1980) with single blasts data compared to scaled distance 92

Figure 5-16 Comparison of residual plot of empirical model for multiple blasts and Studer and Kok (1980) with single blasts data compared to observed *Ru* . 92

Figure 5-12 Blasting Layout and Soil Profile used for Example Design Problem..... 95

Figure 5-13 Multiple Blasts Design Chart for Example Problem..... 96

LIST OF TABLES

Table Page

Table 3.1 – Selected Blast-Induced Liquefaction Studies 21

Table 3.2 – Analysis of results from example blasting study 25

Table 3.3 – Ishikari Pilot Study Blasting Details 29

Table 3.4 – Residual Pore Pressure Results during Maui Blasting Study 37

Table 3.5 – Maximum Residual Pore Pressures during Tokachi Full-Scale Test #1 43

Table 3.6 – Residual Pore Pressure Measurements during TILT Pilot Study 50

Table 3.7 – Soil Conditions for CANLEX study 51

Table 3.8 – Peak Residual Pore Pressure Readings during CANLEX study 53

Table 3.9 – Laboratory Test Results for South Platte River Study 56

Table 3.10 – Peak Residual Pore Pressure Readings during South Platte test 57

Table 4.1 Parameters and Adjusted Correlation Coefficient using in Multiple Regression Analysis for Multiple and Single Blasting Data 69

Table 5.1 –Evaluation of Empirical Model to Maui Blasting Study for both blasts 78

Table 5.2 – Statistical Evaluation of Empirical Model to Vancouver Pilot Study 81

Table 5.3 – Statistical Evaluation of Empirical Model to Tokachi Pilot Study 85

Table 5.4 – Statistical Evaluation of Empirical Model to Ishikari Pilot and Full-Scale Study 88

Table 5.5 – Statistical Evaluation of Studer and Kok (1980) model to Single Blasts Case History Data 93

Table 5.6 – Statistical Evaluation of empirical model for multiple blasts to Single Blasts Case History Data 94

DEDICATION

To my wife, Allison, who has been willing to share life's adventures with me and encourages me so much along the way.

To my daughter, Dayvanee and son, Asher, who constantly remind me how exciting the simple things of life can be.

To my mother, Barbara, for all the sacrifices she gave to help make sure her son was able to pursue a higher education.

PREDICTING PORE PRESSURE RESPONSE IN IN-SITU LIQUEFACTION STUDIES USING CONTROLLED BLASTING

1.0 INTRODUCTION

"Earthquake effects require the most careful attention of the design engineer…[where] failures in previous earthquakes provides little ground for complacency."
- Seed and Whitman, 1970

1.1 SEISMIC DESIGN FOR LIQUEFACTION

The 1995 Hyogoken-Nanbu earthquake in Kobe, Japan on January 17, 1995 (M_w 6.9) tested the resiliency of a nation with modern seismic design codes. Due to strong ground motions, liquefaction occurred and caused major damage to ports, highways, and other critical infrastructure. Many lives were lost as collapsed highway bridges prevented emergency crews from reaching victims. The total aftermath of the earthquake left over 6,300 people dead and over $200 billion in economic losses, with a significant portion of the loss due to damage from liquefaction (Schiff 1988).

Liquefaction began to primarily develop as an important seismic design issue for geotechnical engineers following the 1964 earthquakes in Anchorage, Alaska and Niigata, Japan. Earthquake-induced liquefaction is a "transformation of a granular material from a solid to a liquefied state as a consequence of increased pore-water pressure and reduced effective stress…induced by the tendency of [loose] granular materials to compact when subjected to cyclic shear deformations" (Youd et al. 2001). It can cause significant loss in soil strength, resulting in foundation failures, slope failures, or lateral spreading of soil. Liquefaction is a seismic hazard that becomes a risk when infrastructure is threatened. As urban development and infrastructure within liquefaction-susceptible areas increases, such as in the seismically-active San Francisco Bay area or along the urban coastline of Japan, liquefaction increasingly presents a risk to the lives and economies of the population in such areas.

A major concern when dealing with liquefaction is how to minimize damage to lifelines and maintain performance immediately following an earthquake. Lifelines are defined as the "systems and facilities that provide services vital to the function of an industrialized society and [are] important to the emergency response and recovery of a national disaster" (TCLEE 2010). These systems and facilities include communication, power (electric, liquid fuel, and natural gas), water (clean and wastewater), and transportation (airports, highways, ports, rail and transit). Liquefaction can cause loss or damage of these lifelines, thus impeding emergency response and disaster relief following an earthquake, in addition to the disruption of the normal, day-to-day activities of a society, as witnessed in the 1995 Hyogoken-Nanbu earthquake in Kobe, Japan. Another sobering example is from the 1906 San Francisco earthquake (estimated M7.9) where liquefaction caused significant ground settlement, rupturing gas lines and waterlines that resulted in uncontested fires that destroyed most of the city and claimed nearly 3,000 lives, approximately 8% of the city's population at the time (USGS 2009). Liquefaction is a serious threat to our infrastructure, and with lifelines playing such a vital role in the response effort following an earthquake, there is no room for engineers to exhibit complacency in seismic design.

The current approach to liquefaction design follows three questions, as described by Kramer (2008):

1. Is the soil susceptible to liquefaction?
2. Is the anticipated seismic loading sufficient to initiate liquefaction?
3. What will the effects of liquefaction be?

Much research has been performed in each of these areas, but continued research is necessary to improve our understanding and design techniques. For example, the current technique to assess a soil's resistance to liquefaction under seismic loading has been developed through post-earthquake reconnaissance investigations, laboratory testing, numerical studies, and in-situ testing. However, many of these research methods generally provide results assuming ideal or simplified conditions, which do not always represent actual field conditions. Laboratory testing uncertainties include sample

disturbance, sample size, and misrepresentation of the existing conditions of the site, in addition to human error. Empirical correlations to estimate a soil's resistance to liquefaction have been developed based upon in-situ index tests such as penetration resistance measurements (i.e. SPT, CPT) or shear wave velocities, but they are generally applicable to clean sands or silty sands, becoming unreliable for gravels and clays that have shown to also be susceptible to liquefaction-type behavior (Bray and Sancio 2006). Therefore, to minimize uncertainties and limitations, in-situ assessment techniques using dynamic testing have been developed to evaluate liquefaction susceptibility. Testing the liquefaction susceptibility of the soil in its in-situ state is highly advantageous as it removes sample disturbance effects and accounts for the existing stress conditions, the location of groundwater table, and the soil heterogeneity of the site. Ideally, through the use of a dynamic source, all soil types could be investigated, minimizing the need to idealize any of the site conditions or behavior of the test.

Current methods used in performing in-situ liquefaction tests include vibroseis and controlled blasting. Vibroseis uses controlled vibrations to induce shear strains in the soil, creating pore pressure buildup. The Civil Engineering Department at the University of Texas at Austin has performed small-scale in-situ liquefaction tests using vibroseis to cause strain-controlled pore pressure response (Chang et al. 2007). Controlled blasting has also been used to perform liquefaction evaluations as a means of supplementing other methods (Rollins et al. 2004, Gohl et al. 2009). Through the use of blasting, excess pore pressure can be generated through the shock wave of the blast, eventually building up to liquefaction. Blasting was originally used as a ground improvement method to densify loose soils and later expanded its applicability by becoming a research tool in performing full-scale seismic experiments. One of the first full-scale blast-induced liquefaction experiments was conducted in the San Francisco Bay area in California by Ashford et al. (2004) to induce liquefaction for estimating the lateral load capacity of deep foundations in liquefied sands.

The current standard of practice in designing these tests is to use empirical models to design a pilot study that will in turn identify the optimal layout (i.e. single or multiple blasts, blasting depth, charge weight, number of blasts) to liquefy the target area. The empirical methods currently in place predict residual pore pressure response with the total weight of explosives and distance between the explosives and area of interest. However, these methods do not consider soil conditions, limiting their applicability to the conditions from which they were developed. If a test were designed using these methods and the soil was different than the conditions in which the empirical methods are based upon, then the residual pore pressure may be inaccurately predicted, requiring additional "trial and error" tests to determine the optimal blasting layout. In addition, most empirical models are based upon single blasts, whereas current blasting projects utilize multiple blasts. Although the amount of total energy may be the same between the single and multiple blasts, the pore pressure response can be different.

1.2 STATEMENT OF OBJECTIVES

Controlled blasting has developed to be a viable research tool and ground improvement technique in liquefaction-related studies in geotechnical engineering. However, to promote further use and development of controlled blasting, it would be beneficial to predict excess pore pressure response with blasting as a function of not only the blasting layout but the soil conditions as well. In addition, understanding the effect of multiple blasts versus single blasts on excess pore pressure response would provide insight in to determining a blasting layout to induce liquefaction. Generation of excess pore pressure is the means from which liquefaction is able to occur, and a model that can more accurately predict these pore pressures would prove to be highly useful to future blasting studies used for liquefaction evaluations, full-scale testing, and/or even ground improvement methods.

Based upon the understanding that in-situ conditions play a significant role in pore pressure generation in earthquake-induced liquefaction, the goal of this research is to evaluate if blast-induced pore pressures can be predicted based upon blasting layout and in-situ parameters. This is answered by the following objectives:

a) Develop a standard method to evaluate the effect of multiple blasting in regard to the generation of residual pore water pressure.
b) Perform multiple linear regression analysis to determine the in-situ parameters to be considered in an improved empirical model for single and multiple blasts.
c) Validate the models for single and multiple blasts through statistical evaluations.

These objectives meet the primary goal of the National Science Foundation Grant #0728120 of increasing our knowledge of blast-induced liquefaction. This will help assess whether controlled blasting is appropriate for use in physically modeling earthquake-induced liquefaction, as well as give insight into the possible development of using controlled blasting as an assessment tool to supplement existing liquefaction assessment methods. In addition, this project is intended to increase and promote collaboration with U.S. and Japanese researchers, as it was initiated following a large research project involving U.S. and Japanese participants in Japan in 2007.

1.3 SCOPE OF WORK

The remaining chapters of this thesis are organized as follows: Chapter 2, the "Literature Review" section, provides background on liquefaction and pore pressure development for both earthquake-induced liquefaction and blast-induced liquefaction, with a summary of existing empirical models used to predict blast-induced pore pressure. Chapter 3 is the "Materials and Methods" section, and summarizes select blast-induced liquefaction case histories, presenting the site characteristics, blasting layout, and pore pressure responses of each test. In this chapter a standard method of accounting for multiple blasts in residual pore pressure development is also presented. Chapter 4 presents the results of the analyses, including the empirical models developed for single and multiple blasts from the research. Chapter 5 provides a discussion of the results, including an evaluation of the validity of the newly developed empirical models through comparisons with existing models and case history data. Chapter 6 concludes the research by summarizing the work performed and results, as well as recommendations for possible future work to increase our insight into developing blasting as an in-situ liquefaction assessment tool.

2.0 LITERATURE REVIEW

"Liquefaction is one of the most important, interesting, complex, and controversial topics in geotechnical earthquake engineering."

– Steven L. Kramer, Geotechnical Earthquake Engineering (1996)

2.1 CONTROLLED BLASTING

The use of controlled blasting in civil engineering construction has been used since the 1930's as a ground improvement method to densify sandy soils to increase bearing capacity, decrease hydraulic conductivity, reduce settlements, and even to increase liquefaction resistance (Narin van Court and Mitchell 1994). Commonly referred to as "explosive compaction", this ground improvement technique densifies soil by causing localized liquefaction through compressive shock waves breaking down the soil matrix. Just as in earthquake-induced liquefaction, as the soil matrix collapses, excess pore pressures are generated, reducing the strength of the soil and ultimately causing the soil to behave more like a liquid. As the excess pore pressures begin to dissipate, the soil grains reorganize and settle, forming a new soil skeleton that becomes increasingly denser as additional settlement (compression) occurs during the regaining of effective stresses (Narsilo et al. 2009). Blasting has been used as a cost-effective method to mitigate liquefaction-susceptible soils, particularly clean to silty sands with relative densities less than 50%, up to 40 m in depth (Dickenson et al. 2002, Mitchell 2008, Narsilio et al. 2009).

2.1.1 History of Blasting in Civil Projects

In 1936, Russian engineers attempted to densify loose soils beneath a railway embankment in the former Soviet Union (Ivanov 1967). Although the target soil was densified, the project was deemed unsuccessful due to extensive cracking in the overlying soils (Narin van Court and Mitchell 1994). Blasting to densify soils was later used successfully in the U.S. when foundation soils beneath the Franklin Falls Dam in New Hampshire were densified (Lyman 1942). Later, blasting was performed to densify loose soils at depths up to 40 m beneath the Jebba Dam Hydroelectric plant in Nigeria (Solymar 1984). Blasting was used to densify loose soils deposited during the Mt. St.

Helens eruption in order to reduce the liquefaction potential of the soil underlying Spirit Lake Highway (Kimmerling 1994). Recently, blasting has been used to densify mine tailings within aggregate ponds to increase storage capacity and reduce the liquefaction potential of the tailings (Gohl et al. 2009).

In the 1970's and 1980's, controlled blasting studies transitioned from ground improvement studies to military-based research. During the midst of the Cold War, research studies were motivated through military interest into understanding the threat that a large explosion poses to infrastructure founded on liquefiable soils (Fragaszy and Voss, 1986). Controlled blasting experiments using both nuclear and high-energy chemical explosives were performed to investigate the range of liquefaction based upon the energy of the explosive (Charlie et al. 1988a).

Recently, controlled blasting has been used to physically model liquefaction for large- and full-scale in-situ experiments. Ashford et al. (2004) used controlled blasting to liquefy sandy soils in order to gain insight into the behavior of piles in liquefied sands. The Port and Airport Research Institute (PARI) of Japan performed several blasting studies to investigate the performance of lifelines in liquefied soils, such as pipelines and airport infrastructure (Sugano et al., 2002, PARI 2009). Blasting has been considered as a means to perform an in-situ assessment of the liquefaction potential of soils. Rollins et al. (2004) and Gohl et al. (2001) discuss the use of blasting to perform in-situ liquefaction evaluations as a supplement to existing methods, but this is still in the development stage. Additional blast-induced liquefaction studies have also been performed and are presented in Chapter 3.

2.2 BLAST DESIGN

A blasting program typically consists of charges placed in a grid when a large unit of soil is being liquefied, or a circular array can be used when the center of the testing area is the primary target area, such as testing vertical drains in mitigating pore pressures (Rollins 2004). In blasting studies, a sequence of multiple charges has been found to be more effective in generating residual pore pressures than an energy-equivalent single

blast (Narsilio 2009). This is due to the decrease in cyclic shear stress amplitude with the increase in number of cycles or loads. Typically, the sequential charges are detonated when the excess pore pressure from the preceding charges are greatest, giving a time interval range of 0.03 to 2 seconds (Narin van Court & Mitchell 1994). Further information into the excess pore pressures are provided in Section 2.3.

In performing controlled blasting studies either for ground improvements or for research purposes, the main design considerations include the following, as provided by Charlie (1985):

(1) Charge weight per unit volume of soil,
(2) Charge distribution (array layout, depth placement, and vertical spacing),
(3) Blasting sequence,
(4) Delay time,
(5) Soil and rock properties, and
(6) Groundwater conditions.

From an energy viewpoint, for blasting to be effective in generating liquefaction, the amount of energy from blasting must equal or exceed the energy required to overcome the soil' resistance to liquefaction. The total energy input during blasting is a function of the charge size, charge geometry, type of explosion, distance between detonation and point of interest, soil characteristics and the attenuation of the blast waves (Narin van Court and Mitchell, 1994). The theoretical amount of energy released during blasting is 4.186×10^6 joules (J) per kilogram (kg) of TNT, with only about 67% of this energy converted into mechanical energy that acts on the soil structure while the remaining 33% escaping as heat loss (Charlie & Doehring, 2007; Green & Mitchell, 2004). Therefore, because a dense soil exhibits greater shear strength than a loose soil, more explosive energy (i.e. increase in weight of the charge) is required to cause shear straining and ultimately liquefaction within denser soils. In addition, larger charges are required to liquefy soils at greater depths (Green 2001).

In determining the required amount of explosives necessary to cause liquefaction, the most common approach is the Hopkinson's Number (Narin van Court and Mitchell 1994). The Hopkinson's Number (*HN*) is defined by the following equation:

$$HN = {W^{0.33}}/{R} \qquad 2\text{-}1$$

where *HN* is expressed in $kg^{0.33}/m$, and *W* is the TNT-equivalent charge size in kilograms, and *R* is the radial distance from the center of the charge in meters.

Throughout the literature, the ratio of $W^{0.33}/R$ is commonly inversed to $R/W^{0.33}$ and is referred to as the scaled distance, *SD*. Although the Hopkinson's Number accounts for the charge weight and distance from the charge, it does not account for the geometry of the charge. This makes it more applicable to concentrated charges at shallow depths than for distributed or columnar charges at greater depths (Green 2001). Other methods used to determine required amount of explosives include the Normalized Weight and Powder Factor, which are explained in detail in Narin van Court and Mitchell (1994).

Currently, there are no theoretical design approaches used in practice known to the author except the "cavity expansion theory" described by Gohl et al. (2009) that is used in a finite element model developed by others. This theory assumes that residual pore pressures are governed by accumulated shear strains and large stress changes, and that the effect of the charge changes with depth, thus requiring a larger charge for greater depths. Also, the theory holds that subjecting the soil to multiple blasts rather than a single blast is more effective in generating residual pore pressures.

Additional information regarding the empirical models used in design is presented in Section 2.4. For a thorough summary of design procedures, the author recommends Narin van Court and Mitchell's report on explosive compaction (1994).

2.2.1 Instrumentation

During blasting experiments, robust monitoring equipment to measure pore pressure response and other changes due to blasting must be able to withstand the shock wave generated from the blast pulse. Pore pressure transducers must be able to survive a

transient blast pulse of 41.4 MPa (6,000 psi), while maintaining a tolerance of ± 0.69 kPa (0.1 psi) to record residual pore pressures following the blast (Rollins et al, 2005a). Other key instrumentation used to monitor blasting experiments include accelerometers to measure ground shaking, geophones to measure surface vibrations and Sondex tubes to measure settlements at particular depth intervals following blasting. Ground surface settlements can be measured by conventional "rod-and-level" techniques or settlement plates. For large areas, LIDAR (Light Detection And Ranging), a laser scanning system that can characterize fine-scale topographic changes, can quickly measure ground deformations up to a 1 cm resolution and provide digital plots of the data once converted to the Cartesian coordinate system using GPS coordinates (Kayen et al. 2009).

2.3 PORE PRESSURE RESPONSE DURING BLASTING

Explosives can generate substantial energy through stress waves created by the detonation pressure and pressure due to the expanding blast-generated gases (Narin van Court & Mitchell 1994). Blast pressures travel radially from the explosive as a compression wave throughout the soil, with gas pressures traveling towards the surface. Blast-induced ground motions can cause localized peak accelerations that can be several orders of magnitude greater than earthquake accelerations due to the short travel paths (Charlie 1985). When the compression wave, which travels by contracting and expanding parallel to the direction of travel (Kramer 1996), encounters interfaces such as rock-soil boundaries, the water table or ground surface, shear waves and surface waves can be generated (Charlie 1985).

In example of generalized wave paths is shown in Figure 2-1. A point of interest, as shown in Figure 2-1, will feel the compression waves first as they travel faster than shear waves, followed by the shear waves and lastly, the surface waves. The controlling wave (wave with the most energy) is determined by the distance between the energy source (i.e. explosive) and the point of interest. The compression waves "subject the soil to a large and abrupt, albeit short-lived, pressure and strain pulse" (Dowding and Hryciw 1986), but they attenuate much quicker than shear waves. This is observed in earthquakes where the source is tens to hundreds of kilometers away, causing

compression waves to attenuate significantly while shear waves produce the low-frequency, long-duration waves resulting in ground motions. However, during blasting where the distances are much shorter (meters to tens of meters), the soil is typically subjected to energy derived primarily from compression waves.

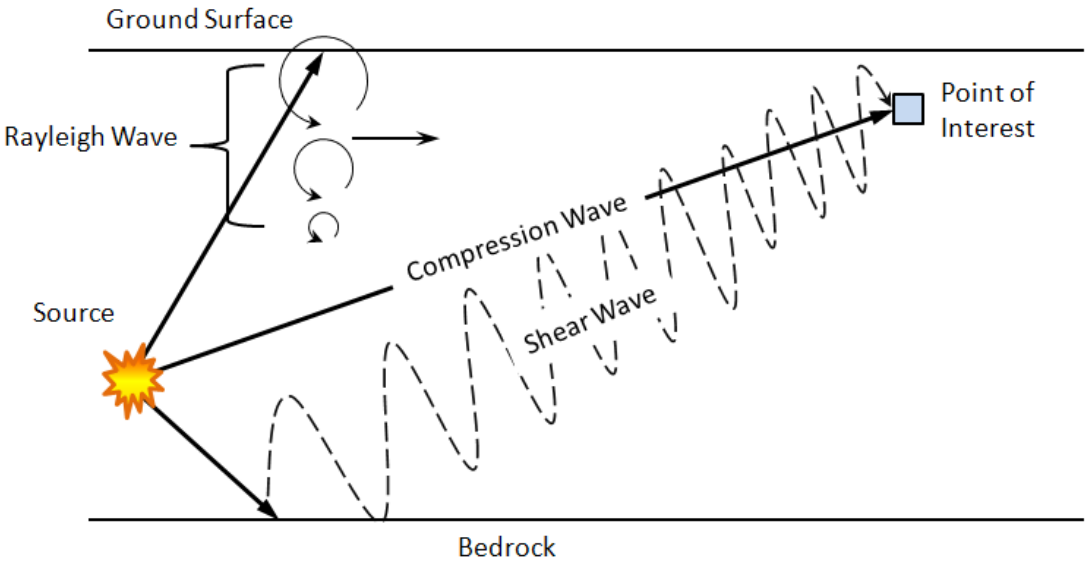

Figure 2-1 Generalized Wave Paths from an Explosion

When multiple blasts are used with time delays between detonations, these compression waves can cyclically load the soil, causing ground motion. The cyclic loading can gradually cause the soil to exhibit shear straining, and may eventually lead to a collapse of the soil matrix. The level of the induced shear strains are influenced by the mechanical properties of the soil such as the soil type, soil density, effective stress, stress history, number of strain cycles, and other properties.

Typically, shear strains within dry soils will cause volumetric contraction in loose soils and dilation in denser soils. However, if the soil consists of saturated loose sand and drainage is impeded (i.e. soils beneath groundwater table), shear straining can cause significant adverse effects to soils. If the soil structure is weak and incapable of fully

supporting the increased stress, it begins to collapse, transferring the load to the pore water. The pore water begins to develop residual (excess) pore pressures, or pressures beyond its hydrostatic state, due to its degree of incompressibility. Simply put, excess pore pressures are generated when the fluid responds elastically while the soil responds plastically (Charlie 1985). The magnitude of the residual pore pressure is a function of the initial stress state, the magnitude of the total stress increase, the loading and unloading moduli of the soil, and the drainage conditions of the soil (Fragaszy and Voss 1986).

During undrained conditions, the residual pore pressures can lead to a reduction in the effective stress of the soil, leading to a complete loss of shear strength when the residual pore pressure is equal to the initial effective vertical stress (Ferritto 1997). At this stage, liquefaction of the soil has occurred. When a soil has reached liquefaction, the individual sand grains are no longer in contact with each other but are in a suspended state, acting more like a viscous liquid than a solid. Liquefaction can be represented by the following equation:

$$PPR = Ru = {}^{\Delta u}/_{\sigma'_{v0}} \qquad 2\text{-}2$$

where the residual pore pressure ratio is represented by *PPR* or *Ru*, and is the change in residual pore pressure (Δu) divided by the initial vertical effective stress (σ'_{v0}). A *Ru* value greater than 0 indicates residual pore pressures have been generated while a *Ru* of 1.0 represents complete liquefaction.

During blasting, a soil will experience three distinct pore pressure response stages:

(1) Peak (transient) pore pressure that is attributed to the compressive wave or shock blast,
(2) Residual (excess) pore pressure, and
(3) Dissipation of pore pressure.

These stages are presented in Figure 2-2, which shows a generalized *Ru* time history during a blasting experiment which utilized three blasts detonated at time intervals of approximately 1.0 second. The peak pore pressures can exceed the theoretical liquefaction boundary of *Ru* = 1.0, but the pressures are short-lived, serving only as a precursor of the residual pore pressure developed by contraction of the soil. The residual pore pressure will maintain a constant level until dissipation initiates. The duration of dissipation is based upon the permeability of the soil, which can change after each blast as the soil densifies, reducing the amount of voids for seepage to occur. In blasting studies, more attention is typically given towards the residual pore pressure as this directly correlates to liquefaction. After the residual pore pressures dissipate, the soil particles begin to settle and rearrange into a denser state than the initial state before blasting. Settlement can reach up to 2 to 10% of the initial thickness of the liquefied layer (Narsilio et al. 2009).

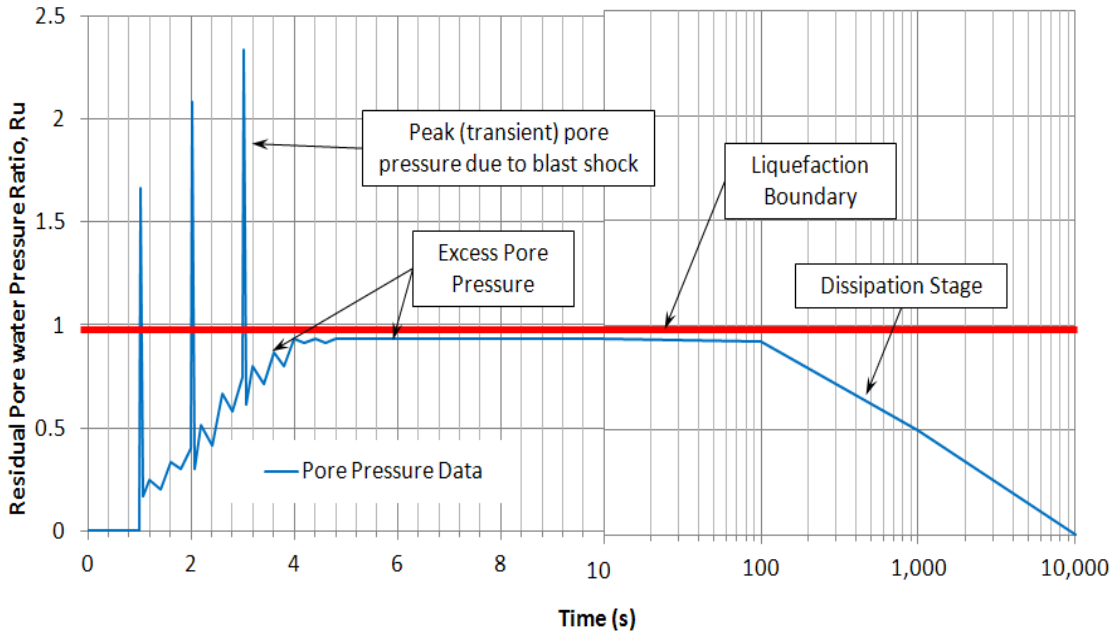

Figure 2-2 Pore pressure response stages during blasting

Typically during a blasting experiment and with earthquake-induced liquefaction, sand boils will occur at the surface as the pore pressures seek out the easiest route to the surface to relieve the pressures. Water flows through the cracks and fissures of the subsurface, carrying sand particles with it. As it reaches the surface, the sand is ejected and is distributed concentrically around the hole. An example of this is shown in Figure 2-3, in which a sand boil was developed following blasting at the Tokachi Study in Japan.

Figure 2-3 Sand Boil due to liquefaction during Tokachi blasting study
©Ashford and Juirnarongrit, 2004

2.3.1 Factors Affecting Pore Pressure Generation

There are four general components that affect pore pressure generation and ultimately, the liquefaction potential of soils: (1) soil type, (2) soil density, (3) saturation, and (4) magnitude of shaking. Changing one or more of these components, such as increasing the density or decreasing the anticipated magnitude of shaking, and the likelihood of

liquefaction occurring will be reduced. The most susceptible soils to liquefaction consist of saturated, loose to medium dense, poorly-graded granular soils with a relatively low permeability, such as clean and silty sands. Recently, research and post-earthquake field reconnaissance have shown that gravelly soils and clayey-silty soils can also be susceptible to liquefaction due to the soil composition factors (Seed et al. 2003, Boulanger & Idriss 2004, Bray & Sancio 2006). Bray and Sancio (2006) identified that liquefaction-type behavior can occur in clayey soils depending on the "amount and type of clay minerals in the soil". Other soil composition factors include confining pressures (e.g. capping soils, overburden stress), soil structure and cementation, thickness of soil deposit, strain history, permeability and drainage, and the amount of entrapped air within the deposit (Charlie et al. 1988b, Figueroa et al. 1994).

2.4 PREDICTING PORE PRESSURE RESPONSE DURING BLASTING

Several studies have been performed to predict the pore pressure response due to blasting. The common method is to relate the residual pore pressure ratio (*Ru*) to the scaled distance ($R/W^{0.33}$), where *W* is the TNT-equivalent charge size in kilograms, and *R* is the radial distance between the point of interest and the explosive charge in meters. Other methods in predicting pore pressure response use peak particle velocity or compressive strain to predict pore pressure response (Charlie 1985, Al-Qasimi et al. 2005). To the author's knowledge, there are no theoretical methods currently in use for estimating residual pore pressure response during blasting.

Most of the past research in estimating residual pore pressures was centered on single charges in saturated sandy soils. Ivanov (1967) observed that liquefaction typically occurred between scaled distances ($R/W^{0.33}$) less than 6 to 8 for sandy soil with a relative density between 30 and 40%. While performing blasting in marine deposits, Kummeneje and Eide (1961) observed that the potential for liquefaction decreases as depth increases due to the increased confining stress. Therefore, in predicting the pore pressure response with blasting, they considered the initial effective vertical stress (σ'_{vo}) as shown in the following equation, where $R/W^{0.33}$ is in $m/kg^{0.33}$, and the initial effective vertical stress (σ'_{vo}) is in kPa:

$$Ru = 65\left(\frac{R}{W^{1/3}}\right)^{-2.2} \cdot (\sigma'_{vo})^{-0.33} \quad 2\text{-}3$$

Although based solely on the scaled distance, the most common empirical method used to predict residual pore pressure response in soils was developed by Studer and Kok (1980) following blasting to densify loose sands within Amsterdam Harbor utilizing single blasts, and is provided below, in addition to the range as provided by Narin van Court and Mitchell (1994):

$$\text{Average: } Ru = 1.65 + 0.64\, ln(W^{0.33}/R) \quad 2\text{-}4$$

$$\text{Range: } Ru = 2.15 + 0.74\, ln(W^{0.33}/R) \quad 2\text{-}5$$

$$Ru = 1.53 + 0.77\, ln(W^{0.33}/R) \quad 2\text{-}6$$

where *Ru* is the pore pressure ratio, *W* is the TNT-equivalent charge weight in kilograms, and *R* is the radial distance between the piezometer and the explosive charge in meters. These are shown graphically in Figure 2-4, with the average shown in the solid line and the range represented by the dashed lines.

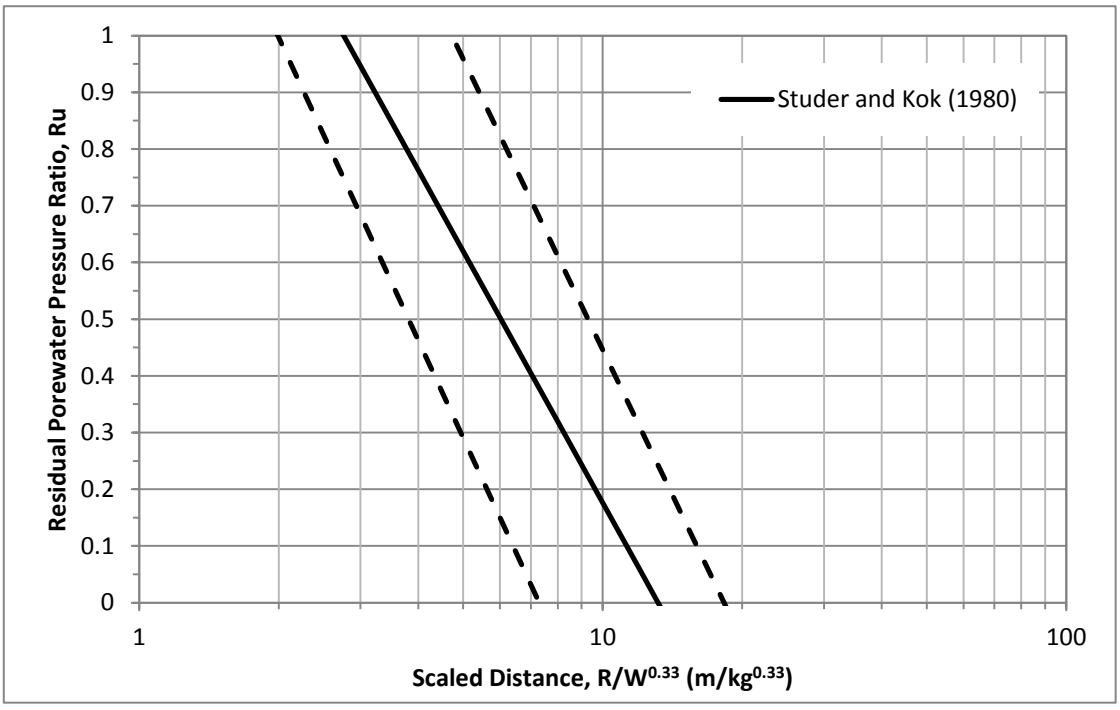

Figure 2-4 Studer and Kok (1980) empirical model

In studying residual pore pressure responses from underground chemical explosions, Charlie and Doehring (2007) identified the upper-bound maximum scaled distance for initial pore pressure generation and ultimately liquefaction. Based upon their analysis, the maximum boundary for pore pressure generation occurred at a scaled distance of 14 $m/kg^{0.33}$, and the maximum boundary for liquefaction occurred at 3 $m/kg^{0.33}$. From these boundaries, it can be deduced that for 1 kg of TNT, any point beyond the 14 m radius is not expected to be subjected to enough strain to cause generation of residual pore pressure. A comparison of the Charlie and Doehring (2007) model, Studer and Kok (1980) model, and the Kummeneje and Eide (1961) model are presented in Figure 2-5. Limitations of these models include omissions such as initial soil properties and depth of placement of the charge, as these can affect the distribution of energy from the charge blast and ultimately, the pore pressure response (Narin van Court & Mitchell 1994).

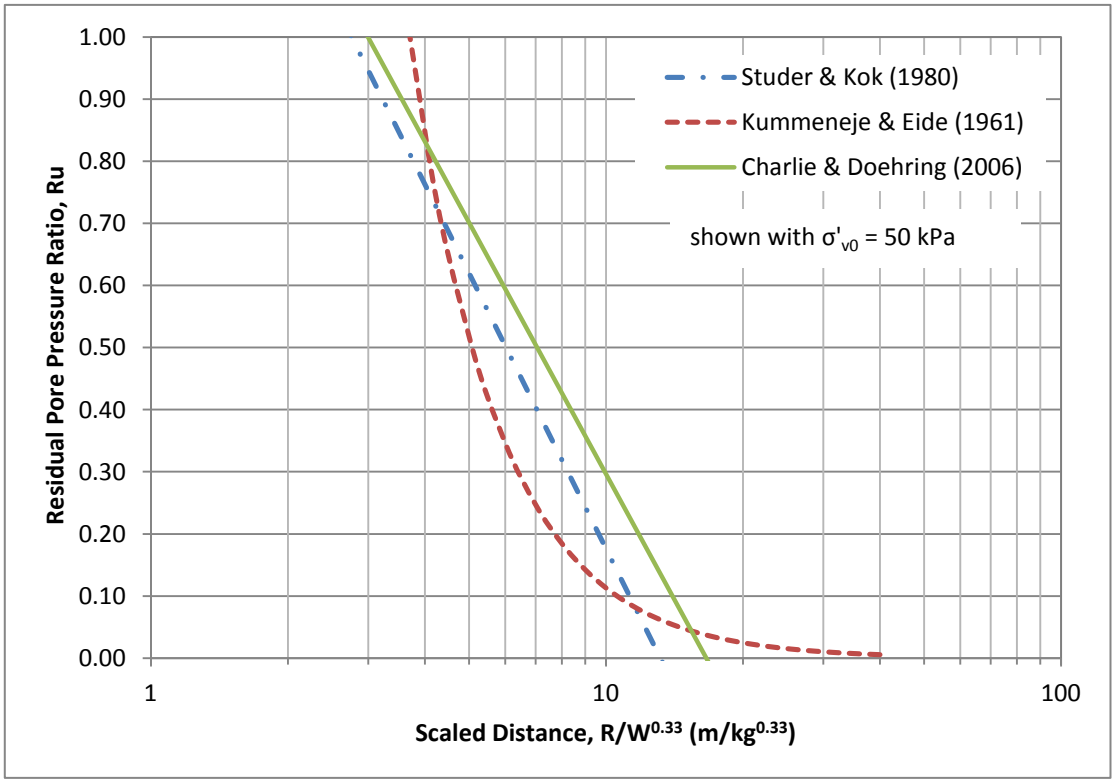

Figure 2-5 Empirical models for predicting *Ru* for single blasts (assuming an initial effective vertical stress of 50 kPa)

Based upon a blasting study using multiple blasts, Rollins et al. (2004) identified a best-fit trend line for the observed residual pore pressure and scaled distances developed from a separate blasting test performed by Rollins (2004). This best-fit trend line can be approximated by Equation 2-7. However, it should be noted that it is unclear if Equation 2-7 considers any other parameters rather than the scaled distance as it was approximated from a graph provided by Rollins et al. (2004). Assuming the trend line is based solely on the scaled distance, the approximate equation is provided below:

$$Ru = 1.89 - 0.621\, ln(R/W^{0.33}) \qquad 2\text{-}7$$

For comparison purposes, the trend lines developed by Studer and Kok (1980) and Rollins et al. (2004) are presented in Figure 2-6.

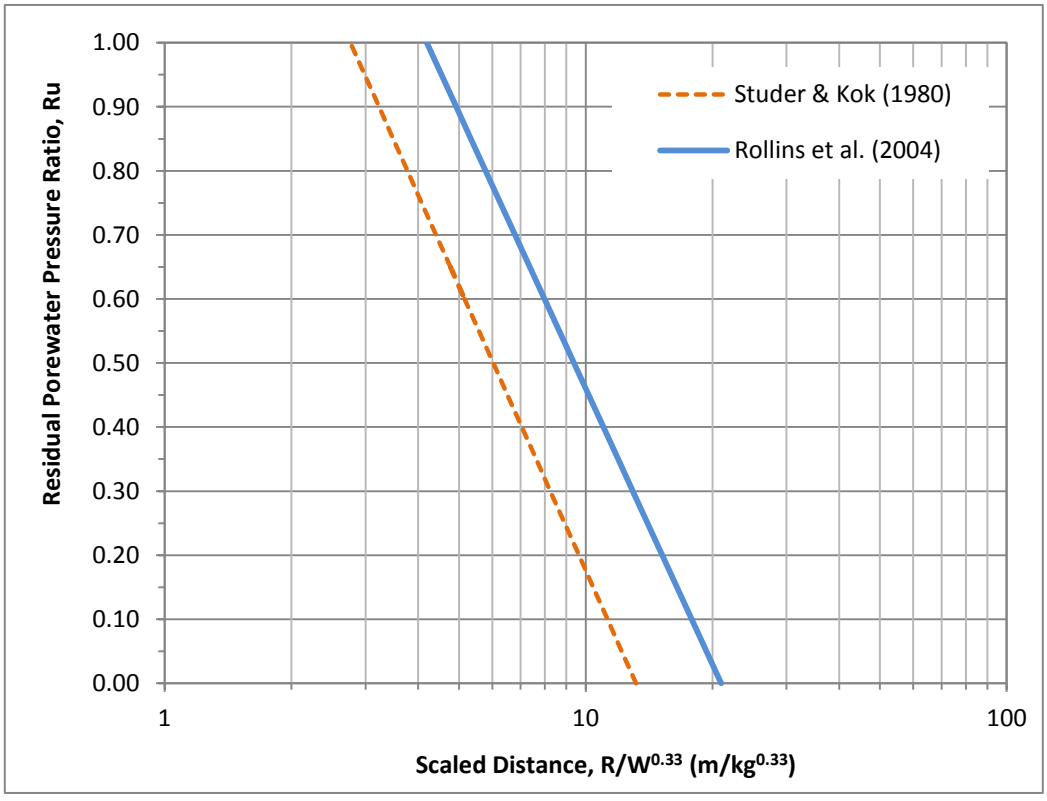

Figure 2-6 Empirical Models predicting *Ru* for single blasts (Studer & Kok 1980) and multiple blasts (Rollins et al. 2004)

From the figure, it is observed that liquefaction can occur at a greater scaled distance for multiple blasting (represented by the Rollins et al. 2004 model) than for single blasts (represented by the Studer and Kok (1980) model), which occurs at a scaled distance of 4.1 $m/kg^{0.33}$ and 2.7 $m/kg^{0.33}$ respectively. For a 1 kg charge, initiation of pore pressure generation for multiple blasts can occur at a scaled distance of approximately 20 m while single blasts may be bounded around 12 m.

2.5 MOTIVATION FOR RESEARCH

After evaluating the current trends for predicting residual pore pressure response with scaled distances, there are two significant observations that have motivated this research. First of all, of the existing empirical models, only one model (Kummeneje and Eide 1961) considers soil conditions as a parameter in predicting the residual pore pressure. If denser soils exhibit more resistance to liquefaction, than it is expected that they would require more energy (lower scaled distance value) to generate residual pore pressure and eventually liquefaction, but this is not accounted for with the empirical methods presented. Therefore, an analysis should be made to evaluate the influence that in-situ conditions have on blast-induced pore pressure generation. Secondly, of all the methods, only Rollins et al. (2004) is applicable to multiple blasts. From our understanding of soil mechanics, more energy is required to cause liquefaction from one load cycle (e.g. 1 blast) than for multiple load cycles (e.g. multiple blasts). Therefore, an empirical model for single blasts would not be the same for multiple blasts, but would actually underestimate the scaled distance (more energy) for a given residual pore pressure. As mentioned in Chapter 1, this research evaluates the pore pressure response for multiple blasts and single blasts as a function of blasting properties and soil conditions. If such a trend exists and is considered an improvement to existing models, then this empirical model may serve as a design tool in planning future blasting studies.

3.0 MATERIALS AND METHODS

"… I was awakened by a tremendous earthquake…and I ran out of my cabin, both glad and frightened shouting, 'A noble earthquake!' feeling sure I was going to learn something."
– John Muir, Our National Parks (1901)

3.1 INTRODUCTION

Geotechnical engineers began to use controlled blasting as a means for densifying loose soils in the 1930's. It has only been relatively recent that controlled blasting has developed into a tool for geotechnical engineers to physically generate liquefaction for seismic-related research. Several experiments have been performed in the last two decades, ranging from investigating the seismic behavior of deep foundations when subjected to liquefaction to developing controlled blasting as a tool to perform liquefaction potential assessments to supplement to existing methods. This section summarizes several blast-induced liquefaction experiments, as shown in Table 3.1, beginning with the most recent test performed in Ishikari, Japan in 2007. These case histories serve as the "Methods and Materials" of this thesis, from which the recorded in-situ soil conditions, blasting layout, and pore pressure results serve as the data for this research.

The case histories presented provide valuable insight into the effect of blasting on pore pressure development. Although this section presents several selected case histories, it should be noted that this does not include all controlled blasting experiments performed to date. Other studies have been performed in the last 30 years that investigated pore pressure generation, including large nuclear experiments, but were not included in this research due to the inapplicability of the data to the specific research hypothesis and/or the availability of published data.

Table 3.1 – Selected Blast-Induced Liquefaction Studies

Test Location (year)	Principal Investigator	Single (S) / Multiple (M) Blasts	Principal References
Ishikari, Hokkaido Island, Japan (2007)	Port and Airport Research Institute (PARI)	M	PARI (2009), Nakazawa & Sugano (2010)
Vancouver, British Columbia, Canada (2004)	Brigham Young University (BYU)	S, M	Rollins (2004), Strand (2008)
Maui, Hawaii (2004)	BYU & University of Hawaii	S, M	Rollins et al. (2004a)
Tokachi, Hokkaido Island, Japan (2002)	PARI & UC San Diego (UCSD)	S, M	Ashford & Juirnarongrit (2004)
Delta, British Columbia, Canada (2000)	Pacific Geodynamics, Inc. & Univ. of British Columbia (UBC)	S, M	Gohl et al. (2001)
Treasure Island, San Francisco, California (1998)	UCSD, BYU, & U.S. Geological Survey	M	Ashford & Rollins (2002), Ashford et al. (2004)
Fort McMurray, Alberta, Canada (1997)	UBC	S, M	Pathirage (2000)
South Platte River, Colorado (1987)	Colorado State University, Fort Collins	S	Charlie et al. (1992)

3.2 ACCOUNTING FOR MULTIPLE BLASTS

As presented in Chapter 2, pore pressure generation due to blasting is often plotted with the scaled distance, $R/W^{0.33}$ (in m/kg$^{0.33}$), between the explosive and point of interest (e.g. pore pressure transducer). Although this is easily estimated for single blasts, it is unclear how to estimate the scaled distance for when multiple blasts are used. If all blasts were detonated at the same time, then one could simply average the scaled distance for each explosive. But is this a valid method when a series of blasts are used, involving different charge weights and radial distances with time intervals between blasts? In order to analyze the pore pressure response with respect to multiple blasts, a consistent method to account for the changing scaled distance with each blast must be established. In order to do so, the following assumptions were made:

- The magnitude of pore pressure generated from each sequential blast is influenced by the previous blast and generated pore pressure. As explained in Chapter 2, soil can lose its stiffness during pore pressure buildup. Therefore, a blast can have a different impact in generating residual pore pressures when *Ru* = 0.5 than it does at the beginning of a blasting study when *Ru* = 0.
- Time intervals between sequential/multiple blasting are short enough to minimize *significant* pore pressure dissipation.
- Blasting patterns (e.g. in-to-out, out-to-in, circular, alternating sides, etc.) are not considered to play a significant role in pore pressure buildup. However, this assumption cannot be verified within the scope of this research.
- Blasts that did not cause an increase in pore pressure, either represented by excess pore pressure or residual pore pressure ratio, are not considered. This requires a decipherable time history to determine pore pressure increase following each blast pulse.
- Blasts that exceeded an individual scaled distance (e.g. simply their specific radial distance divided by the cubed root of their specific charge weight) of 20 $m/kg^{0.33}$ were considered to have an insignificant influence in pore pressure generation based upon observation of data. Therefore, these particular blasts were not considered in the overall analysis.

From these assumptions, a general method was established to account for pore pressure generation for multiple blasts, and is shown in the following equation:

$$R/_{W^{0.33}} = \frac{\overline{R}}{\Sigma W^{0.33}} = \frac{\left(\frac{R_1 + R_2 + \ldots R_i}{N_i}\right)}{\Sigma(W_1 + W_2 + \ldots W_i)^{0.33}} \qquad 3\text{-}1$$

where $R/W^{0.33}$ is the scaled distance between explosive and point of interest, *R* is the radius in meters, and *W* is the equivalent weight of the charge to TNT in kilograms, *N* is the number of blasts, and *1*, *2*, and *i* denotes the associated distance and weight of the charge number.

To provide a clear and concise understanding of this method, an example of a blasting test with pore pressure readings and analysis is displayed in Figures 3-1 through 3-3, and in Table 3-1. In Figure 3-1, the blasting layout is shown. The layout consists of 3 charges with sizes of 0.5, 1.0, and 1.5 kg. The largest charge is placed at a radial distance of 8 m from the center of the test area, and the 1.0 kg charge and 0.5 kg charge placed at radial distances of 6 m and 4 m, respectively. A pore pressure transducer is placed in the center of the test area at a depth of 4 m, which is also the same depth where the explosives were placed. The blasting sequence utilized an "out-to-in" sequence, starting with the farthest charge (i.e. W = 1.5 kg) being detonated first with time delays of 500 ms.

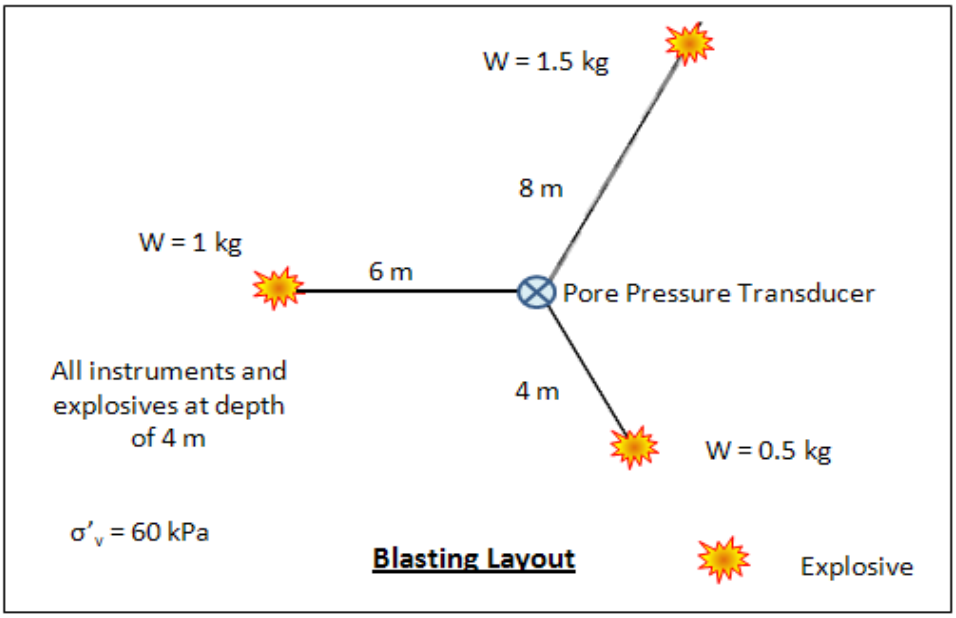

Figure 3-1 Blasting layout from example blasting study

From the pore pressure time history shown in Figure 3-2, each blast is represented initially by the transient pore pressure increase, representing the change in the applied mean normal stresses from the blast pulse, and immediately dissipates. Following the transient pulse the residual pore pressures develop as the soil skeleton progressively collapses. This causes a decrease in effective stress equal to the generated excess pore

pressures. After blasting has concluded, the residual pore pressure reaches a peak and after a period of time it will begin to dissipate, as previously shown in Figure 2-5. In the example, the soil does not achieve liquefaction (e.g. *Ru* = 1.0), but gets relatively close to the boundary. In an actual event, sand boils may appear indicating liquefaction has occurred even though the residual pore pressure has not met that theoretical boundary.

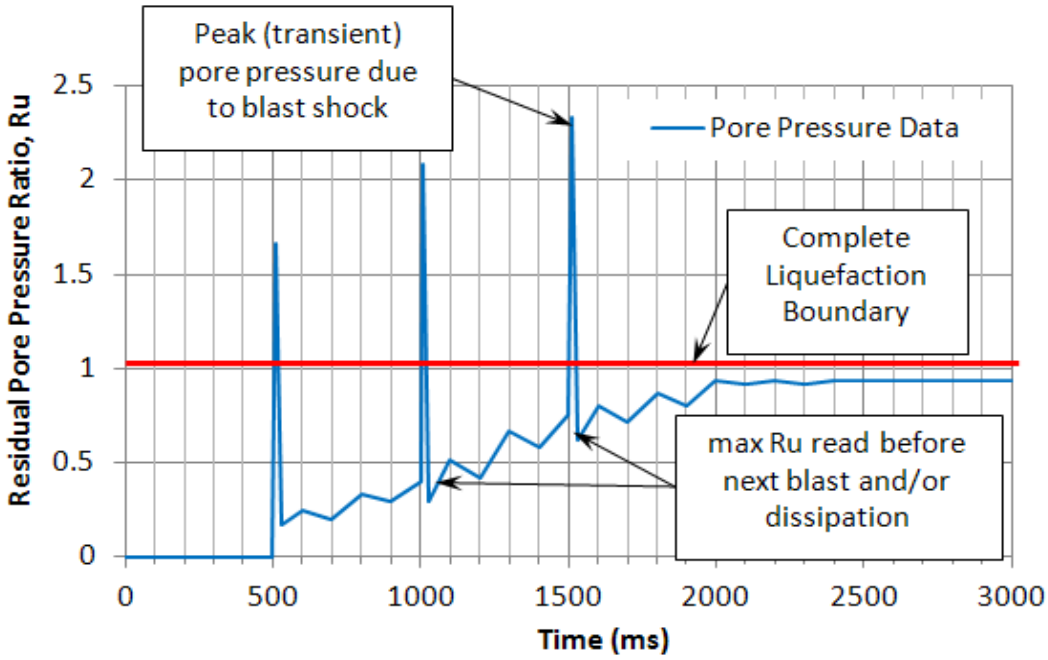

Figure 3-2 Pore pressure time history from example blasting study

In Table 3.2, an analysis is shown how the scaled distance was calculated for each sequential blast. The magnitude of excess pore pressure is dependent upon the blast size and distance, as well as the previous blasts sizes and distances. The residual pore pressure developed for each blast was determined by the maximum pore pressure observed on the chart prior to the next blast and/or dissipation.

Table 3.2 – Analysis of results from example blasting study

Blast No.	Radius R m	Mass W kg	Scaled Distance $R_{ave}/\Sigma(W^{0.33})$ m/kg$^{0.33}$	Excess Pore Pressure kPa	Residual Pore Pressure Ratio R_u
1	8	1.5	7.00	24	0.40
2	6	1	5.17	45	0.75
3	4	0.5	4.18	56	0.93

From Table 3.2, the residual pore pressure ratio, Ru, is plotted in Figure 3-3 with respect to the scaled distance. The increasing *Ru* is plotted as a negative slope with the adjusted scaled distance plotted on a semi-log plot, indicating that each blast reduces the overall scaled distance.

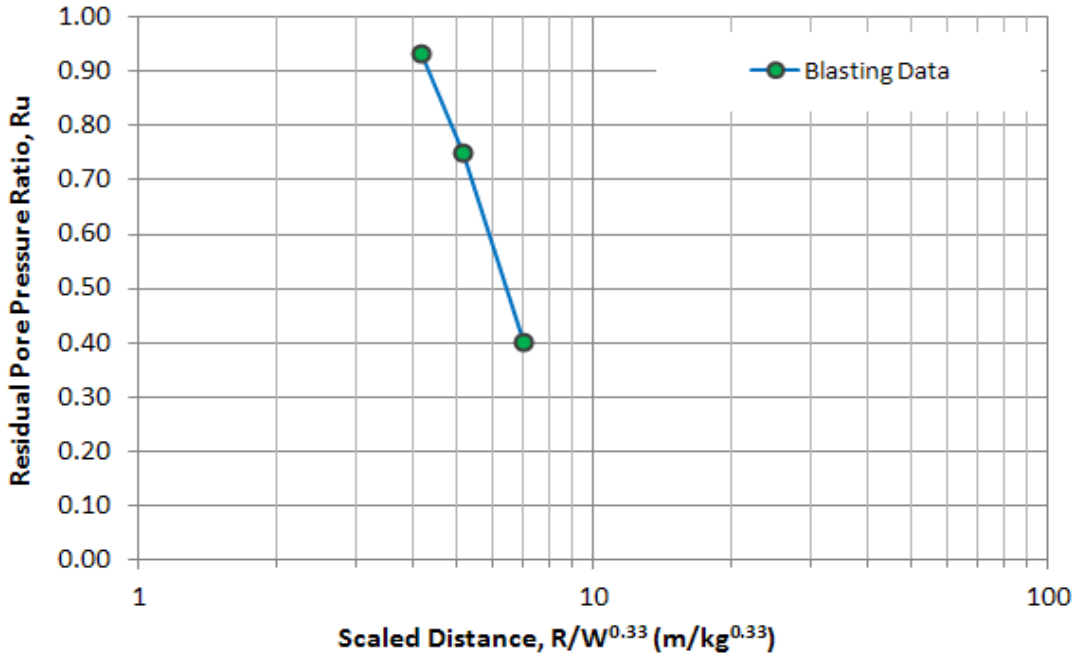

Figure 3-3 Residual pore pressure, *Ru*, vs. scaled distance for example blasting study

3.2 PORT OF ISHIKARI, JAPAN

In the fall of 2007, a full-scale blast-induced liquefaction study was conducted by Japan's Port and Airport Research Institute (PARI) at the Ishikari Bay New Port in Hokkaido Island, Japan, to evaluate the resiliency of airport infrastructure subjected to liquefaction induced from a major earthquake (PARI 2009). Airports play a critical role in a community's response following a natural disaster, providing emergency services and supplies for medical and relief operations. Using controlled blasting to induce liquefaction, the seismic performance of several full-scale airport structures were evaluated, including ground improvement techniques to mitigate liquefaction. The airport structures tested included a mock runway, apron, embankment, and other structures. Ground improvement techniques included compaction grouting and chemical (permeation) grouting, and were compared to the settlement observed in an unimproved area within the blasting area. Chemical grouting was performed with various treatment depths to determine the cost-effective treatment layout. The study emphasized that liquefaction-induced settlement beneath a runway can force closure of the runway following a major earthquake, which can cause significant delays in disaster relief services. However, cost-effective liquefaction countermeasures can be implemented to minimize settlement and maintain serviceability.

The study was largely funded by Japan's Ministry of Land, Infrastructure, and Transportation, and included over forty-seven research groups participating with PARI collaborating on thirty different projects in five research areas. The research areas included (1) observation of liquefaction behavior, (2) pavement management, (3) liquefaction mitigation methods, (4) airport infrastructure, and (5) monitoring techniques. Oregon State University (OSU) and the United States Geological Survey (USGS), with funding provided by the National Science Foundation (NSF), contributed to the study by measuring post-liquefaction settlement using LIDAR (Light Detection And Ranging) to measure fine-scale topographic changes and by performing non-destructive evaluation methods to analyze density changes following dissipation of blast-induced residual pore pressures. To date, this may be the most extensively monitored controlled blasting study performed, providing a wealth of information including soil conditions,

blasting results, and so forth. However, a major obstacle in regard to this information is that most of it is currently in Japanese, requiring a translation to English in order to make it understandable to U.S. researchers.

3.2.1 Site Conditions and Test Layout

The test site consisted of loose, reclaimed sand dredged from Ishikari Bay extending to a depth of approximately 5 to 6 m below the ground surface. The reclaimed sand had an average fines content of 10 to 20% and SPT $(N_1)_{60}$ values ranging from 1 to 8 blows per 30 cm. The reclaimed sand was underlain by several alluvial soil layers consisting of sand, gravel, and clay. SPT $(N_1)_{60}$ values for the alluvial layers ranged from 3 to 12 blows per 30 cm. The average shear wave velocity of the reclaimed sand was approximately 120 m/s. The reclaimed soil was classified as poorly graded and susceptible to liquefaction. The groundwater table was at an approximate depth of 2 to 2.5 m. A typical soil profile is shown in Figure 3-4, including average SPT $(N_1)_{60}$ values.

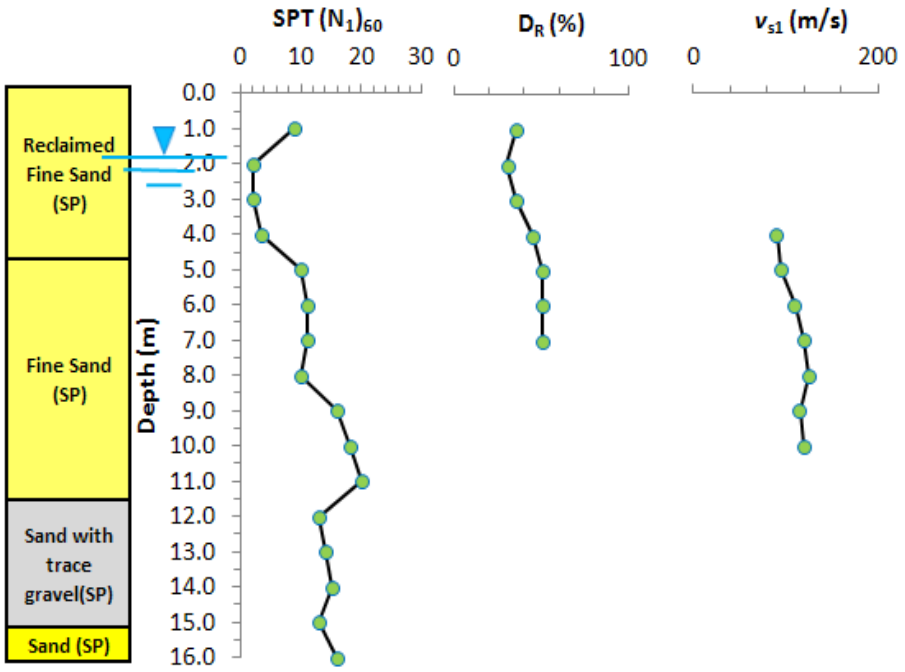

Figure 3-4 Typical Soil Profile for Ishikari Blasting Study

The pilot study consisted of four separate blasting studies using both multiple blasts and single blasts. Pilot study P2, shown in Figure 3-5, utilized a grid array of 16 boreholes spaced on a 6.5 m grid. Charges were placed at depths of 4.5 m and 9.0 m, with charge weights ranging from 2 kg to 4 kg, as shown in Table 3.3. Time delays between each blast with the exception of the first and second blasts was 200 ms. The second blast occurred approximately 34 minutes after the first blast for reasons unknown. During this 34 minute pause between blasting, the pore pressure had enough time to almost fully dissipate within each pore pressure transducer prior to the second blast. For additional information regarding the pilot study, the reader is referred to PARI (2009).

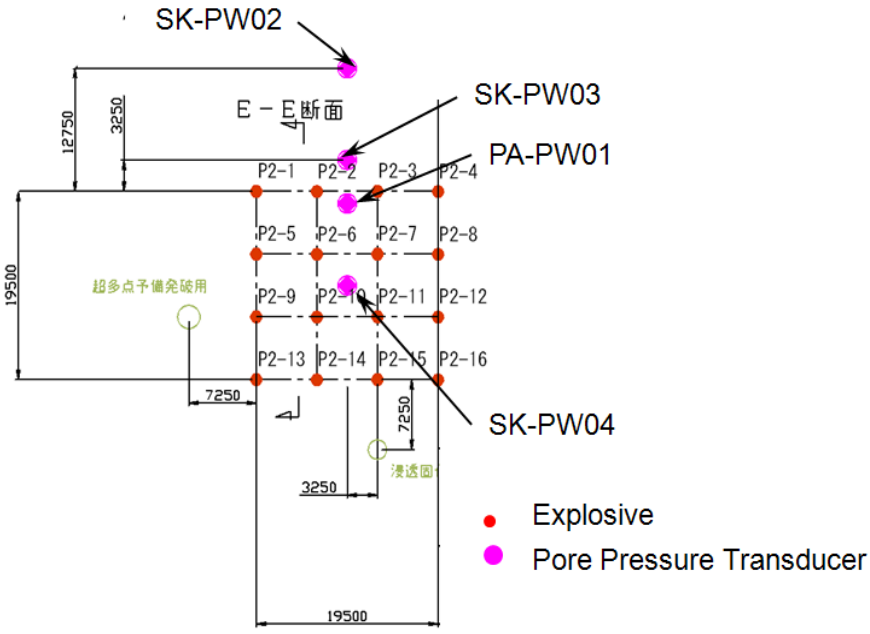

Figure 3-5 Blasting Layout for Ishikari Pilot Study
(adapted from PARI 2009)

Table 3.3 – Ishikari Pilot Study Blasting Details
(adapted from PARI 2009)

Pilot Study, P2	Charge Weight at depth of placement (kg)		Radial Distance of Explosive from Pore Pressure Transducer, PPT (m)				
Blast	at z = 4.5 m	at z = 9.0 m	SK-PW03 (at 4 m)	PA-PW01 (at 4 m)	PA-PW01 (at 8 m)	SK-PW04 (at 4 m)	SK-PW02 (at 4 m)
1	2	4	10.64	10.24	9.94	14.06	16.28
2	2	4	5.36	4.51	3.79	10.64	13.44
3	3	4	5.36	4.51	3.79	10.64	13.44
4	3	4	10.64	10.24	9.94	14.06	16.28
5	3	4	14.06	11.30	11.03	10.64	21.75
6	3	4	10.64	6.57	6.09	5.36	19.72
7	2	4	10.64	6.57	6.09	5.36	19.72
8	2	4	14.06	11.30	11.03	10.64	21.75
9	2	4	19.15	15.33	15.13	10.64	27.67
10	2	4	23.14	18.50	18.33	10.64	32.53
11	3	4	16.80	12.26	12.02	5.36	26.10
12	3	4	24.90	20.65	20.51	14.06	33.80
13	3	4	19.15	15.33	15.13	10.64	27.67
14	3	4	23.14	18.50	18.33	10.64	32.53
15	2	4	16.80	12.26	12.02	5.36	26.10
16	2	4	24.90	20.65	20.51	14.06	33.80

The full-scale study was performed approximately one month following the pilot study. The full-scale study used 269 boreholes with 2-kg and 4-kg charges placed at depths of 4.5 m and 9.0 m, respectively, below the ground surface. The delay interval was 200 ms between each blast, requiring nearly 2.5 minutes to complete blasting. A general layout of the full-scale blasting study is shown below in Figure 3-6, with an additional figure in Appendix A.1.4 displaying the blasting sequencing. In the tarmac area, horizontal blasts were used instead of downhole vertical blasts to liquefy the immediate area beneath the

pavement. A specific layout identifying specific pore pressure transducers is included in Appendix A.1.5. Recorded time histories from the transducers following the pilot test are provided in Appendix A.1.1 and A.1.2, and the full-scale test readings are in Appendix A.1.3. Many of the transducers were damaged or affected by the blast pulse, causing their readings to not be included in the analysis portion of the study.

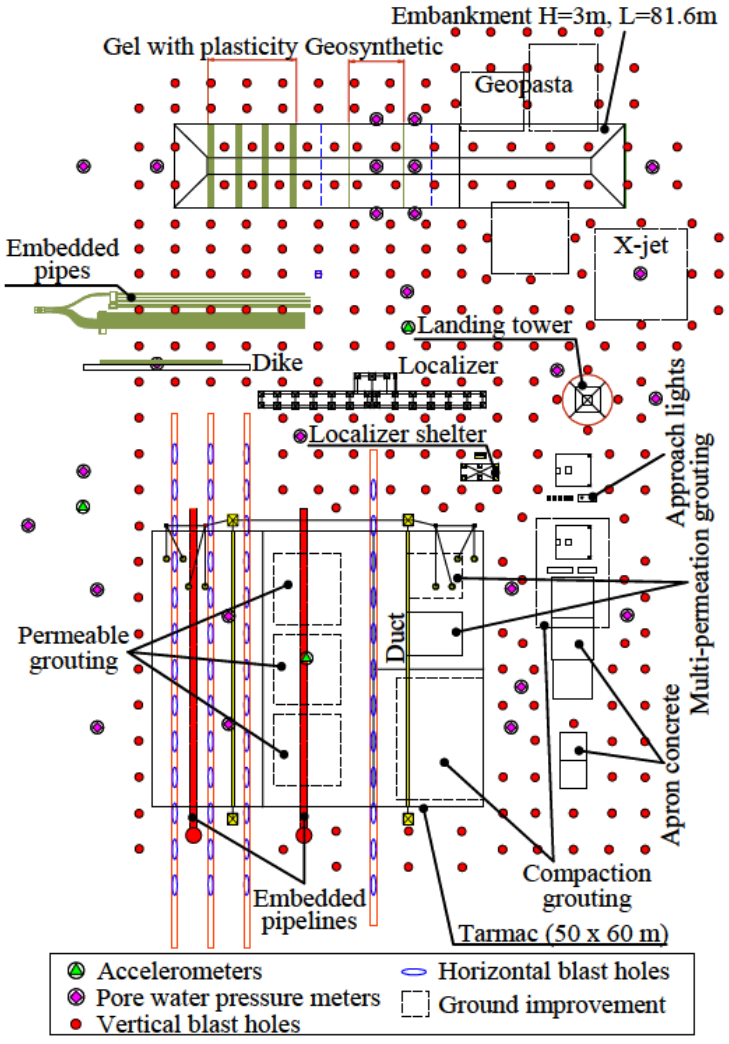

Figure 3-6 Blasting Layout for Ishikari Full-Scale Blasting Study (from Ashford et al. 2008)

3.2.2 Test Results

In both the pilot study and the full-scale study, sand boils and flowing of groundwater to the surface indicated that liquefaction had occurred. Maximum residual pore pressure ratios recorded from several transducers from the pilot and full-scale studies are plotted in Figure 3-7 based upon scaled distance estimated using the procedure shown previously in Equation 3-1. From the results, the data follows the expected trend of increasing *Ru* values with decreasing scaled distance. Generally, transducers closer to the explosives experienced higher residual pore pressures during blasting.

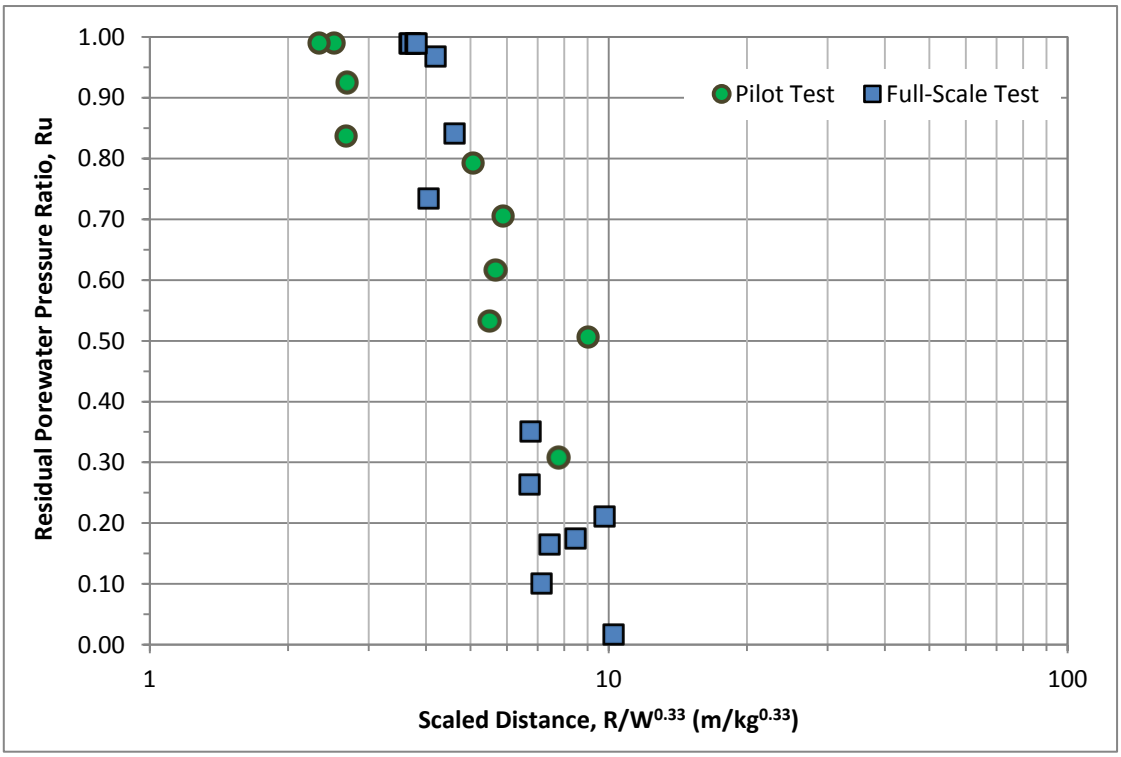

Figure 3-7 Maximum Residual Porewater Pressure Ratios from Ishikari Pilot Study P2 and Full-Scale Study

3.3 VANCOUVER, BRITISH COLUMBIA, CANADA, 2004

An in-situ liquefaction study using controlled blasting was performed near the Massey Tunnel in Vancouver, British Columbia with the objective of evaluating the performance of vertical composite earthquake drains to mitigate liquefaction (Rollins 2004, Strand 2008). Prior to the full-scale test of the composite drains, a pilot study was performed to

design the blasting layout and to serve as the baseline for comparison purposes of the drains. Multiple blasting was to be used over a period of 10 to 16 seconds to liquefy the soils surrounding the composite drains.

3.3.1 Site Conditions and Blasting Layout

The soil consisted of young alluvial sand/silty sand that extended to a depth of 6 m to approximately 15 m, as shown in Figure 3-8. The sand layer had an average shear wave velocity of 180 m/s and an average relative density of approximately 40%. CPT-based correlations provided by Kulhawy and Mayne (1990) estimated the SPT $(N_1)_{60}$ values to range from 8 to 14 per 30 cm, with an average of 10 blows per 30 cm.

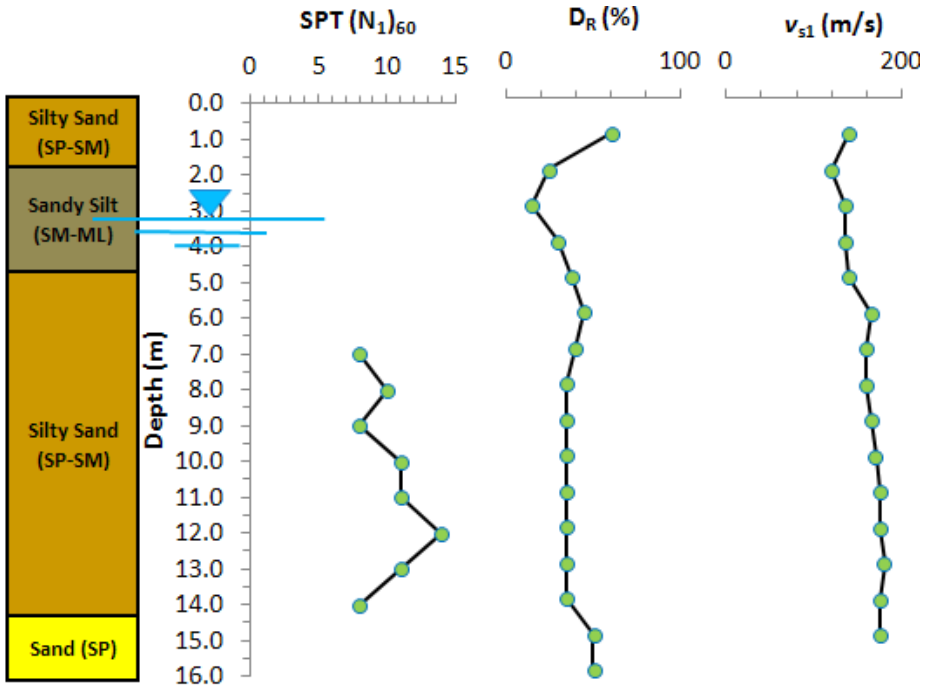

Figure 3-8 Typical Soil Profile for Vancouver, British Columbia Blasting Study

The soil blasting layout was designed to provide a relatively broad zone of liquefaction while preventing adverse impacts to nearby infrastructure. A total of 3 pilot test blasts were performed along a circular array 10 m in diameter, as shown in Figure 3-9. The first test consisted of 8 holes with 3 decks of 0.227 kg charges. The blast holes were placed at depth intervals of 6.4 m, 8.5 m, and 10.1 m beneath the surface. The first pilot

test did not generate high residual pore pressures within the soil, so a single charge was used in test #2 to evaluate pore pressure response with an increased charge weight. A single blast was performed with an increased charge size of 1.135 kg placed at a depth of 8.5 m. The results from test #2 are unknown. The third test blast consisted of 7 boreholes with 3 charges in each borehole at the same depths as test #1, with charge sizes increased to 1.36 kg.

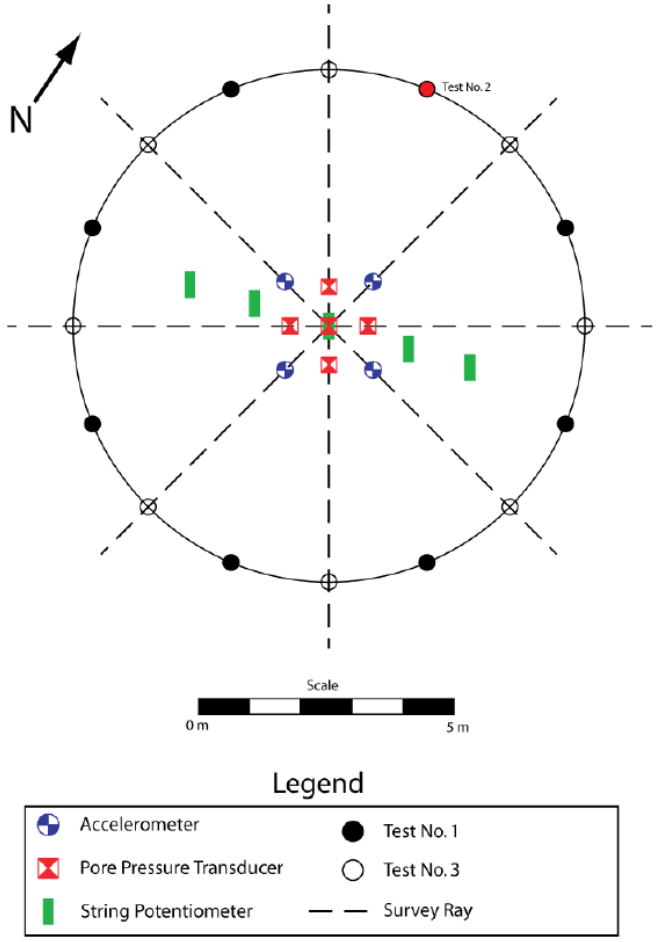

Figure 3-9 Blasting Layout for Pilot Study at Vancouver, British Columbia Test (from Strand 2008)

3.3.2 Test Results

Time histories of residual pore pressure, *Ru,* were measured during the first and third blasts and are shown in Appendix A.2. From the time histories, the increase in *Ru* with

each blast was able to be estimated and plotted as a sequence with respect to scaled distance as shown in Figure 3-10. In Figure 3-10, the maximum recorded *Ru* for each transducer is represented by the larger marker in the sequence of blasts. During the first blast sequence, the maximum *Ru* was approximately 0.70, indicating that liquefaction did not occur. It was observed that pore pressure transducers (PPT) installed at greater depths experienced less *Ru* than PPT's closer to the surface, perhaps due to the increase in scaled distance and the increase in soil density (Strand, 2008). During the third blast, the maximum *Ru* typically exceeded 0.90, indicating that the soil was nearly liquefied completely.

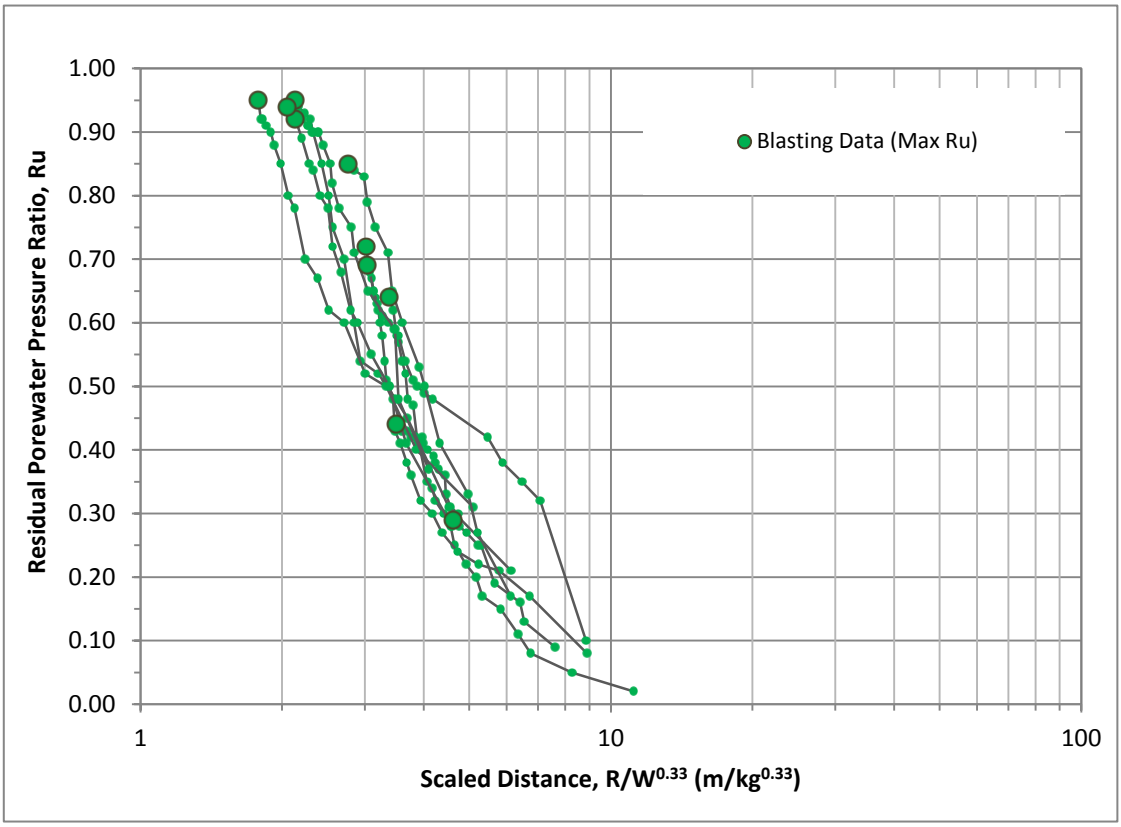

Figure 3-10 Sequential Change in Residual Porewater Pressure Ratio, *Ru*, with respect to Scaled Distance from Vancouver Blasting Study

3.4 MAUI, HAWAII, 2002

In order to assess the in-situ potential of liquefaction in coralline sands, researchers from Brigham Young University and the University of Hawaii performed a controlled

blasting experiment in Maui, Hawaii (Rollins et al. 2004). Prior to the blasting experiment, an SPT-based liquefaction assessment based on clean non-coralline sands indicated that the soil was liquefiable. However, shear velocity measurements were high enough to categorize the site as not being susceptible to liquefaction. Blasting was performed as a supplemental method to assess the liquefaction potential of the coralline sand.

3.4.1 Site Conditions and Blasting Layout

The site consisted of clayey silt and fine volcanic sand overlying coralline silty sand and gravel, the layer of interest in the liquefaction study. SPT $(N_1)_{60}$ values ranged from 2 to 8 blows per 30 cm, with an average of 5 blows for 30 cm for the coralline sand while shear wave velocities ranged from 200 to 215 m/s. Based upon the SPT test, the coralline sand was considered susceptible to liquefy for a design-level earthquake while the shear wave velocity evaluation showed the soil to be able to resist liquefaction. A typical soil profile is shown in Figure 3-11.

Two different controlled blasting tests utilizing multiple blasts were performed to provide an in-situ liquefaction assessment of the coralline sands, with layouts shown in Figure 3-12. All explosives and pressure transducers were placed at a depth of 5.35 m. The individual charge sizes were 0.45 kg, with a total of 8 charges used for each test. In test #1, the charge line was placed at a perpendicular distance of approximately 8 m, while test #2 was moved closer to a perpendicular distance of approximately 4 m.

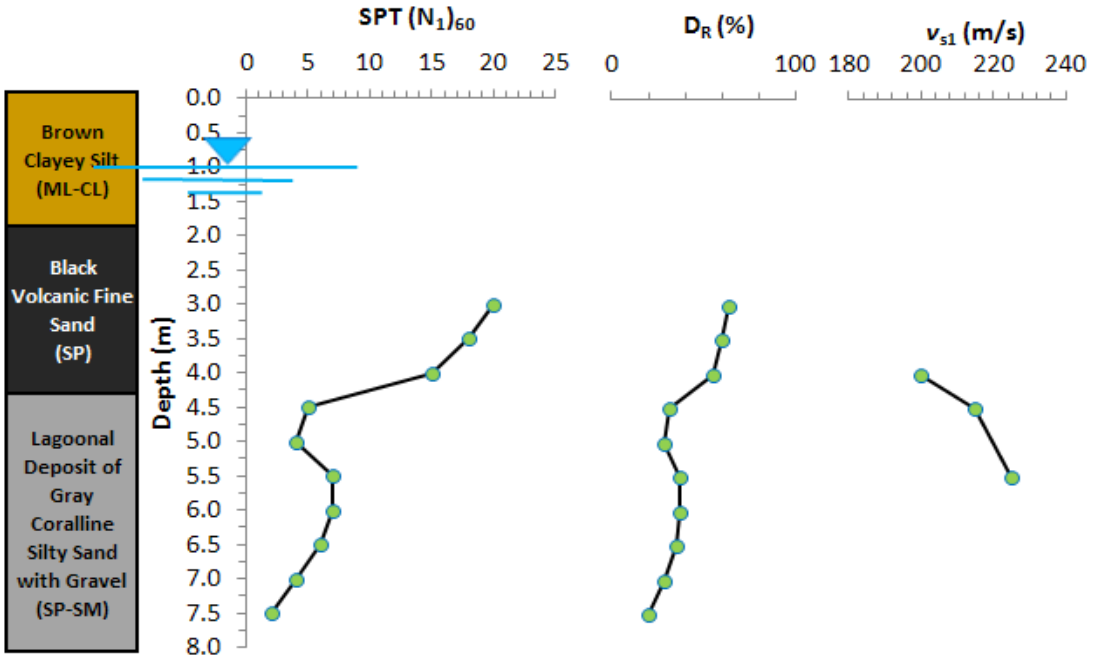

Figure 3-11 Typical Soil Profile for Maui Blasting Study

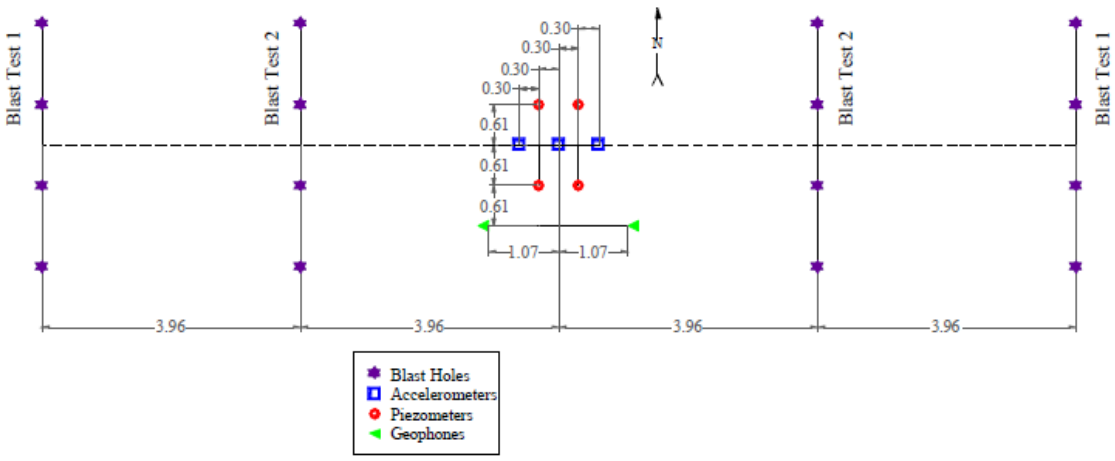

Figure 3-12 Blasting and Instrumentation Layout at Maui (distances in meters) (from Rollins et al. 2004)

3.4.2 Test Results

Pore pressures (both peak and residual), ground motions, and settlements were measured during both tests. Pore pressure time histories are included in Appendix A.3. It was uncertainty of which pore pressure transducer the results came from, further analysis was performed using the center transducer. Table 3.4 summarizes the residual pore pressures recorded with each charge during blast #1 and #2. The first charge during blast #1 consisted of two charges detonated simultaneously. During the test, changes in *Ru* were recorded with each blast and plotted in Figure 3-13 for blast #1 and blast #2 with the calculated scaled distance. During blast #1 and #2, the peak pore pressure ratio reached a value of 0.91 and 0.96, respectively, indicating that blast sequence effectively liquefied the soil in each case. Based upon their results, Rollins et al. (2004) concluded that the coralline sand was indeed susceptible to liquefaction, and that correction factors should be made to shear wave velocity tests performed in such soils.

Table 3.4 – Residual Pore Pressure Results during Maui Blasting Study
Adapted from Rollins et al. (2004)

Charge Number	Test Blast #1			Test Blast #2		
	Charge Mass (kg)	Change in Pore Pressure, Δ*Ru*	Residual Pore Pressure Ratio, *Ru*	Charge Mass (kg)	Change in Pore Pressure, Δ*Ru*	Residual Pore Pressure Ratio, *Ru*
1	0.90	0.53	0.53	0.45	0.58	0.58
2	0.45	0.12	0.65	0.45	0.14	0.72
3	0.45	0.09	0.74	0.45	0.07	0.79
4	0.45	0.06	0.80	0.45	0.05	0.84
5	0.45	0.03	0.83	0.45	0.05	0.89
6	0.45	0.04	0.87	0.45	0.01	0.90
7	0.45	0.04	0.91	0.45	0.04	0.94
8	-	-	-	0.45	0.02	0.96

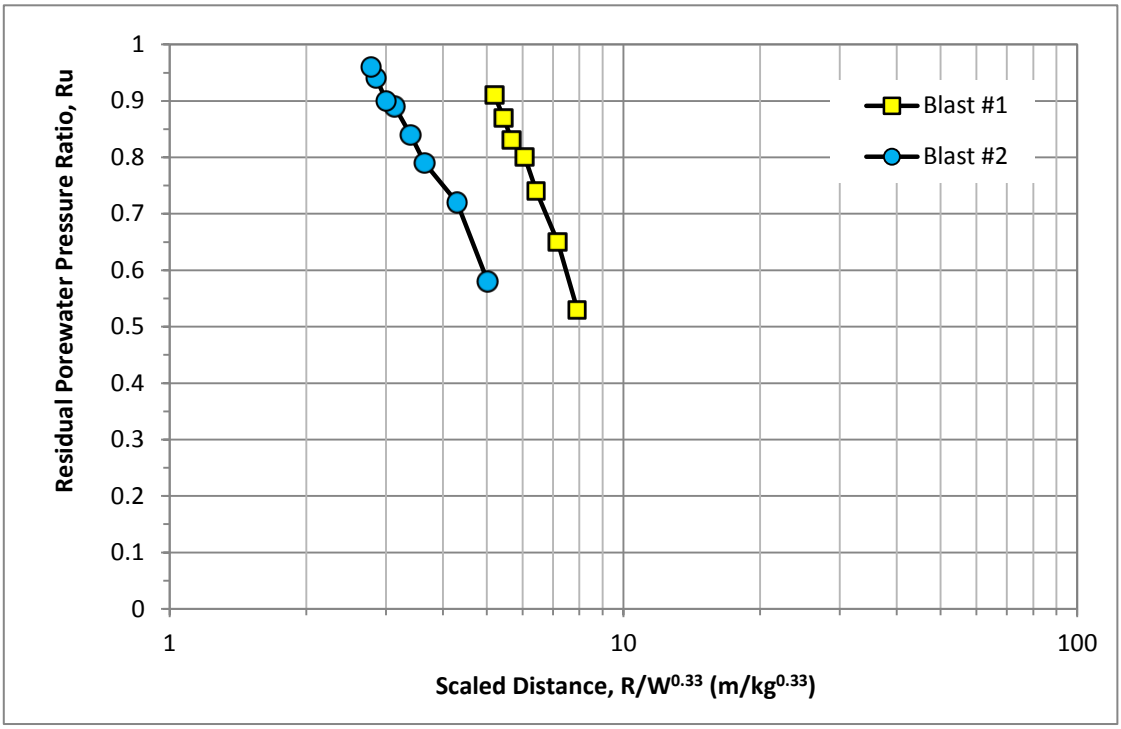

Figure 3-13 Residual Pore Pressure Response vs. Scaled Distance for Maui Blasting Study

3.5 PORT OF TOKACHI, HOKKAIDO ISLAND, JAPAN, 2001

Lead by the Port and Airport Research Institute (PARI) of Japan, a multi-participant, full-scale blast-induced liquefaction experiment was performed to assess the performance of piles, pipelines, and quay walls against lateral spreading based upon static and seismic design. Universities and industries from Japan and the U.S. also contributed to the study, experimenting with mitigation techniques and response of lifelines to liquefaction. Blasting was performed to induce lateral spreading of a hydraulic fill placed less than 2 years prior to the test (Sugano et al. 2002). Prior to the full-scale experiment, pilot tests were performed to determine the optimal blasting layout to ensure liquefaction, such as charge weights, locations of charges, and delay in blasts (Ashford and Juirnarongrit, 2004).

3.5.1 Site Conditions and Blasting Layout

The site consisted of young hydraulic fill that was mostly loose silty sand. In-situ measurements recorded average $(N_1)_{60}$ values of 3 blows per 30 cm, shear wave

velocities averaging 100 m/s, and a relative density of approximately 30% from CPT measurements for the upper 7 m. A typical soil profile for the site is provided in Figure 3-14. The soil was considered very susceptible to liquefaction, as observed by the loose density of the sand indicated by the low SPT $(N_1)_{60}$ values.

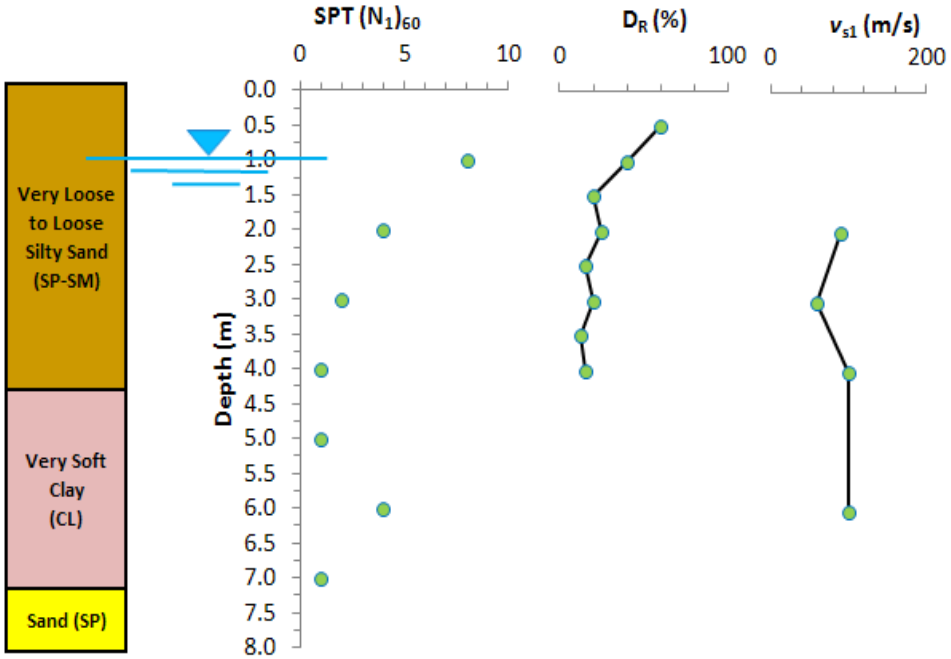

Figure 3-14 Typical Soil Profile for Tokachi Blasting Study

The first pilot test consisted of several single borehole tests and was performed to determine the blasting sequence, the optimum depth of the charge, and the optimum explosive weight. The boreholes were spaced at the corners of a square area with border lengths of 10 m. The explosives were placed at a depth of 5 m below the ground surface for boreholes S1 and S2, and decked at depths of 5 m and 10 m for S3 and S4. The soil conditions for the 10 m depth is unknown except that it was a dense sand with SPT $(N_1)_{60}$ values exceeding 40 blows per 30 cm. The individual charge weights were 2 kg for S1, and 3 kg for the remaining charges. Each borehole was detonated upon dissipation of residual pore pressures from the previous borehole explosion. During test S3, blasting started from the bottom-up, while in S4 it was performed from the top-down, with a time delay of 300 ms.

For the full-scale tests, sequential blasting was performed utilizing a grid pattern covering an area of approximately 4,800 m^2 as shown in Figure 3-15. During the first test, explosives were placed in a 6 m grid, with charges placed at depths of 3.5 m and 7.5 m below the ground surface. Charge sizes ranged from 3 to 5 kg along the outer perimeter, while 2 kg charges were used near the test piles to prevent damage due to the shock blast. The blasting interval was 750 ms between boreholes, requiring approximately 35 seconds for the 60 charges to be detonated within the test area. Blasting was performed in an "out-to-in" pattern. Pore pressure transducers were placed near the pile groups at depths of 2, 4, and 6 m beneath the surface, as shown in Figure 3-16.

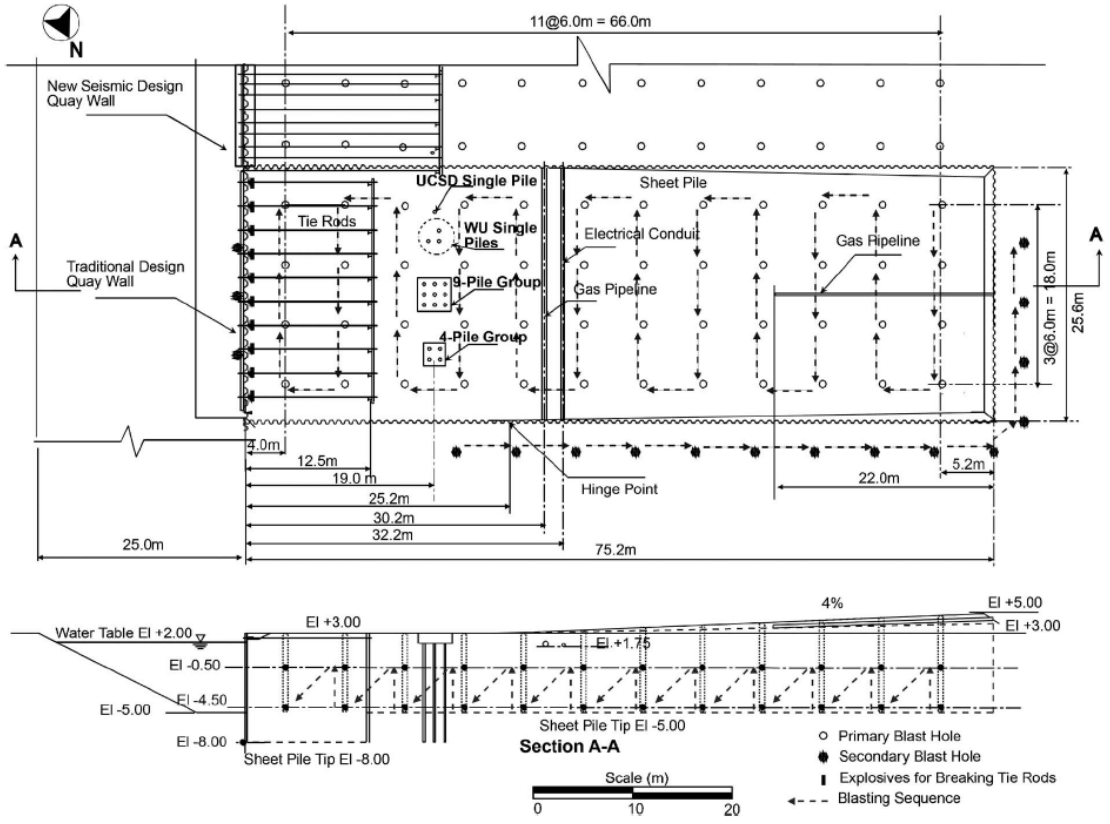

Figure 3-15 Blasting Layout and Sequence during Tokachi Full-Scale Blast #1 (from Ashford and Juirnarongrit 2004)

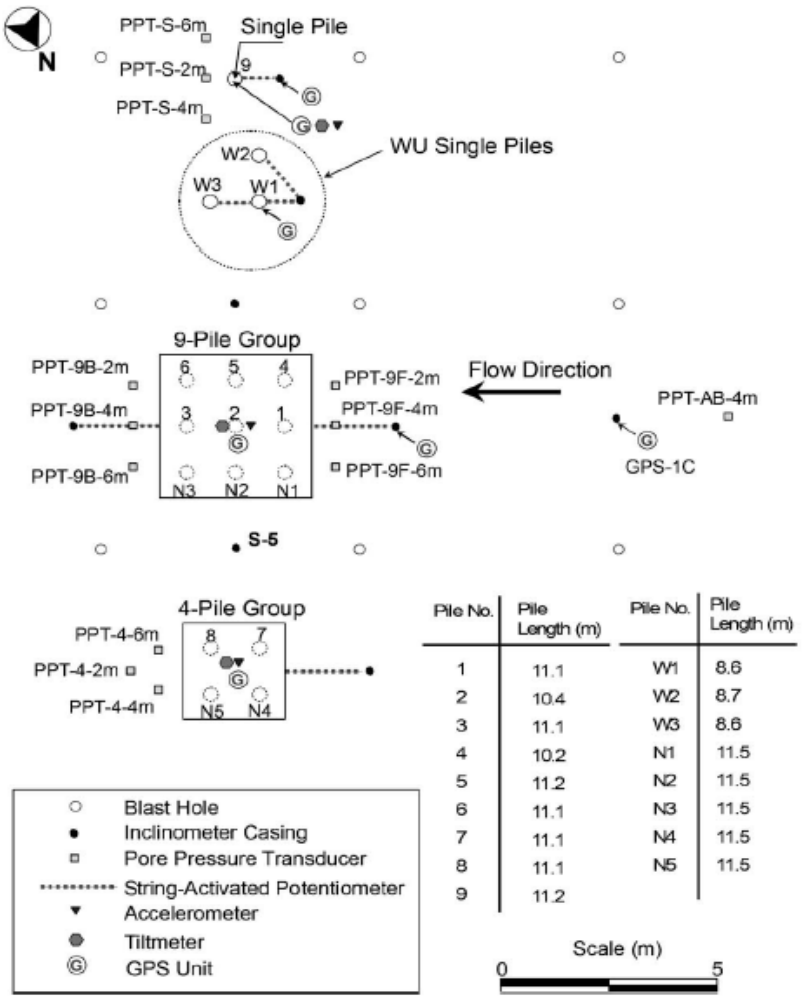

Pile No.	Pile Length (m)	Pile No.	Pile Length (m)
1	11.1	W1	8.6
2	10.4	W2	8.7
3	11.1	W3	8.6
4	10.2	N1	11.5
5	11.2	N2	11.5
6	11.1	N3	11.5
7	11.1	N4	11.5
8	11.1	N5	11.5
9	11.2		

Figure 3-16 Pore Pressure Transducer Layout during Tokachi Full-Scale Blast #1 (from Ashford and Juirnarongrit 2004)

3.5.2 Test Results

Pore pressure time histories are provided in Appendix A.4. During pilot test #1, the maximum residual excess pore pressures were observed to increase with increased charge size in tests S1 and S2. In tests S3 and S4, it was observed that a maximum *Ru* was achieved when blasting was performed from the bottom-up rather than top-down sequence. The change in *Ru* observed in the pilot studies is plotted with respect to scaled distance in Figure 3-17. The maximum recorded *Ru* is shown as the larger, darker marker on the figure.

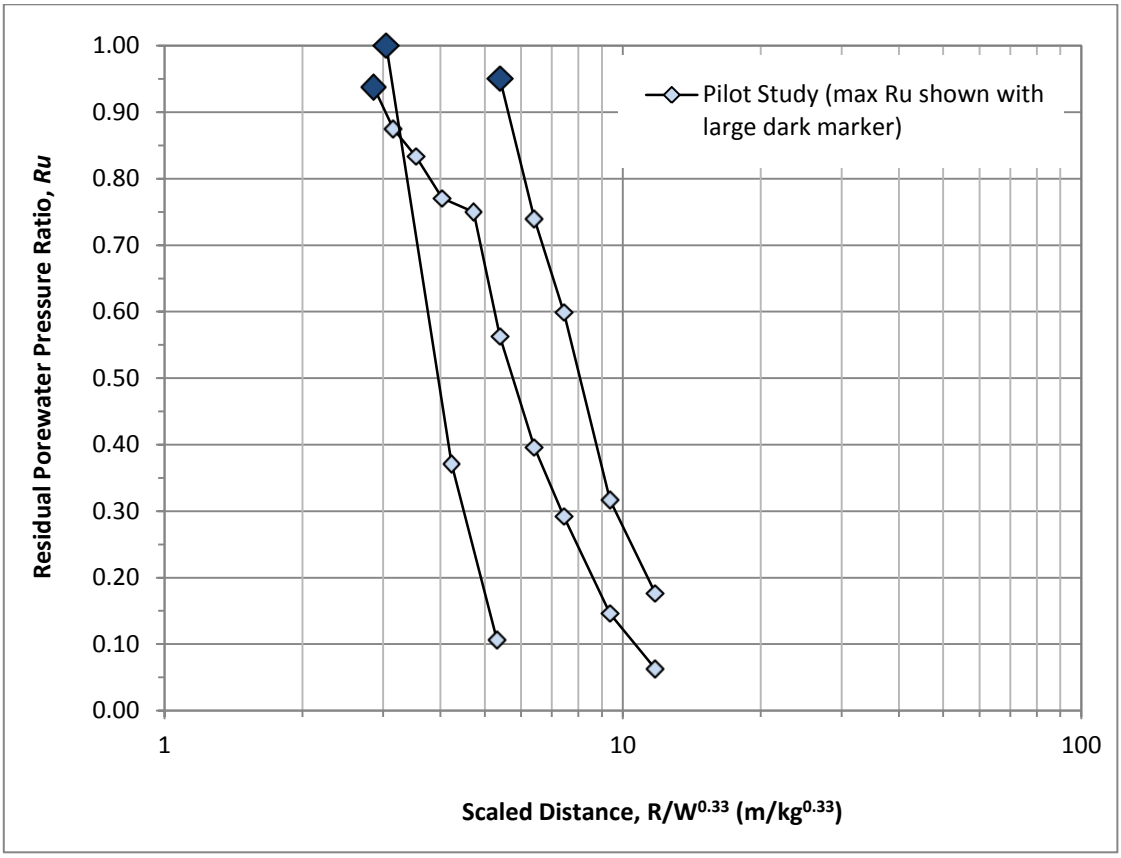

Figure 3-17 Residual Pore Pressures vs. Scaled Distance during Tokachi Blasting Study, Pilot Test

During the full-scale blast #1, residual pore pressures near the transducers increased rapidly as the blasting approached the transducer locations. *Ru* measurements showed that liquefaction occurred within 25 seconds, and sand boils appeared at the ground surface shortly thereafter, indicating that liquefaction had indeed occurred. The change in *Ru* observed in individual transducers is plotted in Figure 3-18 with respect to scaled distance. The maximum *Ru* recorded for each pore pressure transducer are denoted by the larger, darker marker on the figure as well as presented below in Table 3.5.

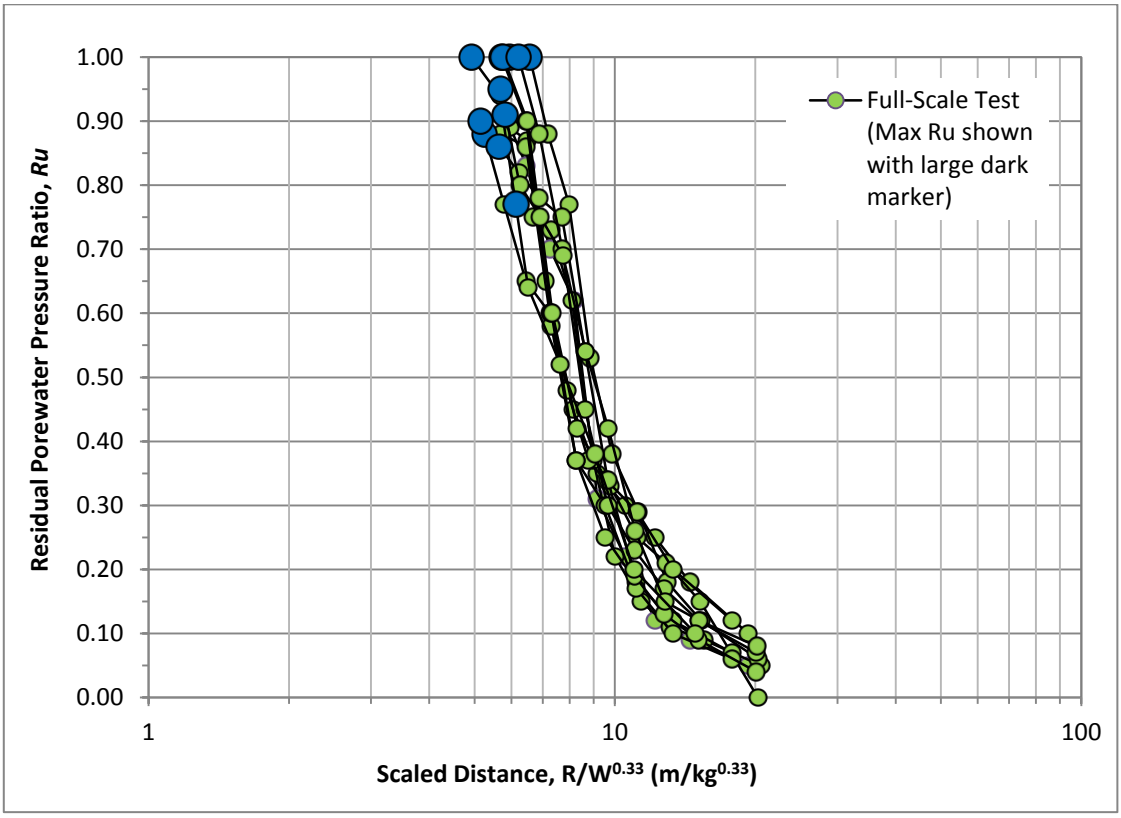

Figure 3-18 Residual Pore Pressures vs. Scaled Distance during Tokachi Blasting Study, Full-Scale Test #1

Table 3.5 – Maximum Residual Pore Pressures during Tokachi Full-Scale Test #1

Pore Pressure Transducer (PPT)	Depth of PPT (m)	Residual Pore Pressure, *Ru*
S-2	2.00	0.91
S-6	6.20	0.88
4-2	2.00	0.77
4-4	4.00	1.00
4-6	6.63	1.00
9F-2	2.00	0.90
9F-4	4.00	1.00
9F-6	6.00	1.00
9B-2	2.00	0.86
9B-4	4.00	1.00
9B-6	6.00	0.95
AB-4	4.00	1.00

3.6 VANCOUVER, BRITISH COLUMBIA, CANADA, 2000

Controlled blasting was used to perform an in-situ liquefaction field test in Delta, British Columbia, Canada by Pacific Geodynamics Inc. and the University of British Columbia in 2000 (Gohl et al. 2001). The goal of the blast-induced liquefaction experiment was to develop a downhole in-situ liquefaction test to supplement existing penetration test-based methods and cyclic laboratory tests, particularly for problematic soils such as low-plasticity silts, and sand and gravel deposits that are difficult to perform conventional liquefaction assessments in. Sequential blasting using multiple charges was performed to generate shear and compressive strain pulses to cyclically load the soil to the equivalent shear strain that would be expected from anticipated ground motions created from the design-level earthquake.

3.6.1 Site Conditions and Blasting Layout

The site was composed of estuarine deposits consisting of interlayered sand, silt and clayey silt. The target layer for the liquefaction study was low plasticity silty sand at a depth of 10 to 12 m. Shear wave velocities for the target layer averaged around 160 m/s, with $(N_1)_{60}$ values ranging from 5 to 10 blows per 30 cm. Empirical liquefaction relationships indicated that the soil was susceptible to liquefaction for the design-level earthquake for the area, a M_w 7 earthquake capable of producing shear strains ranging from 0.4% to 2%. A typical soil profile for the site is provided in Figure 3-19.

A circular array was used for the blasting layout, with explosives spaced at alternating radial distances of 6 m and 12 m from the center. A total of 16 explosives were used, with two 6-kg charges used in the 12 m radius holes and two 2-kg charges used in the 6 m radius hole spaced at depths of 8 m and 12 m. Prior to the main blasting event a single 8-kg charge was detonated at a distance of 12 m from the center of the blasting area to verify that all instrumentation was functioning. The blasting and instrumentation layout is shown in Figure 3-20. The blasts were delayed by an average of 500 ms between each deck, and 1 second between each borehole.

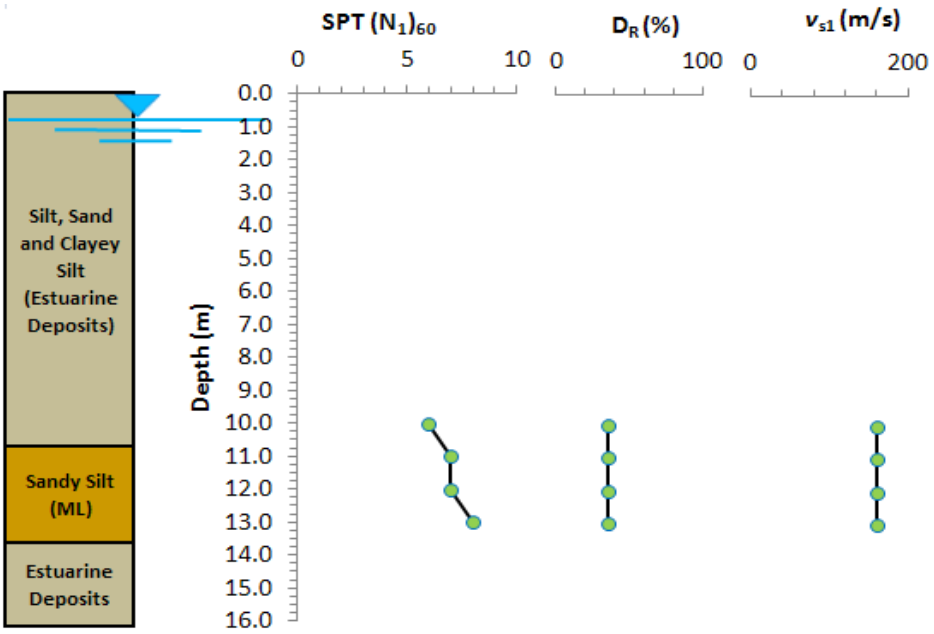

Figure 3-19 Typical Soil Profile for Delta, British Columbia Blasting Study

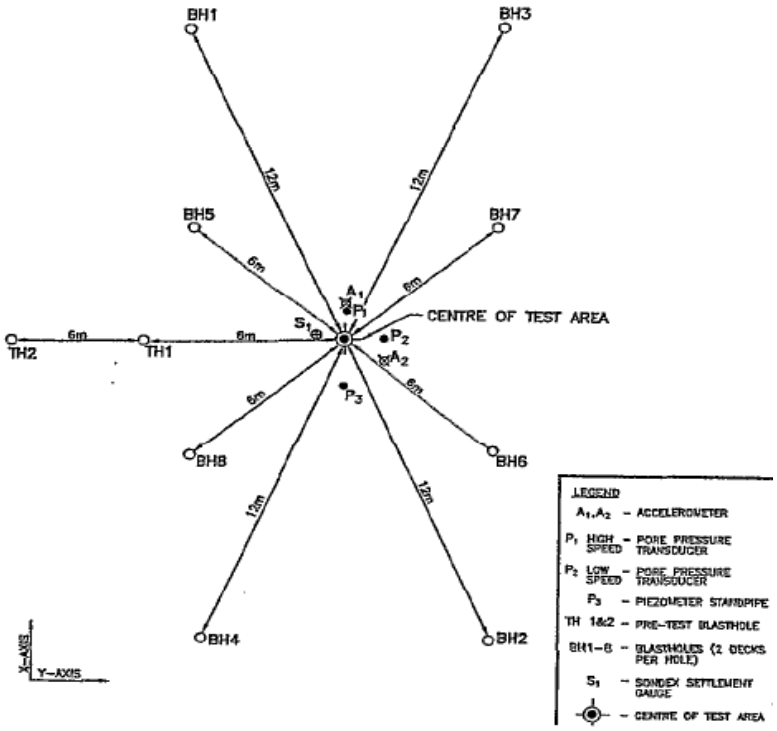

Figure 3-20 Blasting and Instrumentation Layout at Delta, British Columbia Study (from Gohl et al. 2001)

3.6.2 Test Results

The change in the residual pore pressure following the single 2-kg test blast and after all blasts were detonated were 0.15 and 0.48, respectively, for a maximum residual pore pressure of 0.63. This pore pressure ratio indicates that complete soil liquefaction was not achieved, as confirmed by a lack of sand boils at the surface. Following their study, Gohl et al. (2001) recommended a similar downhole in-situ controlled blasting experiment to be performed on clean sand to serve as a baseline for future liquefaction evaluations. The maximum *Ru* recorded for the single blast and the multiple blasts are plotted in Figure 3-21 with respect to the scaled distance.

Figure 3-21 Maximum Residual Pore Pressure Ratio vs. Scaled Distance for Delta, British Columbia Blasting Study

3.7 SAN FRANCISCO, CALIFORNIA, 1998

To improve seismic design for lateral load capacity of deep foundations, a full-scale in-situ liquefaction study was performed by UC San Diego and Brigham Young University. Other participants collaborated on the project, including the U.S. Geological Survey. The test was performed at the National Geotechnical Experimentation Site (NGES) located on Treasure Island in the San Francisco Bay of California. This full-scale study, called the Treasure Island Liquefaction Test (TILT), focused on developing lateral load-displacement relationships for a variety of individual piles and pile groups in liquefied sand under full-scale conditions (Ashford & Rollins 2002, 2004; Ashford et al. 2006). Controlled blasting was used to induce liquefaction in the surrounding soil prior to conducting the lateral load pile tests. In order to determine the blasting layout that would sufficiently induce liquefaction for the full-scale test, two pilot tests were performed. The second pilot test was conducted to verify if the soil could be liquefied at a site more than once using the same blasting design.

3.7.1 Site Conditions and Blasting Layout

Treasure Island is a man-made island consisting of hydraulically-placed sands. The site investigation identified the sand fill extended to a depth of approximately 6 m below the ground surface, and having a relative density ranging from 20% to 70%. SPT $(N_1)_{60}$ values ranged from 2 to 19 blows per 30 cm, with the highest penetration values within 1 m of the surface. Underlying the hydraulic fill are sandy silts and Young Bay Mud. The hydraulic fill is considered liquefiable based upon previous liquefaction during the Loma Prieta earthquake in 1989 (M_w 6.9). A typical soil profile for the pilot liquefaction study is provided below in Figure 3-22. The water table was approximately 0.5 m beneath the excavated surface during this study. The pilot study involved two blasting events separated by three days. The blasting layout consisted of 0.5 kg TNT-equivalent charges placed at approximately 3 m beneath the excavated surface, spaced evenly in a circular array with horizontal radius of approximately 2 m, with pore pressure transducers spaced at depths ranging from 1 m to 6 m throughout the testing area, as shown in Figure 3-23. During the second blast, the blasting layout was rotated clockwise 0.3 m, maintaining the same radial distance used during the first test.

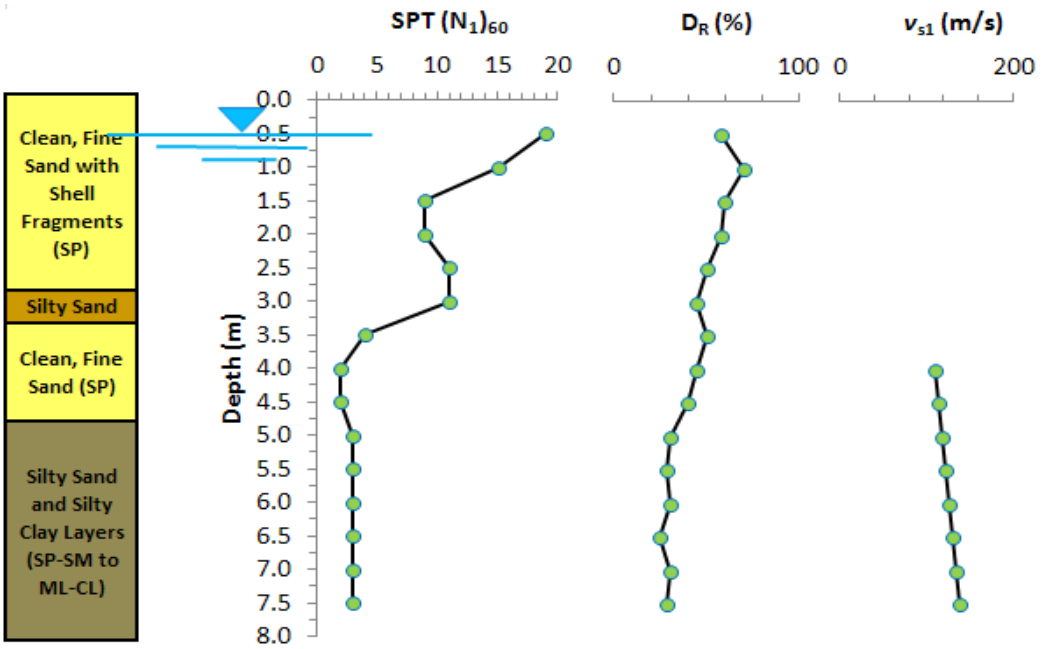

Figure 3-22 Typical Soil Profile for Treasure Island, California Pilot Study

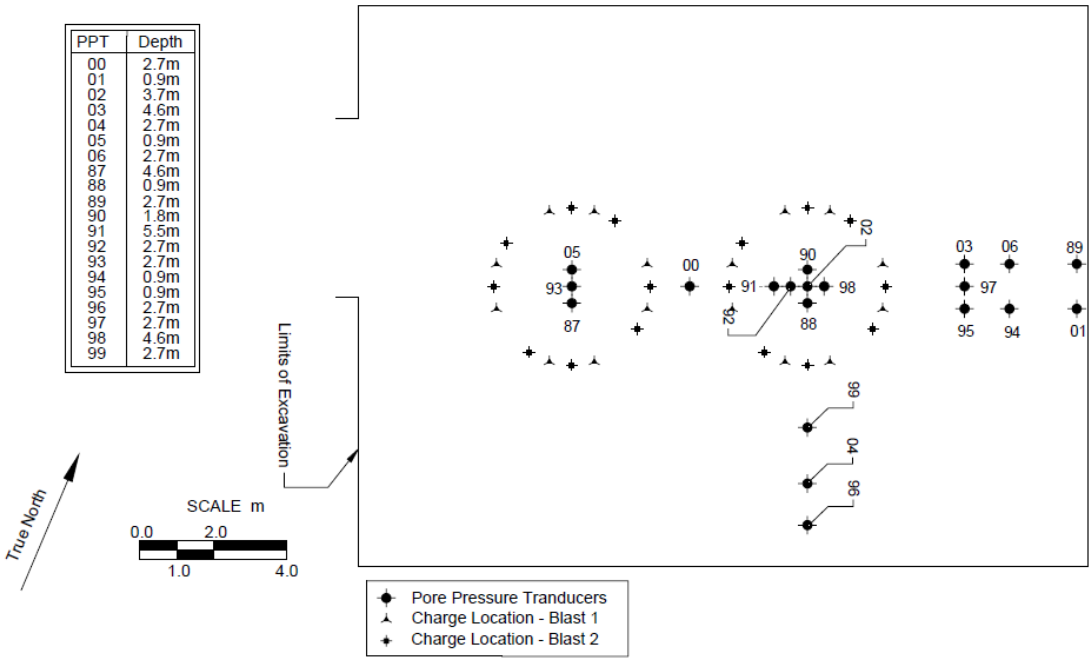

Figure 3-23 Blasting and Instrumentation Layout for Treasure Island Pilot Study (from Ashford et al. 2004)

3.7.2 Test Results

During both blasts, pore pressure ratios of more than 80% were consistently achieved throughout the soil profile, with many transducers indicating that liquefaction had occurred. Sand boils appeared at the ground surface about 5 minutes after blasting had finished, and continued to eject material for over 20 minutes. Residual pore pressures measured during the first and second blasts are included in Appendix A.5 of this thesis. The maximum residual pore pressures are plotted in Figure 3-24 with respect to scaled distance for both Blast #1 and Blast #2. Table 3.6 summarizes the maximum recorded *Ru* from each PPT during the blast #1 and blast #2 of the pilot study. Additional information regarding TILT is provided by Kayen et al. (2000), Ashford et al. (2004), and Rollins et al. (2005a, 2005b).

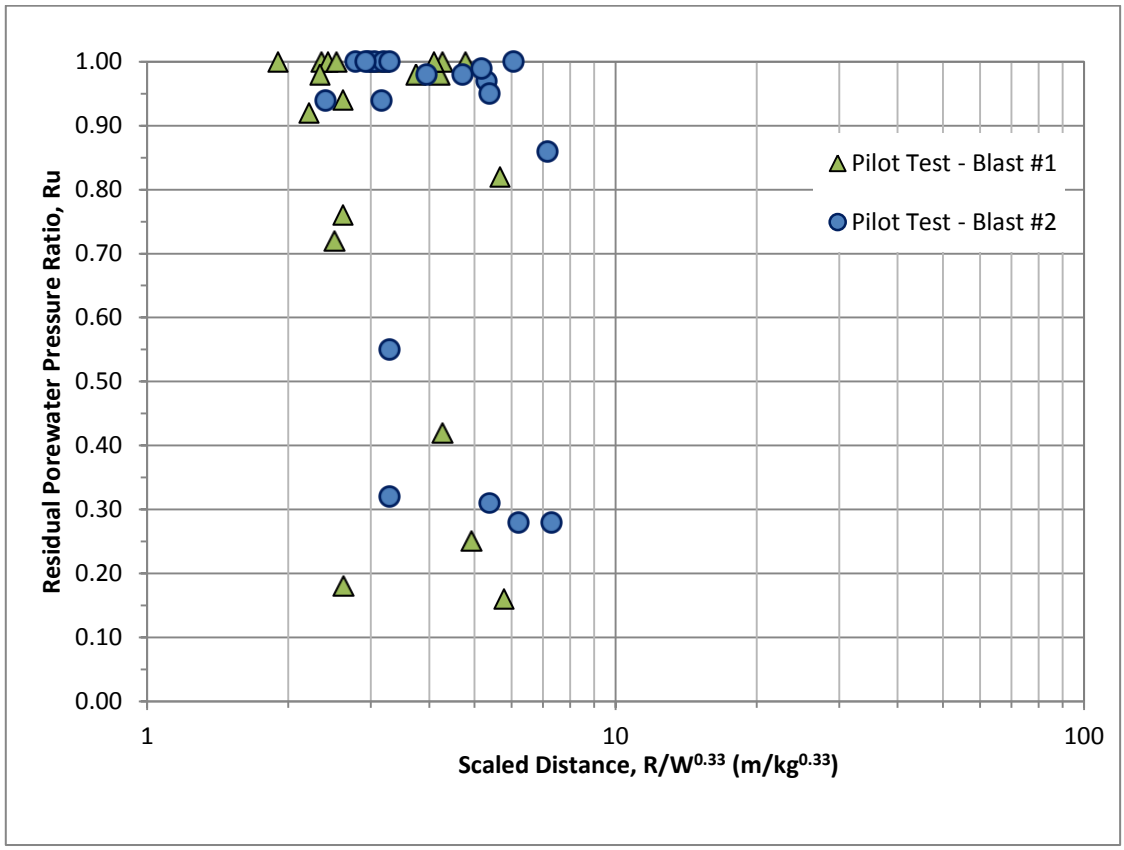

Figure 3-24 Maximum Pore Pressure Ratio vs. Scaled Distance for Treasure Island Pilot Study

Table 3.6 – Residual Pore Pressure Measurements during TILT Pilot Study

Pore Pressure Transducer (PPT)	Depth of PPT (m)	Residual Pore Pressure Ratio, *Ru*	
		Blast #1	Blast #2
00	2.70	1.00	0.94
01	0.90	0.16	0.28
02	3.70	1.00	1.00
03	4.60	0.98	0.97
04	2.70	0.98	0.98
05	0.90	0.18	0.32
06	2.70	1.00	1.00
87	4.60	0.72	0.94
88	0.90	0.76	0.55
89	2.70	0.82	0.86
90	1.80	1.00	1.00
91	5.50	1.00	1.00
92	2.70	0.92	1.00
93	2.70	0.98	1.00
94	0.90	0.25	0.28
95	0.90	0.42	0.31
96	2.70	1.00	0.95
97	2.70	1.00	0.99
98	4.60	0.94	1.00
99	2.70	1.00	0.98

3.8 FORT MCMURRAY, ALBERTA, CANADA, 1997

In 1997, a fourth phase of the Canadian Liquefaction Experiment (CANLEX), was performed by researchers from the University of British Columbia near Fort McMurray, Alberta, Canada to investigate the potential of using controlled blasting as a liquefaction assessment technique (Pathirage 2000). This study was a part of a multi-phase study aimed in developing liquefaction prediction methods using controlled blasting. The researchers were attempting to use controlled blasting to match ground motion characteristics from earthquakes.

3.8.1 Site Conditions and Blasting Layout

The blasting was performed at a quarry where previous blasting experiments were performed during earlier studies of the CANLEX studies. The soil consisted of artificially-deposited medium dense silty sand to sandy silt, with an average corrected SPT blow

count of 3 blows per 30 cm, and average shear wave velocity of 127 m/s (Pathirage 2000). The groundwater table was approximately 0.5 m below the surface. Additional soil information from Pathirage (2000) is provided in Table 3.7.

Table 3.7 – Soil Conditions for CANLEX study

Soil Type	Silty sand to sandy silt
Mean Grain Size, D_{50} (mm)	0.17
Effective Grain Size, D_{10} (mm)	0.08
Specific Gravity of Soil, G_s	2.62
Minimum Void Ratio, e_{min}	0.461
Maximum Void Ratio, e_{max}	0.986
In-situ Void Ratio, e_0	0.765
Total Unit Weight, γ_t (kN/m^3)	19.5
Relative Density, D_R(%)	43

A total of six blast events were performed, with half involving single blasts and half multiple blasts. Charge weights ranged from 1 kg to 4.5 kg, with placement depths ranging from 3 m to 9 m. Based upon the available results, only blast tests #2 and #6 were evaluated. Blast #2 is a single blast event, and blast #6 is a multiple blast event involving 4 bore holes (G,H,I, and J) with 3 decks of charges each (1,2, and 3). The layout for Blast #2 and Blast #6 are shown in Figures 3-25 and 3-26, respectively. The charges were cylindrical, and detonated from the bottom up with a delay time of 250 ms between decks and 500 ms between bore holes. Additional details regarding the blasting study are provided by Pathirage (2000) and Al-Qasimi et al. (2005).

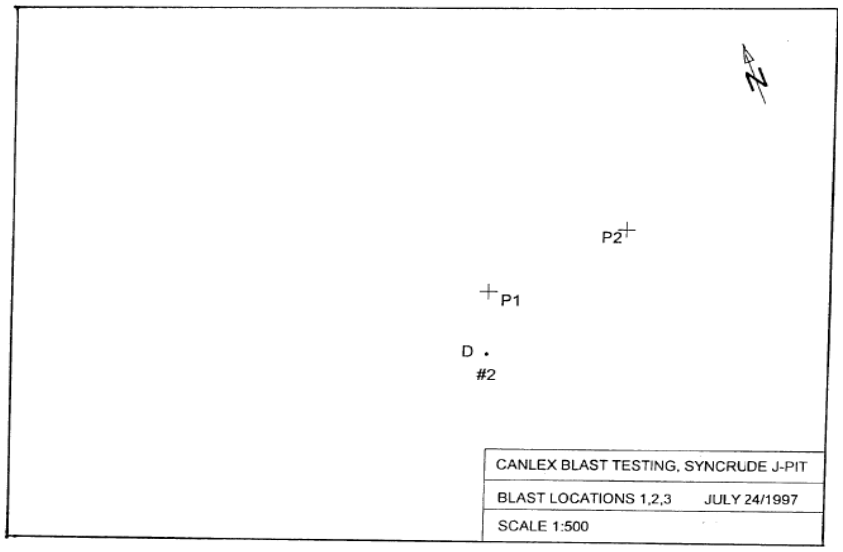

Figure 3-25 Blasting Layout for CANLEX Blast Testing, Blast #2 ©Pathirage 2000

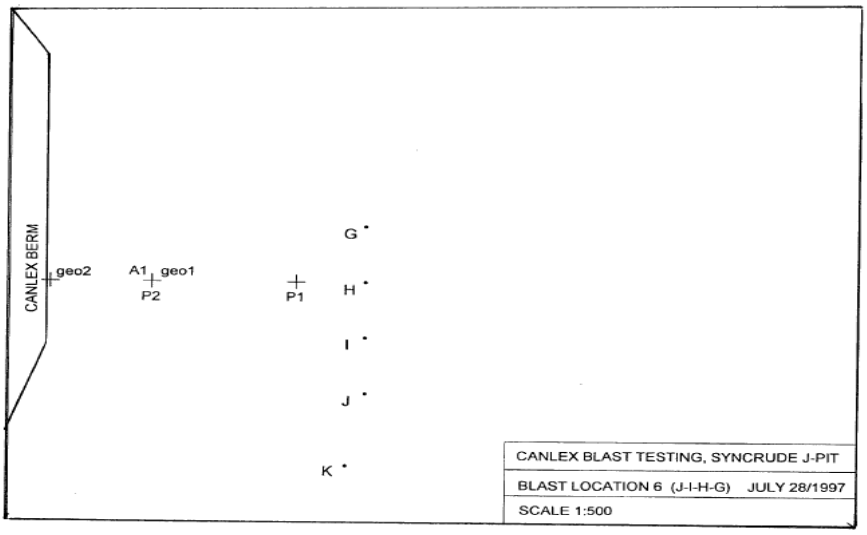

Figure 3-26 Blasting Layout for CANLEX Blast Testing, Blast #6 ©Pathirage 2000

3.8.2 Test Results

Residual pore pressure measurements recorded following blasting are summarized in Table 3.8 below. The recorded *Ru* with respect to scaled distance are plotted in Figure 3-27. Although Table 3.8 shows *Ru* values decreasing during some blasts, Figure 3-27 was

developed on the assumption that dissipation of excess pore pressures are not occurring. Therefore, the data shown in Figure 3-27 show only the increasing *Ru* values and their respective scaled distances. Pathirage (2000) identified a best-fit trend line to the data, but the change in scaled distance was accounted for in a different manner than presented in Equation 3-1. For further information on the trend line developed from this study, the reader is referred to Pathirage (2000).

Table 3.8 – Peak Residual Pore Pressure Readings during CANLEX study

Single Blast

Test Number	Charge Weight (kg)	Distance from PPT (m)		Residual Pore Pressure Ratio, *Ru*	
		PPT 1	PPT 2	PPT 1	PPT 2
Blast #2	1.5	5.5	20.0	0.46	0.10

Multiple Blast

Test Number	Charge Weight (kg)			Average Radial Distance (m)		Residual Pore Pressure Ratio, *Ru*	
	at 3 m	at 6 m	at 9 m	PPT 1	PPT 2	PPT 1	PPT 2
Blast #6							
J-1			4.5	22.14	27.75	0.00	0.27
I1 + I2		3.0	4.5	13.54	21.52	0.00	0.28
I3	1.5			13.45	21.47	0.11	0.30
J2		3.0		21.93	27.59	0.13	0.25
J3+H1	1.5		4.5	13.45	21.47	0.13	0.38
H2		3.0		9.00	19.00	0.24	0.46
H3+G1	1.5		4.5	10.30	19.65	0.31	0.38
G2		3.0		13.45	21.47	0.86	0.38
G3	1.5			13.78	21.68	0.88	0.35

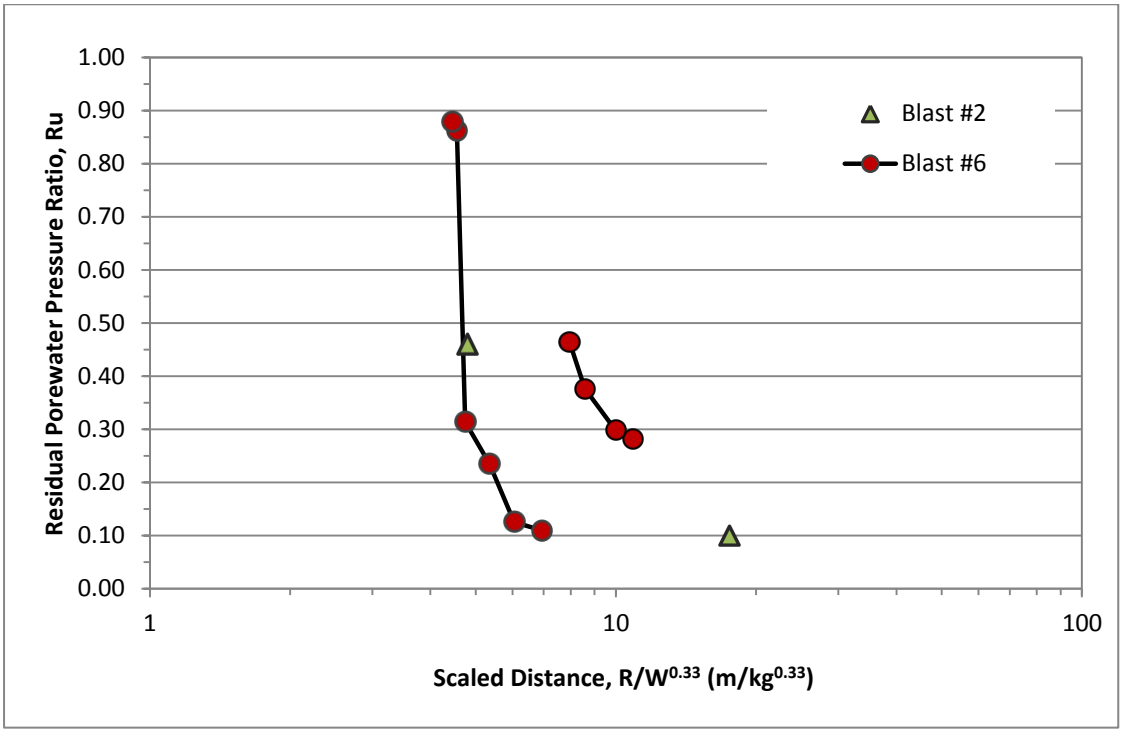

Figure 3-27 Pore Pressure Ratio vs. Scaled Distance at CANLEX

Through this study, Pathirage (2000) concluded that "to simulate actual earthquake ground motions by blasting is not feasible, because frequency characteristics of earthquakes cannot be 'created' with the type of explosives used for CANLEX test." Also, he observed that multiple blasts required less energy than a single blast to generate a specific pore pressure ratio because of the cyclic loading and induced shear strains. The study did show that sequential detonation can be used to investigate "the response of installations to the effects of liquefaction during an earthquake." Additional information and discussion regarding the test is provided by Pathirage et al. (2000), Byrne et al. (2000) and Al-Qasimi et al. (2005).

3.9 SOUTH PLATTE RIVER, COLORADO, 1987

Researchers from Colorado State University, Fort Collins performed controlled blasting on a saturated, *dense*, natural soil deposit along the South Platte River in Colorado with the objective of developing relationships for peak pore pressure response, residual pore pressure response, and peak particle velocity.

3.9.1 Site Conditions and Blasting Layout

The site was an alluvial deposit consisting of approximately 3.65 m of poorly graded coarse sand underlain by silt. CPT measurements indicated that the sand had a relative density of 70 to 90%, and downhole seismic surveys measured shear wave velocities ranging from 190 m/s to 270 m/s, categorizing the sand as dense. The sand layer was underlain by a lean silt layer. A typical soil profile is shown in Figure 3-28 with additional soil information provided in Table 3.9.

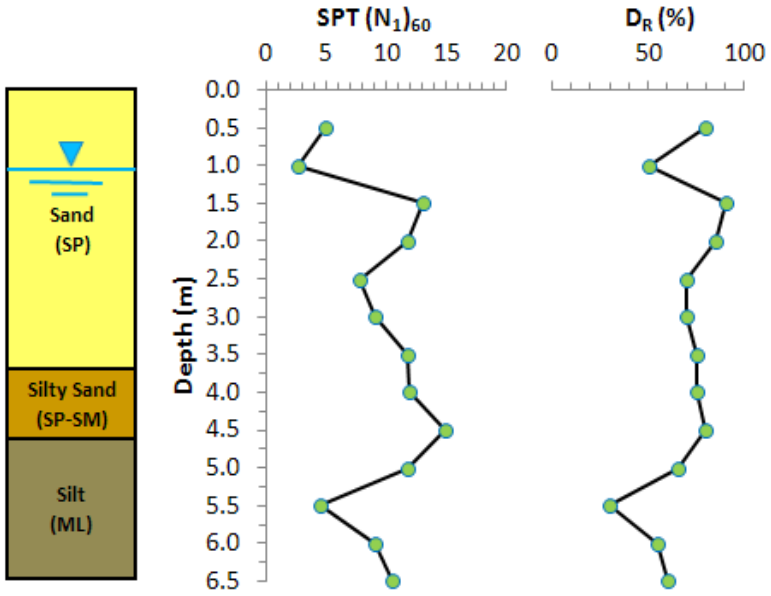

Figure 3-28 Typical Soil Profile for South Platte River Study

Using six single blasts placed at a depth of 3 meters with charge weights ranging from 0.0045 kg to 9.06 kg, peak and residual pore pressures were generated and monitored at several locations, as shown in Figure 3-29. Table 3.10 includes the residual pore pressure data and blasting properties recorded for all the detonations, as provided by Charlie et al. (1992).

Table 3.9 – Laboratory Test Results for South Platte River Study (adapted from Charlie et al. 1992)

	Sand Layer	Silt Layer
Soil Type	SP	ML
Depth (m)	0 – 3.65	> 3.65
Mean Grain Size, D_{50} (mm)	1 to 3	-
Effective Grain Size, D_{10} (mm)	0.3 to 0.7	-
Specific Gravity of Solids, G_s	2.63	-
Minimum Void Ratio, e_{min}	0.373	-
Maximum Void Ratio, e_{max}	0.564	-
Total Unit Weight, γ_t (kN/m^3)	18.4 above GWT	-
	21.2 below GWT	-
Permeability, k (cm/s)	$3x10^{-2}$	-
Atterberg Limits – LL/PI	-	29 – 41 / 24 – 26
Natural Water Content, w_n (%)	-	28 - 29

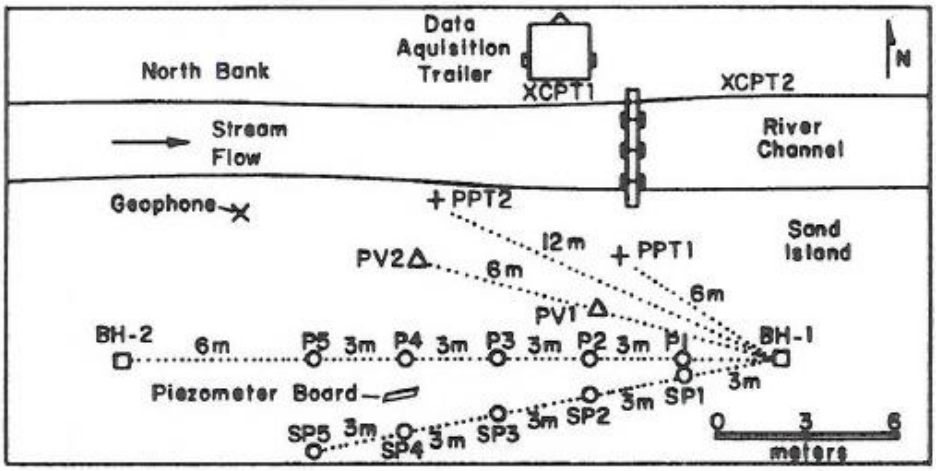

Figure 3-29 Blasting and Instrumentation Layout for South Platte River Liquefaction Study (from Charlie et al. 1992)

Table 3.10 – Peak Residual Pore Pressure Readings during South Platte test
Adapted from Charlie et al. (1992)

Detonation Number	Charge Weight (kg)	Maximum Residual Pore Pressure Ratio, *Ru*				
		PPT 1	PPT 2	PPT 3	PPT 4	PPT 5
1	0.0068	NR	NR	NR	NR	NR
2	0.068	0.012	NR	NR	NR	NR
3	0.081	0.236	0.114	0.114	0.024	NR
4	0.405	0.315	0.212	0.094	0.047	0.016
5	2.024	0.456	0.299	0.157	0.087	0.031
6	8.138	0.234	0.275	0.398	0.417	0.645
NR = No reading recorded (i.e. blast too small to generate significant *Ru*						

3.9.2 Test Results

Following the blasts, the residual pore pressures were measured and plotted with scaled distance to blast weight for all detonations, as shown in Figure 3-30. A "best-fit" line was estimated for the data, and had a correlation value of 0.59. The equation is developed specifically for single blasts, and is provided below:

$$PPR = 2.60\left(\frac{W^{0.33}}{R}\right)^{-1.37} \qquad 3\text{-}2$$

The highest *Ru* was 0.65, indicating that liquefaction was not achieved. Based upon their results, Charlie et al. (1992) extrapolated that liquefaction could be produced in dense sand through explosives at a scaled distance of 3 $m/kg^{1/3}$, with an overburden pressure at 38 kPa when the peak compressive strain had exceeded 0.01%. The threshold for residual pore pressure generation was observed to be at a scaled distance of 16 $m/kg^{1/3}$, or at the peak compressive strain of 0.002%. The study concluded that pore pressure generation to liquefaction at a "given peak compressive strain decreases with increasing effective stress", indicating that more energy is required to liquefy denser soils than looser soils at the same depth.

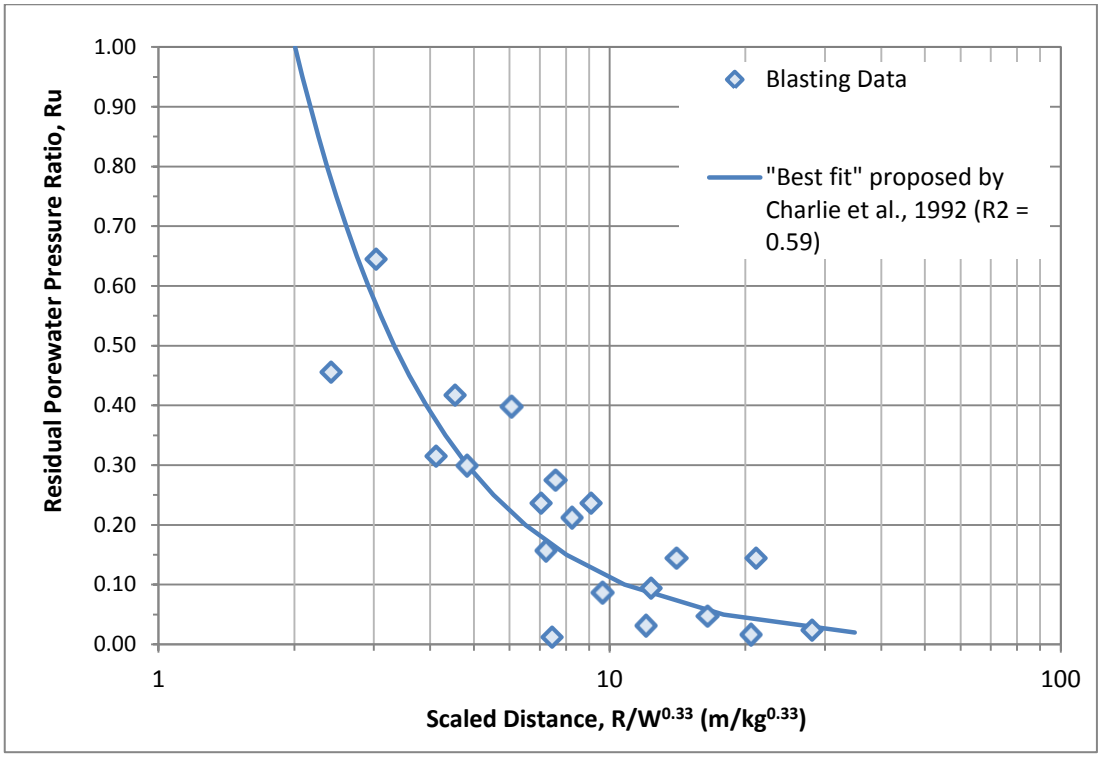

Figure 3-30 Measured residual PPR vs. scaled distance in South Platte River blasting study

4.0 RESULTS

"A good scientist is a person with original ideas. A good engineer is a person who makes a design that works with as few original ideas as possible."

– Freeman Dyson, American Physicist and Mathematician

4.1 PORE PRESSURE RESULTS FROM CASE HISTORIES

Using Equation 3-1 to estimate the scaled distances, the measured residual pore pressure ratios, *Ru*, for multiple blasts from the case histories in Chapter 3 are plotted in Figure 4-1. Results for the single blasts are plotted in Figure 4-2. The data is also included in Appendix B. In all the succeeding figures for multiple blasts, it should be noted that the scaled distance was estimated using Equation 3-1, where as the scaled distance for single blasts is simply $R/W^{0.33}$.

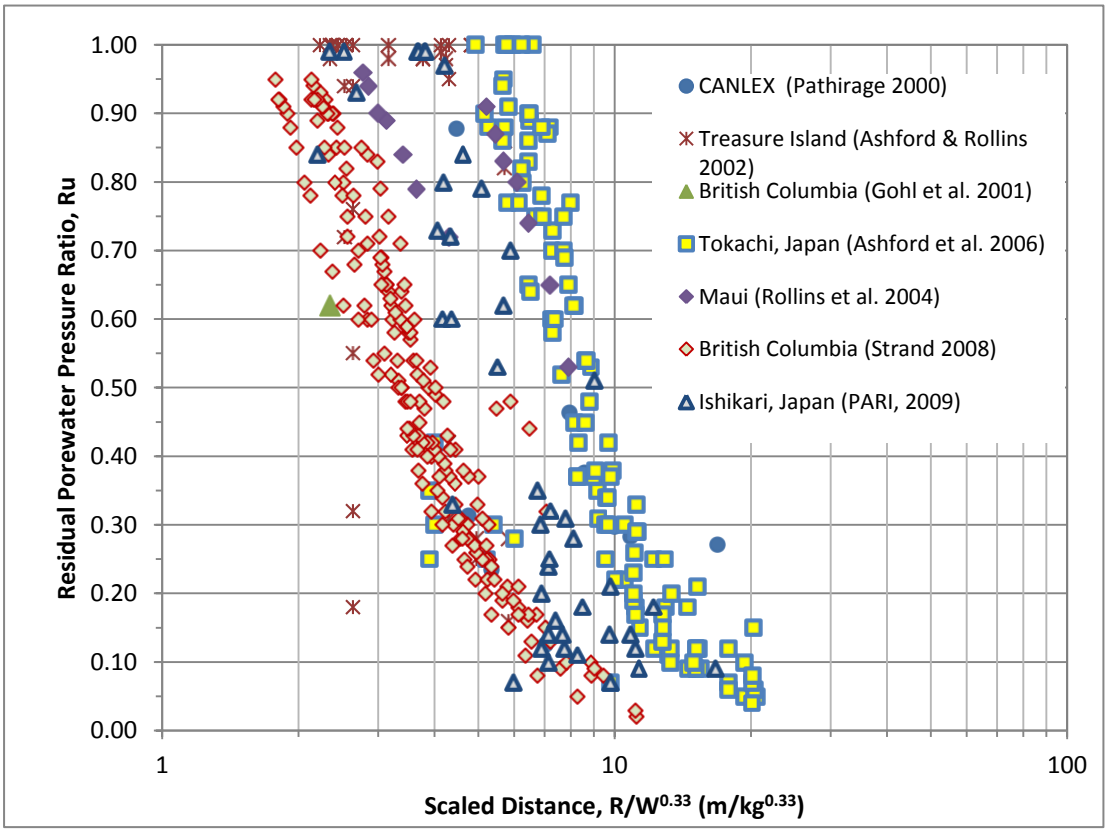

Figure 4-1 Pore Pressure Response vs. Scaled Distance for Multiple Blasts

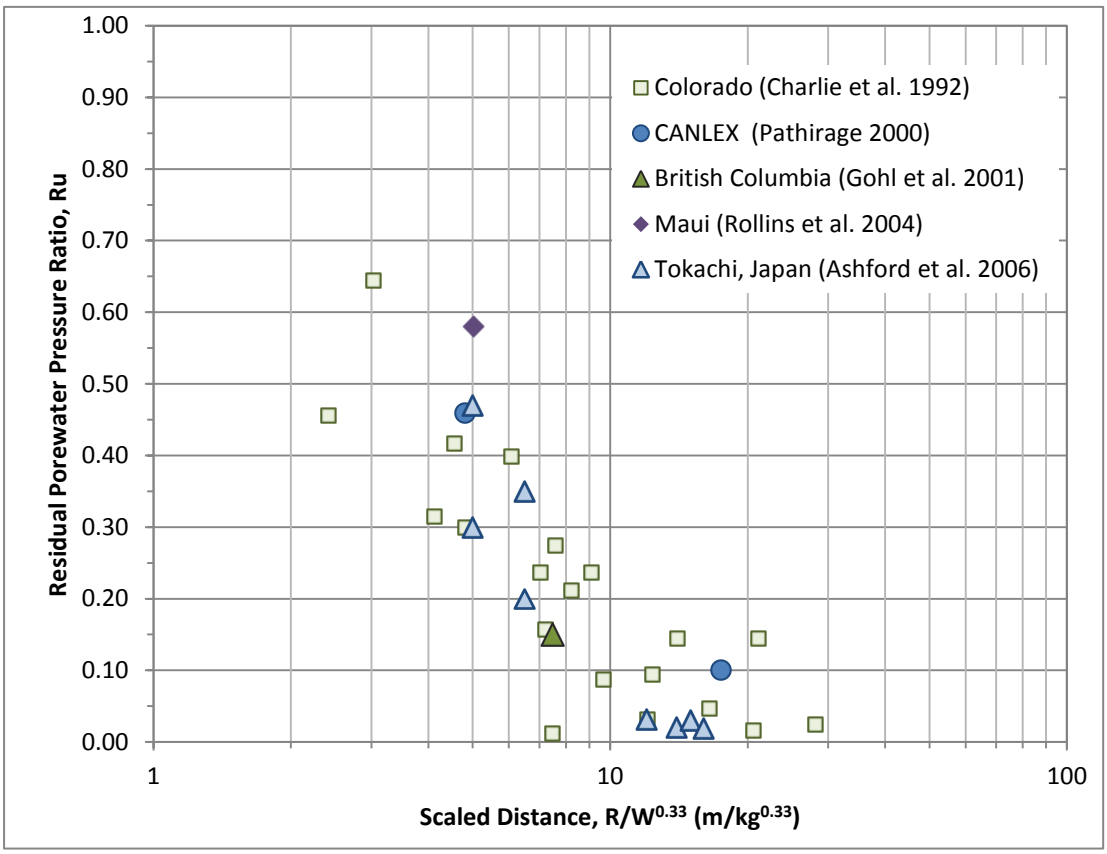

Figure 4-2 Pore Pressure Response vs. Scaled Distance for Single Blasts

Upon first observation, the results follow a general trend of an increasing residual pore pressure ratio (*Ru*) with a decrease in scaled distance (*SD*) for both multiple and single blasts. In a comparison between the multiple blasts and the single blasts in Figures 4-1 and 4-2, respectively, it appears that the slope of *Ru* with *SD* is steeper for multiple blasts than for single blasts. A steeper slope indicates that at a given scaled distance multiple blasts would generate a larger pore pressure response than a single charge of equivalent weight. By using the scaled distance as a proxy for energy, a steeper slope would also indicate that less energy is required to develop residual pore pressure. This observation agrees with the current practice of using multiple blasts to more effectively generate residual pore pressures rather than a large single blast based upon the fact that pore pressure is more efficiently generated during cyclic loading than monotonic loading.

4.2 EVALUATION OF EXISTING EMPIRICAL MODELS

Current empirical models used to predict pore pressure response based upon scaled distance were presented in Chapter 2.3. As described in that section, most of the empirical models were developed for single blasts, and typically do not account for soil or site conditions. The most referenced empirical model used in blasting studies is the Studer and Kok (1980) model which was developed for single blasts. In regards to multiple blasts, the Rollins et al. (2004) empirical model is the only referenced model for multiple blasts found in the literature and is explained in more detail in Section 2.4. These trend lines are plotted with the results for single and multiple blasts from the case histories in Figure 4-3.

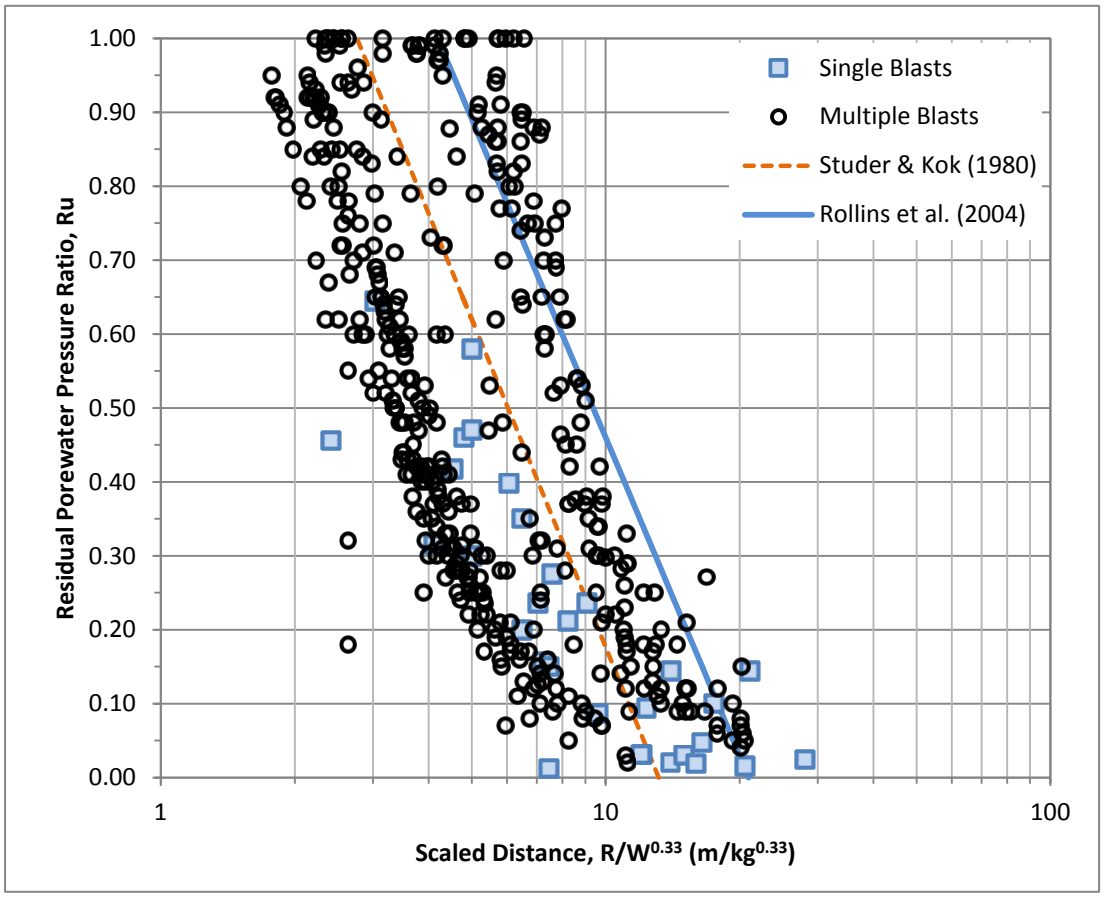

Figure 4-3 Studer & Kok (1980) and Rollins et al. (2004) empirical models compared with single and multiple blasts results

4.2.1 Single Blast Comparison to Empirical Model

In evaluating the single blast data, a residual plot was developed comparing the *Ru* observed to the *Ru* predicted by the Studer and Kok (1980) model and is provided in Figure 4-4. From observation of Figure 4-3, the Studer and Kok (1980) model estimates excess pore pressure generation to initiate at a scaled distance of approximately 13, wherein fact observed data showed that excess pore pressures were generated at scaled distances greater than 13. Therefore, in performing the residual analysis for values with scaled distances greater than 13, the observed *Ru* was the residual value. In observing the residual plot, the Studer and Kok (1980) provides an average residual value of -0.2 for scaled distances less than 10, which is typically the area of interest. From this analysis it can be concluded that the Studer and Kok (1980) does not provide a good fit to the analyzed data and may in fact not provide a good fit to data with soil properties outside the conditions from which it was developed.

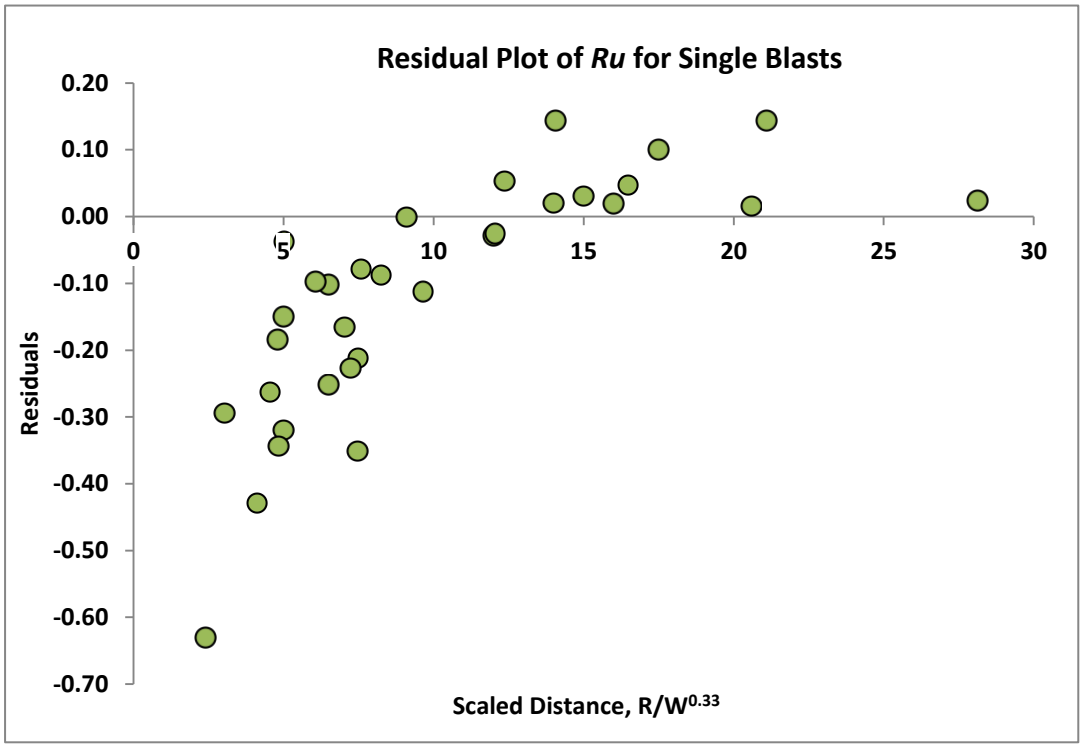

Figure 4-4 Residual Plot of Single Blasts Data to Studer and Kok (1980) model

In Figure 4-5, the single blasts are plotted against the Studer and Kok (1980) model including the range of the model provided by Narin van Court and Mitchell (1994). In addition, the observed trend line is graphed with an equation and the correlation coefficient, R^2 value, provided. From this figure it is readily observed that the "best fit" trend line plotted for the data is significantly different than Studer and Kok (1980). The slope of the best fit line is significantly lower than Studer and Kok (1980), and appears to provide a much better fit to the data.

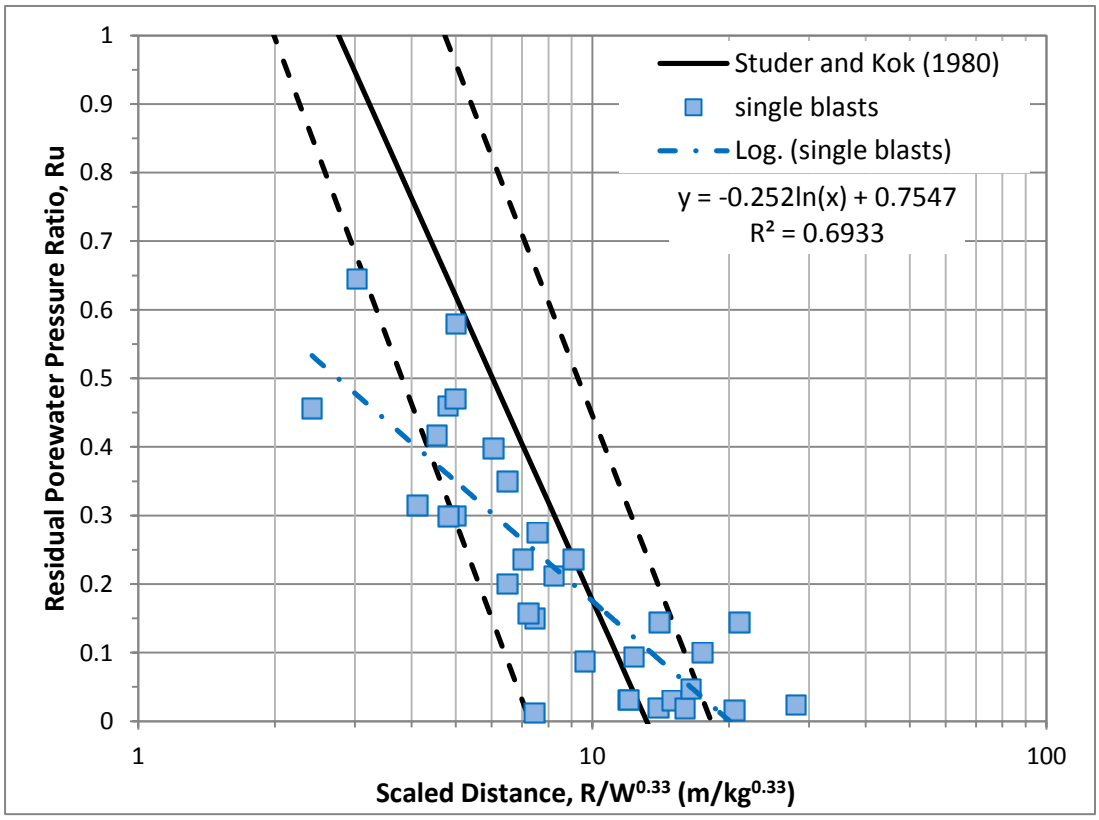

Figure 4-5 Residual Plot of Single Blasts Data to Studer and Kok (1980) model

4.2.2 Comparison of Multiple Blasts to Empirical Model

In Figure 4-6, the multiple blasts data is plotted with the Studer and Kok (1980) average and range trend lines as well as the Rollins et al. (2004) trend line. The Studer and Kok (1980) model appears to bisect the multiple blasts data while the model proposed by

Rollins et al. (2004) appears to serve more as a outer boundary for the data. This does not invalidate Rollins et al. (2004) but suggests that the method in accounting for the change in scaled distance is different than that used to develop the data. A linear (based upon the semi-log plot) trend line is provided in Figure 4-6. With an R^2 value of 0.44, the trend line indicates that blasting conditions (i.e. scaled distance) alone does not provide a good representation or fit to the data. Therefore, it is conclusive that additional parameters should be considered to provide a better fit to the data.

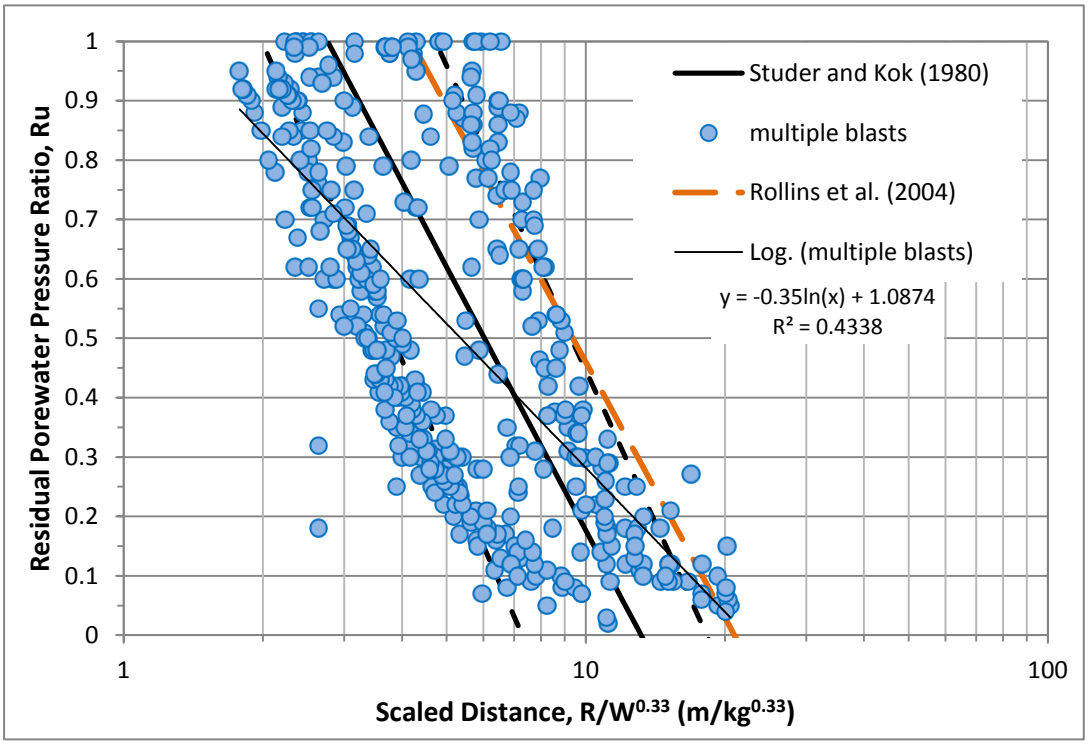

Figure 4-6 Multiple Blasts comparison to existing empirical models and observed trend lines

In a comparison plot of the residuals shown in Figure 4-7, the existing empirical models can be evaluated. The Studer and Kok (1980) exhibits a lot of scatter for scaled distances less than 10, and then transitions to under-predicting the *Ru* values for scaled distances greater than 10 at a relatively constant residual of 0.20. The Rollins et al. (2004) exhibits scatter for scaled distances less than 8, but mostly over-predicts the observed *Ru* for scaled distances greater than 0.8.

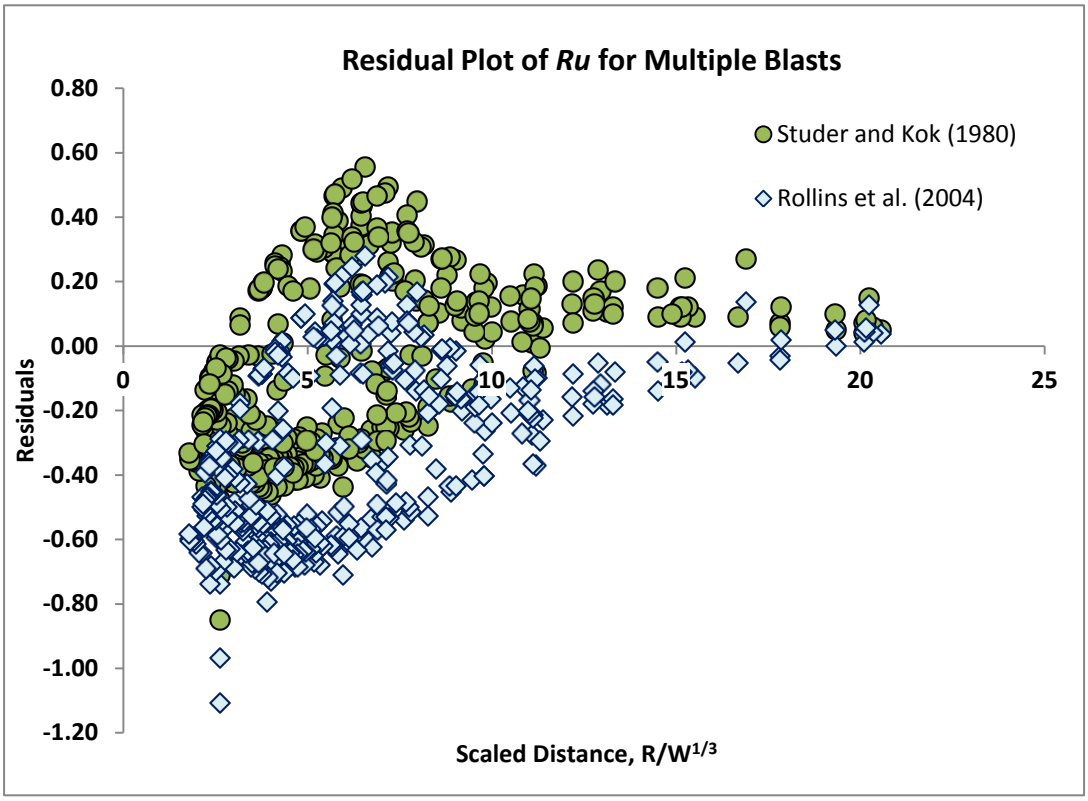

Figure 4-7 Residual Plot of Multiple Blasts Data to Studer and Kok (1980) model and Rollins et al. (2004) model

Both of the existing models presented are solely based on scaled distance and neglect the possible influence that in-situ conditions may have on the generation of pore pressures, either for single blasts or multiple blasts. Although these models may have provided a reasonable fit for the site/soil conditions from which they were developed, they do not serve as a good "general" fit to the case history data investigated in this research.

4.3 DEVELOPMENT OF A NEW EMPIRICAL MODEL

4.3.1 Pore Pressure Effect due to Relative Density

Generally for liquefaction to occur, the soil needs to be loose, saturated granular material. Assuming that the soil consists of sand to silty sand below the groundwater table, the remaining independent parameter is the in-situ relative density of the soil. As described in Chapter 2, the relative density (D_R) is commonly correlated to SPT $(N_1)_{60}$

values (as well as CPT tip resistance) because of the difficulty in measuring it accurately due to sample disturbance. Based upon the case histories data, the blasting results were categorized based upon the reported relative densities from the boring logs, or if they were unavailable, from the SPT $(N_1)_{60}$ correlated values based upon Kulhawy and Mayne (1990). The relative densities were categorized into 4 groups: (1) very loose (D_R of 0 – 15%), (2) loose (D_R of 15 – 35%), (3) medium dense (D_R of 35 – 65%), and (4) dense (D_R of 65 – 85%). Figures 4-8 and 4-9 display the distribution of relative densities for the multiple and single blasts, respectively.

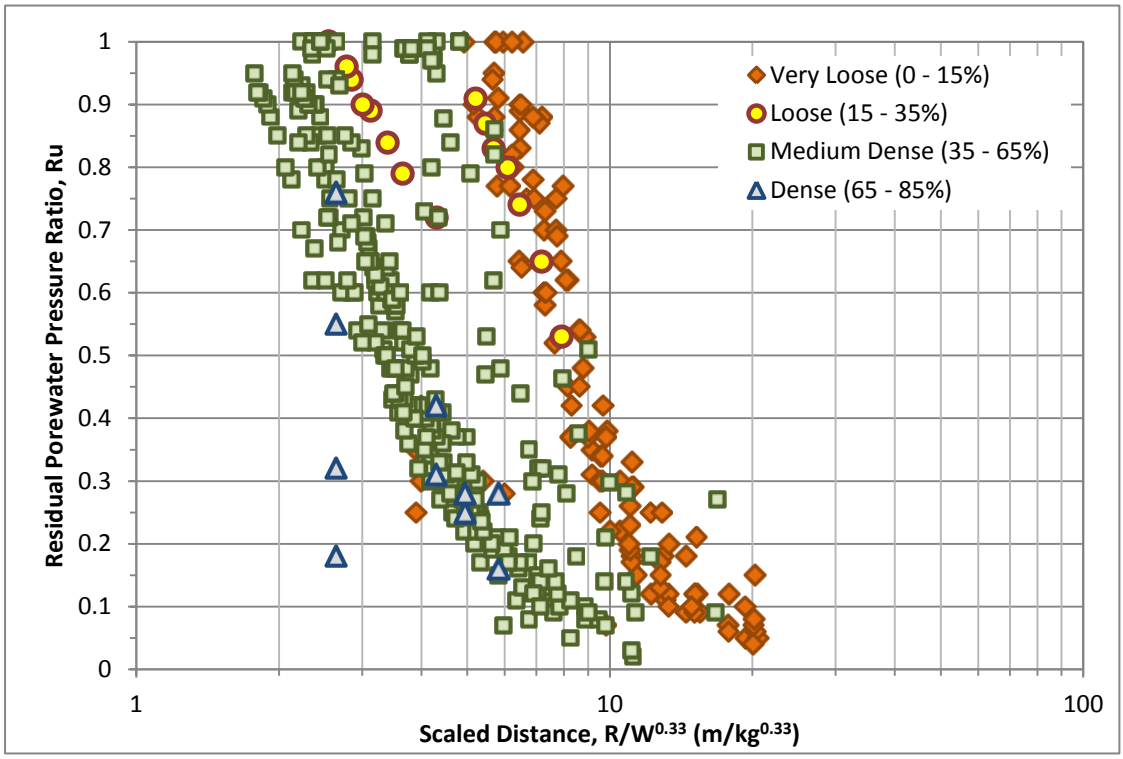

Figure 4-8 Pore pressure response for multiple blasts categorized by relative density

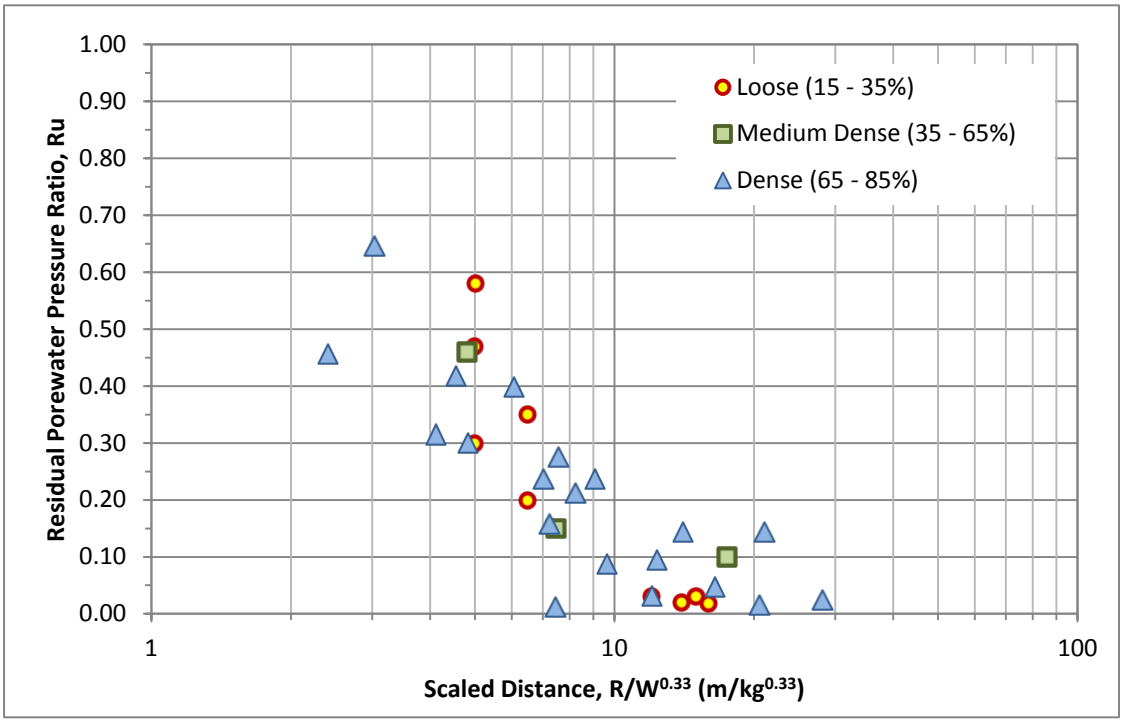

Figure 4-9 Pore pressure response from single blasts categorized by relative density

From these figures, it is observed that for a given scaled distance, the looser soils can generate a higher *Ru* than for denser soils. This agrees with the fact that the looser soils are more susceptible to liquefaction than denser soils, thus requiring less energy (i.e. larger scaled distance) to generate residual pore pressures. Also from these results, it appears that significant excess pore pressures were able to be generated in the denser soils, which may not be typically encountered in actual soils following earthquake-induced shaking. This could possibly indicate that the soil was subjected to a greater amount of energy during blasting than would be realistic during a large earthquake.

Based upon the distribution of data with respect to relative density, it is evident that in-situ conditions do play a role in the pore pressure generation for multiple blasts and perhaps even with single blasts. Generally, the denser the soil, more energy is required to increase the pore pressure ratio and ultimately reach liquefaction. However, too much energy can cause significant pore pressure generation that would not be expected, even for a large earthquake.

4.3.2 Multiple Regression Analysis

To identify which in-situ parameters may play a significant role in the pore pressure generation during blasting, several multiple regression analyses were performed on both the multiple and single blasting data using different combinations of common in-situ parameters with respect to the scaled distance. The parameters chosen to use in the analysis were those that were consistently provided on boring logs and laboratory reports, or those that could easily be calculated based upon the provided information, and included corrected SPT $(N_1)_{60}$ values, initial relative densities D_r, corrected shear wave velocities v_{s1}, initial effective overburden pressure σ'_{vo}, and the cyclic resistance ratio (*CRR*) as determined from the Youd et al. (2001) simplified method. However, it should be noted that these parameters are not solely independent parameters, but some are dependent on one another. For example, the SPT $(N_1)_{60}$ values, corrected shear wave velocities, and *CRR* are all influenced by the effective overburden pressure σ'_{vo} in their calculations.

Therefore, to evaluate the data, Microsoft Excel 2007's multiple regression analysis tool was used to perform several multiple regression analyses using the conventional logarithmic-based fit that provides a linear trend line on the semi-log plot. However, upon observing the development of pore pressure with each successive blast followed a curved trend as shown in Figures 3-10 and 3-18 for Vancouver and Tokachi, respectively, a power-based analysis was also provided. The resulting correlation coefficients, R^2, from selected tests are summarized in Table 4.1 for the specific in-situ parameters analyzed for multiple and single blasts. Additional tests were performed, including variations in accounting for the in-situ parameters (i.e. the product of $(N_1)_{60}$ and σ'_{vo}, etc.) but were not included in this table as they did not improve the fit to the data. Complete results of the analysis are provided in Appendix C.

Table 4.1 Parameters and Adjusted Correlation Coefficient using in Multiple Regression Analysis for Multiple and Single Blasting Data

Test No.	Blasting parameters		In-situ parameters					Adjusted Correlation Coefficient, R^2 Log / Power	
	Residual Pore Pressure, *Ru*	Scaled Distance, $R/W^{0.33}$ ($m/kg^{0.33}$)	Relative Density, D_R (%)	Effective Overburden Pressure, σ'_{vo} (kPa)	SPT $N_1(_{60})$ value	Cyclic Resistance Ratio, CRR	Shear Wave Velocity, v_{s1} (m/s)		
Multiple Blasts									
1	X	X						0.43	0.49
2	X	X	X					0.49	0.56
3	X	X		X				0.52	0.55
4	X	X			X			0.57	0.61
5	X	X				X		0.53	0.59
6	X	X					X	0.56	0.59
7	X	X		X	X			0.64	0.65
8	X	X		X	X	X		0.60	0.63
9	X	X		X	X		X	0.62	0.64
10	X	X	X	X	X	X	X	0.64	0.66
11	X	X			X	X	X	0.62	0.64
Single Blasts									
1	X	X						0.69	0.58
2	X	X	X					0.67	0.57
3	X	X		X				0.68	0.59
4	X	X			X			0.67	0.56
5	X	X				X		0.67	0.57
6	X	X					X	0.67	0.57

The correlation coefficient, R^2, describes the variability of the predicted data (i.e. *Ru*) as explained by the predictor (i.e. scaled distance, in-situ conditions, etc.). In other terms, the correlation coefficient forecasts how well future events are able to be predicted by the model by describing the linear association of the dependent factor (in this case, *Ru*) to the regressors (i.e. scaled distance and the in-situ parameters), with a R^2 approaching ± 1 indicating a good fit of the model to the data. The adjusted R^2 indicates that the original R^2 has been negatively adjusted to compensate for using multiple parameters in the regression model (Montgomery and Runger 2003).

In performing the regression analysis, p-value tests were also calculated for each parameter used in the regression. A p-value test represents the probability that the test statistic will take on a value that is at least as extreme as the observed value of the statistic when the null hypothesis is true (Montgomery and Runger 2003). Typically, p-values less than 0.05 indicate that the parameter should be included in the analysis while p-values greater than 0.05 would indicate that the parameter can be excluded confidently from the regression analysis. In the regression analyses performed for single blasts, when in-situ conditions were considered, the p-value tests for each in-situ index was greater than 0.05, indicating that it did not provide an improved fit to the data. This is also represented by the decrease in the correlation coefficient when in-situ conditions were considered.

4.4.1 Empirical Model for Multiple Blasts

The regression analysis for multiple blasts provided many helpful insights to understanding the effects due to blasting. From Table 4.1, Test #1 confirms statistically that scaled distance alone is not a sufficient parameter to estimate pore pressure as the R^2 value is 0.43. Although Figure 4-4 indicated that relative density clearly played a role in the pore pressure response during blasting, the R^2 of 0.49 for the log-based analysis and 0.56 for the power-based analysis indicates that scaled distance and relative density are not sufficient either in providing a decent fit to the data. Test #4 with SPT $(N_1)_{60}$ values, producing an R^2 of 0.57 for the log-based analysis and 0.61 for the power-based analysis provided the best fit of the in-situ parameters when used with scaled distance. And when effective overburden stress was included with SPT $(N_1)_{60}$ values and scaled distance in Test #7, the R^2 was 0.64 for the logarithmic-based analysis and 0.65 for the power-based analysis. This is considered the most practical of the models as SPT in-situ are typically performed during blasting experiments and the effective overburden pressure much be estimated in calculating SPT $(N_1)_{60}$.

The equation for the empirical model for Test #7 based upon the logarithmic-based fit and power-based fit are provided in Equations 4-1 and 4-2, respectively.

$$Ru_{multiple-log} = 1.747 - 0.512 \ln\left({R}/{W^{0.33}}\right) - 0.032(N_1)_{60} - 0.002\sigma'_{v0}\,(kPa) \qquad 4\text{-}1$$

$$Ru_{multiple-power} = 8.810 \cdot \left(\frac{R}{W^{0.33}}\right)^{-1.343} \cdot e^{-0.0802(N_1)_{60} - 0.0037 \cdot \sigma'_{v0}\,(kPa)} \qquad 4\text{-}2$$

where $R/W^{0.33}$ is the scaled distance between explosive and point of interest in m/kg$^{0.33}$, and the effective overburden pressure, σ'_{v0}, is in kPa. Based upon the p-value test shown in Appendix C, the SPT $(N_1)_{60}$ values play a more significant role than the effective overburden pressure. Each of the models and their calculated 95% confidence intervals are displayed in Figures 4-10 and 4-11, assuming an effective overburden pressure of 50 kPa and SPT $(N_1)_{60}$ value of 5. The equations for the confidence intervals are provided in Appendix C.

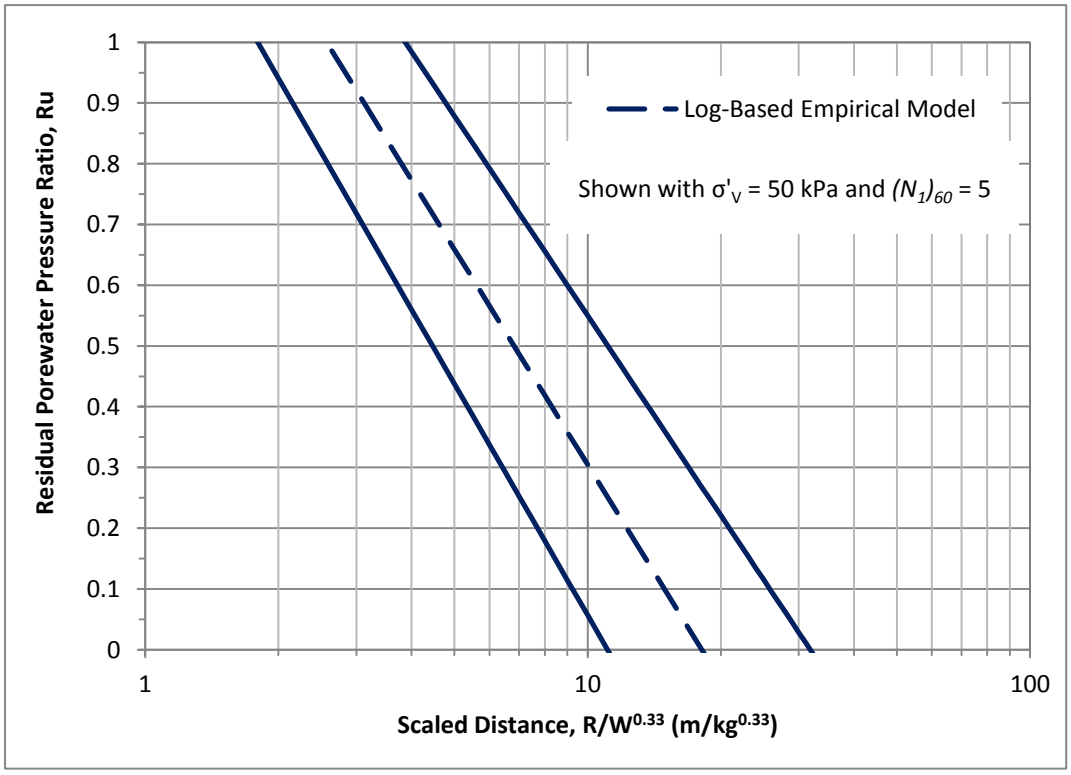

Figure 4-10 Log-based Empirical Model developed for Multiple Blasts (shown with 95% confidence limits)

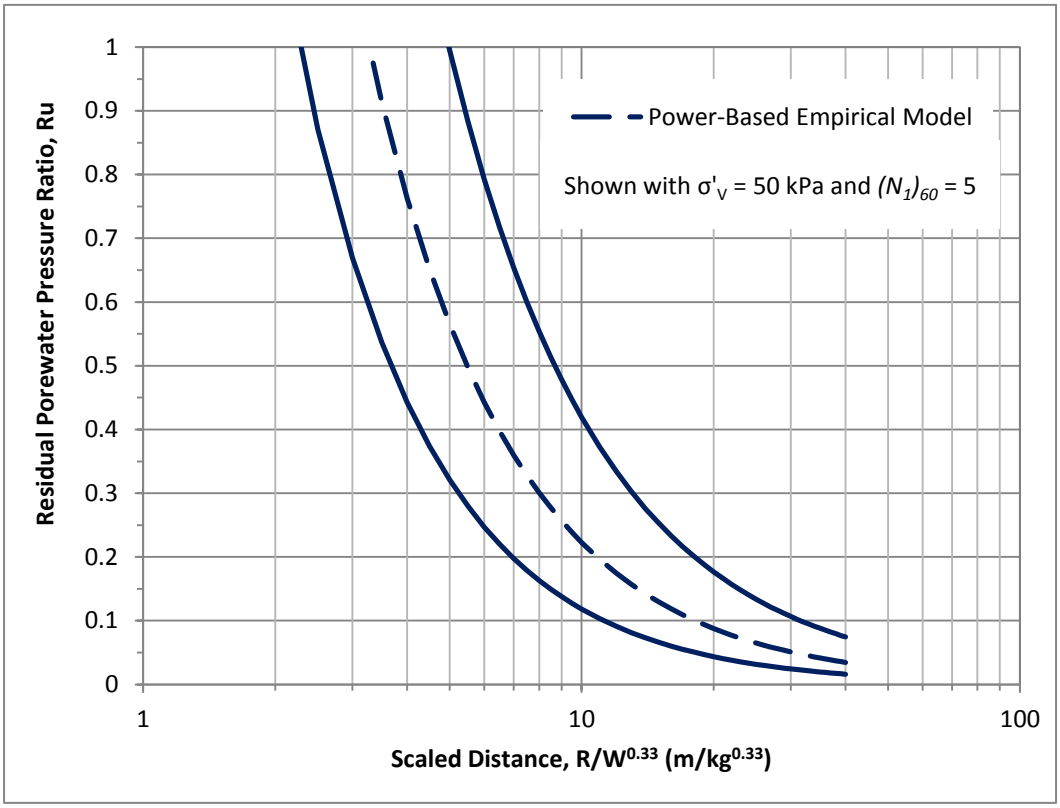

Figure 4-11 Power-based Empirical Model developed for Multiple Blasts (shown with 95% confidence intervals)

A comparison of these two models are plotted with SPT $(N_1)_{60}$ values of 5 and 20 in Figure 4-12 with an effective overburden pressure of 50 kPa. For loose soils (SPT $(N_1)_{60}$ value of 5), the scaled distance for liquefaction to occur for the log-based model and power-based model is 2.5 and 3.6 m/kg$^{0.33}$, respectively, a difference of approximately 30%. It is approximately the same difference with the denser soil (SPT $(N_1)_{60}$ value of 20). The models are relatively similar for *Ru* greater than 0.1, with the greatest difference between the two observed as *Ru* approaches 1.0. For *Ru* values less than 0.1, the models are significantly different but it is considered not a great concern as blasting studies are concerned with generating *Ru* much greater than 0.1.

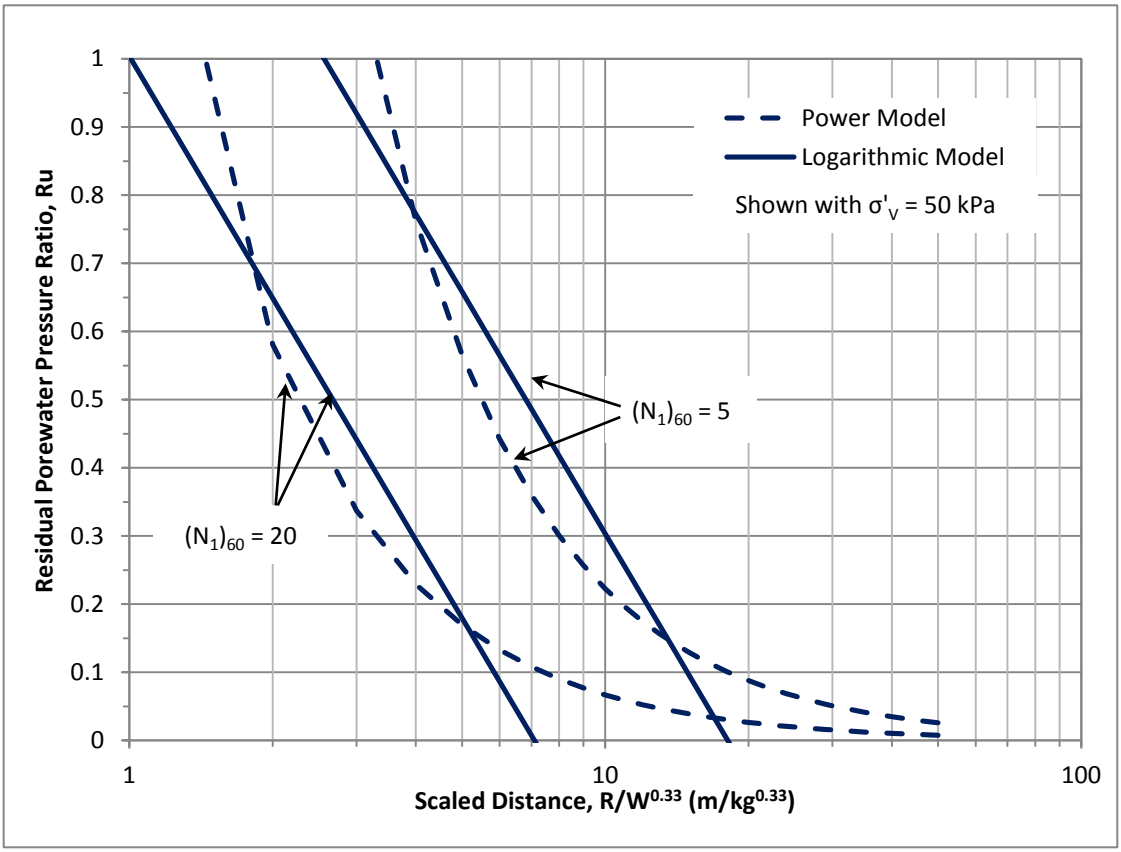

Figure 4-12 Comparison of Logarithmic Model and Power Model for Multiple Blasts

Although it has been determined that the models are relatively similar, the deciding factor in which model is the best can be determined in a comparison of the models to the observed blasting data. In Figure 4-13, the residual plots of the observed *Ru* and the predicted *Ru* by each of the models are shown. The power-based empirical model provides a better fit to the observed data for scaled distances greater than 10, but for scaled distances less than 10 it may be difficult to identify which model provides the better fit. Both models produce a lot of scatter for scaled distances less than 10. However, when looking at scaled distances less than 5, which is typically the zone of liquefaction observed in the blasting studies, the power-based model begins to consistently overestimate the *Ru*. Therefore, from this observation and the goal being to determine which model would serve as the better predictor of liquefaction, the log-based model is the better choice.

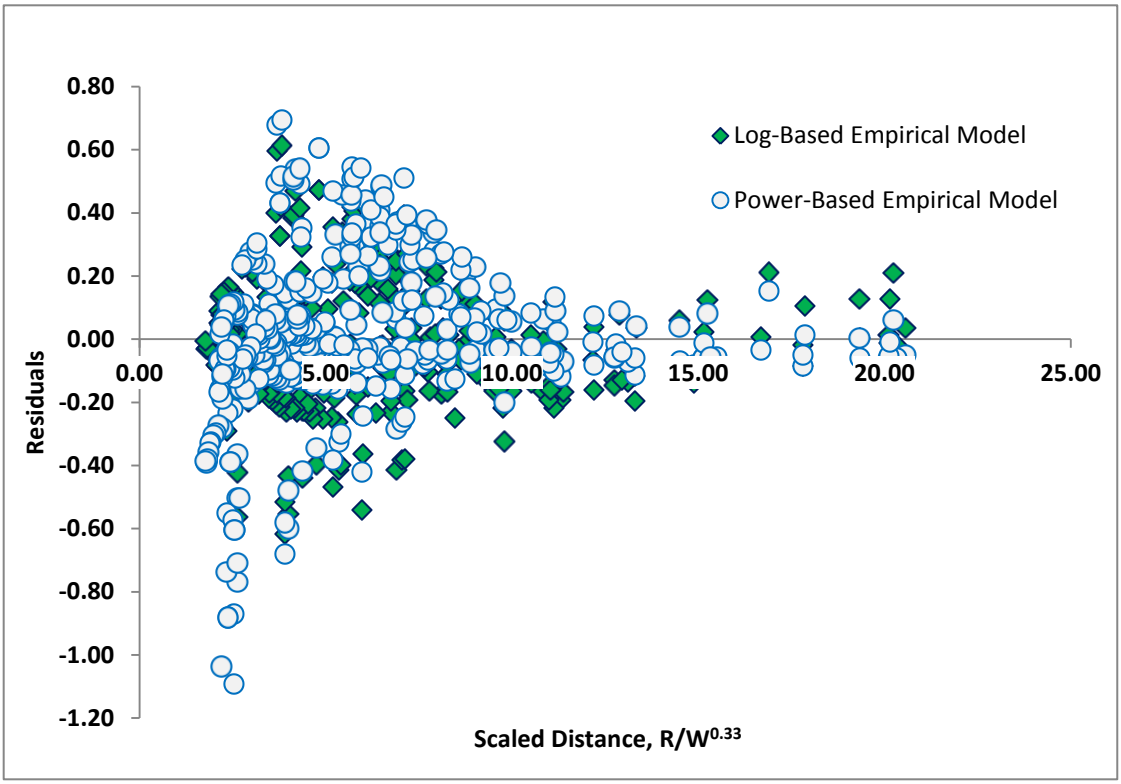

Figure 4-13 Residual plot for log-based and power-based empirical models

4.4.2 Empirical Model for Single Blasts

For the multiple regression analyses for single blasts in Table 4.1, the results show that even though in-situ parameters played a significant role for residual pore pressure generation in multiple blasts, the best fit of the data was based on the scaled distance alone. In fact, all of the tests using in-situ parameters had p-value tests greater than 0.05, indicating that their contribution to the overall regression is influential. However, this is could be due to multiple reasons. One explanation is that there is simply not enough data and that a large portion of the data analyzed came from one test. Therefore, the best model is represented by the logarithmic fit of scaled distance alone as shown in test #1 with an R^2 of 0.69. This empirical model is represented by equation 4-3.

$$Ru_{single} = 0.754 - 0.252 \ln\left({}^{R}/_{W^{0.33}}\right) \qquad 4\text{-}3$$

Figure 4-14 provides a comparative plot of this model with the data used in the analysis. For scaled distances smaller than 2.2 and greater than 30, the empirical model is extrapolated to show its projected path.

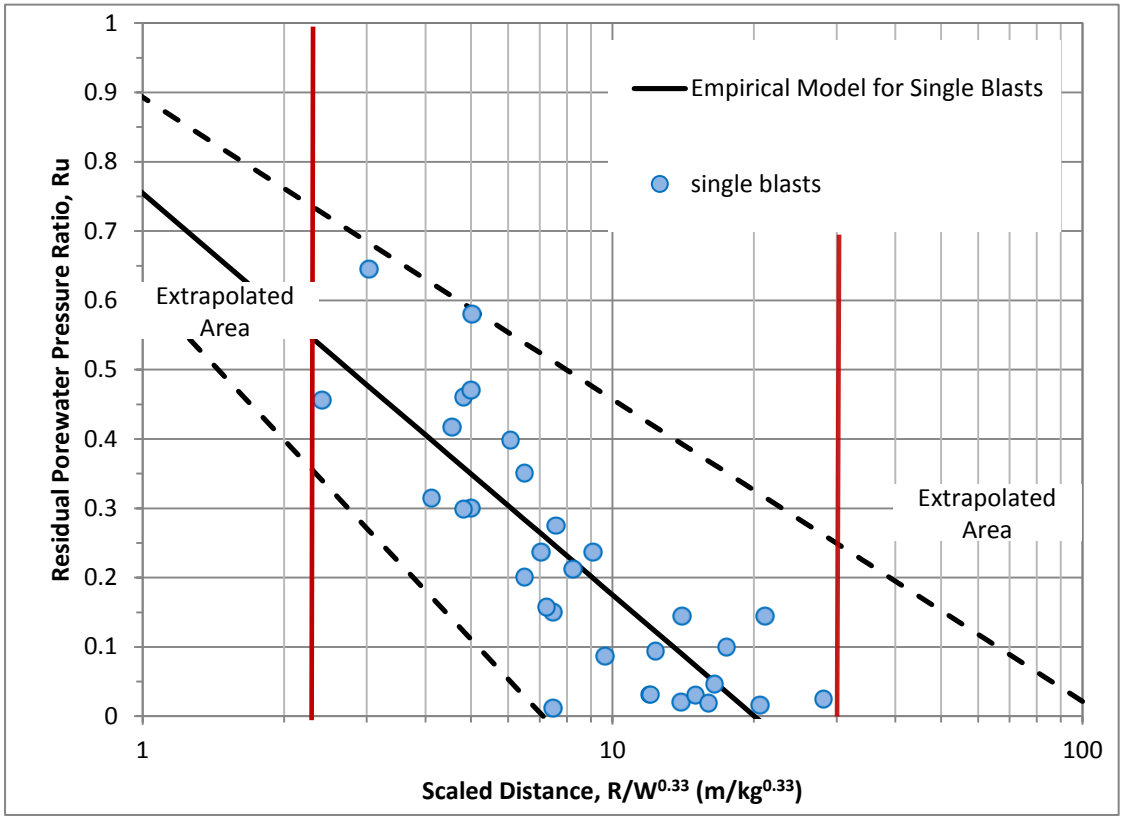

Figure 4-14 Empirical Model for Single Blasts shown with 95% confidence intervals

5.0 DISCUSSION

Engineering is the art of modeling materials *we do not wholly understand,* ***into shapes*** *we cannot precisely analyze so as* ***to withstand forces*** *we cannot properly assess, in such a way that the public has no reason to suspect the extent of our ignorance.*

– Dr. A.R. Dykes, British Institution of Structural Engineers

5.1 VALIDATING EMPIRICAL MODELS

Empirical models for estimating buildup of residual pore pressure for controlled blasting studies using both multiple blasts and for single blasts have been developed based upon case history data. A model is best evaluated under rigorous testing. Unfortunately, the empirical models presented in Chapter 4 are based solely upon case history data and are not able to be tested experimentally in the field. Although it would have been useful to validate these models through actual blasting experiments, this was the beyond the scope of this proposed research. Therefore, in order to evaluate if the models are an improvement to existing models, comparisons will be made to several case histories.

5.2 EVALUATION OF EMPIRICAL MODEL FOR MULTIPLE BLASTS

5.2.1 Maui Comparison

The Maui study (Rollins et al. 2004) as presented in Section 3.4, provided a unique opportunity to observe pore pressure generation with each blast for a relatively simple blasting layout. The site conditions consisted of an effective overburden pressure of 60 kPa and SPT $(N_1)_{60}$ value of 6 blows per 30 cm. Two blasting sequences consisting of 8 charges each were performed, with the second blast utilizing explosives at approximately half the distance to the center than the first blast. The results are plotted against the empirical model developed for multiple blasts (Equation 4-1) as well as the model proposed by Rollins et al. (2004) in Figure 5-1. As shown in Figure 5-1, the first blast was well-represented by the Rollins et al (2004) model, while the second blast was better represented by the empirical model. This is interesting because the only reported change that occurred was the blasting layout. However, one possible explanation is that both blasts were performed within the same area with 24 hours in between studies and

during the first blast study, there was significant settlement (40 cm) that undoubtedly would have affected the in-situ soil conditions by increasing the density which may result in an increase in SPT $(N_1)_{60}$ value and effective overburden pressure. This would theoretically require more energy to achieve liquefaction during the second blasts than observed in the first blast.

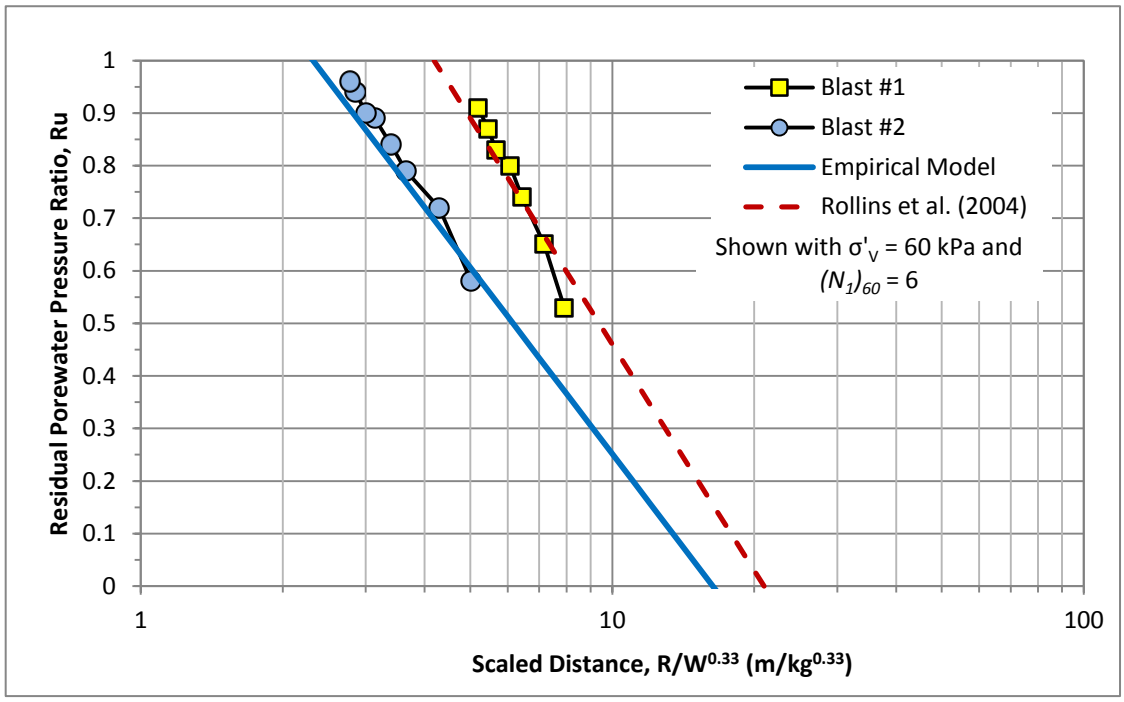

Figure 5-1 Comparison of the Empirical Model to the Maui Blasting Study

A plot of the residuals from the blast #1 and blast #2 is shown in Figure 5-2. The average difference in *Ru* between the observed and predicted were 0.27 and 0.03 in blasts #1 and #2, respectively. This portrays the data from blast #1 as possibly being an outlier, perhaps due to an inaccurate SPT $(N_1)_{60}$ value or effective overburden pressure. However, to compare how well the model represents the actual data, a paired t-test using Microsoft Excel Statistical Data Analysis was performed on the observed *Ru* values and the *Ru* values predicted by the model, with results provided in Table 5-1. From the two-tailed P-test attained from the paired t-test, the results (P(T<=t) two-tail = 0.00082) indicate that the model provides a statistically good fit to the data as the P-test is less than the 0.05, with a much better fit being achieved when only looking at blast #2.

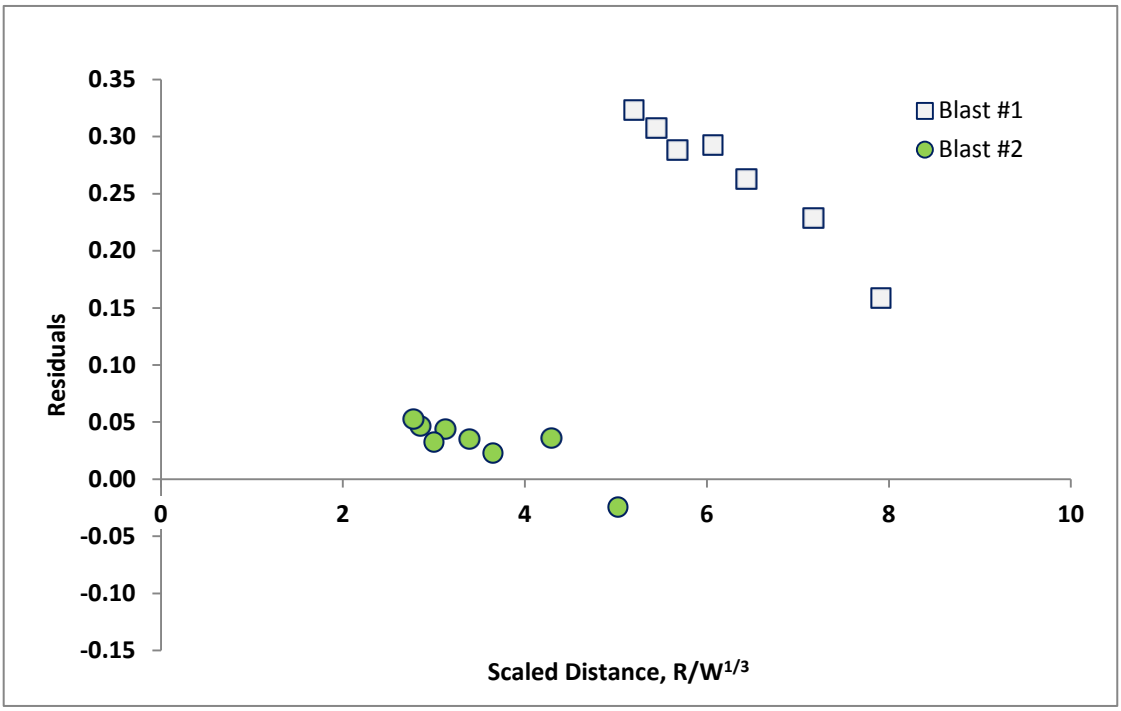

Figure 5-2 Residual plot of Blast #1 and Blast #2 of Maui Blasting Study

Table 5.1 –Evaluation of Empirical Model to Maui Blasting Study for both blasts

t-Test: Paired Two Sample for Means

	Ru - Observed	*Ru – Predicted (from model)*
Mean	0.796666667	0.65623467
Variance	0.016895238	0.03251004
Observations	15	15
Pearson Correlation	0.703744077	
Hypothesized Mean Difference	0	
df	14	
t Stat	4.244638427	
P(T<=t) one-tail	0.000408296	
t Critical one-tail	1.761310115	
P(T<=t) two-tail	0.000816593	
t Critical two-tail	2.144786681	

The difference between the empirical model and the model developed by Rollins et al. (2004) indicates that there may be a difference on how the scaled distance may be accounted for. Therefore, a residual plot was not performed between the two models. The results do not invalidate the Rollins et al. (2004) model but simply imply that it was developed on a different basis.

5.2.2 Vancouver Comparison

The Vancouver (Strand 2008, Rollins et al. 2004) pilot study utilized a simple circular array for the charge layout as explained in Section 3.3. The site conditions were generalized throughout the soil profile, with an average effective overburden pressure of 100 kPa and average SPT $(N_1)_{60}$ value of 10 blows per 30 cm. A comparison plot of the blasting data to the empirical model with 95% confidence intervals is provided in Figure 5-3. From observation, the average predicted trend (represented by the dashed line) provides a decent fit to the data.

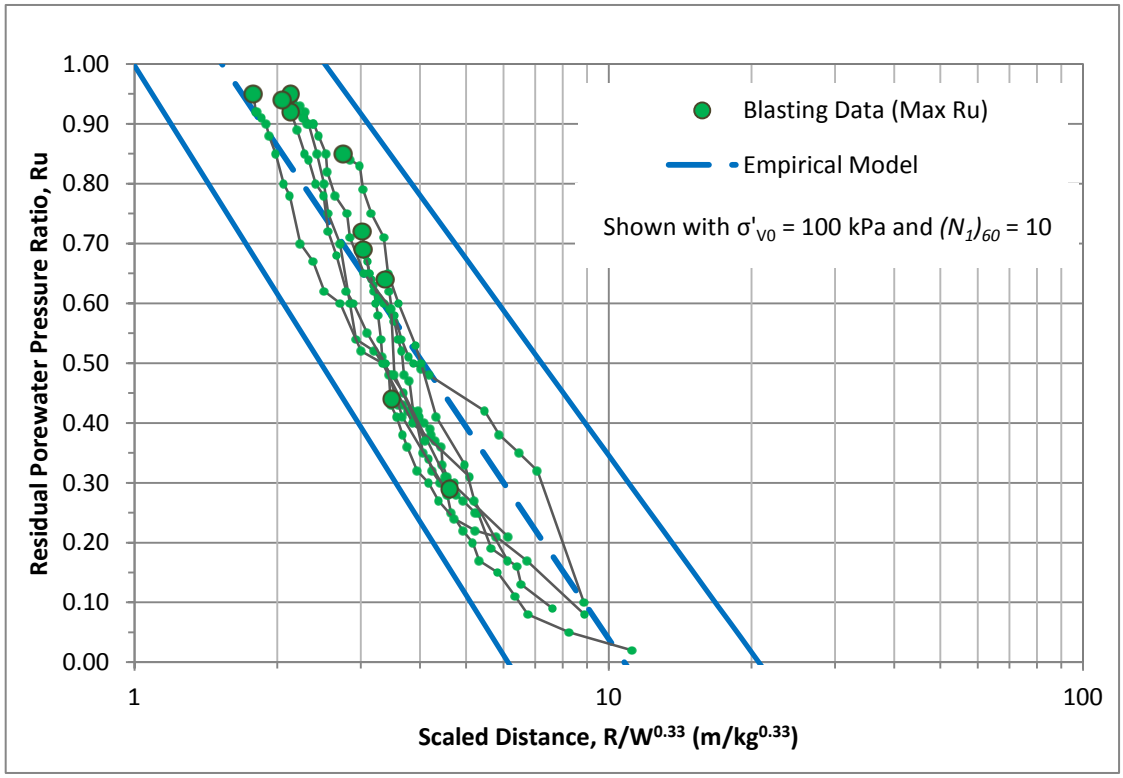

Figure 5-3 Comparison of empirical model to Vancouver pilot study with incremental values shown

In order to statistically evaluate the model, the same approach used in the Maui comparison (Section 5.2.1) is used here as well. The residuals of the observed *Ru* and the predicted *Ru* by the empirical model are plotted against the scaled distance and the observed *Ru* in Figures 5-4 and 5-5, respectively. From Figure 5-4, the average residual values for blast #1 and blast #2 are -0.07 and 0.01, respectively. From Figure 5-5, it is observed that the model mostly over-predicts the *Ru* for blast #1, while transitioning to over-predicting the observed *Ru* for values approaching 1.0 as seen during blast #3. However, there does not appear to be any outliers that can be identified. A paired t-test was performed to further determine how well the model fit the data, and the results are provided in Table 5-2. The two-tailed P-test obtained from the t-test performed on the observed *Ru* and predicted *Ru* indicated that the model provides a good statistical fit to the data.

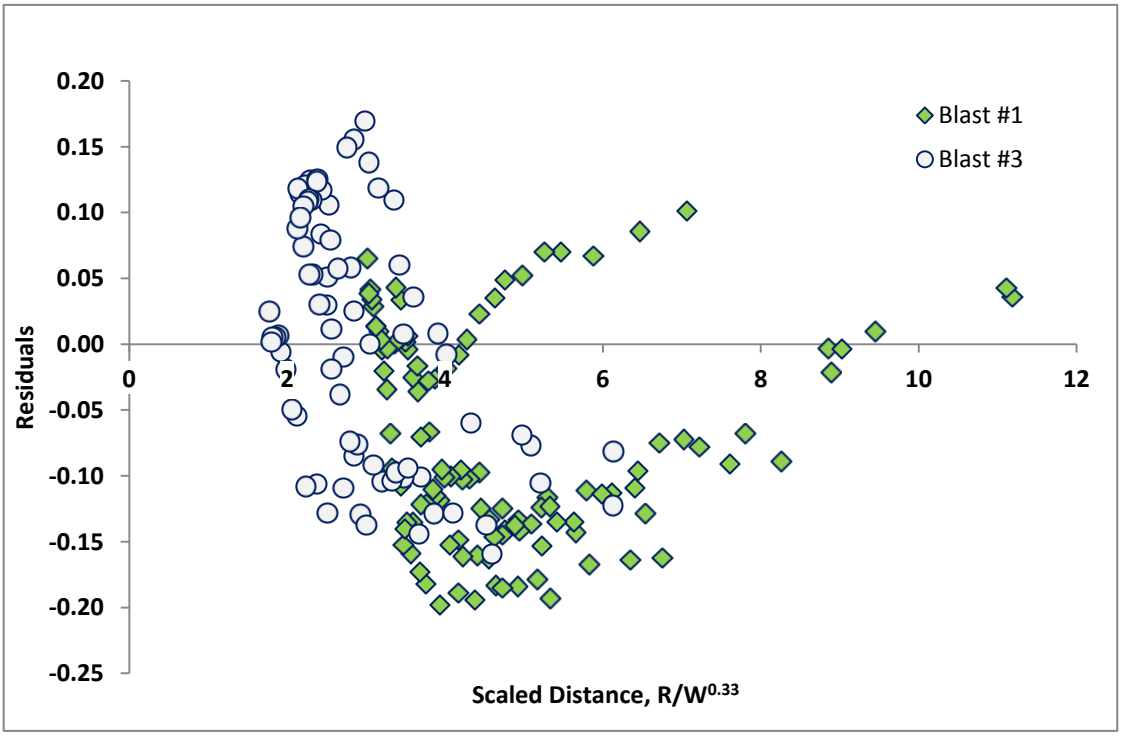

Figure 5-4 Residual plot from Vancouver Pilot Test compared to scaled distance

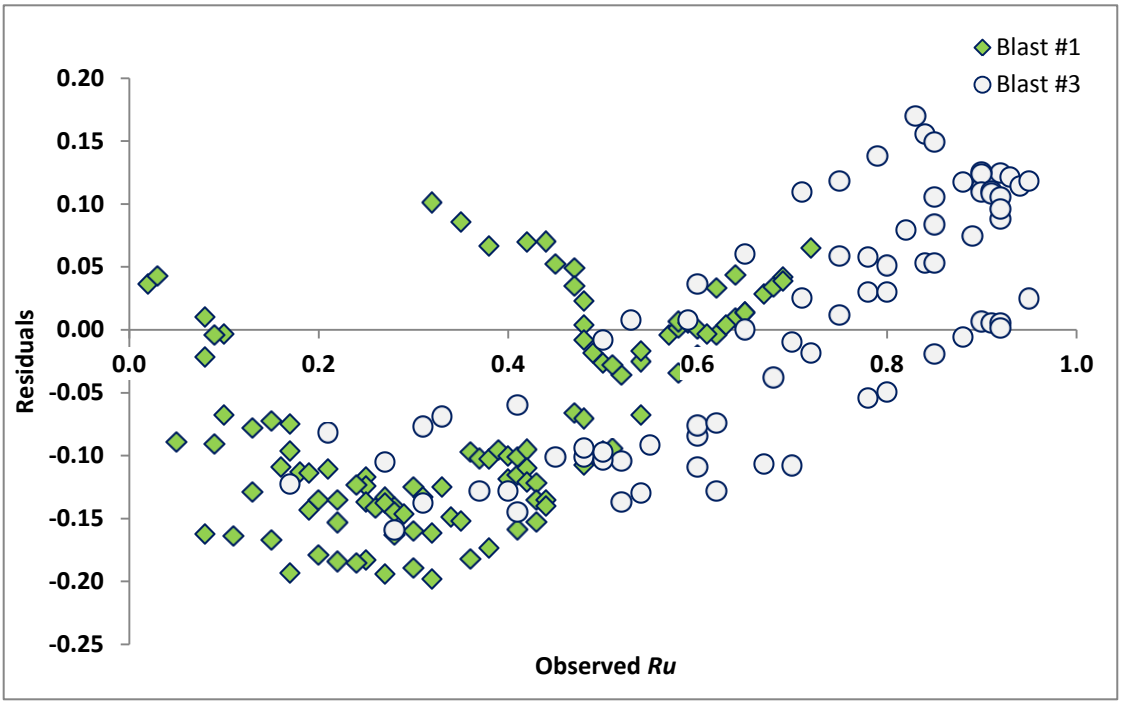

Figure 5-5 Residual plot from Vancouver Pilot Test compared to observed *Ru*

Table 5.2 – Statistical Evaluation of Empirical Model to Vancouver Pilot Study

t-Test: Paired Two Sample for Means

	Ru - Observed	*Ru - Predicted*
Mean	0.500314136	0.542828013
Variance	0.06185148	0.037861325
Observations	191	191
Pearson Correlation	0.940136128	
Hypothesized Mean Difference	0	
df	190	
t Stat	-6.290996493	
P(T<=t) one-tail	1.06147E-09	
t Critical one-tail	1.65291295	
P(T<=t) two-tail	2.12295E-09	
t Critical two-tail	1.972528138	

5.2.3 Tokachi Comparison

The Tokachi experiment consisted of a much more complex blasting layout than the Maui and Vancouver studies, using a larger blasting area with over 120 charges used to liquefy the soil as explained in Section 3.5. A plot of the blasting data from the full-scale test #1 is compared with the empirical model and 95% confidence intervals in Figure 5-6 based upon the generalized site conditions of an average effective overburden pressure of 45 kPa and SPT $(N_1)_{60}$ value of 2. In observing Figure 5-6, the blasting data follows more of an exponential increase (based upon the semi-log plot) in *Ru* with scaled distance rather than the projected linear trend (on a semi-log plot) by the empirical model. As *Ru* approaches 1.0, it falls outside the 95% confidence intervals of the empirical model. However, the model appears to provide a good fit to the data that fall below *Ru* of 0.60.

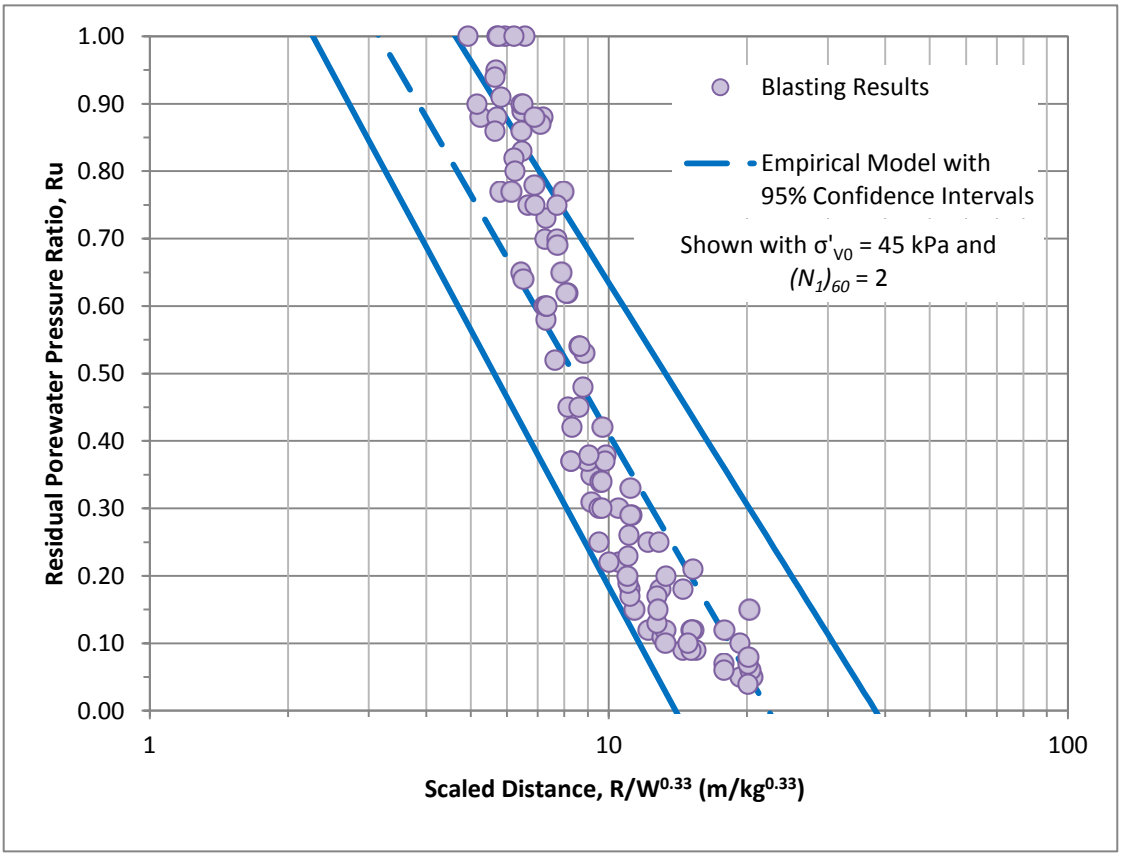

Figure 5-6 Comparison of the empirical model to the Tokachi Full-Scale Test #1

To further investigate the validity of the model for the Tokachi blast results, a residual plot compared to scaled distance and observed *Ru* were developed based upon the pore pressure transducer (PPT) depths of 2, 4 and 6 m, and are shown in Figures 5-7 and 5-8, respectively. In these figures, it is observed that the *Ru* measured by PPT at 2 m and 6 m was similar to the predicted values from the empirical model, while values measured at 4 m were significantly different and for the most part, inconsistent. In Figure 5-7, the graphs shows that at a depth of 4 m, the empirical model overestimated the *Ru* for scaled distances greater than 10 and transitioned to underestimating the *Ru* for scaled distances less than 10. In Figure 5-8, the results show that the model over-predicted the observed *Ru* for PPT at 2 m and 6 m for observed *Ru* values less than 0.45, and then transitioned to under-prediction for observed *Ru* values greater than 0.45. From the same figure, the results for PPT at 4 m showed that the empirical model overestimated the *Ru* for lower observed *Ru* values while underestimating the *Ru* for higher observed *Ru* values.

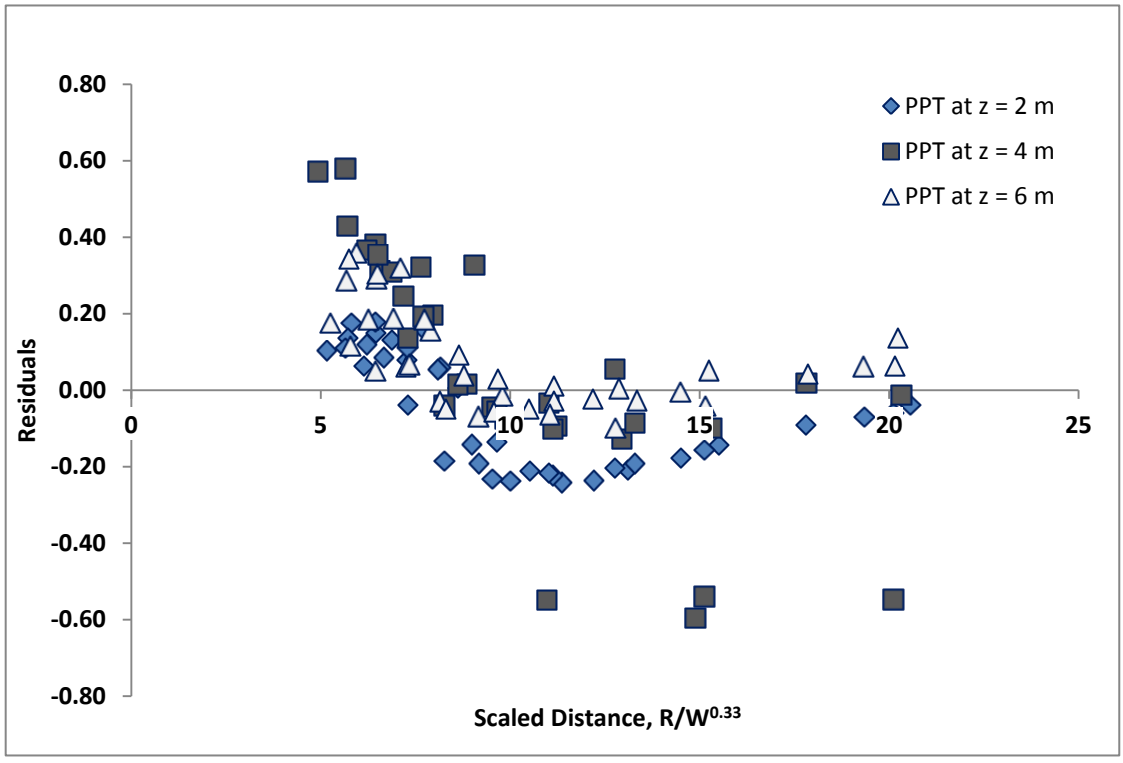

Figure 5-7 Residual plot of the Tokachi full-scale blast #1 compared to scaled distance (categorized by depth of pore pressure transducer)

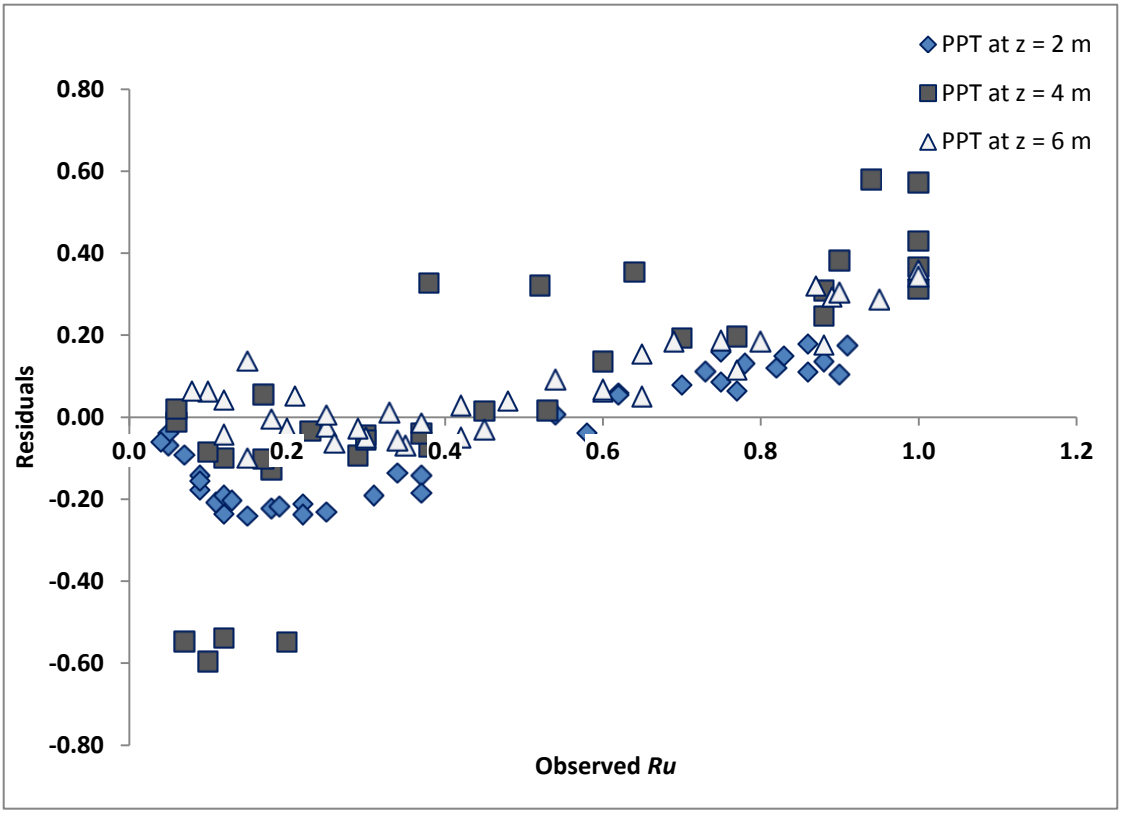

Figure 5-8 Residual plot of the Tokachi full-scale blast #1 compared to observed *Ru* (categorized by depth of pore pressure transducer)

As with the previous case histories, a paired t-test was performed to evaluate how well the model represented the data, with results shown in Table 5-3. Based upon the two-tail P-test, the result of 0.183 indicates that the model does not provide a good fit to the data. One significant factor to this result is that the blasting layout was much more complex than that used at Maui or Vancouver, and that the method used to account for the change in scaled distance (Equation 3-1) may be inapplicable to such blasting layouts. In addition, the soil profile used in the analysis was a generalized profile and may not accurately represent the soil conditions existing during blasting.

Table 5.3 – Statistical Evaluation of Empirical Model to Tokachi Pilot Study

t-Test: Paired Two Sample for Means

	Ru - Observed	*Ru - Predicted*
Mean	0.460825688	0.433694043
Variance	0.096950238	0.03990854
Observations	109	109
Pearson Correlation	0.741123013	
Hypothesized Mean Difference	0	
df	108	
t Stat	1.340394362	
P(T<=t) one-tail	0.09146504	
t Critical one-tail	1.659085144	
P(T<=t) two-tail	0.182930081	
t Critical two-tail	1.982173424	

5.2.4 Ishikari Comparison

In the Ishikari blasting study described in Chapter 3.3, the site conditions were considered to be similar for both the pilot and full-scale study (in the unimproved area), with blasting performed mostly in reclaimed sand with an average effective overburden pressure of 45 kPa and average SPT $(N_1)_{60}$ value of 5 at a depth of 4 m. Blasting during the pilot study followed a simple square-grid layout using 32 blasts while the full-scale study used over 500 blasts and consisted of a much more complex blasting layout and sequence than seen in previous case histories.

The blasting results for the 2 studies are plotted with the empirical model accompanied with the 95% confidence intervals in Figure 5-9. From the figure, the model appears to provide a better fit to the pilot test, while the full-scale test results are not well-represented by the model. In predicting liquefaction, the model provides a slightly overestimate of the scaled distance for the pilot study while being off by nearly 60% for the full-scale test.

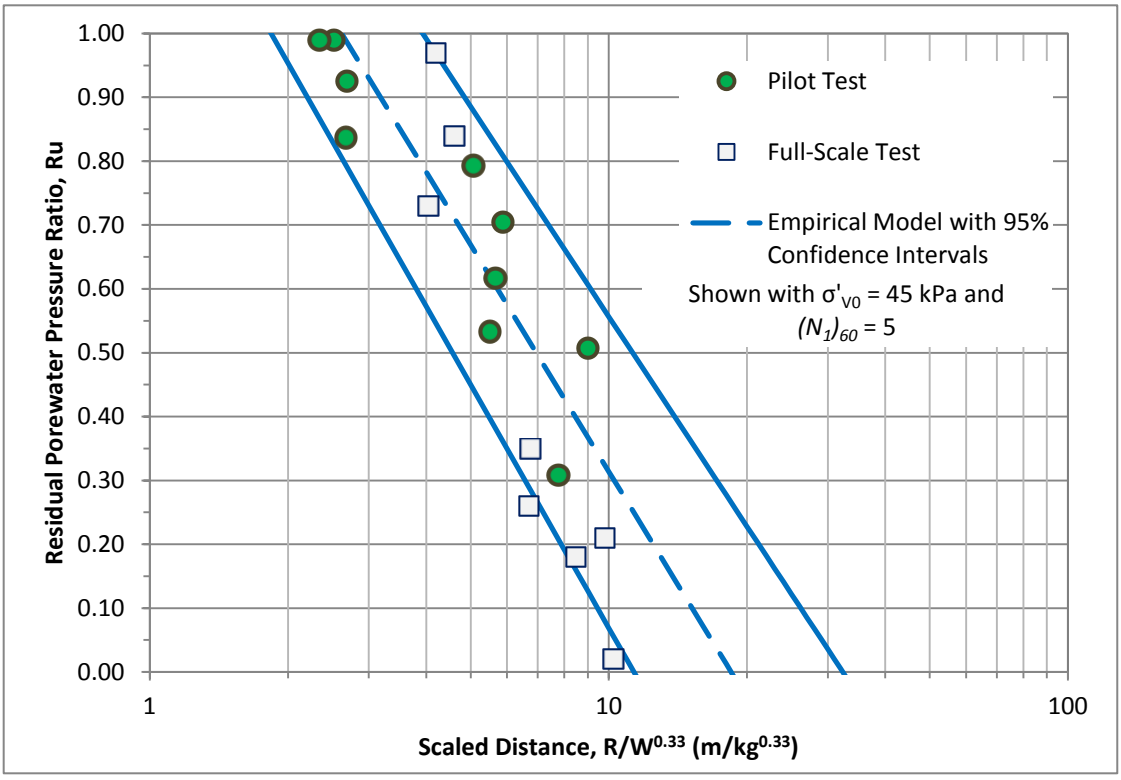

Figure 5-9 Comparison of empirical model to Ishikari pilot test

The residuals for both the pilot study and full-scale study are plotted against the scaled distance and observed *Ru,* and are shown in Figures 5-10 and 5-11 respectively. The residuals for the pilot test generally range from -0.15 to 0.15, while the full-scale study residuals range from -0.30 to 0.20. This may indicate that there is a significant difference between the two tests.

A paired t-test was performed on the data to determine the fit of the model to the data. From the two tail P-test result of 0.177, the model was concluded as not providing a good fit to the combined pilot and full-scale study data. To determine if the model provided a better fit to the individual studies, separate paired t-tests were performed on both the pilot test and full-scale test. However, in performing these separate paired t-tests, the p-test indicated the same conclusion: that the model does not provide a good fit to the data.

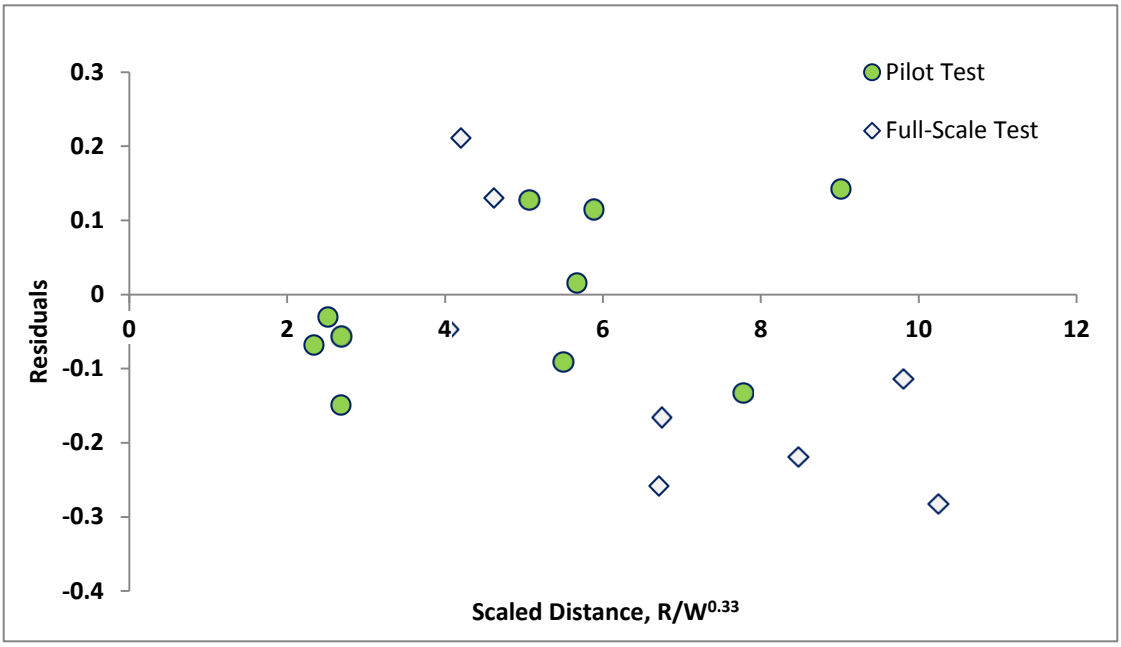

Figure 5-10 Residual plot of Ishikari pilot study and full-scale test to empirical model compared to scaled distance

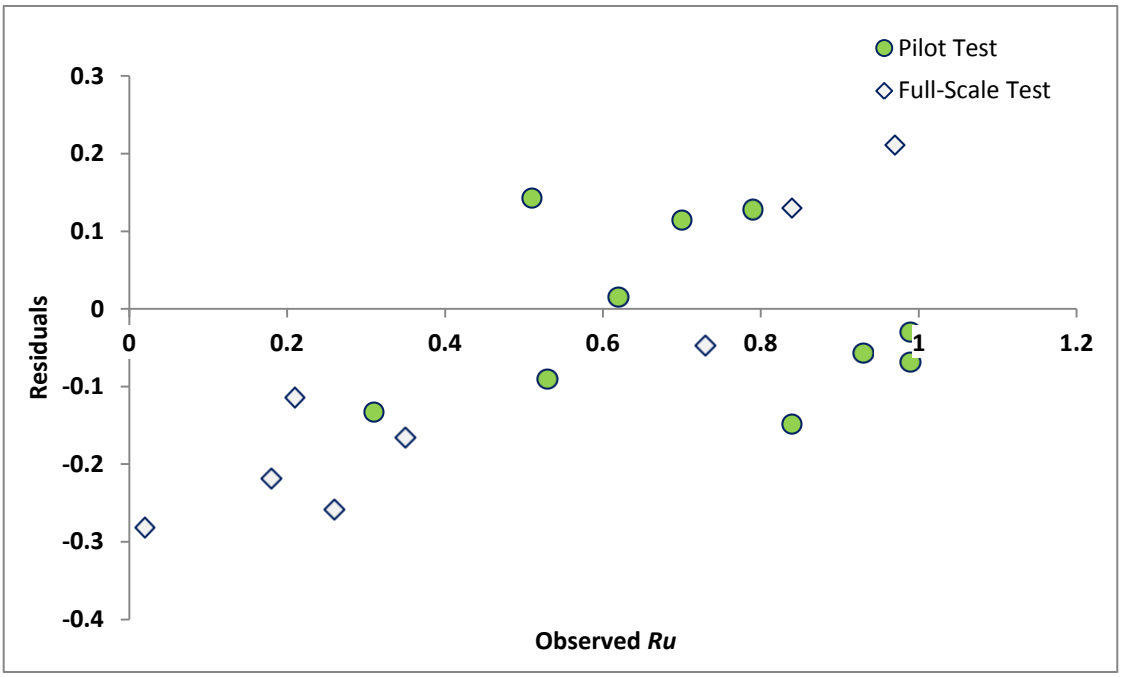

Figure 5-11 Residual plot of Ishikari pilot study and full-scale test to empirical model compared to observed *Ru*

Table 5.4 – Statistical Evaluation of Empirical Model to Ishikari Pilot and Full-Scale Study

t-Test: Paired Two Sample for Means

	Ru - observed	*Ru - predicted*
Mean	0.598333333	0.646873272
Variance	0.098155882	0.059912963
Observations	18	18
Pearson Correlation	0.891321559	
Hypothesized Mean Difference	0	
df	17	
t Stat	-1.408935779	
P(T<=t) one-tail	0.088441457	
t Critical one-tail	1.739606716	
P(T<=t) two-tail	0.176882913	
t Critical two-tail	2.109815559	

In reviewing the results, there were two main concerns that may explain why the model did not provide a good fit to the data. The pilot study consisted of a relatively simple layout, but the time delay between blasts #1 and #2 was over 30 minutes, which could affect pore pressure generation if the pore pressure did not completely dissipate during that period. The analysis assumed that full dissipation did occur, but it was unknown if this was actually the case. The full-scale study utilized a very complex blasting pattern, using over 500 charges placed throughout the site. During the blasting sequence, the soil may be subjected to the blast loads in the beginning, but begins to be unaffected as the blasting occurs at farther distances. During this time pore pressure dissipation can occur before it is subjected to a "second round" of blasts as the sequence returns within the radius of influence of the pore pressure transducers.

5.2.5 Overall Evaluation of Empirical Model for Multiple Blasts

To evaluate the validity of the model, graphical comparisons and paired t-tests of the empirical model were made to four different blasting studies consisting of different blasting layouts. It was observed that the empirical model provided a statistically good

fit to the data for case histories that consisted of simple blasting layouts, such as a simple square grid or circular array. As the blasting layout becomes more complex, such as an increase in the number of blasts or the sequence of blasting, the model did not provide a good fit to the data as shown on both the graphs and paired t-tests. The R^2 value of the empirical model was 0.65, indicating that there are other uncertainties that must be considered to develop a model that will provide a much better fit. These uncertainties can include blasting layout, as shown above, as well as blasting pattern and time delays between blasts. Other considerations may be in regards to additional in-situ soil conditions, such as the soil permeability, cementation, or other aging factors that may exist.

5.3 EVALUATION OF EMPIRICAL MODEL FOR SINGLE BLASTS

Figure 5-12 shows the empirical method developed for single blasts (Equation 4-3) plotted with the models developed by Studer and Kok (1980), Kummeneje and Eide (1961), and Charlie and Doehring (2006) with the observed case history data. An effective overburden pressure of 50 kPa is assumed for the Kummeneje and Eide (1961) model. From observation, the best fitting models are the Kummeneje and Eide (1961) model and the empirical model. The Kummeneje and Eide (1961) model appears to do a better job in predicting high *Ru* values than the empirical model, and appears to do an overall better job representing the data. The data used in the analysis had a maximum *Ru* value of 0.64, which caused the empirical model to be subject to extrapolation for *Ru* values that exceed that value.

To evaluate how the model compared to the existing models, residual plots were developed based upon the scaled distance and the observed *Ru,* and are shown in Figures 5-13 and 5-14. The existing models overestimate the *Ru* for scaled distances less than 10 while the new model under-predicts the *Ru*. For the observed *Ru* residual plot, the empirical model consistently under-predicts the *Ru* for the range of *Ru* values investigated (0 to 0.64). Based upon the residual plots, the empirical model provided the best fit to the data.

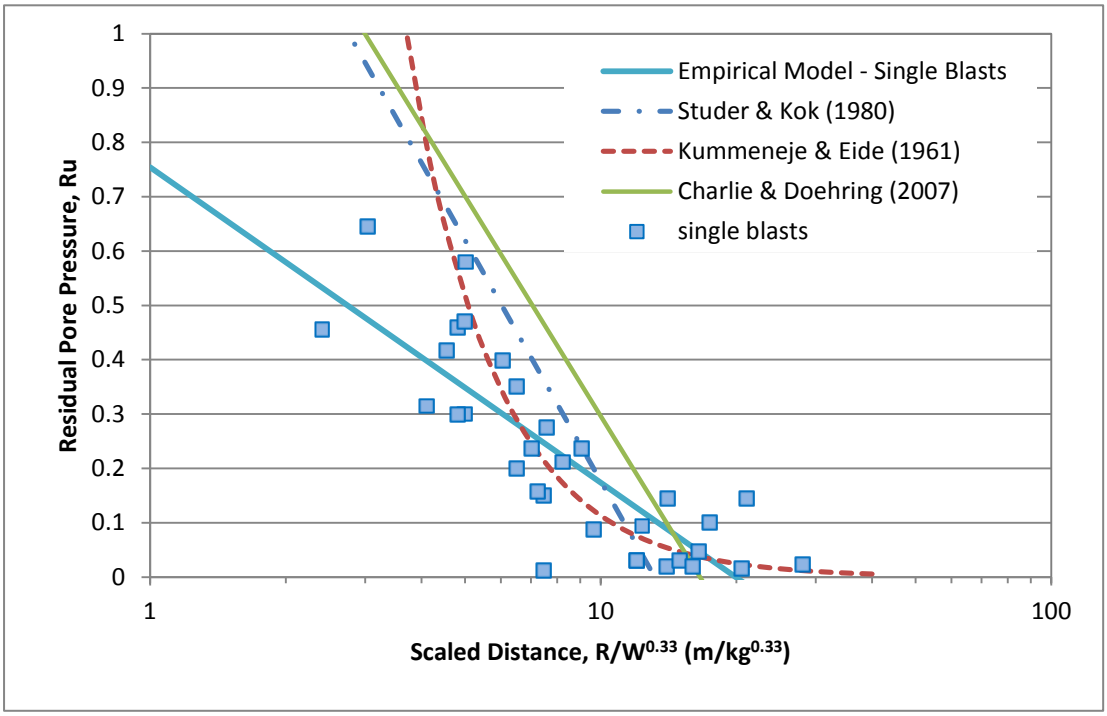

Figure 5-12 Comparison of empirical model for single blasts to existing models

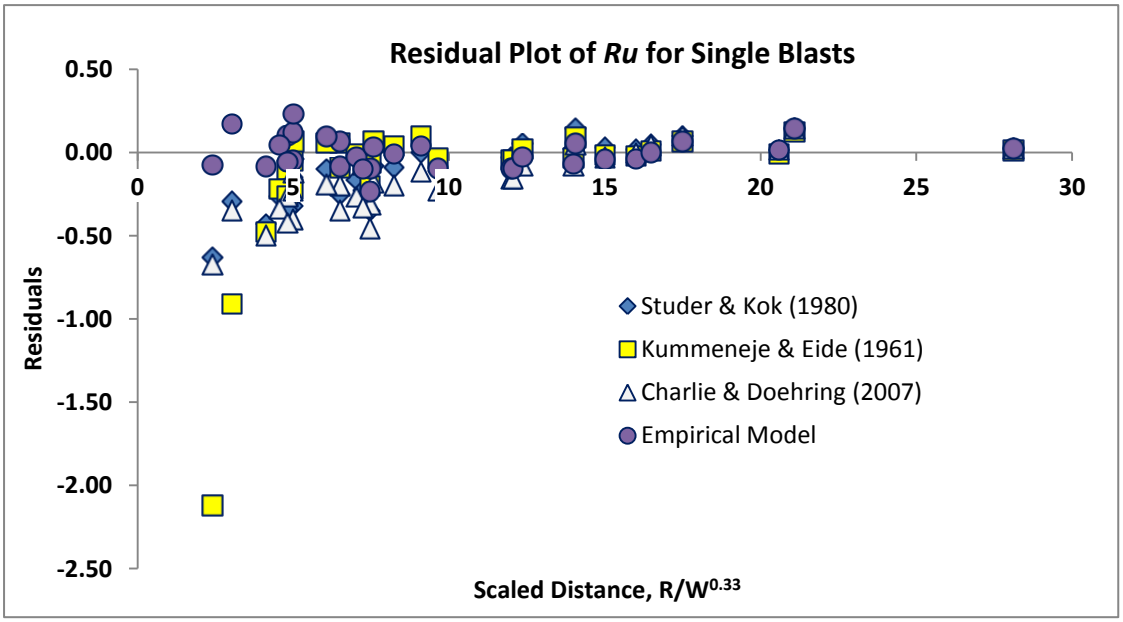

Figure 5-13 Comparison of empirical model for single blasts with existing models with recorded case history data

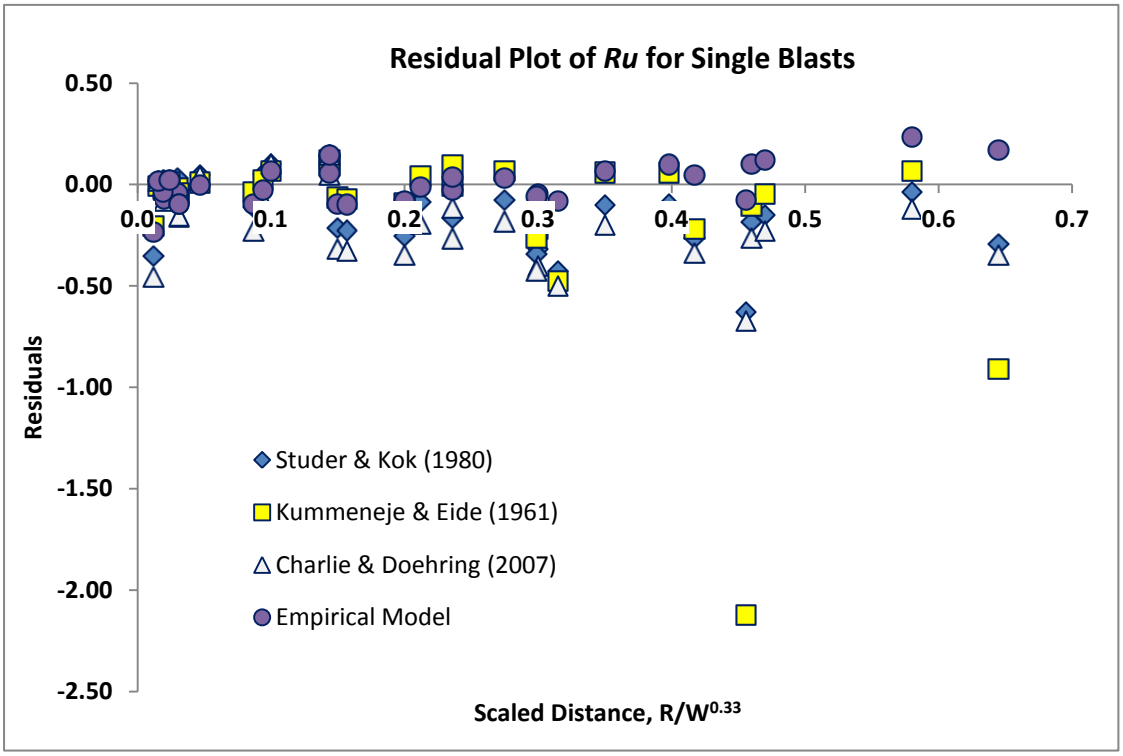

Figure 5-14 Comparison of empirical model for single blasts with existing models with recorded case history data

5.4 MULTIPLE BLAST MODEL AND SINGLE BLAST MODEL COMPARISON

In an attempt to be practical for blasting experiments, a question arose about the difference between the multiple blast empirical model (equation 4-1) and the empirical model for single blasts. Using the case history data developed from single blasts, an evaluation was made into how well the empirical model developed for multiple blasts compared to the single blasts empirical model in predicting *Ru* values for single blasts. Based upon the observed *Ru* and the predicted *Ru* using the models, residual plots based upon scaled distance and observed *Ru* are shown in Figures 5-15 and 5-16, respectively. In Figure 5-15, both models underestimate the *Ru* for scaled distances greater than approximately 13 and then overestimate the *Ru* for scaled distances less than 13. Both models overestimate the *Ru* for observed *Ru* greater than 0.2, but the Studer and Kok (1980) produces a greater range of residual values.

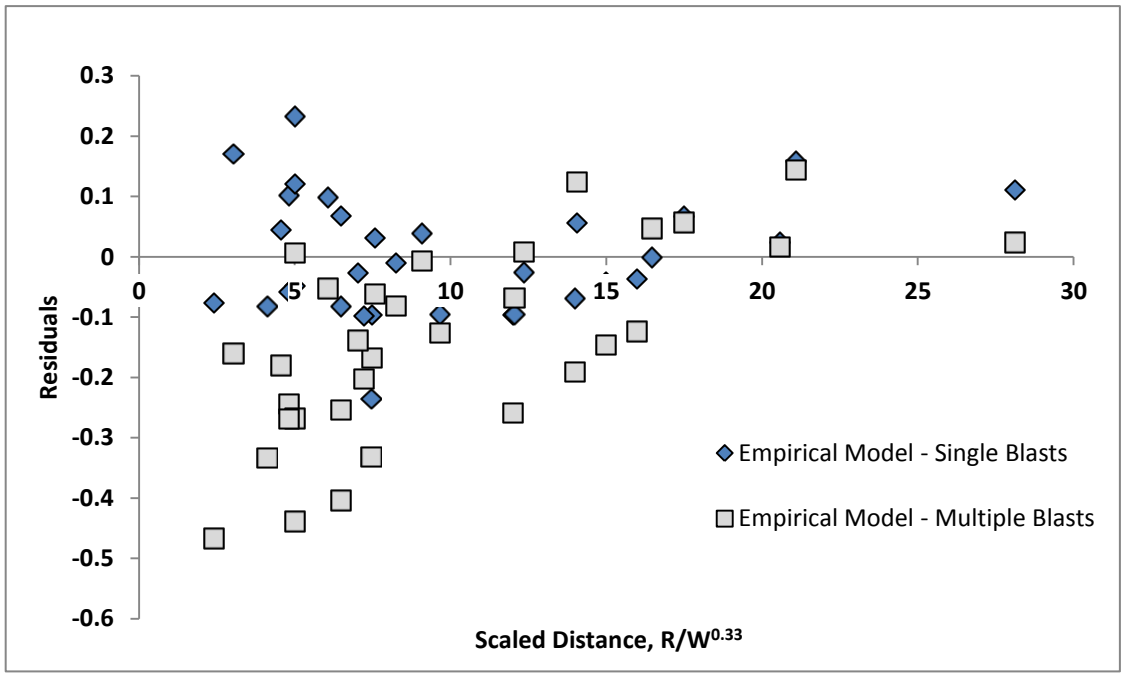

Figure 5-15 Comparison of residual plot of empirical models for multiple blasts and single blasts with single blasts data compared to scaled distance

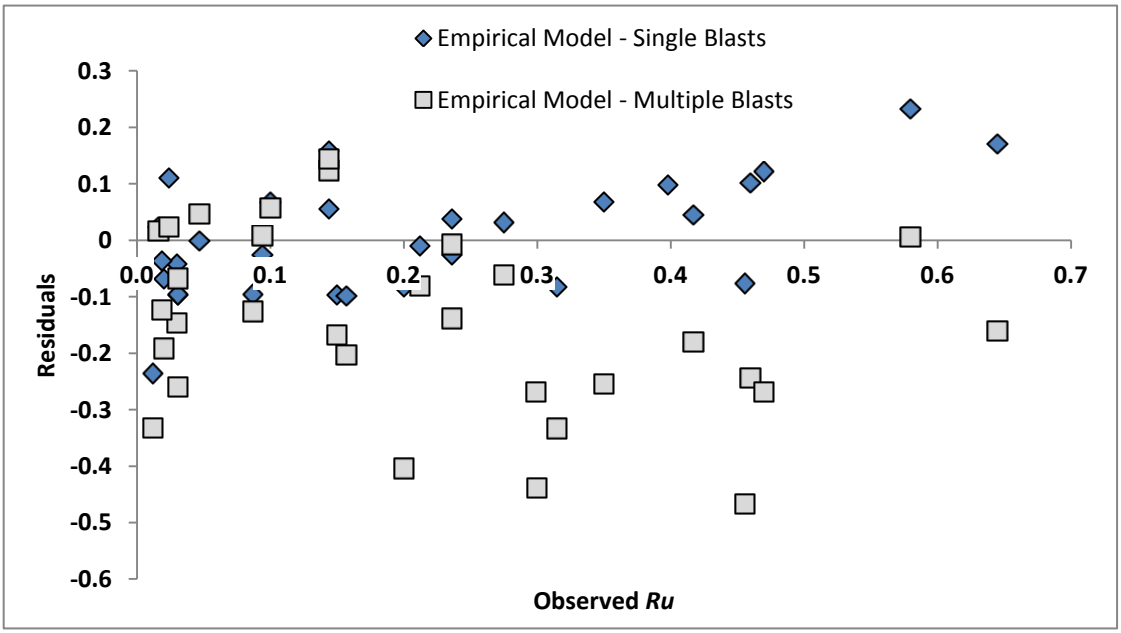

Figure 5-16 Comparison of residual plot of empirical models for multiple blasts and single blasts with single blasts data compared to observed *Ru*

To further compare the models against the single blasts data, paired t-tests were performed between the observed *Ru* and the predicted values from the single blast model and the multiple blasts empirical model, with results shown in Tables 5-5 and 5-6 respectively. Using the two-tail P-test as a determining factor of how well the model fits the data, the models were able to be evaluated for best fit. From Table 5-5, the P-test from the single blasts was 0.91, indicating that it is not a good fit to the data as it exceeds the determining value of 0.05. However, in Table 5-6, it is observed that the P-test value for the empirical model for multiple blasts is well below 0.05, indicating that empirical model statistically provides a good fit to the single blasts data. Therefore, it can be concluded that the empirical model developed for multiple blasts can be used for single blasts as well.

Table 5.5 – Statistical Evaluation of Studer and Kok (1980) model to Single Blasts Case History Data

t-Test: Paired Two Sample for Means

Empirical Model - Single Blasts

	Ru - Observed	*Ru - Predicted*
Mean	0.21734375	0.219289412
Variance	0.03252933	0.020827998
Observations	32	32
Pearson Correlation	0.843482574	
Hypothesized Mean Difference	0	
df	31	
t Stat	-0.113239315	
P(T<=t) one-tail	0.455285499	
t Critical one-tail	1.695518742	
P(T<=t) two-tail	0.910570999	
t Critical two-tail	2.039513438	

Table 5.6 – Statistical Evaluation of empirical model for multiple blasts to Single Blasts Case History Data

t-Test: Paired Two Sample for Means

Empirical Model - Multiple Blasts

	Ru - Observed	*Ru - Predicted*
Mean	0.21734375	0.359448651
Variance	0.03252933	0.074293303
Observations	32	32
Pearson Correlation	0.830747538	
Hypothesized Mean Difference	0	
df	31	
t Stat	-5.069576921	
P(T<=t) one-tail	8.79723E-06	
t Critical one-tail	1.695518742	
P(T<=t) two-tail	1.75945E-05	
t Critical two-tail	2.039513438	

5.5 DESIGN EXAMPLE

From this research, it has been shown that when in-situ conditions such as SPT $(N_1)_{60}$ values and effective overburden pressure are considered, the *Ru* is better predicted than with the conventional method of using the scaled distance. With the use of this model, design of blasting studies may be able to minimize the number of pilot tests performed, as well as having a good approximation of the zone of liquefaction. This can prevent adverse effects of pore pressure buildup in areas adjacent to the blasting zone. To demonstrate how this model can be used in design of a blasting experiment, an example is provided below:

Example:

Given: A blasting study will be performed on loose saturated sand within a 6 m radius using a circular array of explosives, as shown in Figure 5-12. The sand layer is approximately 10 m in depth, with the groundwater table at the surface. The saturated unit weight (γ_{sat}) is 20 kN/m^3 and the average SPT $(N_1)_{60}$ value was 5 blows per 30 cm. A pore pressure transducer will be placed

at the center of the array at a depth of 5 m. The explosives will also be at a depth of 5 m (this can be an average depth of a decked explosives or just one explosive) and placed in eight different boreholes as shown in Figure 5-12.

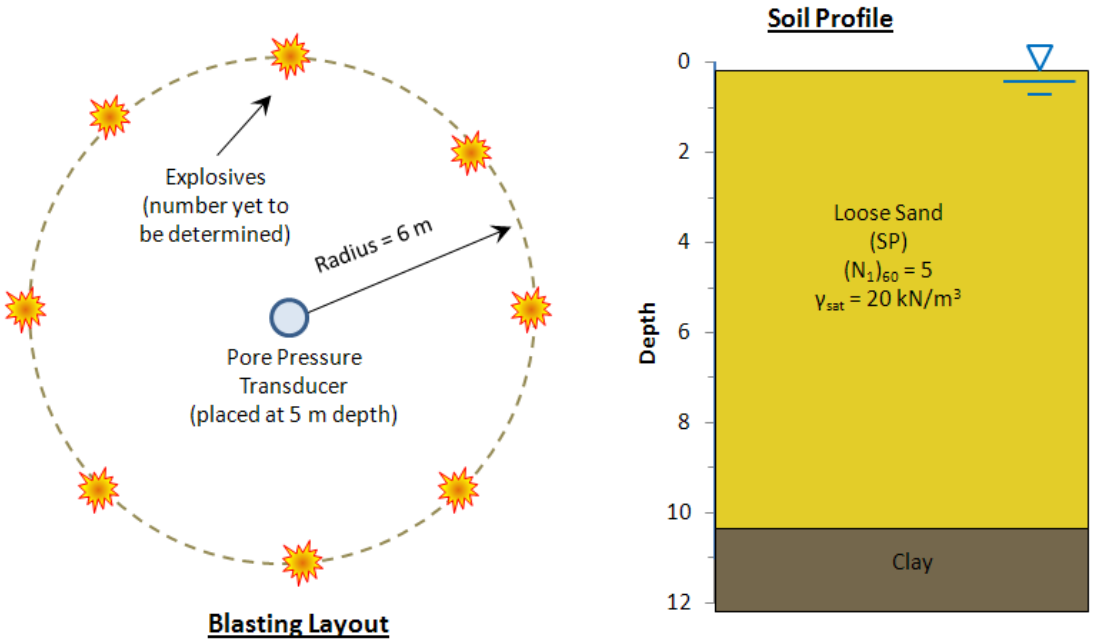

Figure 5-17 Blasting Layout and Soil Profile used for Example Design Problem

Find: Determine the required charge weight to cause liquefaction (*Ru* = 1.0) in the center of the blasting area as measured by the pore pressure transducer.

Solution:

Step 1: Design Curve

Plot the empirical model (Equation 4.1) with the in-situ measurements in order to develop the design curve (shown in Figure 5-13). Confidence intervals for the 95% limits are provided (see Appendix C).

Step 2: Extent of Liquefaction

From Figure 5-14, the extent of liquefaction using the average scaled distance value (solid line) is approximately 2.3 m/kg$^{0.33}$, with confidence intervals ranging from 1.9 to 4.0 m/kg$^{0.33}$.

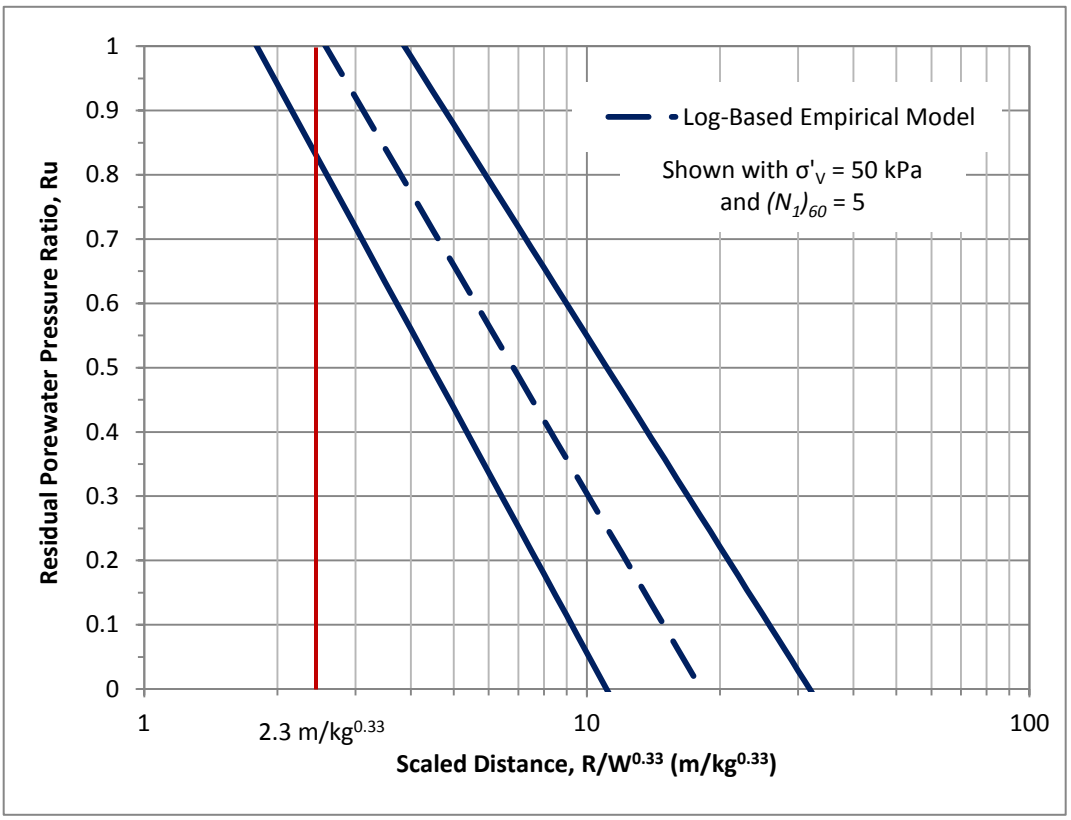

Figure 5-18 Multiple Blasts Design Chart for Example Problem

Step 3: Required Charge Weight

Based upon the scaled distance of 2.3 m/kg$^{0.33}$ from the figure, estimate the required weight of explosives to liquefy within the 6 m radius:

$$\frac{R}{W^{0.33}} = \frac{6\ m}{{W_{req}}^{0.33}} = 2.3\ \frac{m}{kg^{0.33}}$$

Solving for W_{req}:

$$W_{req} = \left(\frac{1\ kg^{0.33}}{2.3\ m} \cdot 6\ m\right)^3 = 17.8\ kg$$

Step 4: Estimate Boreholes and individual charge sizes

For this particular example, the designer would like to use 8 boreholes spaced evenly around the perimeter. To aid in the distributing of explosives, the total weight is increased to 18 kg. Dividing the required weight by the number of boreholes, the amount of explosives (TNT-equivalent) in each borehole would be a total of 2.25 kg of TNT-equivalent explosive. From the 95% confidence intervals, the required charge weight for each borehole would range from 0.45 kg to 4.0 kg approximately.

5.6 LIMITATIONS AND CONSIDERATIONS

An empirical model predicting pore pressure response in controlled blasting studies has been developed and has been shown to be applicable to both single and multiple blasts. As previously mentioned this model is based upon case history data and has yet to be evaluated with actual field experiments. Some uncertainties that may exist within this model include:

- Blasting layout and blasting pattern: circular array versus grid layout may affect how pore pressure is generated and how scaled distances are accounted for. It was observed that simpler layouts with less charges (less than 30) produced similar results predicted by the model while results from complex blasting layouts and patterns created more of a significant difference in the results.
- Time delays between blasts: is *significant* drainage occurring within the soil? If so, there would affect the incremental increase in the residual pore pressure with each blast and perhaps the overall pore pressure ratio.
- The model was developed for a specific range of effective overburden pressures from 14 to 136 kPa, and SPT $(N_1)_{60}$ values of 1 to 16 blows per 30 cm. Anything outside of this range would be subjected to extrapolation that may diverge off the projected trend of the regression line.

- Although the influence of fines content was indirectly considered in the regression analysis by the unit-less cyclic resistance ratio (CRR) developed from the Youd et al. (2001) method from the SPT test, it is not considered directly in this analysis. Fines content has been shown to have a significant influence on the liquefaction potential of a soil.
- A significant majority of the soil information was based on a few tests at selected depths and applied throughout the soil column. Many times an average value was provided in the case history references which may actually not provide an accurate or true representation of the soil conditions through the profile.
- For the single blasts, there were only 32 data points from which the empirical model was developed, and many of the data points came from one test. This can have a significant impact to the data. To better evaluate the model to single blasts, more data points should be used.

6.0 SUMMARY AND CONCLUSIONS

"We can do little to reduce the hazard embodied in an active fault or a major earthquake, but we can do a lot about the risk to the structures we design and build. It is important to remember the frequently quoted observation that earthquakes do not kill, but collapsed buildings and facilities do."

- Professor Thomas O'Rourke, Cornell University

6.1 SUMMARY OF WORK PERFORMED

Controlled blasting has been used as a ground improvement method in densifying loose soils for nearly 70 years, and has recently emerged as a tool to physically generate liquefaction or to even supplement current in-situ liquefaction assessment techniques. Typically, a small blasting study is performed to determine the blasting layout to use in the full-scale tests. Sometimes, multiple "trial and error" studies must be performed to identify the optimal layout of explosives to liquefy the given volume of soil. Empirical models exist that can help predict the pore pressure with the scaled distance, but they are limited in the fact that they do not consider in-situ soil conditions and that they were developed primarily for single blasts, whereas current blasting experiments utilize multiple blasts to liquefy the soil.

To promote the use of controlled blasting as a research tool and liquefaction assessment technique, this research aims to minimize the uncertainty by understanding the role that in-situ conditions and blasting layout play in the generation of residual pore pressures. Through the use of several case histories in which controlled blasting was utilized, a statistical analysis was performed to identify whether residual pore pressures could be predicted based upon the blasting layout and in-situ soil conditions for single and multiple blasts. Empirical models were developed for both multiple and single blasts, and were evaluated through residual plots and paired t-tests.

6.2 SUMMARY OF RESULTS AND LESSONS LEARNED

From this investigation, there were many insights gained into understanding the response of residual pore pressure in controlled blasting studies. Although the loading upon the soil during an earthquake is shear wave-dominated while controlled blasting is typically compression wave-dominated, controlled blasting is a valuable research tool to physically generate liquefaction and investigate soil-structure interaction during liquefied conditions. The intent of this research is to increase the knowledge base of controlled blasting by the following conclusions:

- A higher residual pore pressure is expected in using multiple blasts than one large single blast of an equivalent scaled distance, $R/W^{0.33}$.
- In-situ conditions play a significant role in development of residual pore pressures and should be accounted for in blasting design.
- A consistent method to account for the changing scaled distance in multiple blasts should be used in evaluating pore pressure response due to the observation that the magnitude of residual pore pressure generated from each blast is influenced by the pore pressure generated from the previous blast.
- In developing an empirical model to predict residual pore pressure with each blast, in-situ conditions such as effective overburden pressure and SPT $(N_1)_{60}$ values accompanied with scaled distance provide the best fit, with an R^2 value of 0.64. The SPT $(N_1)_{60}$ values have a more significant effect on the model than the effective overburden pressure. The empirical model is as follows, as defined in Equation 4-1:

$$Ru = 1.747 - 0.512 \ln\left(R/W^{0.33}\right) - 0.032(N_1)_{60} - 0.002\sigma'_{v0}\ (kPa)$$

- An empirical model developed for single blasts was shown to provide a better fit to the observed data than observed in the existing models. However, it was found that the empirical model developed for multiple blasts provided a better fit to the single blasts data than the single blasts empirical model. Therefore, it was concluded that the empirical model for multiple blasts can be used for single blasts as well.

- The empirical model should be improved as the case history data increases.
- The model was shown to be valid for blasting layouts that were relatively simple, such as a square grid or circular array, and consisted of less than 25 charges. The model was not able to predict the *Ru* values on a consistent basis when the layout consisted of many charges (more than 30) and a complex sequence.
- Additionally, this research emphasized the benefit of increased collaboration between U.S and Japanese researchers

6.3 FUTURE WORK AND RESEARCH

Although this empirical model may provide a statistically good fit to the case history data from which it was developed, a field experiment is considered the best means of scrutinizing and evaluating the validity of the model and is recommended as the first step to be performed in regard to the future work stemming from this research. If the model is validated, this information can be used in future blasting studies including the development of in-situ liquefaction assessments using controlled blasting. In addition, this model may serve as a tool in the development of an energy-based procedure for predicting pore pressure response for soil densification and ground improvement procedures.

BIBLIOGRAPHY

Al-Qasimi, E.M.A., Charlie, W.A., and Woeller, D.J. (2005). "Canadian Liquefaction Experiment (CANLEX): Blast-Induced Ground Motion and Pore Pressure Experiments." *Geotechnical Testing Journal,* 28(1), January 2005, pp. 9-21.

Andrus R.D., and Stokoe, K.H. II (2000). "Liquefaction Resistance of Soils from Shear-Wave Velocity." *Journal of Geotechnical and Geoenvironmental Engineering.* 126(11), November 2000, pp. 1015 – 1025.

ASCE Technical Council on Lifeline Earthquake Engineering (TCLEE). American Society of Civil Engineers (ASCE). http://apps.asce.org/instfound/techcomm_tclee.cfm. (accessed January 2010).

Ashford, S.A. and Rollins, K.M. (2002). TILT: Treasure Island Liquefaction Test: Final Report. Report SSRP-2001/17, Department of Structural Engineering, University of California, San Diego.

Ashford, S.A., and Juirnarongrit, T. (2004). Performance of Lifelines Subjected to Lateral Spreading. Report SSRP-04/18, Department of Structural Engineering, University of California, San Diego.

Ashford, S.A., Rollins, K.M., and Lane, J.D. (2004). "Blast-Induced Liquefaction for Full-Scale Foundation Testing." *Journal of Geotechnical and Geoenvironmental Engineering*. 130(8), August 2004, pp 798 – 806.

Ashford, S.A., Juirnarongrit, T., Sugano, T, and Hamada, M. (2006). Soil-Pile Response to Blast-Induced Lateral Spreading. 1: Field Test. *Journal of Geotechnical and Geoenvironmental Engineering*. February 2006. pp. 152 – 162.

Ashford, S.A., Kawamata, Y., Rollins, K.M., Kayen, R.E., Weaver, T.J., and Juirnarongrit, T. (2008). The Use of Controlling Blasting for Evaluating Seismic Performance. Not yet published.

Boulanger, R.W., and Idriss, I.M. (2007). "Evaluation of Cycling Softening in Silts and Clays." *Journal of Geotechnical and Geoenvironmental Engineering.* 133(6), June 2007, pp. 641 – 652.

Bray, J.D., and Sancio, R.B. (2006). "Assessment of the Liquefaction Susceptibility of Fine-Grained Soils." *Journal of Geotechnical and Geoenvironmental Engineering.* 132(9), September 2006, pp. 1165 – 1177

Byrne, P.M., Puebla, H., Chan, D.H., Soroush, A., Morgenstern, N.R., Cathro, D.C., Gu, W.H., Phillips, R., Robertson, P.K., Hofmann, B.A., Wride, C.E., Sego, D.C., Plewes, H.D., List, B.R., and Tan, S. (2000). "CANLEX Full-Scale Experiment and Modeling." *Canadian Geotechnical Journal*, 37(3), pp. 543-562.

Chang, W.J., Rathje, E.M., Stokoe II, K.H., and Hazirbaba, K. (2007). "In Situ Pore-Pressure Generation Behavior of Liquefiable Sand." *Journal of Geotechnical and Geoenvironmental Engineering*, 133(8), August 2007, pp. 921 – 931.

Charlie, W.A. (1985). Review of Present Practices used in Predicting the Effects of Blasting on Pore Pressure. U.S. Department of the Interior, Bureau of Reclamation. Report GR-85-9, 21 pp.

Charlie, W.A., Hubert, M.E., Schure, L.A., Veyera, G.E., Bretz, T.E., and Hassen, H.A. (1988a). Blast Induced Liquefaction: Summary of Literature. Air Force Office of Scientific Research, Washington D.C., 316 pp.

Charlie, W.A., Doehring, D.O., Veyera, G.E., and Hassen, H.A. (1988b). Blast Induced Liquefaction of Soils: Laboratory and Field Tests. Air Force Office of Scientific Research, Washington D.C., 184 pp.

Charlie, W.A., Jacobs, P.J., and Doehring, D.O. (1992). "Blast Induced Liquefaction of an Alluvial Sand Deposit." *Geotechnical Testing Journal.* 15(1), pp. 14-23.

Charlie, W.A., and Doehring, D.O. (2007). "Groundwater Table Mounding, Pore Pressure, and Liquefaction Induced by Explosions: Energy-Distance Relations." *Reviews of Geophysics*. 45, RG4006. December 2007, pp. 1 – 9.

Dickenson, S.E., McCullough, N.J., Barkau, M.G., and Wavra, B.J. (2002). Assessment and Mitigation of Liquefaction Hazards to Bridge Approach Embankments in Oregon – Final Report. SPR 361. Oregon Department of Transportation. November 2002.

Dowding, C.H., and Hryciw, R.D. (1986). "A Laboratory Study of Blast Densification of Saturated Sand." *Journal of Geotechnical Engineering*, 112(2), February 1986, pp. 187 – 199.

Ferrito, J.M. (1997). Seismic Design Criteria for Soil Liquefaction. Technical Report TR-2077-SHR. Naval Facilities Engineering Center. June 1997.

Figueroa, J.L., Saada, A.S., Liang, L., and Dahisaria, N.M. (1994). "Evaluation of Soil Liquefaction by Energy Principles." *Journal of Geotechnical Engineering.* 120(9), September 1994, pp. 1554 – 1569.

Fragaszy, R.J., and Voss, M.E. (1986). "Undrained Compression Behavior of Sand." *Journal of Geotechnical Engineering*. 112(3), March 1986, pp. 334 – 347.

Gohl, W.B., Howie, J.A., and Rea, C.E. (2001). Use of Controlled Detonation of Explosives for Liquefaction Testing. *Proceedings: Fourth International Conference on Recent Advances in Geotechnical Earthquake Engineering and Soil Dynamics and Symposium in Honor of Professor W.D. Liam Finn*, San Diego, March 26 – 31.

Gohl, W.B., Martin, T., and Elliott, R.J. (2009). Explosive Compaction of Granular Soils and In Situ Liquefaction Testing Using Sequential Detonation of Explosives. http://www.explosivecompaction.com/Papers/EC%20of%20Granular%20Soils%20and%20Insitu%20Liq%20testing.pdf (accessed December 2009).

Green, R.A. (2001). *Energy-Based Evaluation and Remediation of Liquefiable Soils,* Ph.D. Dissertation. Virginia Polytechnic Institute and State University, 397 pp. (http://scholar.lib.vt.edu/theses/available/etd-08132001-170900/).

Green, R.A., and Mitchell, J.K. (2004). Energy-Based Evaluation and Remediation of Liquefiable Soils. Geotrans 2004, ASCE, Proc*. Geotech. Eng. For Transportation Projects*. 1961 – 1970.

Ivanov, P.L. (1967). Compaction of Noncohesive Soils by Explosions (translated from Russian). National Technical Information Service Report No. TT70-57221. U.S. Department of Commerce, Springfield, VA, 211 pp.

Kayen, R.E., Barnhardt, W.A., Ashford, S.A., and Rollins, K.M. (2000). Non-destructive Measurement of Soil Liquefaction Density Change by Crosshole Radar Tomography, Treasure Island, California. Computer Simulation of Earthquake Effects. ASCE Research Library.

Kayen, R.E., Minasian, D., Ashford, S.A., Kawamata, Y., Sugano, T., Nimityongskul, N., and Nakazawa, H. (2009). "Terrestrial LIDAR Study of the Blast-Induced Liquefaction of a Simulated Airport Tarmac, Ishikari Port, Hokkaido, Japan." Paper Grant No. CMMI-0728120. *NSF CMMI Engineering Research and Innovation Conference 2009,* Honolulu, Hawaii, June 22-25, 2009.

Kimmerling, R.E. (1994). Blast Densification for Mitigation of Dynamic Settlement and Liquefaction – Final Report WA-RD 348.1. Washington State Department of Transportation. 135 pp.

Kramer, S.L. (1996). *Geotechnical Earthquake Engineering*. Prentice Hall, Inc. Upper Saddle River, New Jersey. 653 p.

Kramer, S.L. (2008). Evaluation of Liquefaction Hazards in Washington State. Final Research Report, Agreement T2695, Task 66, Liquefaction Phase III. Washington State Transportation Commission.

Kulhawy, F.H. and Mayne, P.W. (1990). *Manual of Estimating Soil Properties for Foundation Design*. Report No. EL-6800, Electric Power Research Institute, Palo Alto, CA.

Kummeneje, O. and Eide, O. (1961). Investigation of Loose Sand Deposits by Blasting. Proc. 5th International Conf. Soil Mechanics and Foundation Engineering. Vol. 1, pp. 491-497.

Lyman, A.K.B. (1942). Compaction of Cohesionless Foundation Soils by Explosives. Transactions ASCE (107) pp. 1330 – 1348.

Mitchell, J.K. (2008). "Mitigation of Liquefaction Potential of Silty Sands." From Research to Practice in Geotechnical Engineering Congress 2008, pp 453-451.

Montgomery, D.C., and Runger, G.C. (2003). *Applied Statistics and Probability for Engineers*, 3rd Edition. John Wiley & Sons, Inc., New York, 706 pp.

Nakazawa, H., and Sugano, T. (2010). Full-Scale Field Test on Liquefaction-Induced Damage of Runway Pavement by Controlled Blast Technique. In preparation.

Narin Van Court, W.A., and Mitchell, J.K. (1994). Explosive Compaction: Densification of loose, saturated, cohesionless soils by blasting. Geotechnical Engineering Report No. UCB/GT/94-03. May 1994. 116 pp.

Narsilio, G.A., Santamarina, J.C., Hebeler, T., and Bachus, R. (2009). "Blast Densification: Multi-Instrumented Case History." *Journal of Geotechnical and Geoenvironmental Engineering*, 135(6), June 2009, pp. 723 – 734.

Port and Airport Research Institute (PARI), Japan. (2009). Technical Note of the Port and Airport Research Institute: Full-Scale Field Experiment of Airport Facilities during Liquefaction Induced by Controlled Blasting Technique. Independent Administrative Institution, Port and Airport Research Institute, Japan. 338 pp. (in Japanese).

Pathirage, K.S. (2000). *Critical Assessment of the CANLEX Blast Experiment to Facilitate a Development of an In-Situ Liquefaction Methodology Using Explosives.* Thesis in partial fulfillment of the requirements for the Degree of Master of Science, Department of Civil Engineering, The University of British Columbia, December.

Rollins, K.M. (2004). Liquefaction Mitigation Using Vertical Composite Drains: Full Scale Testing. Final Report for Highway IDEA Project 94. Transportation Research Board, February 2004, 105 pp.

Rollins, K.M., Lane, J.D., Nicholson, P.G., and Rollins, R.E. (2004). "Liquefaction Hazard Assessment using Controlled-Blasting Techniques." *Proc. 11th International Conference on Soil Dynamics & Earthquake Engineering.* Vol. 2, 2004, pp. 630 – 637.

Rollins, K.M., Lane, J.D., Dibb, E., Ashford, S.A., and Mullins, A.G. (2005a). Pore Pressure Measurement in Blast-Induced Liquefaction Experiments. Transportation Research Record 1936, Soil Mechanics 2005, TRB, Washington D.C., pp. 210-220.

Rollins, K.M., Gerber, T.M., Lane, J.D., and Ashford, S.A. (2005b). Lateral Resistance of a Full-Scale Pile Group in Liquefied Sand. *Journal of Geotechnical and Geoenvironmental Engineering*. January 2005, pp. 115 – 125.

Schiff, A.J., editor. (1998). *Hyogoken-Nanbu (Kobe) Earthquake of January 17, 1995: Lifeline Performance.* ASCE Technical Council on Lifeline Earthquake Engineering Monograph No. 14, September 2008.

Seed, H.B., and Whitman, R.V. (1970). "Design of Earth Retaining Structures for Dynamic Loads." *Proceedings, ASCE Specialty Conference on Lateral Stresses in the Ground and Design of Earth Retaining Structures.* pp. 103-147.

Seed, H.B., and Idriss, I.M. (1971). "Simplified procedure for evaluation of soil liquefaction potential." *Journal of the Soil Mechanics and Foundations Division*, ASCE, 107(9), pp. 1249 – 1274.

Seed, R.B., Cetin, K.O., Moss, R.E.S., Kammerer, A.M., Wu, J., Pestana, J.M., and Riemer, M.F. (2003). "Recent Advances in Soil Liquefaction Engineering and Seismic Site Response Evaluation: A Unified and Consistent Framework." *Proceedings: Fourth International Conference on Recent Advances in Geotechnical Earthquake Engineering and Soil Dynamics and Symposium in Honor of Professor W.D. Liam Finn*, San Diego, March 26 – 31.

Solymar, S.V. (1984). "Compaction of Alluvial Sands by Deep Blasting". *Canadian Geotechnical Journal*, 21(2), pp. 305 – 321.

Strand, S.R. (2008). *Liquefaction Mitigation using Vertical Composite Drains and Liquefaction-Induced Downdrag on Piles: Implications for Deep Foundation Design.* A Dissertation in partial fulfillment of the requirement for the degree of Doctor of Philosophy, Department of Civil and Environmental Engineering, Brigham Young University, April 2008.

Studer, J. and Kok, L. (1980). Blast-Induced Excess Porewater Pressure and Liquefaction Experience and Application. International Symposium on Soils under Cyclic and Transient Loading, Swansea, UK, January 7 – 11, pp. 581 - 593.

Sugano, T., Kohama, E., Mitoh, M., and Shiozaki, Y. (2002). Seismic Performance of Urban, Reclaimed and Port Areas – Full Scale Experiment at Tokachi Port by Controlled Blasting Technique. The Earthquake Engineering Symposium Proceedings, Vol. 11, pp. 901 – 906.

USGS Earthquakes Hazards Program. The Great 1906 San Francisco Earthquake. United States Geological Survey (USGS). http://earthquake.usgs.gov/regional/nca/1906/18april/casualties.php (accessed December 2009).

Youd, T.L., et al.. (2001). "Liquefaction Resistance of Soils: Summary Report from the 1996 NCEER and 1998 NCEER/NSF Workshops on Evaluation of Liquefaction Resistance of Soils." *Journal of Geotechnical and Geoenvironmental Engineering.* ASCE, 127(10), pp. 817-833.

APPENDICES

APPENDIX A – SITE & TEST INFORMATION FOR CASE HISTORIES

A.1 PORT OF ISHIKARI, HOKKAIDO ISLAND, JAPAN

Note: All pore pressure data was provided by Dr. Hideo Nakazawa of the Port and Airport Research Institute (PARI).

A.1.1 Residual Pore Pressure Results during First Blast of Pilot Test #2

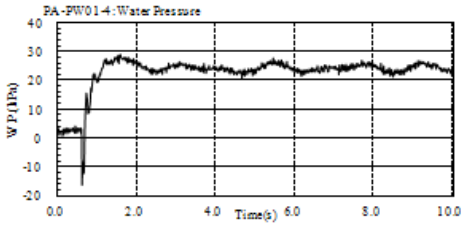

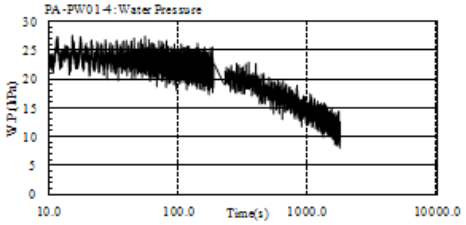

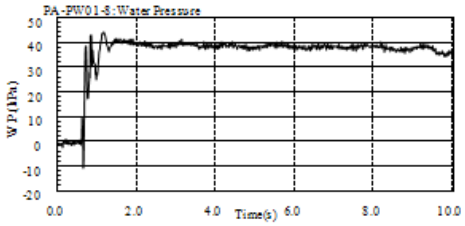

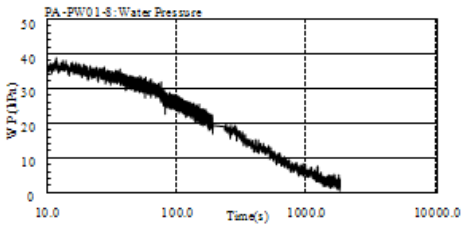

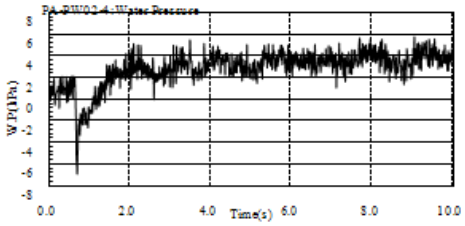

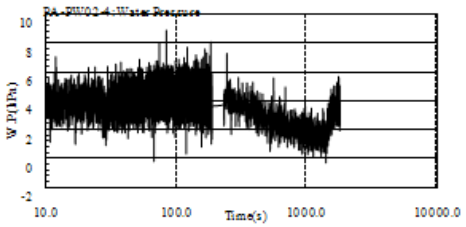

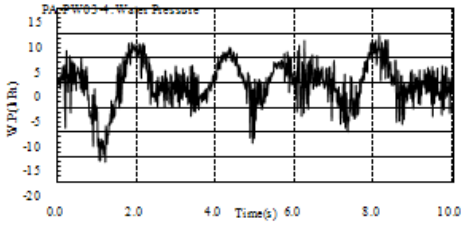

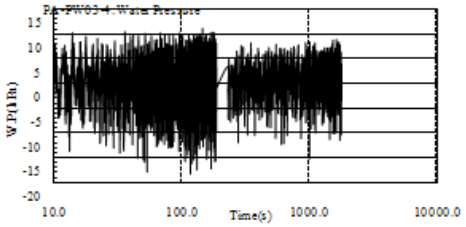

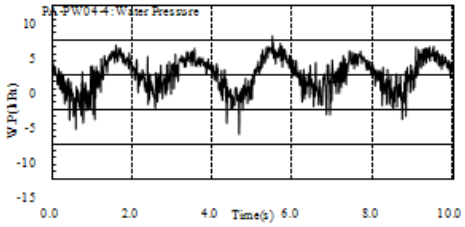

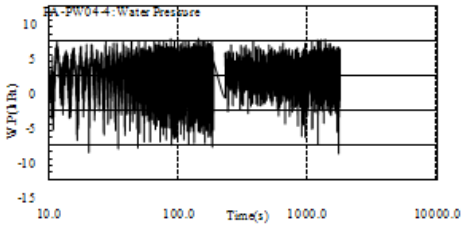

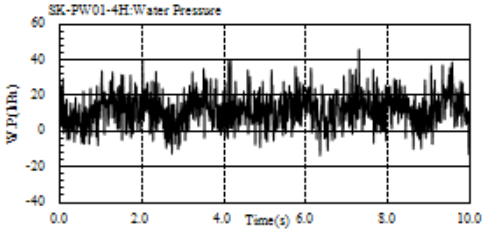
SK-PW01-4H:Water Pressure
W P(Bh)
Time(s)

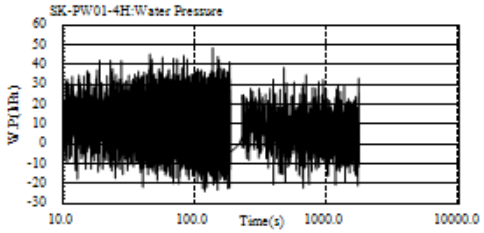
SK-PW01-4H:Water Pressure
W P(Bh)
Time(s)

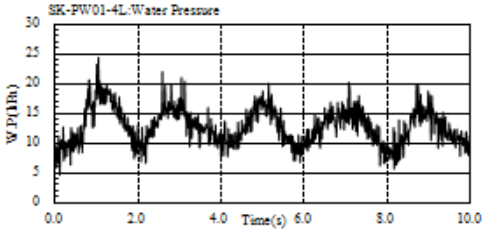
SK-PW01-4L:Water Pressure
W P(Bh)
Time(s)

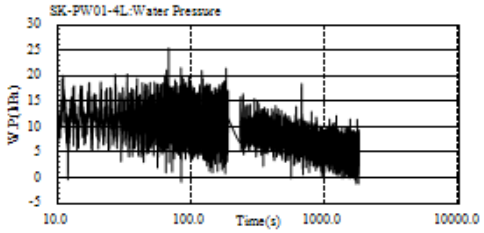
SK-PW01-4L:Water Pressure
W P(Bh)
Time(s)

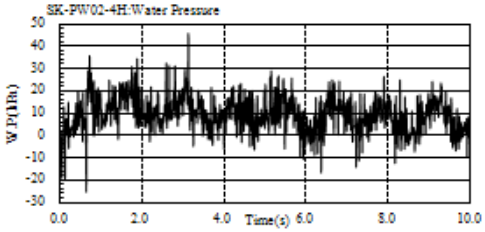
SK-PW02-4H:Water Pressure
W P(Bh)
Time(s)

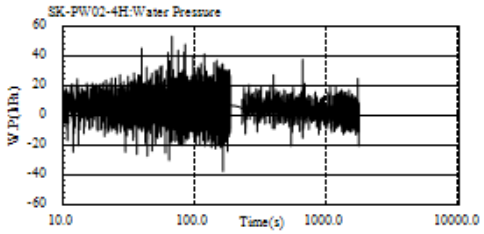
SK-PW02-4H:Water Pressure
W P(Bh)
Time(s)

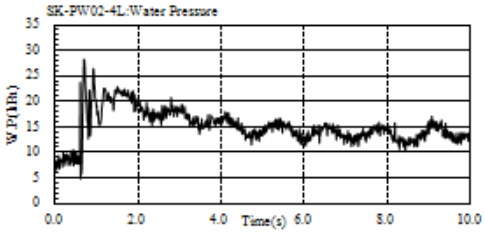
SK-PW02-4L:Water Pressure
W P(Bh)
Time(s)

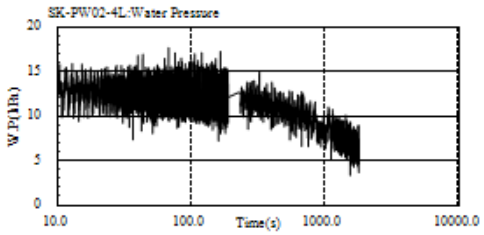
SK-PW02-4L:Water Pressure
W P(Bh)
Time(s)

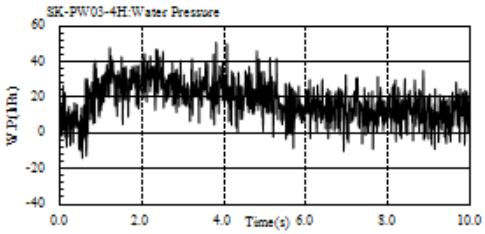
SK-PW03-4H:Water Pressure
W P(Bh)
Time(s)

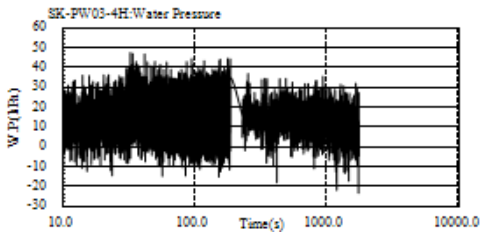
SK-PW03-4H:Water Pressure
W P(Bh)
Time(s)

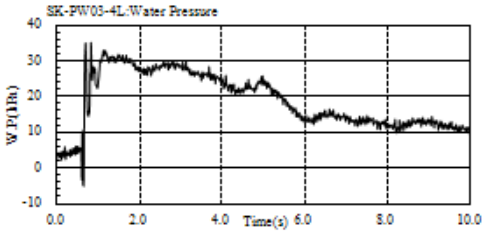
SK-PW03-4L:Water Pressure
W P(Mb)
Time(s)

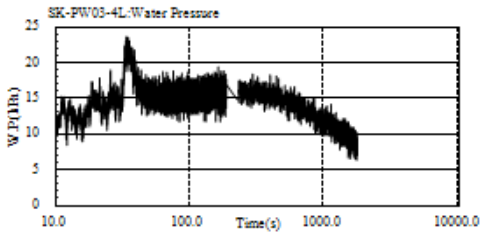
SK-PW03-4L:Water Pressure
W P(Mb)
Time(s)

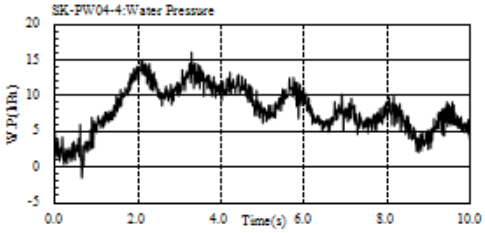
SK-PW04-4:Water Pressure
W P(Mb)
Time(s)

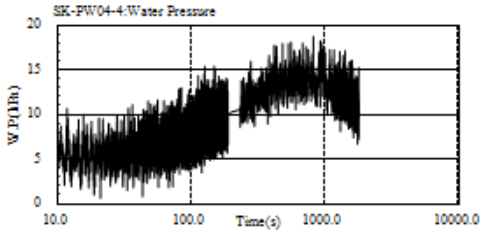
SK-PW04-4:Water Pressure
W P(Mb)
Time(s)

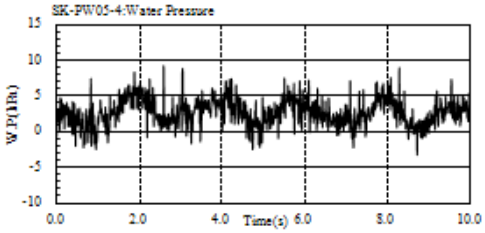
SK-PW05-4:Water Pressure
W P(Mb)
Time(s)

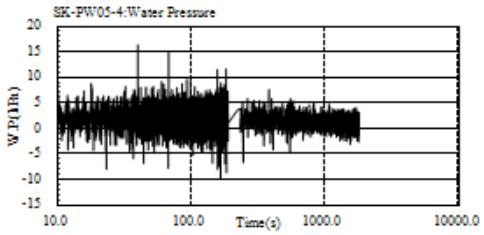
SK-PW05-4:Water Pressure
W P(Mb)
Time(s)

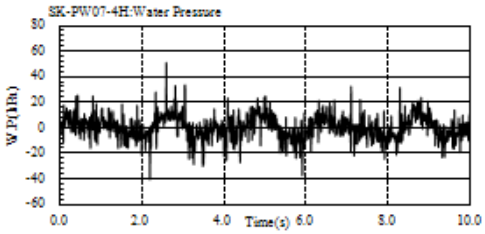
SK-PW07-4H:Water Pressure
W P(Mb)
Time(s)

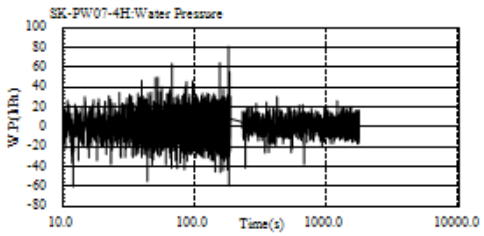
SK-PW07-4H:Water Pressure
W P(Mb)
Time(s)

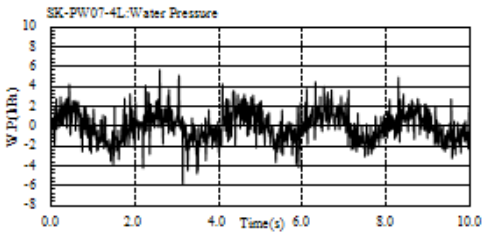
SK-PW07-4L:Water Pressure
W P(Mb)
Time(s)

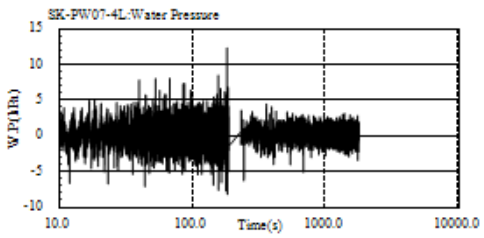
SK-PW07-4L:Water Pressure
W P(Mb)
Time(s)

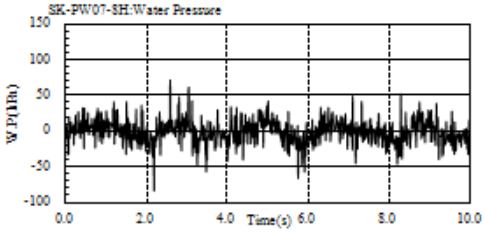
SK-PW07-SH:Water Pressure
W P(lBf)
Time(s)

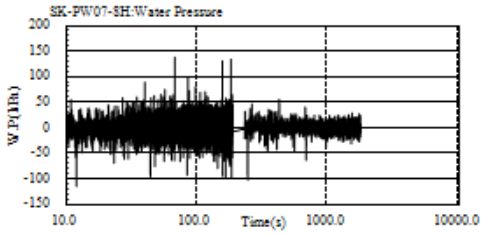
SK-PW07-SH:Water Pressure
W P(lBf)
Time(s)

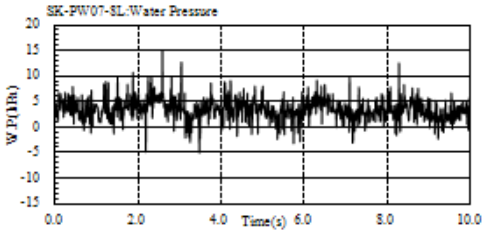
SK-PW07-SL:Water Pressure
W P(lBf)
Time(s)

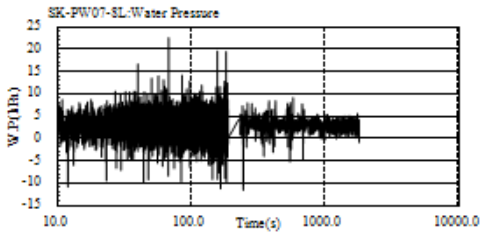
SK-PW07-SL:Water Pressure
W P(lBf)
Time(s)

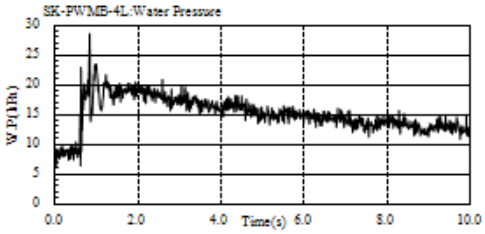
SK-PWMB-4L:Water Pressure
W P(lBf)
Time(s)

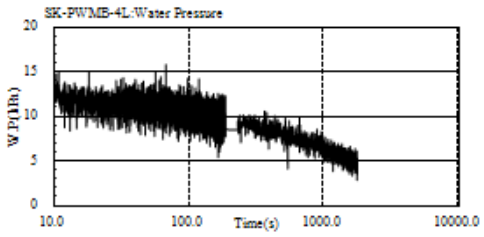
SK-PWMB-4L:Water Pressure
W P(lBf)
Time(s)

A.1.2 Residual Pore Pressure Results during Remaining Blasts of Pilot Test #2

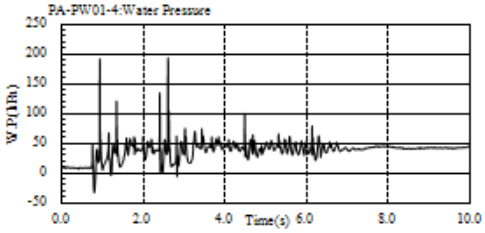

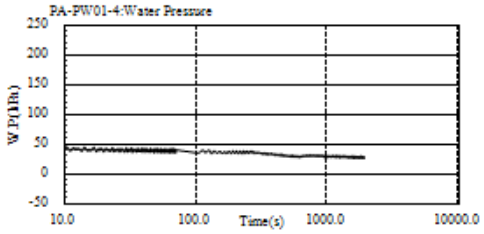

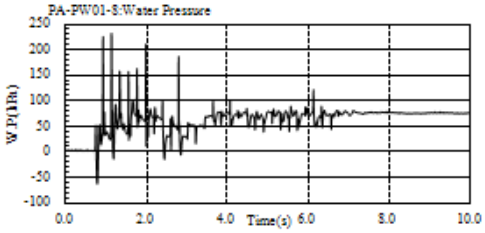

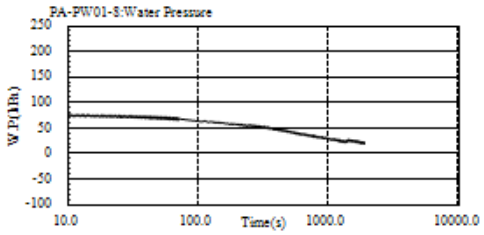

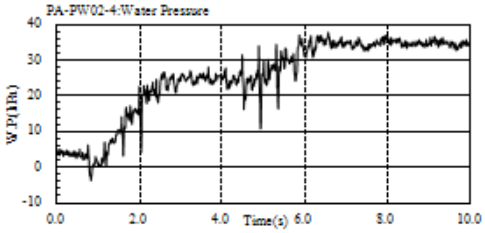

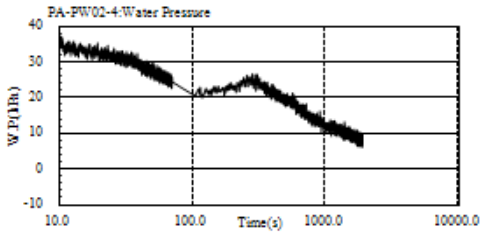

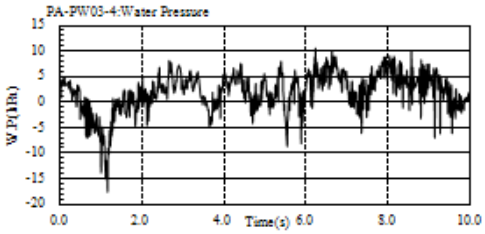

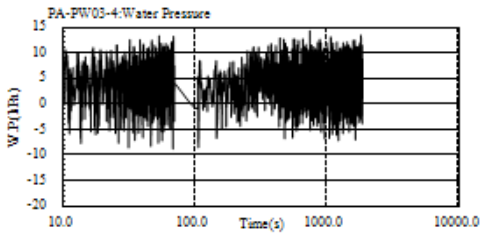

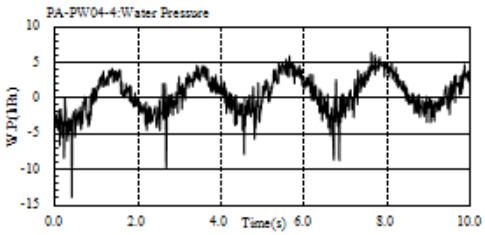

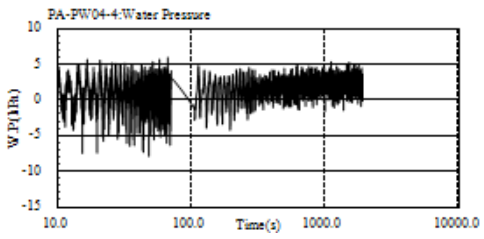

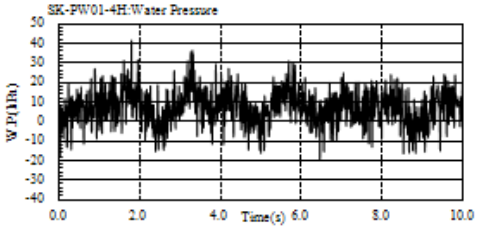
SK-PW01-4H:Water Pressure
WP(kPa)
Time(s)

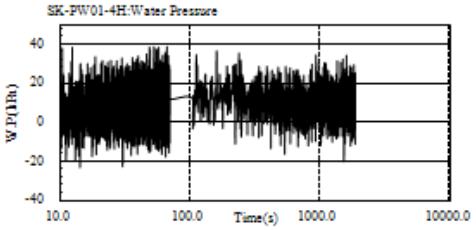
SK-PW01-4H:Water Pressure
WP(kPa)
Time(s)

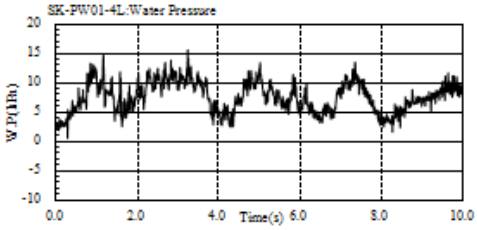
SK-PW01-4L:Water Pressure
WP(kPa)
Time(s)

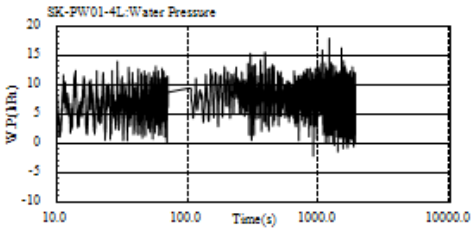
SK-PW01-4L:Water Pressure
WP(kPa)
Time(s)

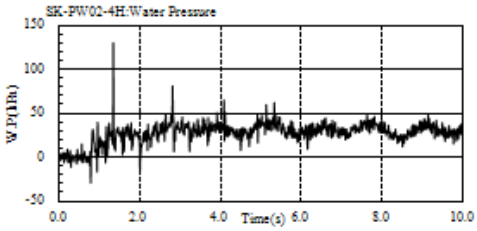
SK-PW02-4H:Water Pressure
WP(kPa)
Time(s)

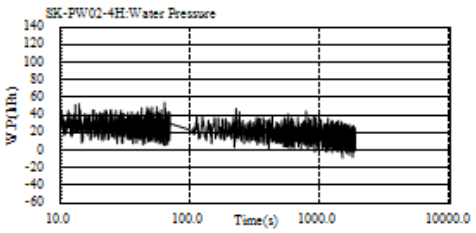
SK-PW02-4H:Water Pressure
WP(kPa)
Time(s)

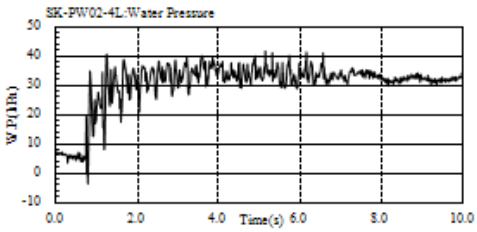
SK-PW02-4L:Water Pressure
WP(kPa)
Time(s)

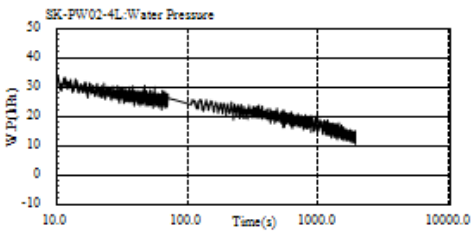
SK-PW02-4L:Water Pressure
WP(kPa)
Time(s)

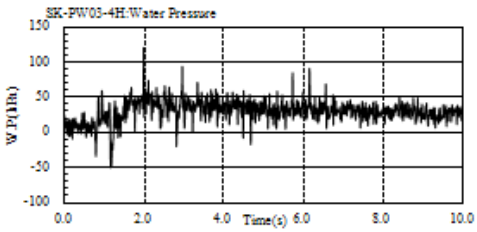
SK-PW03-4H:Water Pressure
WP(kPa)
Time(s)

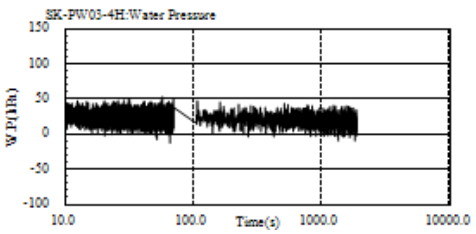
SK-PW03-4H:Water Pressure
WP(kPa)
Time(s)

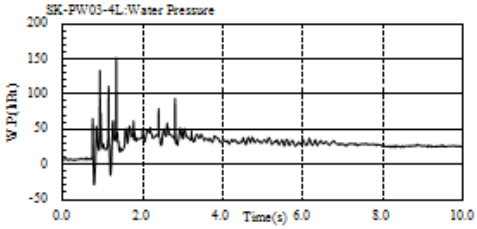
SK-PW03-4L:Water Pressure
W.P(kPa)
Time(s)

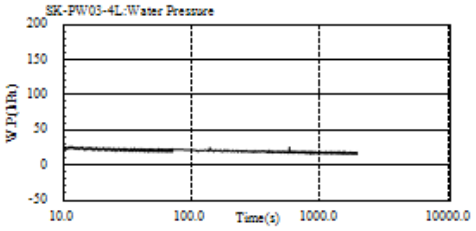
SK-PW03-4L:Water Pressure
W.P(kPa)
Time(s)

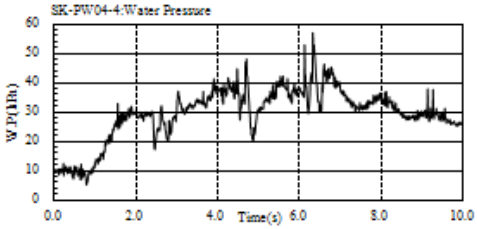
SK-PW04-4:Water Pressure
W.P(kPa)
Time(s)

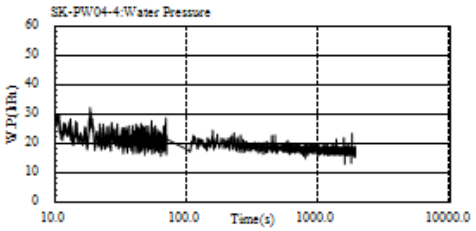
SK-PW04-4:Water Pressure
W.P(kPa)
Time(s)

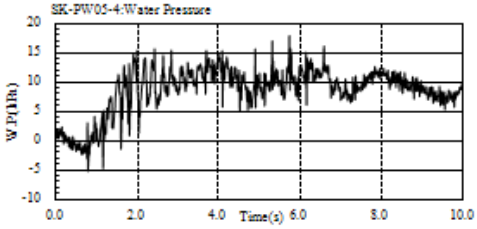
SK-PW05-4:Water Pressure
W.P(kPa)
Time(s)

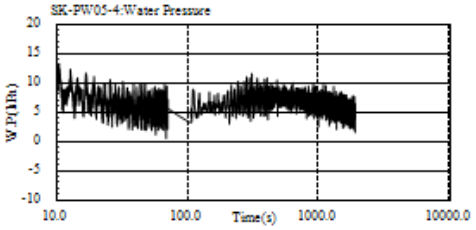
SK-PW05-4:Water Pressure
W.P(kPa)
Time(s)

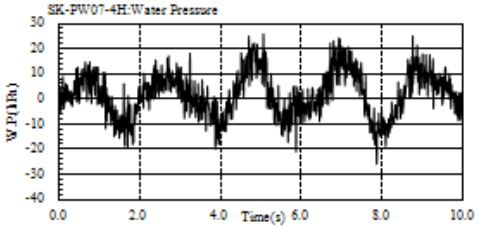
SK-PW07-4H:Water Pressure
W.P(kPa)
Time(s)

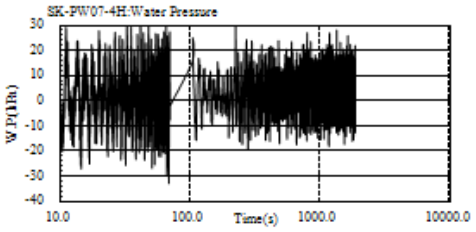
SK-PW07-4H:Water Pressure
W.P(kPa)
Time(s)

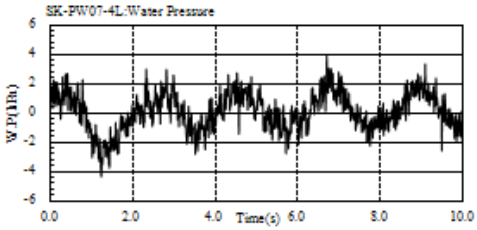
SK-PW07-4L:Water Pressure
W.P(kPa)
Time(s)

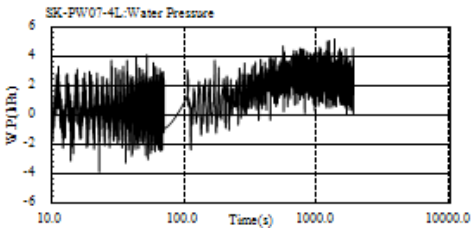
SK-PW07-4L:Water Pressure
W.P(kPa)
Time(s)

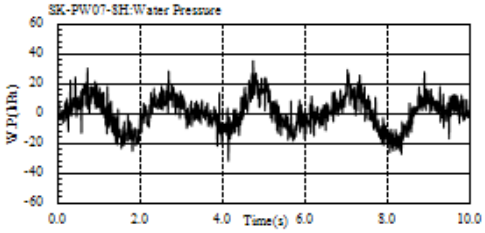
SK-PW07-SH:Water Pressure
W.P(kPa)
Time(s)

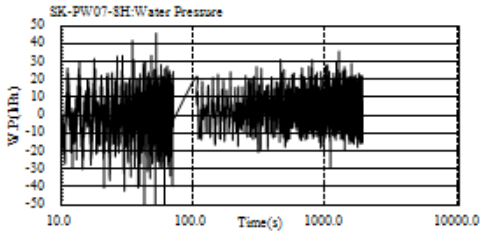
SK-PW07-SH:Water Pressure
W.P(kPa)
Time(s)

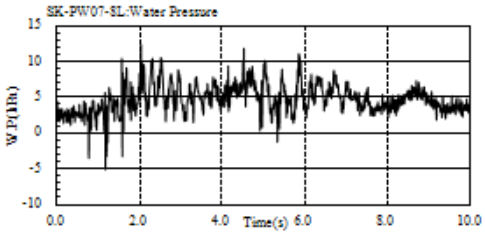
SK-PW07-SL:Water Pressure
W.P(kPa)
Time(s)

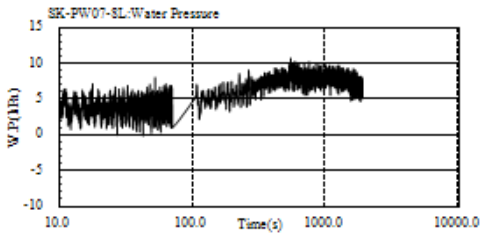
SK-PW07-SL:Water Pressure
W.P(kPa)
Time(s)

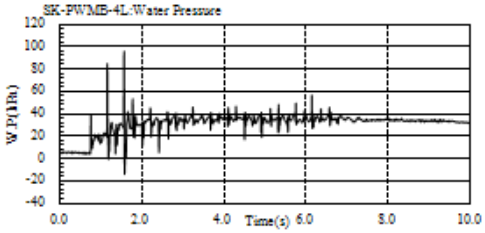
SK-PWMB-4L:Water Pressure
W.P(kPa)
Time(s)

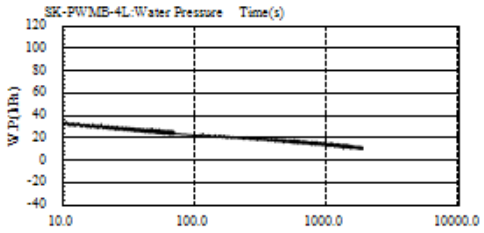
SK-PWMB-4L:Water Pressure
Time(s)
W.P(kPa)

A.1.3 Residual Pore Pressure Results during Full-Scale Test, Ishikari

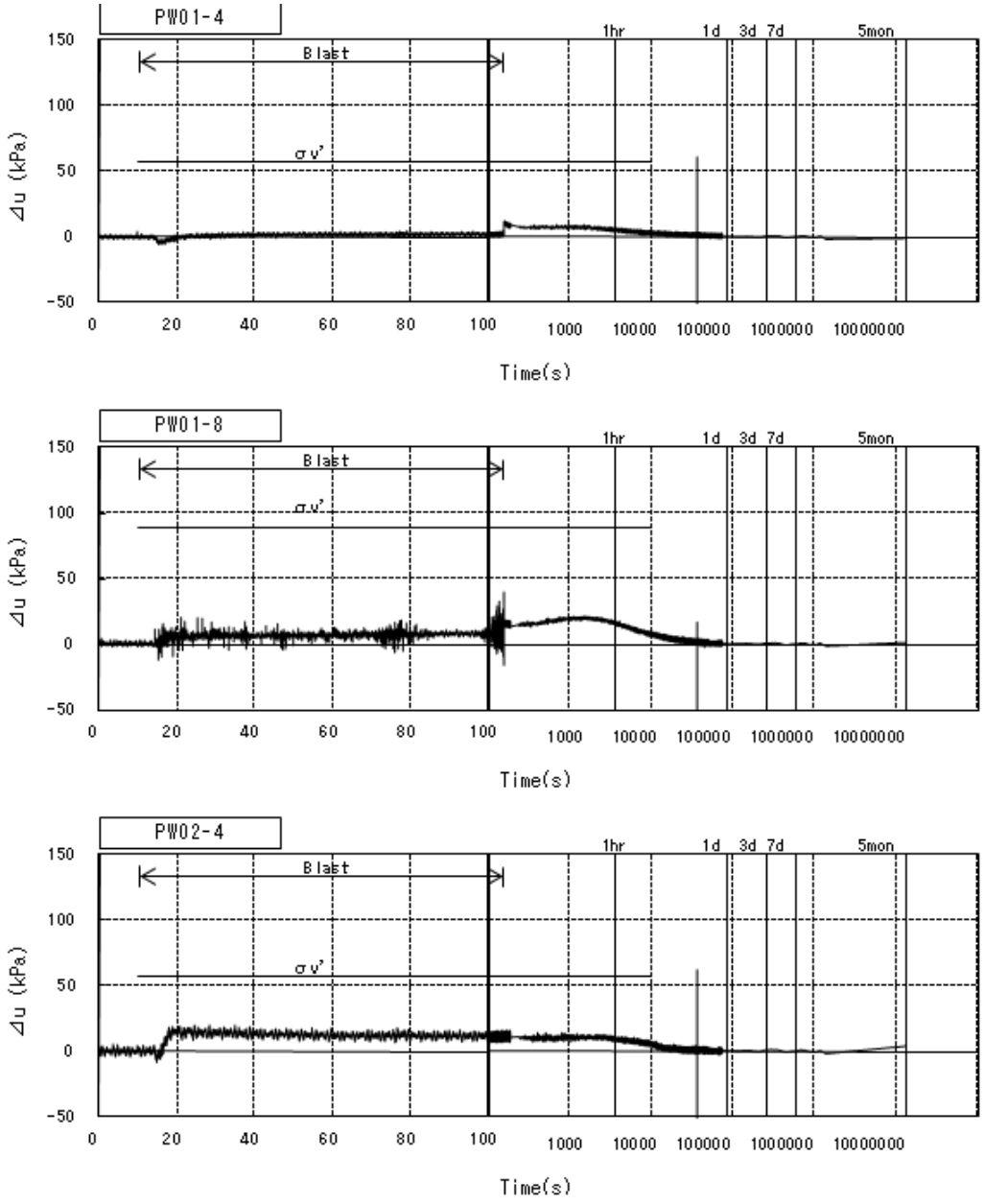

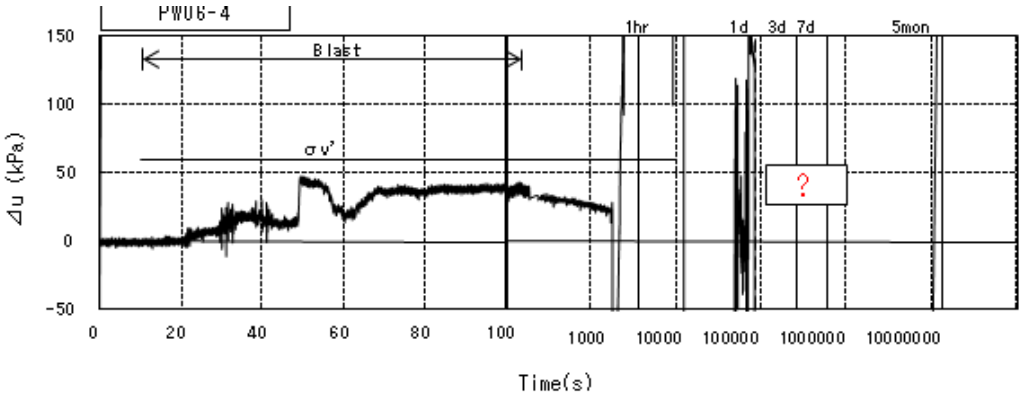
PWU6-4
Blast
1hr
1d
3d
7d
5mon
σv'
?
Δu (kPa)
Time(s)

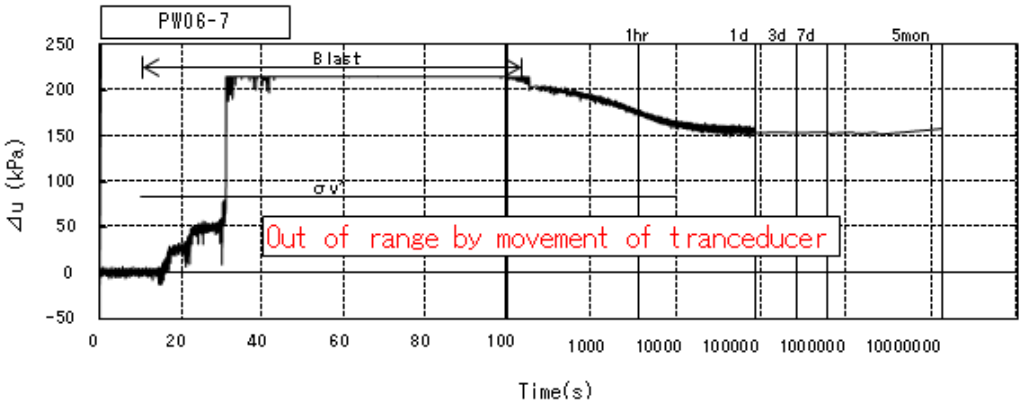
PW06-7
Blast
1hr
1d
3d
7d
5mon
σv'
Out of range by movement of tranceducer
Δu (kPa)
Time(s)

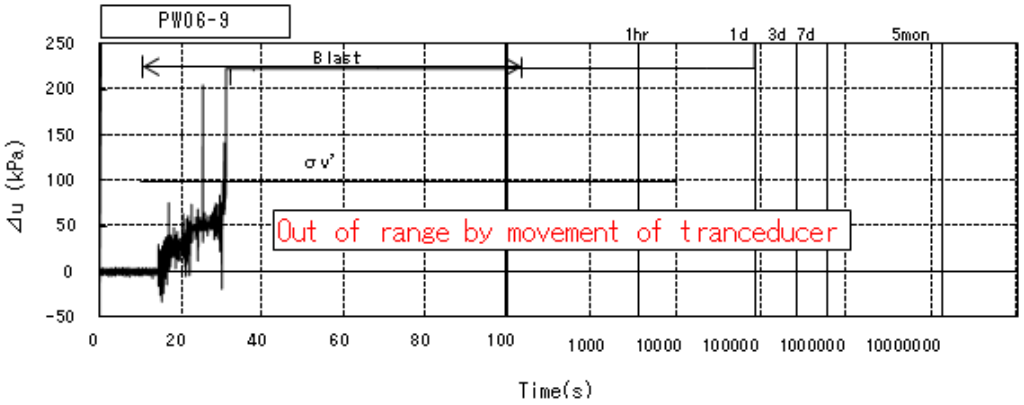
PW06-9
Blast
1hr
1d
3d
7d
5mon
σv'
Out of range by movement of tranceducer
Δu (kPa)
Time(s)

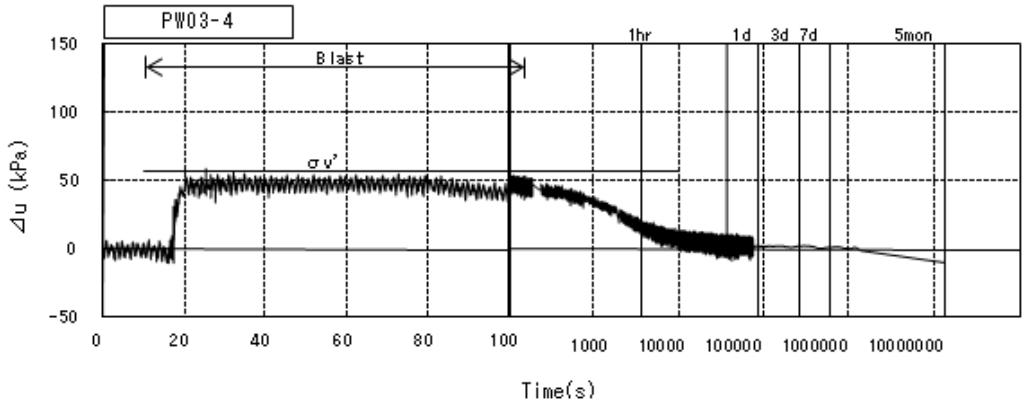
PW03-4
Blast
σv'
1hr
1d
3d
7d
5mon
Δu (kPa)
150
100
50
0
-50
0
20
40
60
80
100
1000
10000
100000
1000000
10000000
Time(s)

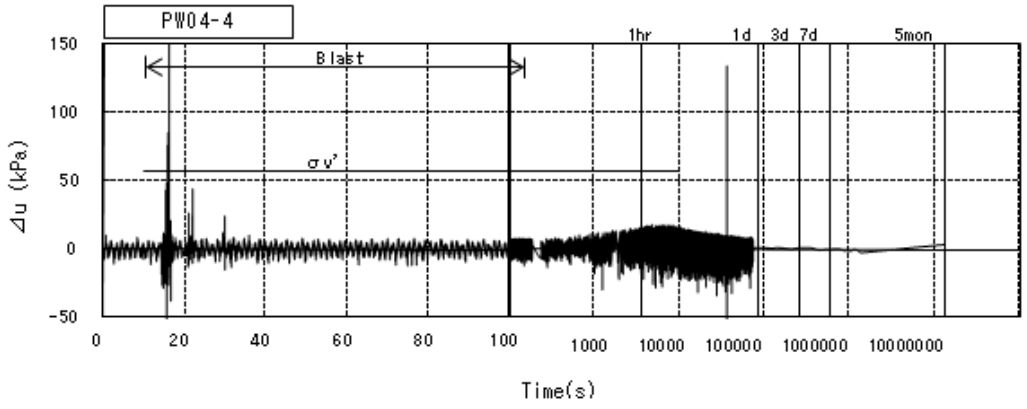
PW04-4
Blast
σv'
1hr
1d
3d
7d
5mon
Δu (kPa)
150
100
50
0
-50
0
20
40
60
80
100
1000
10000
100000
1000000
10000000
Time(s)

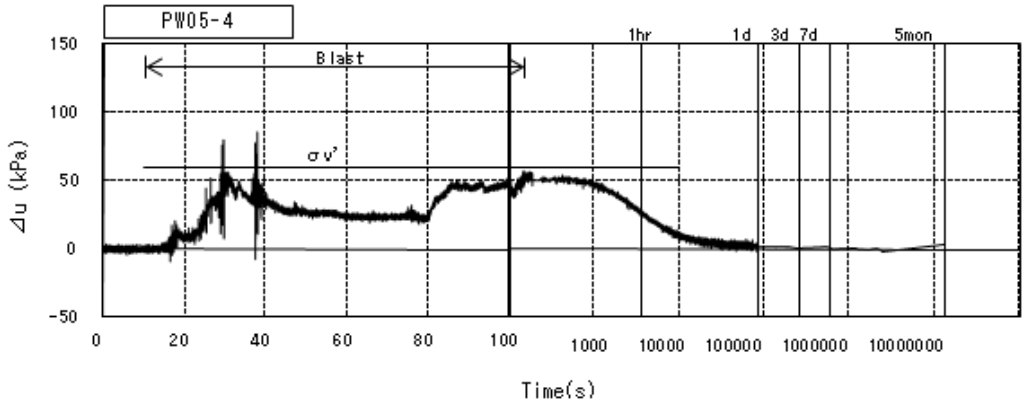
PW05-4
Blast
σv'
1hr
1d
3d
7d
5mon
Δu (kPa)
150
100
50
0
-50
0
20
40
60
80
100
1000
10000
100000
1000000
10000000
Time(s)

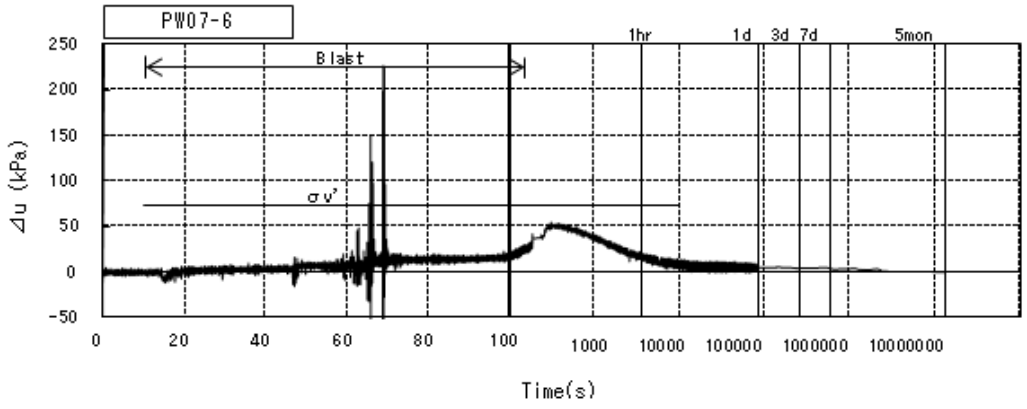
PW07-6
Blast
1hr
1d
3d
7d
5mon
σv'
Δu (kPa)
Time(s)

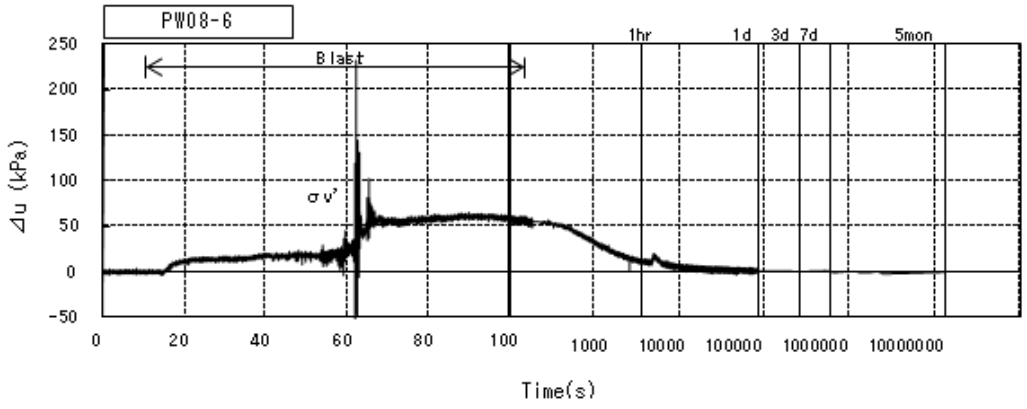
PW08-6
Blast
1hr
1d
3d
7d
5mon
σv'
Δu (kPa)
Time(s)

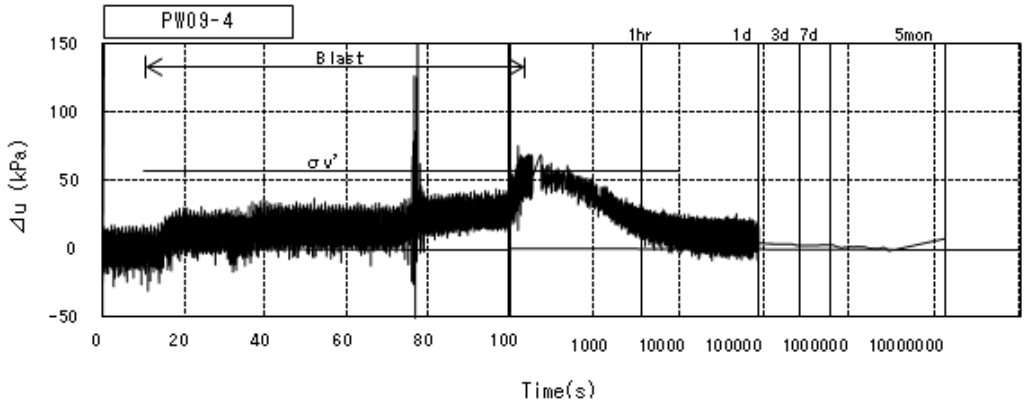
PW08-4
Blast
1hr
1d
3d
7d
5mon
σv'
Δu (kPa)
Time(s)

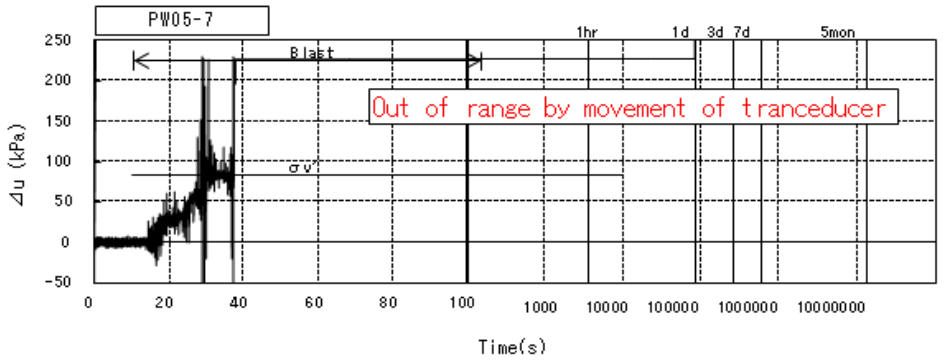
PW05-7
Blast
1hr
1d
3d
7d
5mon
Out of range by movement of tranceducer
σv'
Δu (kPa)
Time(s)

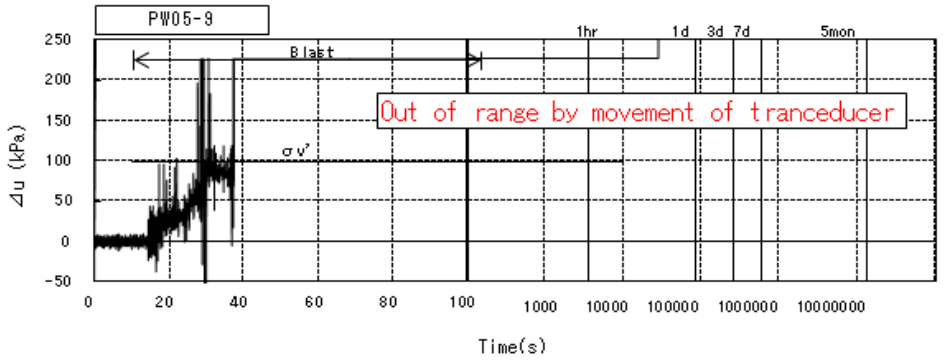
PW05-9
Blast
1hr
1d
3d
7d
5mon
Out of range by movement of tranceducer
σv'
Δu (kPa)
Time(s)

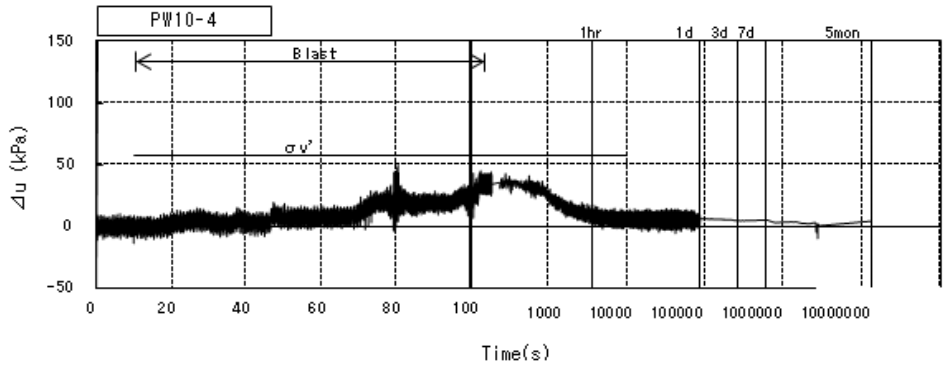
PW10-4
Blast
1hr
1d
3d
7d
5mon
σv'
Δu (kPa)
Time(s)

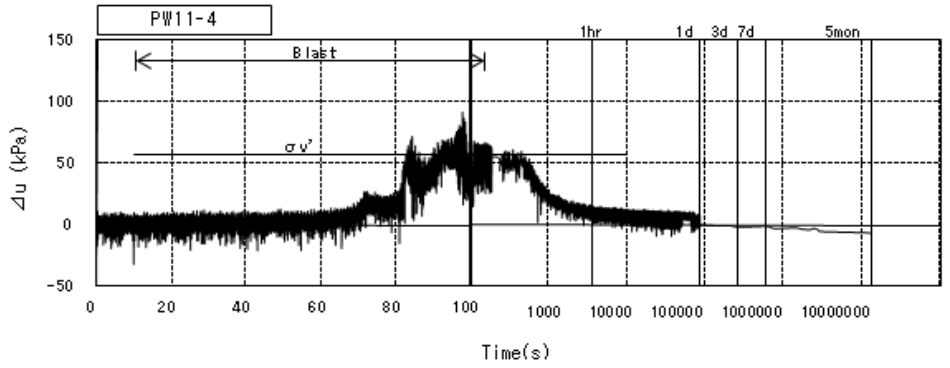
PW11-4
Blast
1hr
1d
3d
7d
5mon
σv'
Δu (kPa)
Time(s)

A.1.4 Blasting Layout for Full-Scale Test at Ishikari (PARI, 2009)

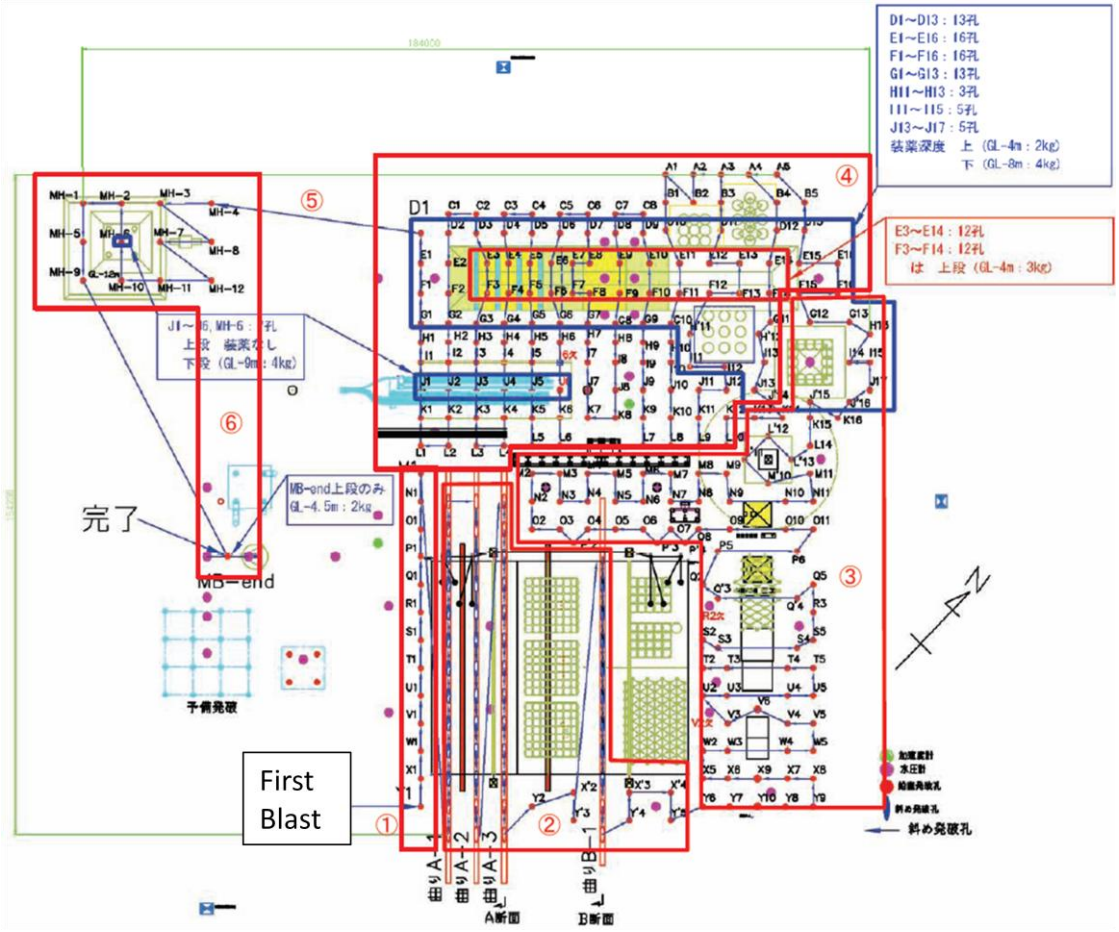

A.1.5 Pore Pressure Transducer layout for Full-Scale Test at Ishikari (PARI, 2009)

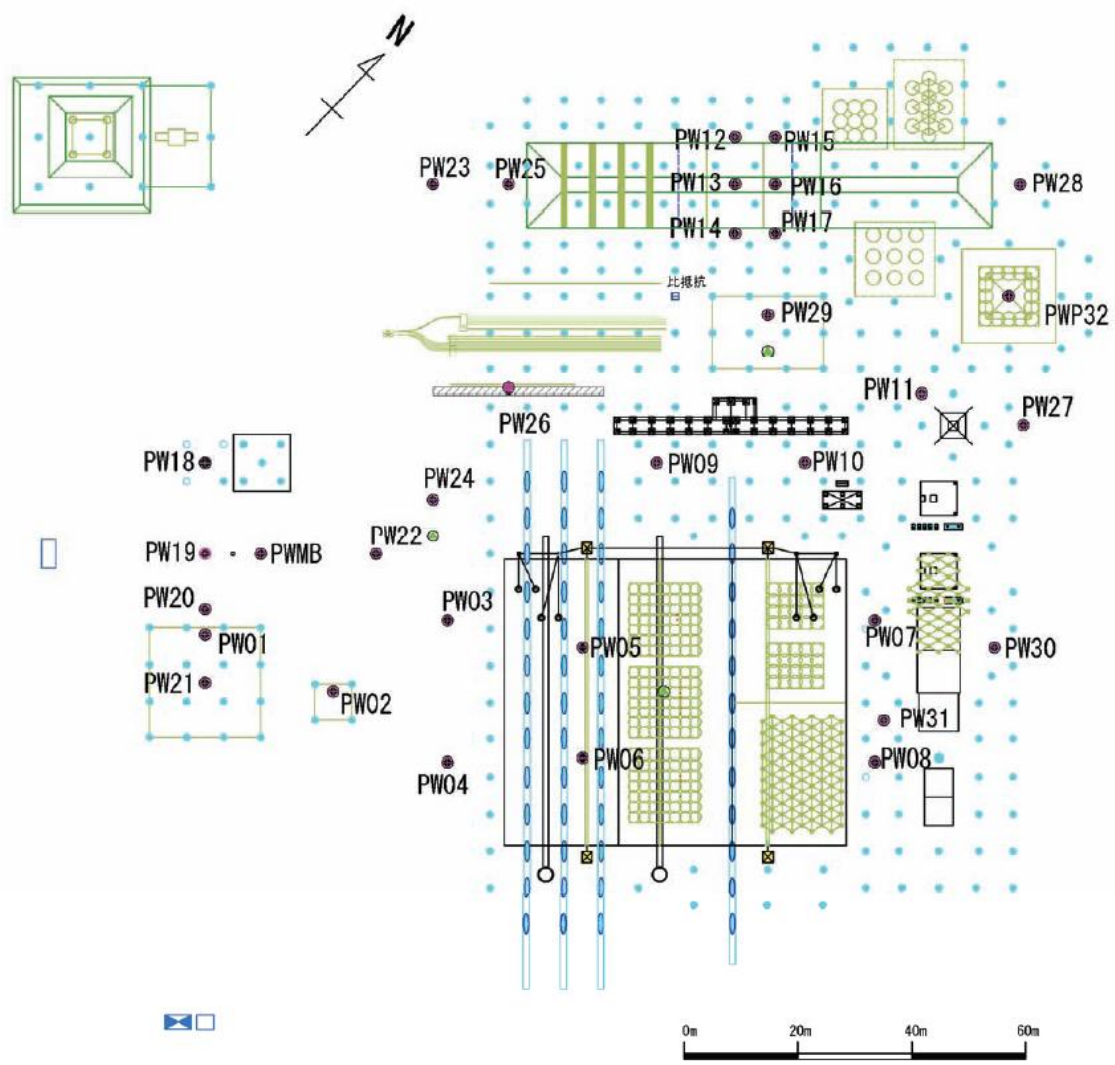

A.2 VANCOUVER, BRITISH COLUMBIA, CANADA, 2004

A.2.1 Residual Pore Pressure Results during the Pilot Study Blast #1

From Strand 2008

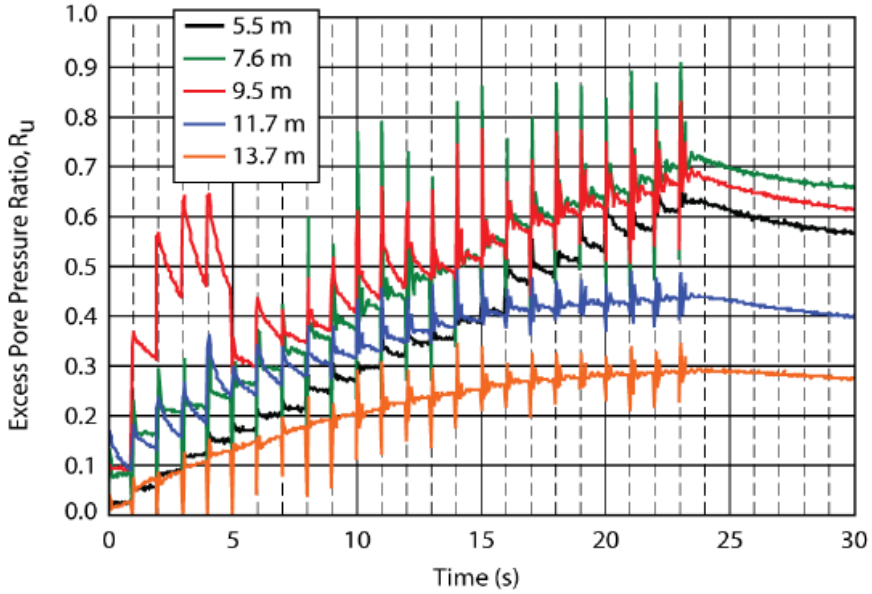

A.2.2 Residual Pore Pressure Results during the Pilot Study Blast #3

From Strand 2008

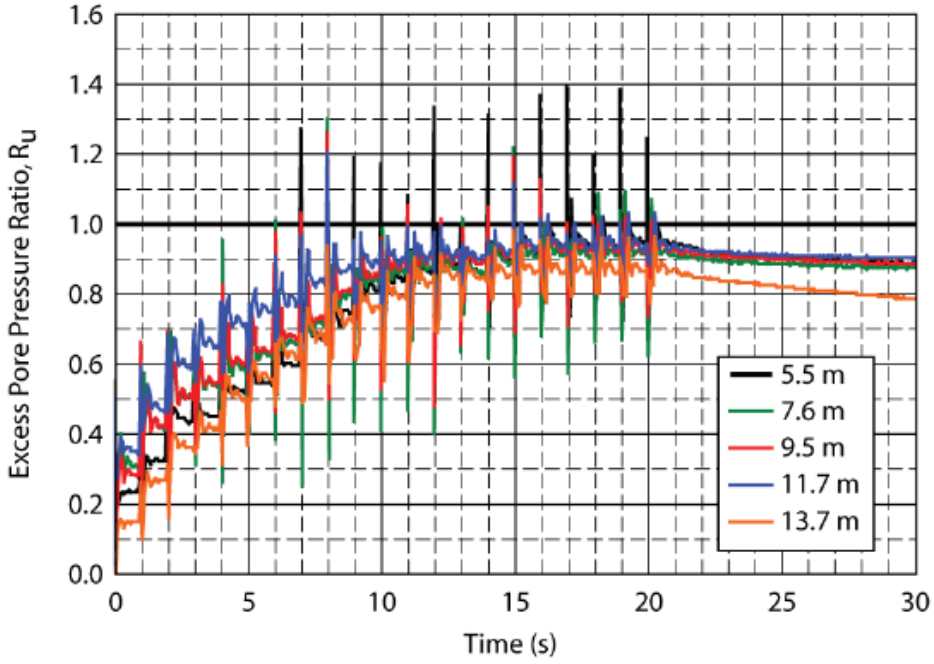

A.3 MAUI, HAWAII, 2004

A.3.1 Residual Pore Pressure Results during Blast #1

From Rollins et al. (2004)

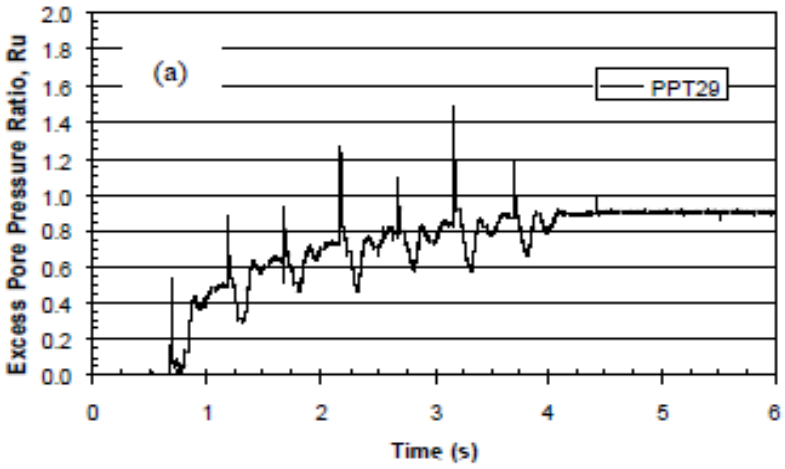

A.3.2 Residual Pore Pressure Results during Blast #2

From Rollins et al. (2004)

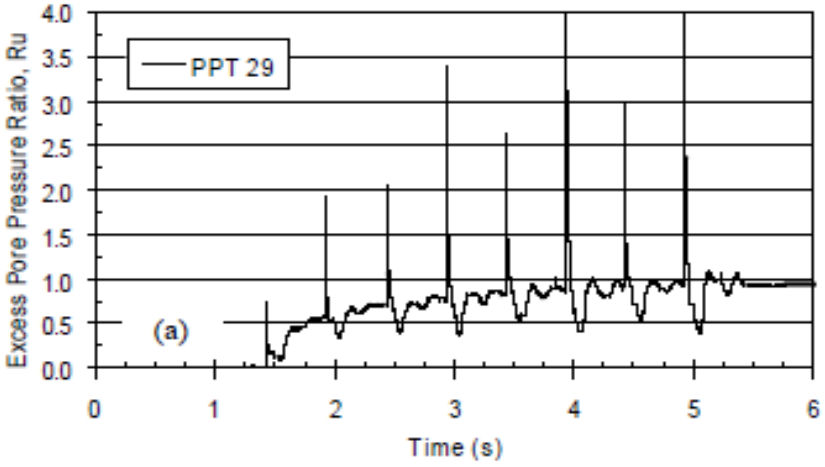

A.4 PORT OF TOKACHI, HOKKAIDO ISLAND, JAPAN

A.4.1 Residual Pore Pressure Results during Full-Scale Test #1

from Ashford and Juirnarongrit, 2004

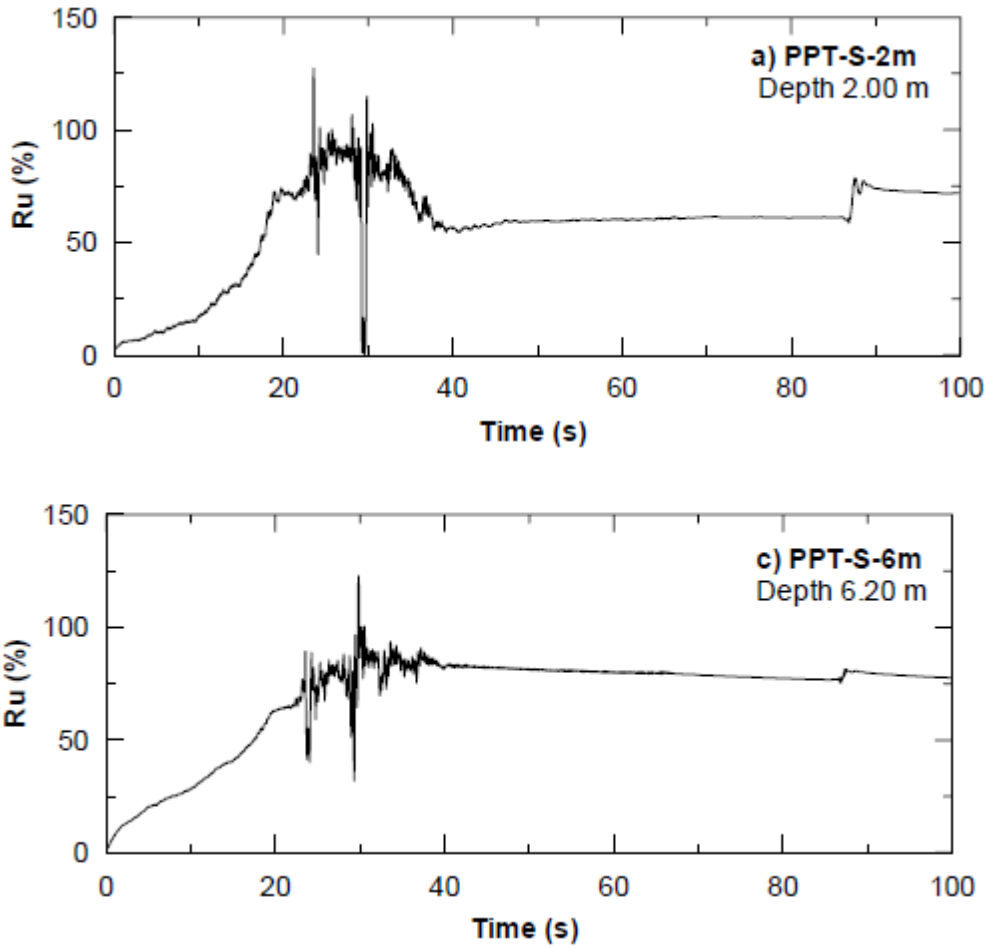

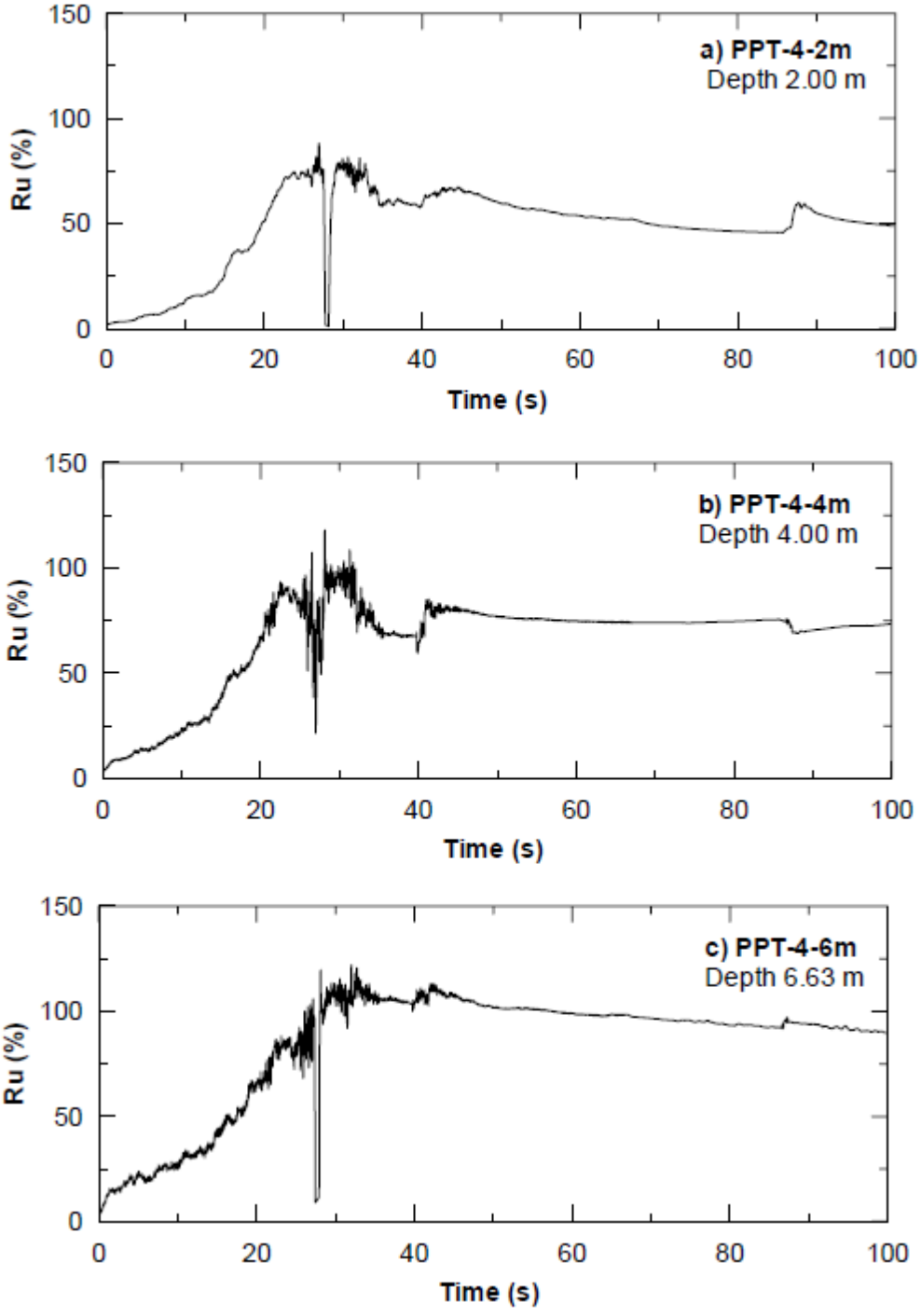
a) PPT-4-2m
Depth 2.00 m
b) PPT-4-4m
Depth 4.00 m
c) PPT-4-6m
Depth 6.63 m
Ru (%)
Time (s)
0
50
100
150
0
20
40
60
80
100

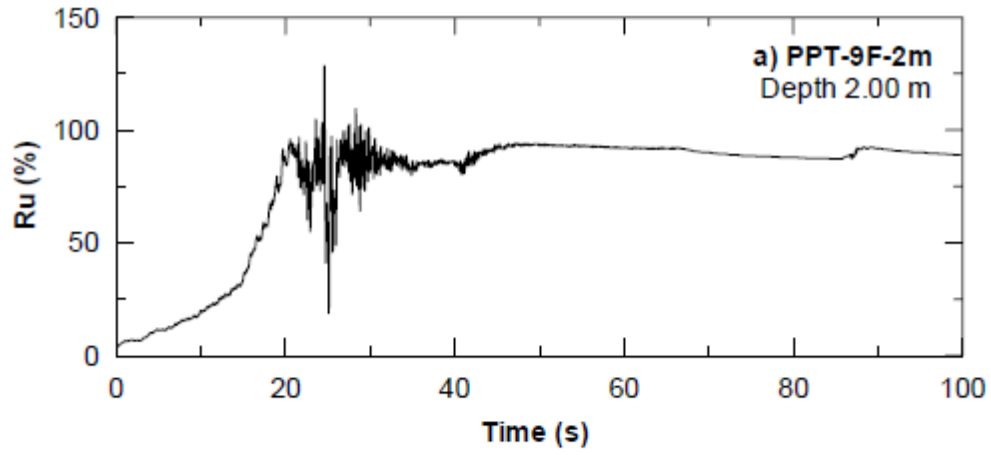
a) PPT-9F-2m
Depth 2.00 m
Ru (%)
Time (s)
0
50
100
150
0
20
40
60
80
100

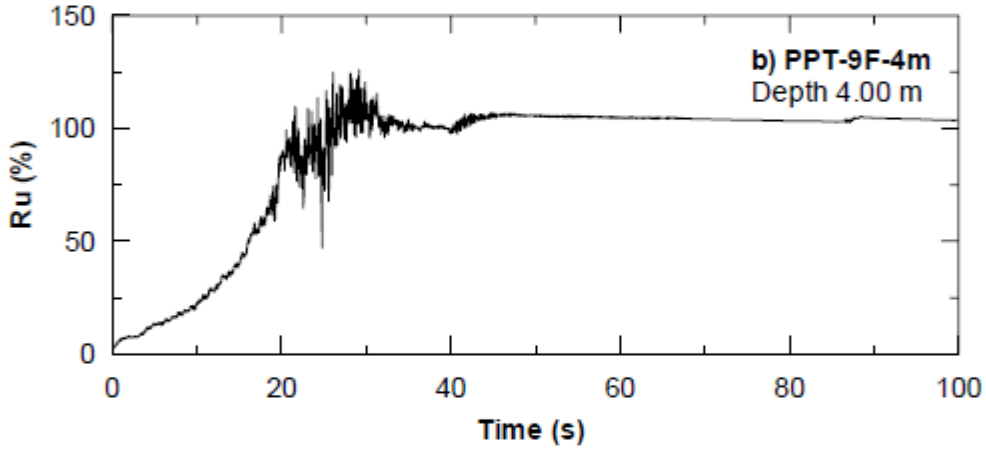
b) PPT-9F-4m
Depth 4.00 m
Ru (%)
Time (s)
0
50
100
150
0
20
40
60
80
100

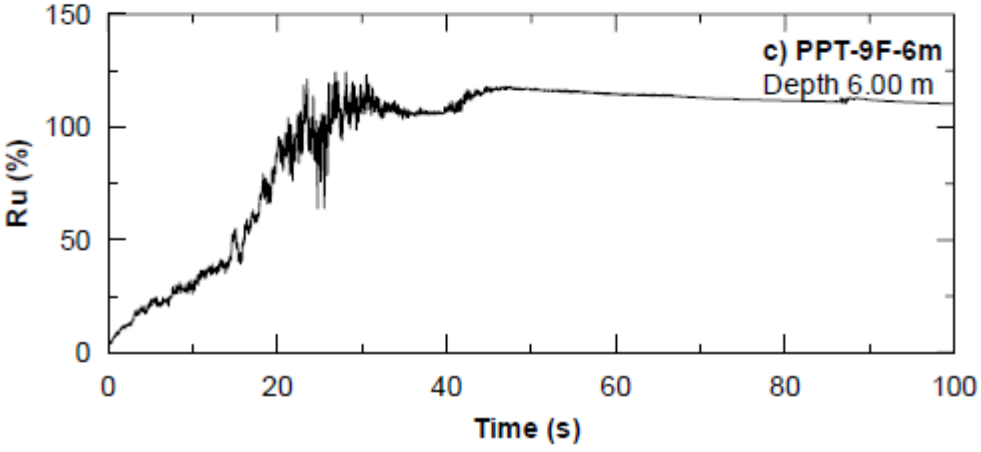
c) PPT-9F-6m
Depth 6.00 m
Ru (%)
Time (s)
0
50
100
150
0
20
40
60
80
100

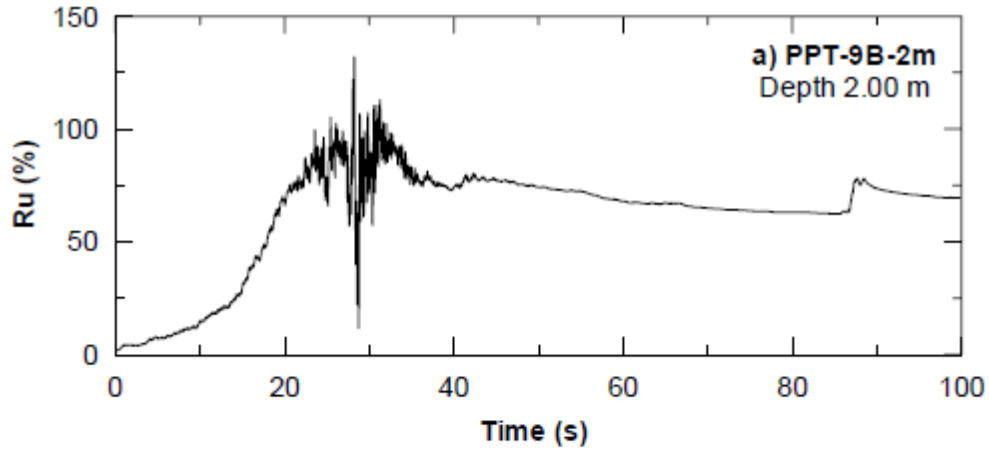
a) PPT-9B-2m
Depth 2.00 m
Ru (%)
Time (s)
0
50
100
150
0
20
40
60
80
100

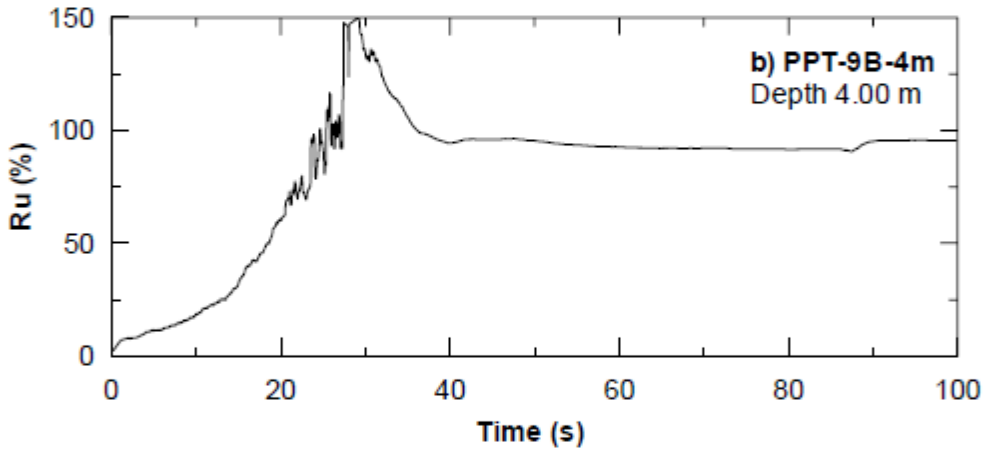
b) PPT-9B-4m
Depth 4.00 m
Ru (%)
Time (s)
0
50
100
150
0
20
40
60
80
100

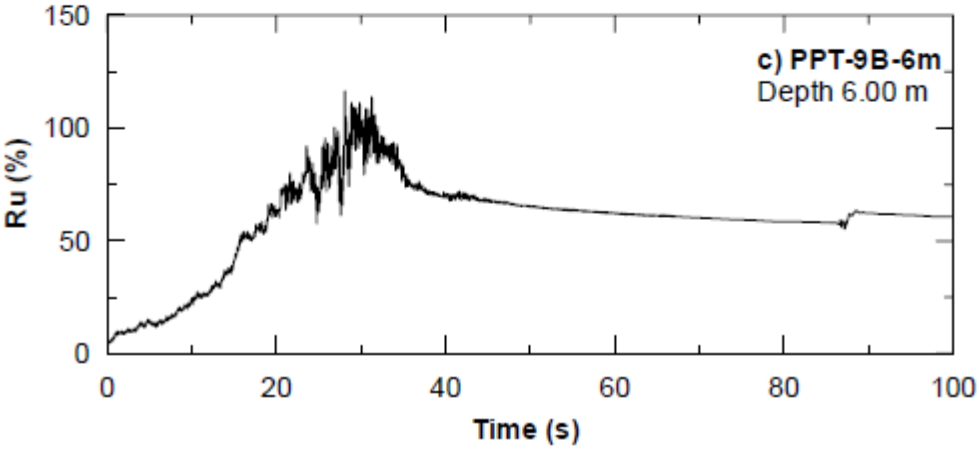
c) PPT-9B-6m
Depth 6.00 m
Ru (%)
Time (s)
0
50
100
150
0
20
40
60
80
100

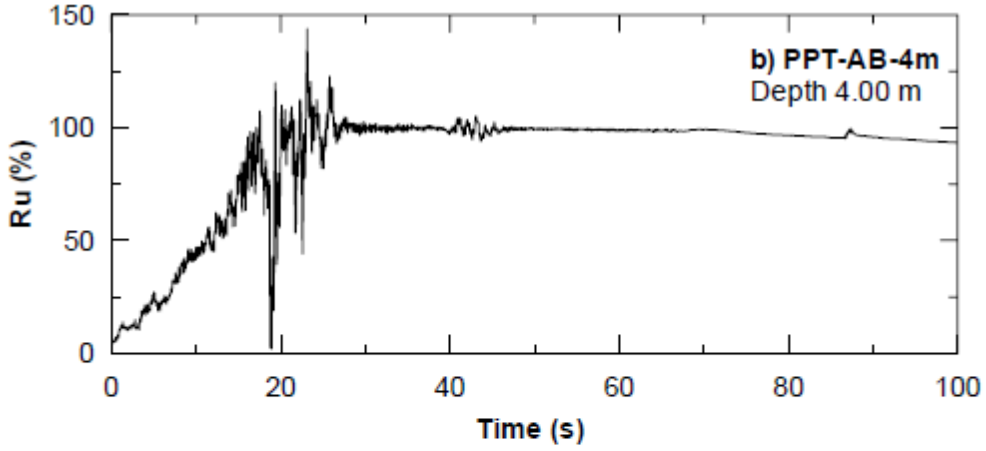
b) PPT-AB-4m
Depth 4.00 m
Ru (%)
Time (s)
0
50
100
150
0
20
40
60
80
100

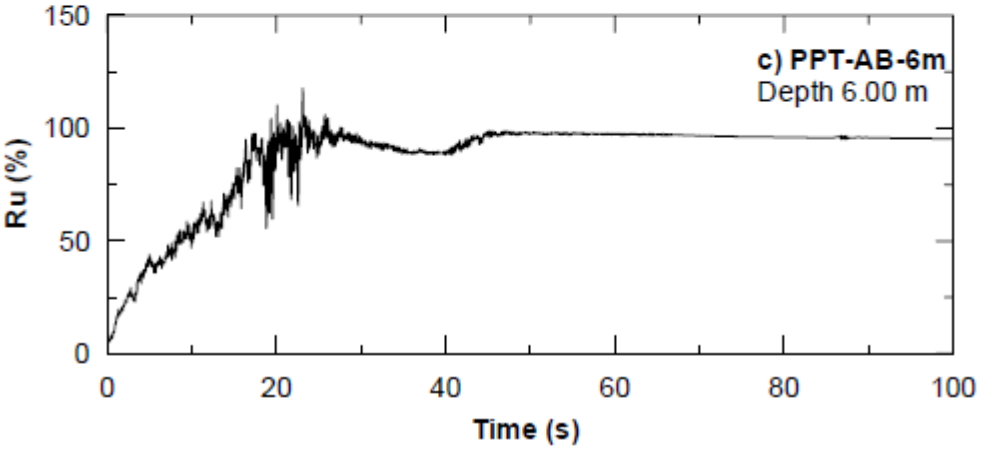
c) PPT-AB-6m
Depth 6.00 m
Ru (%)
Time (s)
0
50
100
150
0
20
40
60
80
100

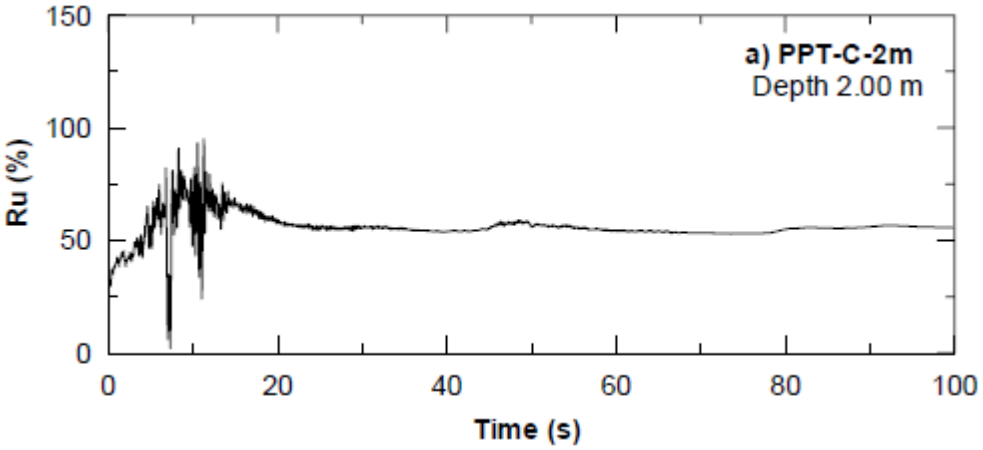
a) PPT-C-2m
Depth 2.00 m
Ru (%)
Time (s)
0
50
100
150
0
20
40
60
80
100

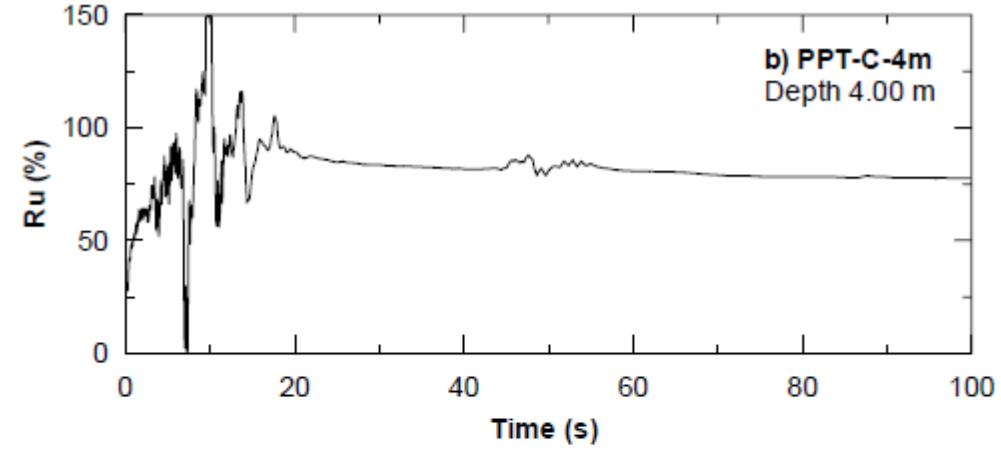
b) PPT-C-4m
Depth 4.00 m
Ru (%)
Time (s)
0
50
100
150
0
20
40
60
80
100

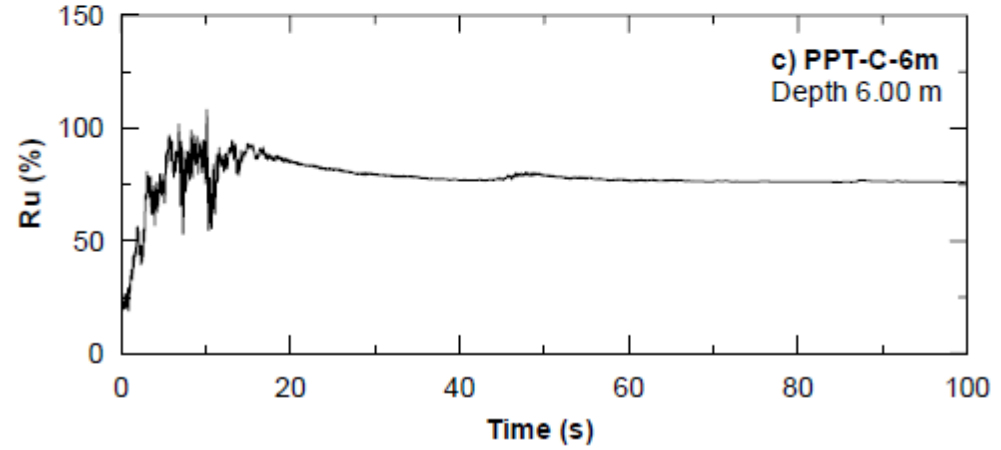
c) PPT-C-6m
Depth 6.00 m
Ru (%)
Time (s)
0
50
100
150
0
20
40
60
80
100

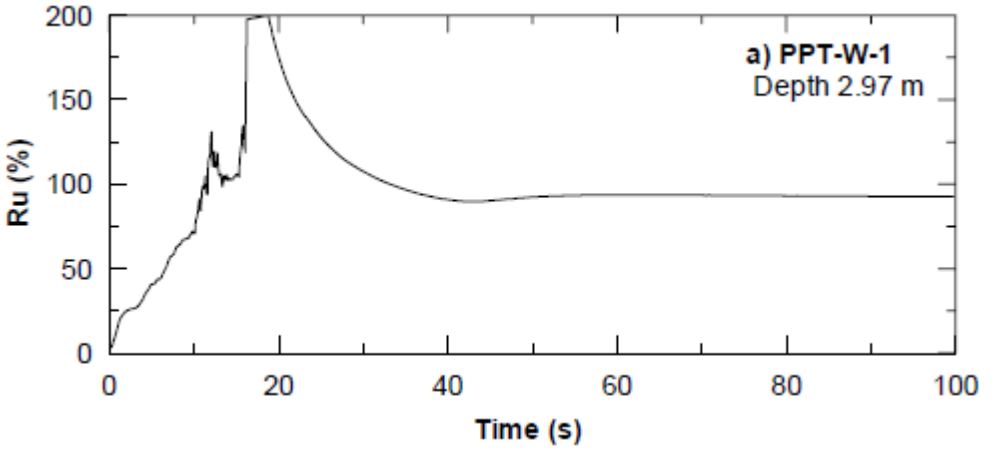
a) PPT-W-1
Depth 2.97 m
Ru (%)
Time (s)
0
50
100
150
200
0
20
40
60
80
100

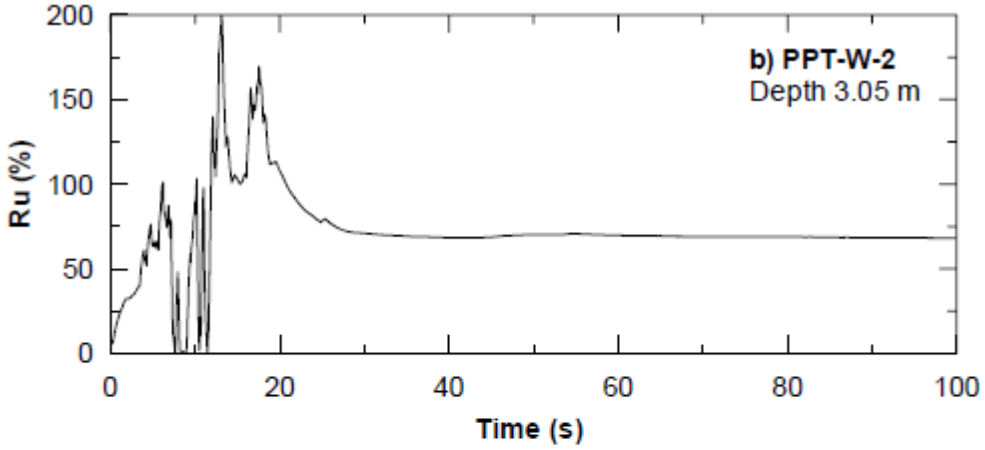
b) PPT-W-2
Depth 3.05 m
Ru (%)
Time (s)
0
50
100
150
200
0
20
40
60
80
100

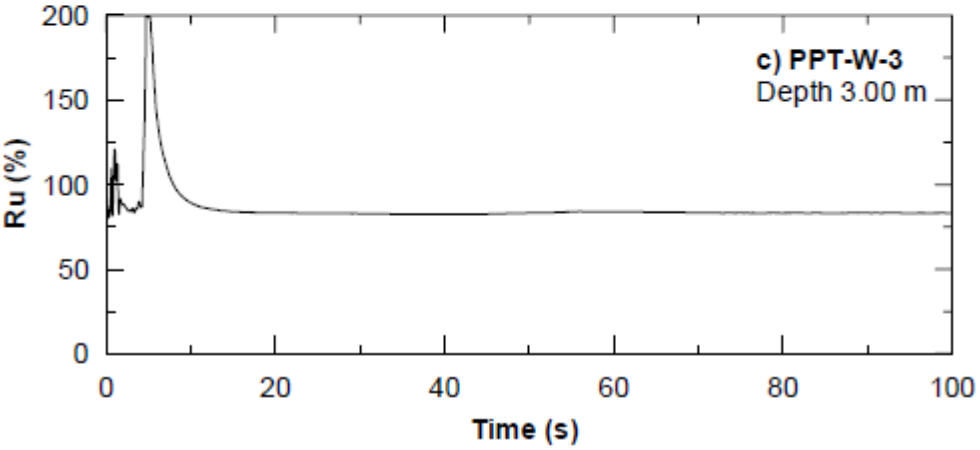
c) PPT-W-3
Depth 3.00 m
Ru (%)
Time (s)
0
50
100
150
200
0
20
40
60
80
100

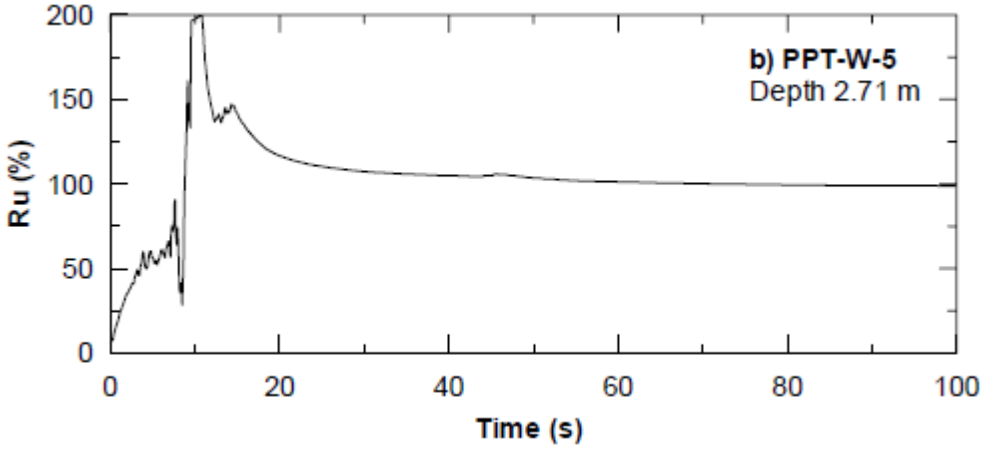
b) PPT-W-5
Depth 2.71 m
Ru (%)
Time (s)
0
50
100
150
200
0
20
40
60
80
100

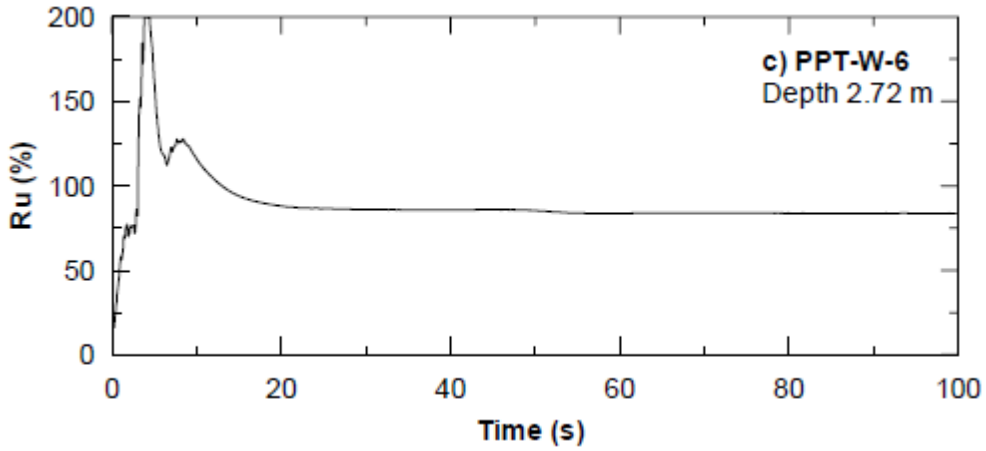
c) PPT-W-6
Depth 2.72 m
Ru (%)
Time (s)
0
50
100
150
200
0
20
40
60
80
100

A.5 TREASURE ISLAND, SAN FRANCISCO, CALIFORNIA

A.5.1 Pilot Study Blast #1 – Residual Pore Pressures

(from Ashford and Rollins, 2002)

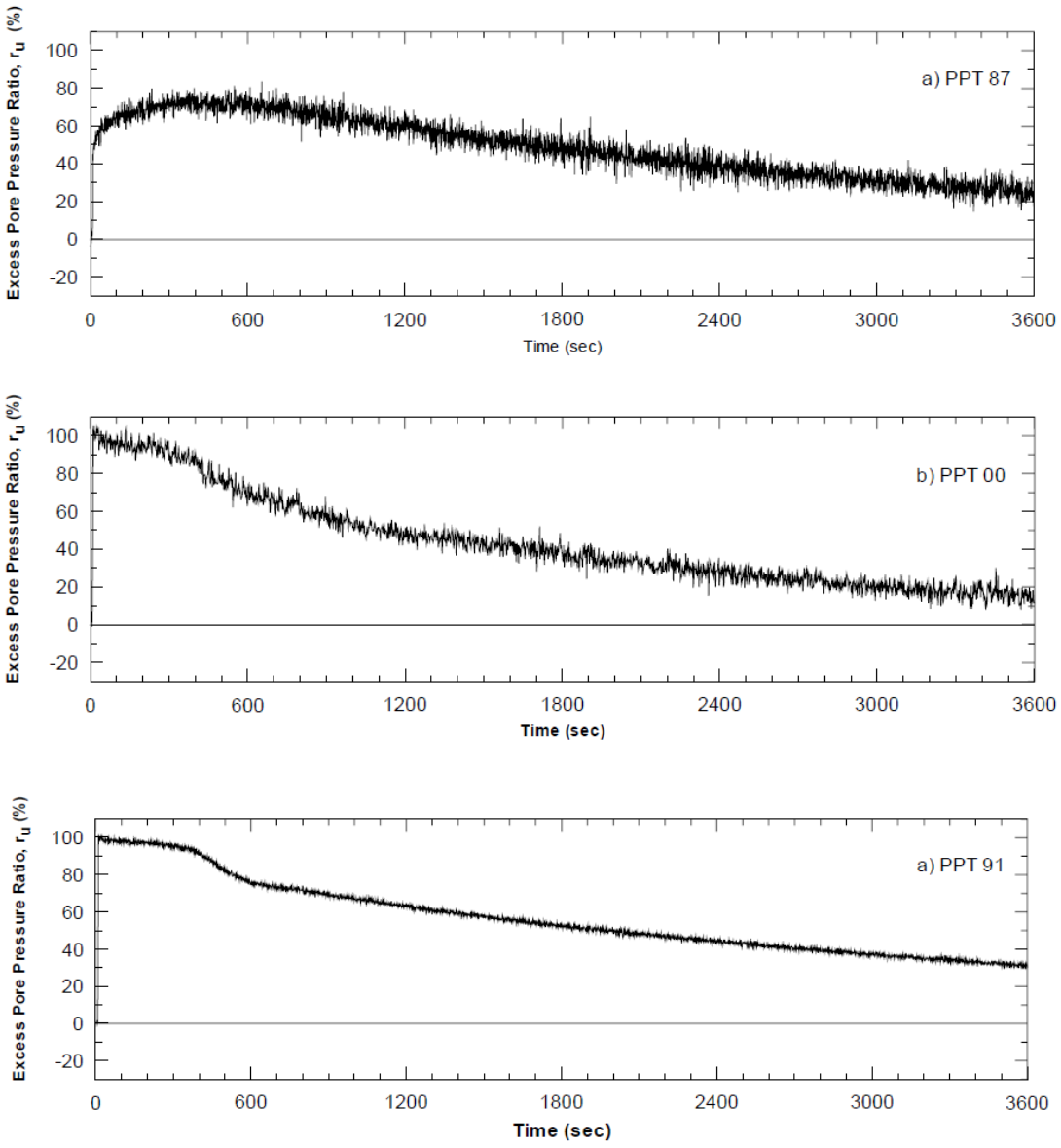

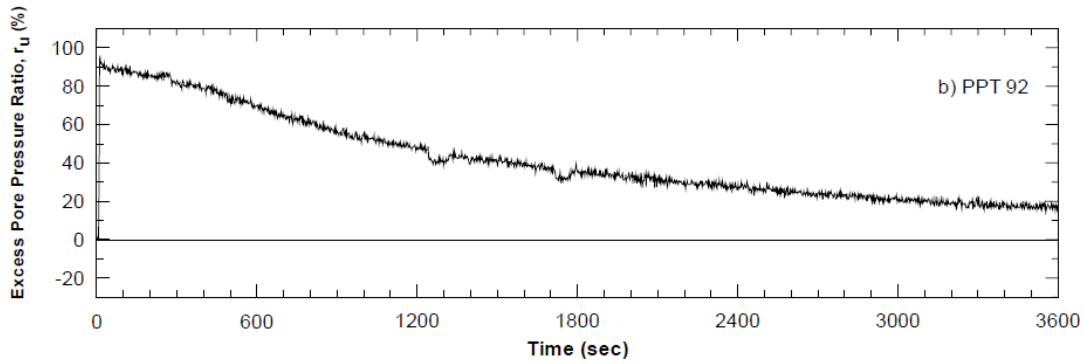
Excess Pore Pressure Ratio, r_u (%)
100
80
60
40
20
0
-20
b) PPT 92
0
600
1200
1800
2400
3000
3600
Time (sec)

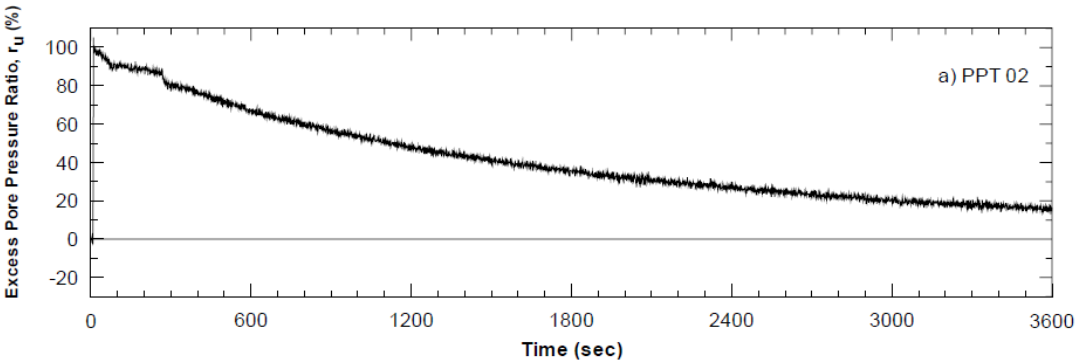
Excess Pore Pressure Ratio, r_u (%)
100
80
60
40
20
0
-20
a) PPT 02
0
600
1200
1800
2400
3000
3600
Time (sec)

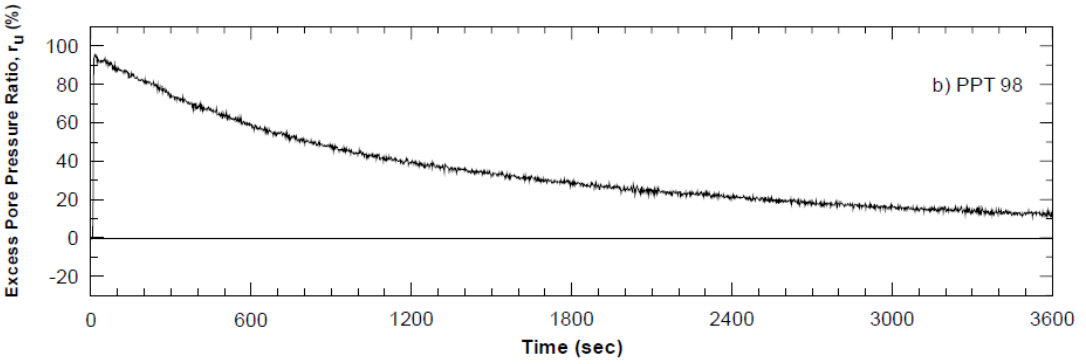
Excess Pore Pressure Ratio, r_u (%)
100
80
60
40
20
0
-20
b) PPT 98
0
600
1200
1800
2400
3000
3600
Time (sec)

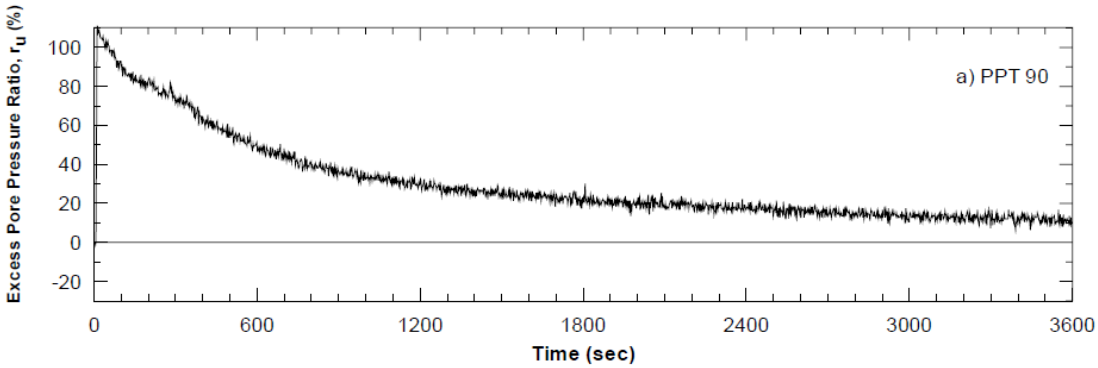
Excess Pore Pressure Ratio, r_u (%)
100
80
60
40
20
0
-20
a) PPT 90
0
600
1200
1800
2400
3000
3600
Time (sec)

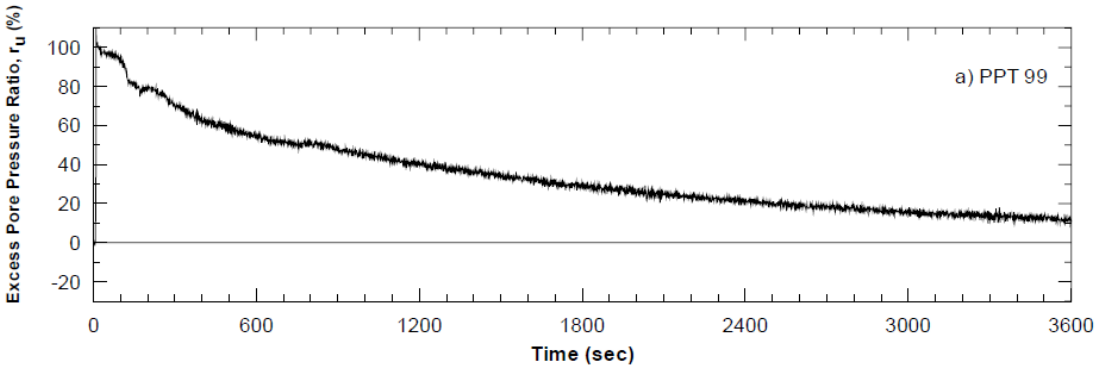
Excess Pore Pressure Ratio, r_u (%)
100
80
60
40
20
0
-20
a) PPT 99
0
600
1200
1800
2400
3000
3600
Time (sec)

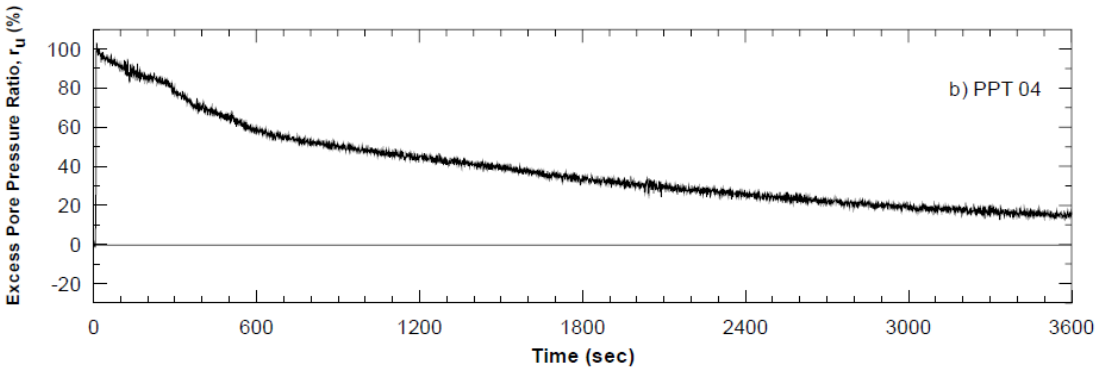
Excess Pore Pressure Ratio, r_u (%)
100
80
60
40
20
0
-20
b) PPT 04
0
600
1200
1800
2400
3000
3600
Time (sec)

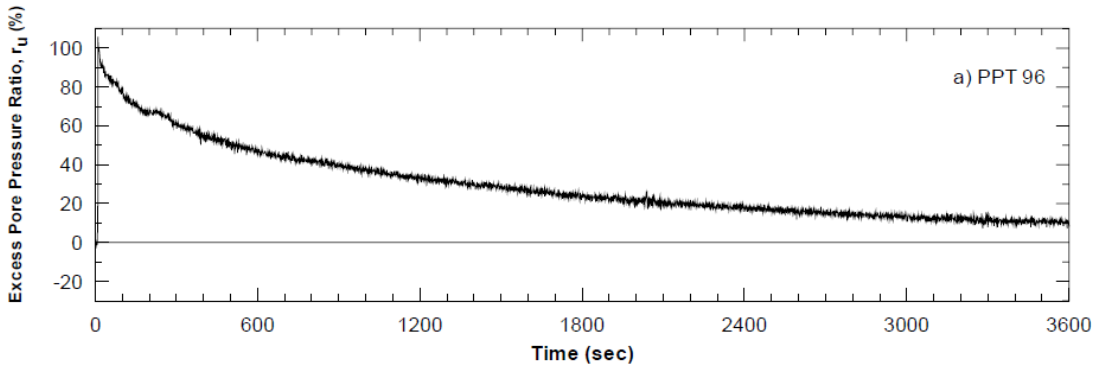
Excess Pore Pressure Ratio, r_u (%)
100
80
60
40
20
0
-20
a) PPT 96
0
600
1200
1800
2400
3000
3600
Time (sec)

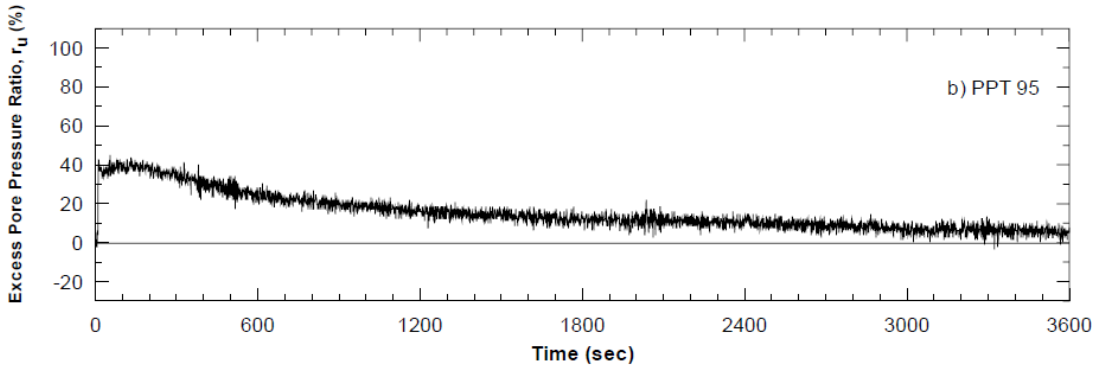
Excess Pore Pressure Ratio, r_u (%)
100
80
60
40
20
0
-20
b) PPT 95
0
600
1200
1800
2400
3000
3600
Time (sec)

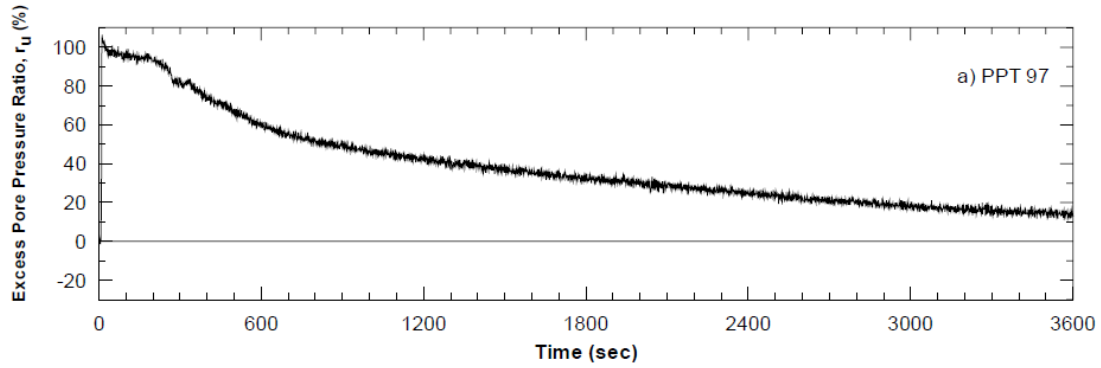
Excess Pore Pressure Ratio, r_u (%)
100
80
60
40
20
0
-20
a) PPT 97
0
600
1200
1800
2400
3000
3600
Time (sec)

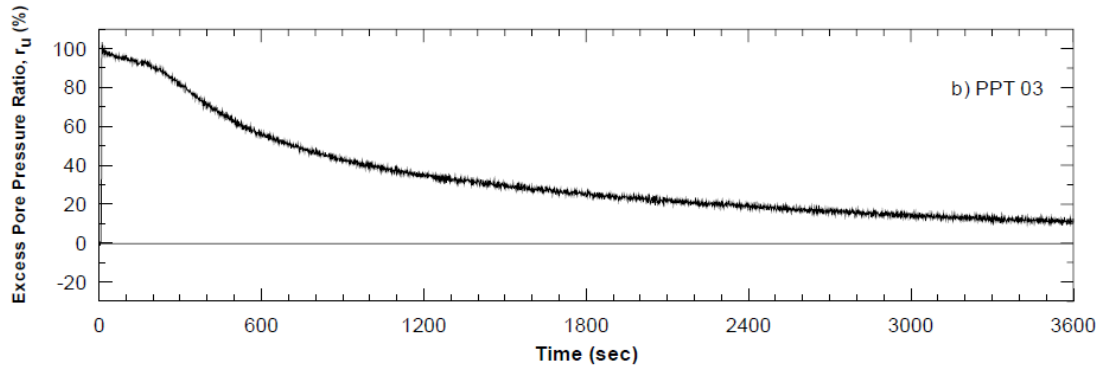
Excess Pore Pressure Ratio, r_u (%)
100
80
60
40
20
0
-20
b) PPT 03
0
600
1200
1800
2400
3000
3600
Time (sec)

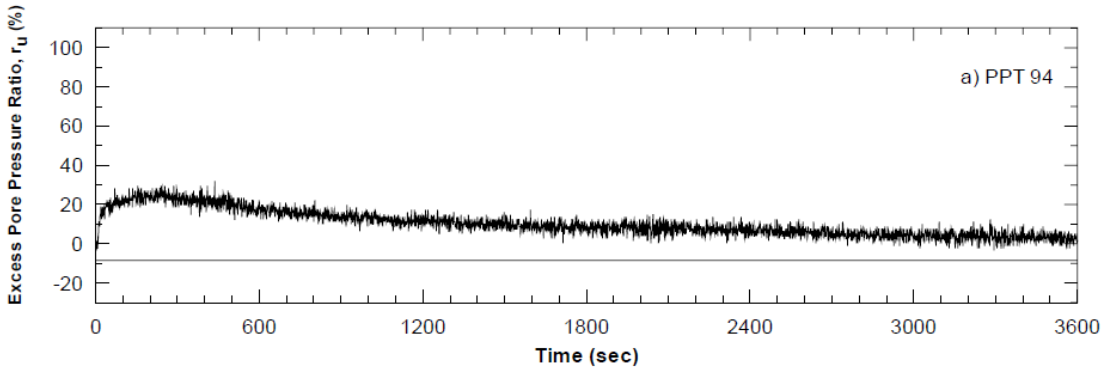
Excess Pore Pressure Ratio, r_u (%)
100
80
60
40
20
0
-20
a) PPT 94
0
600
1200
1800
2400
3000
3600
Time (sec)

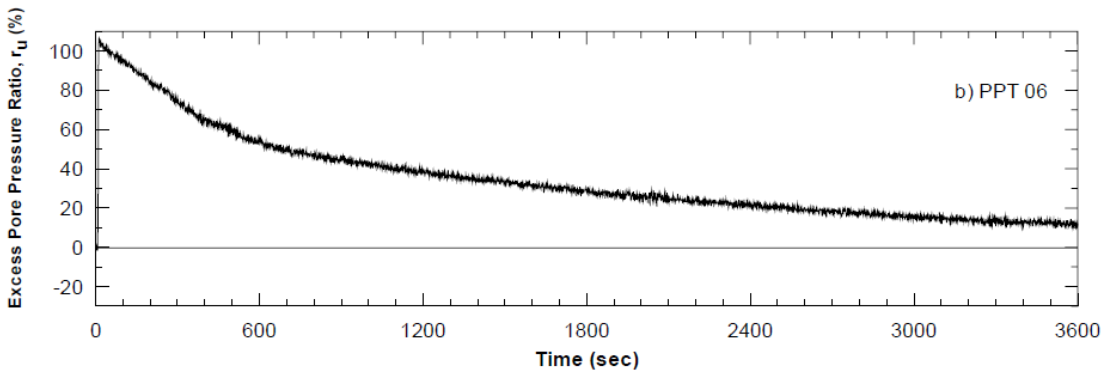
Excess Pore Pressure Ratio, r_u (%)
100
80
60
40
20
0
-20
b) PPT 06
0
600
1200
1800
2400
3000
3600
Time (sec)

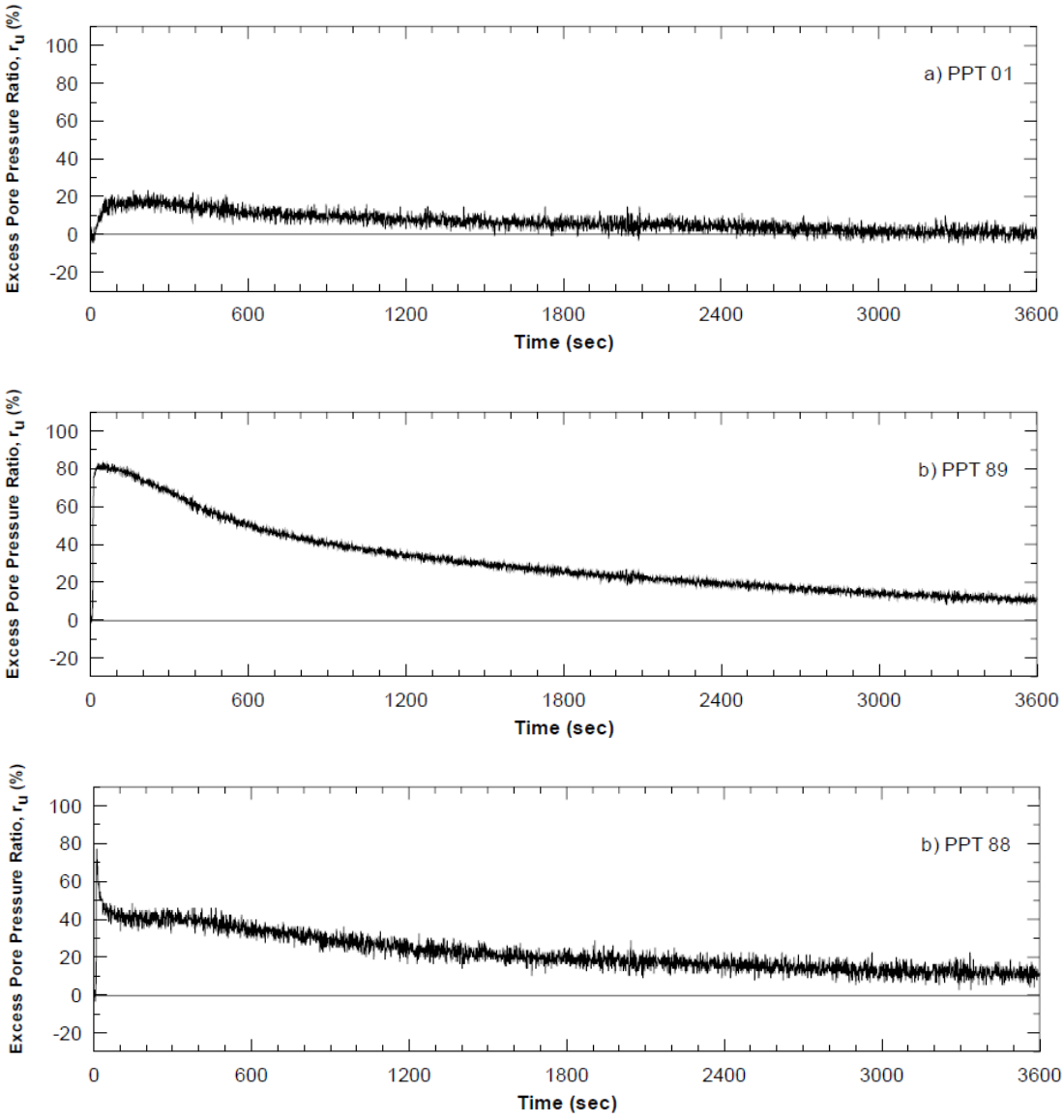
Excess Pore Pressure Ratio, r_u (%)
100
80
60
40
20
0
-20
a) PPT 01
0
600
1200
1800
2400
3000
3600
Time (sec)
Excess Pore Pressure Ratio, r_u (%)
b) PPT 89
Time (sec)
Excess Pore Pressure Ratio, r_u (%)
b) PPT 88
Time (sec)

A.5.2 Pilot Study Blast #2 – Residual Pore Pressures

(from Ashford and Rollins, 2002)

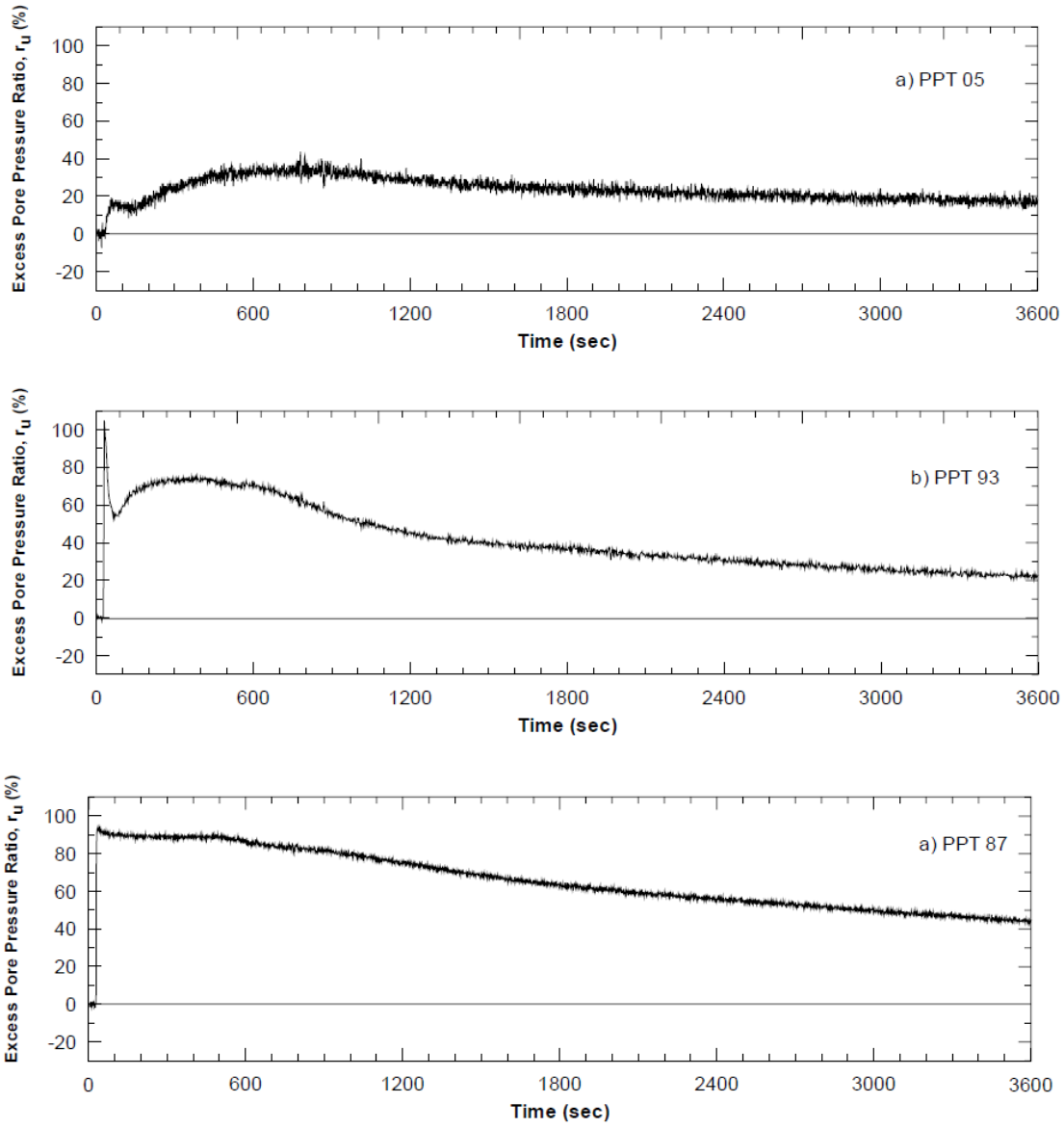

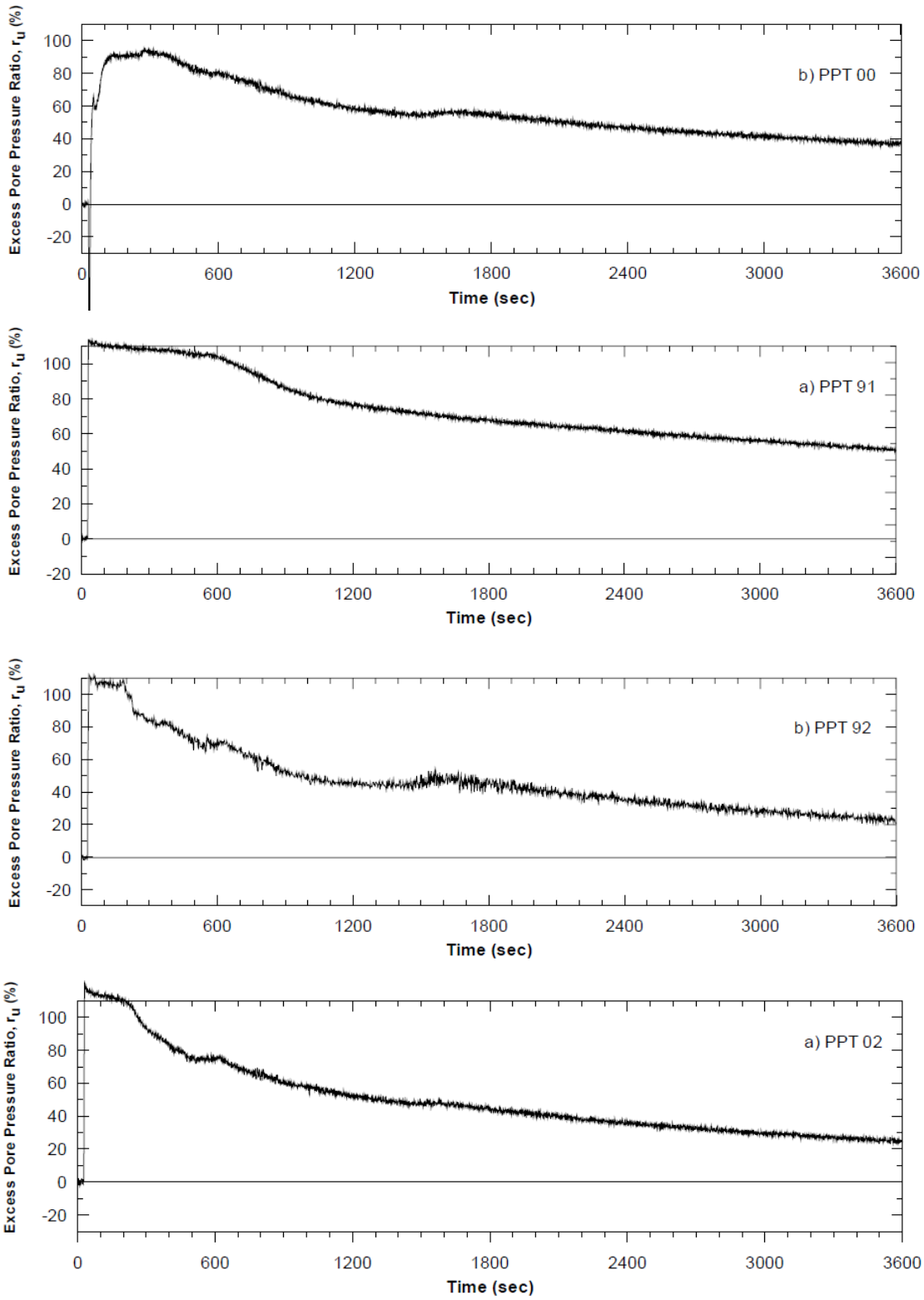
Excess Pore Pressure Ratio, r_u (%)
b) PPT 00
a) PPT 91
b) PPT 92
a) PPT 02
100
80
60
40
20
0
-20
0
600
1200
1800
2400
3000
3600
Time (sec)

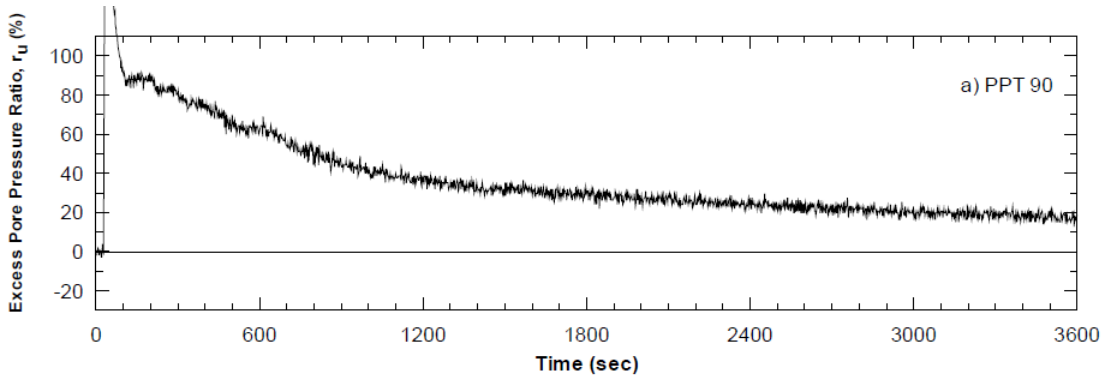
Excess Pore Pressure Ratio, r_u (%)
100
80
60
40
20
0
-20
a) PPT 90
0
600
1200
1800
2400
3000
3600
Time (sec)

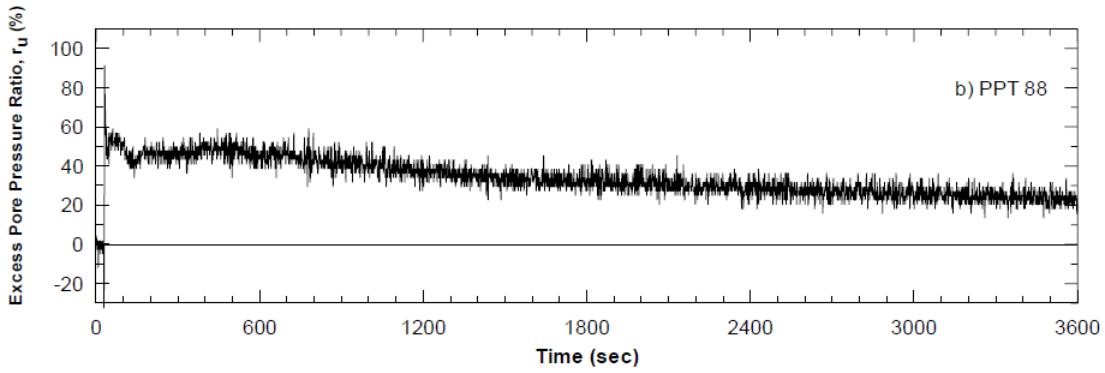
Excess Pore Pressure Ratio, r_u (%)
100
80
60
40
20
0
-20
b) PPT 88
0
600
1200
1800
2400
3000
3600
Time (sec)

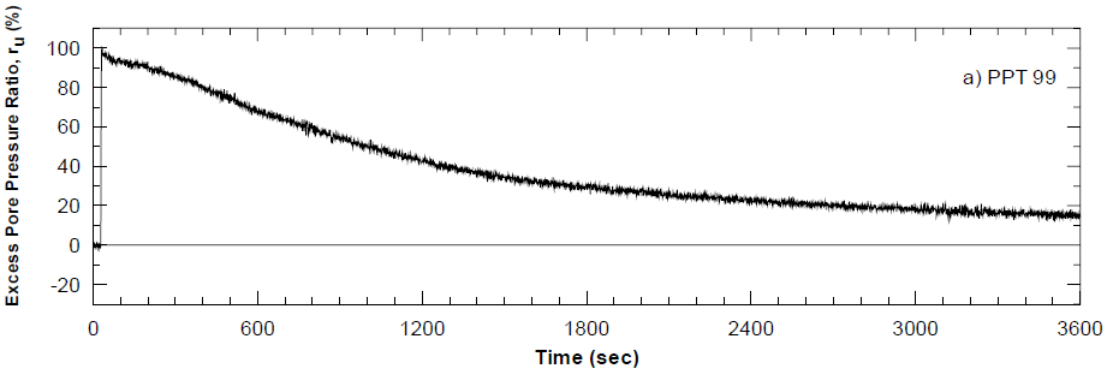
Excess Pore Pressure Ratio, r_u (%)
100
80
60
40
20
0
-20
a) PPT 99
0
600
1200
1800
2400
3000
3600
Time (sec)

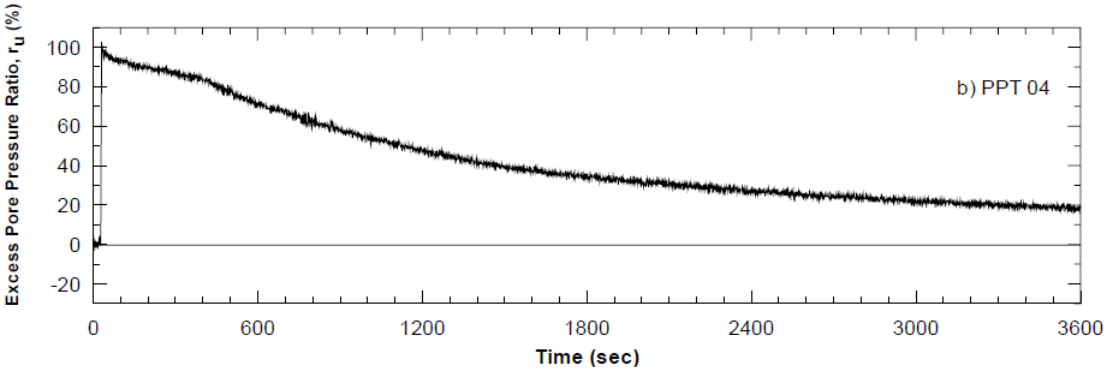
Excess Pore Pressure Ratio, r_u (%)
100
80
60
40
20
0
-20
b) PPT 04
0
600
1200
1800
2400
3000
3600
Time (sec)

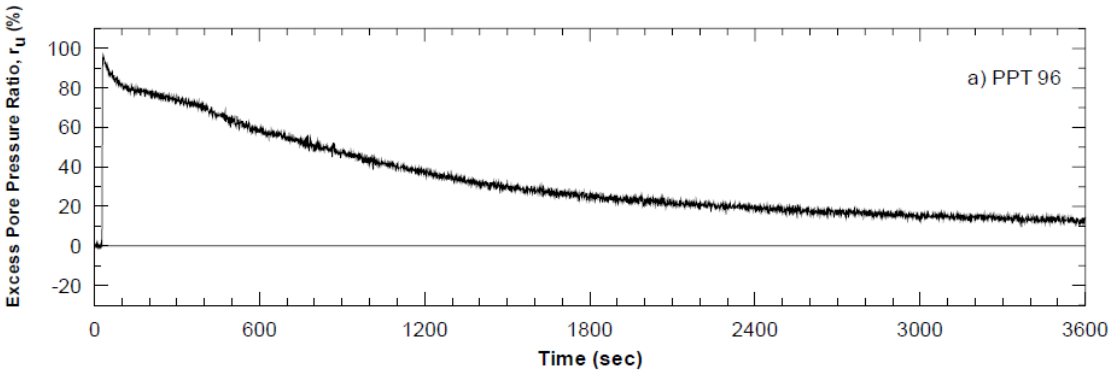
Excess Pore Pressure Ratio, r_u (%)
100
80
60
40
20
0
-20
a) PPT 96
0
600
1200
1800
2400
3000
3600
Time (sec)

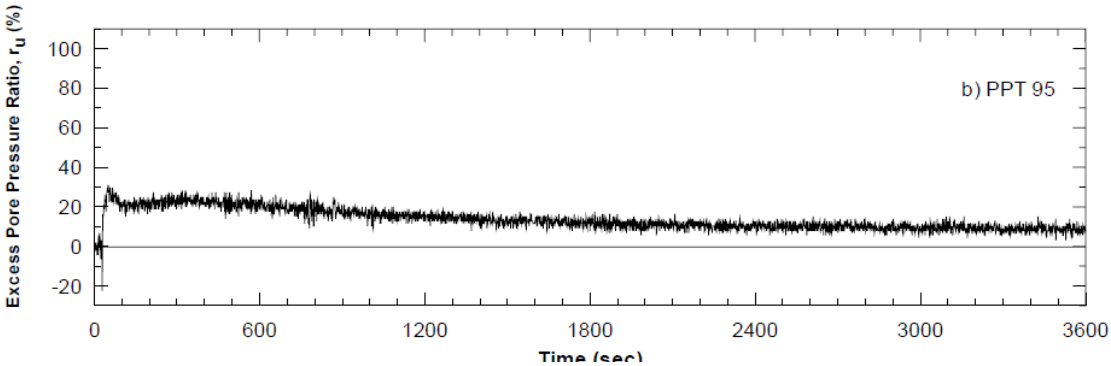
Excess Pore Pressure Ratio, r_u (%)
100
80
60
40
20
0
-20
b) PPT 95
0
600
1200
1800
2400
3000
3600
Time (sec)

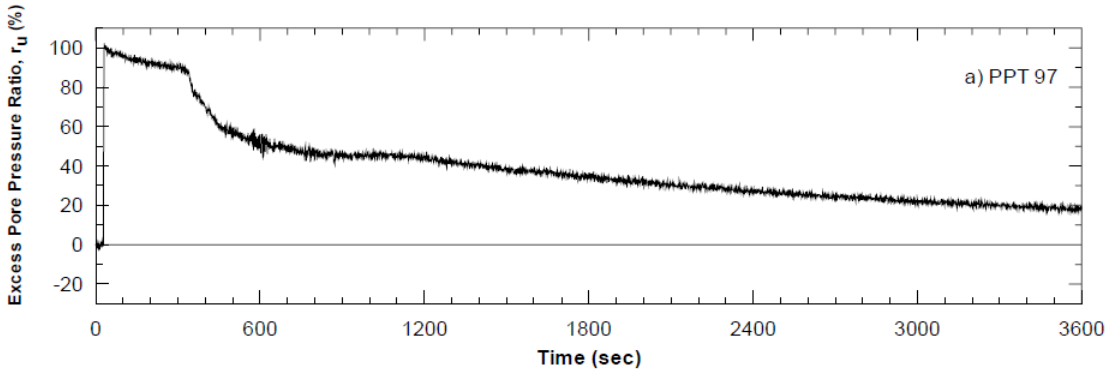
Excess Pore Pressure Ratio, r_u (%)
100
80
60
40
20
0
-20
a) PPT 97
0
600
1200
1800
2400
3000
3600
Time (sec)

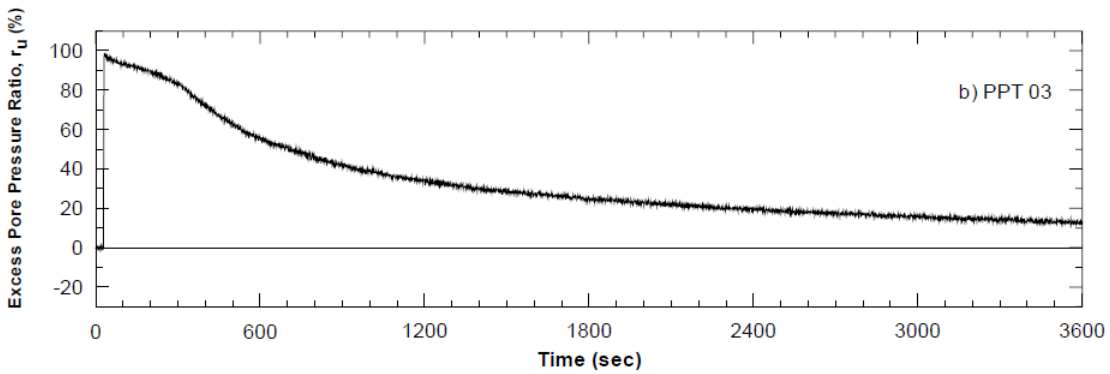
Excess Pore Pressure Ratio, r_u (%)
100
80
60
40
20
0
-20
b) PPT 03
0
600
1200
1800
2400
3000
3600
Time (sec)

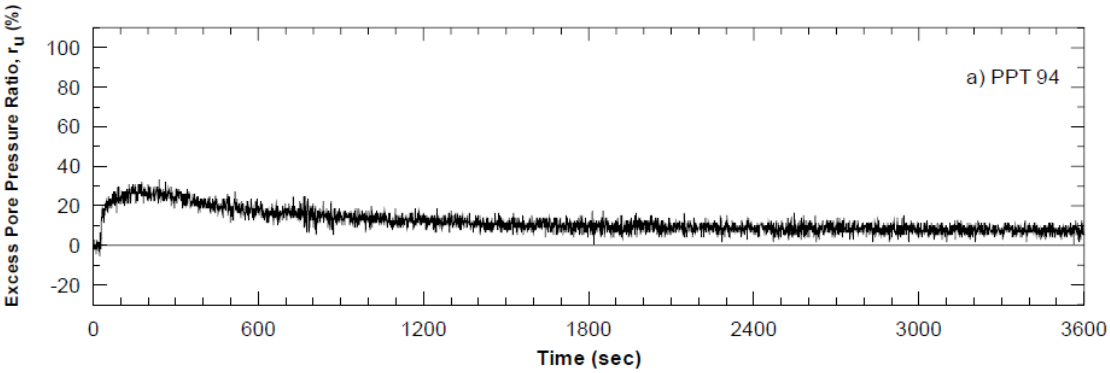
Excess Pore Pressure Ratio, r_u (%)
100
80
60
40
20
0
-20
a) PPT 94
0
600
1200
1800
2400
3000
3600
Time (sec)

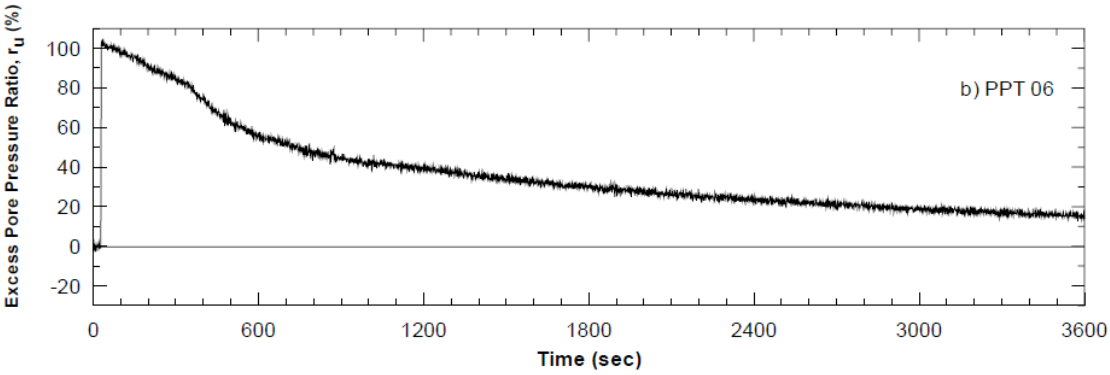
Excess Pore Pressure Ratio, r_u (%)
100
80
60
40
20
0
-20
b) PPT 06
0
600
1200
1800
2400
3000
3600
Time (sec)

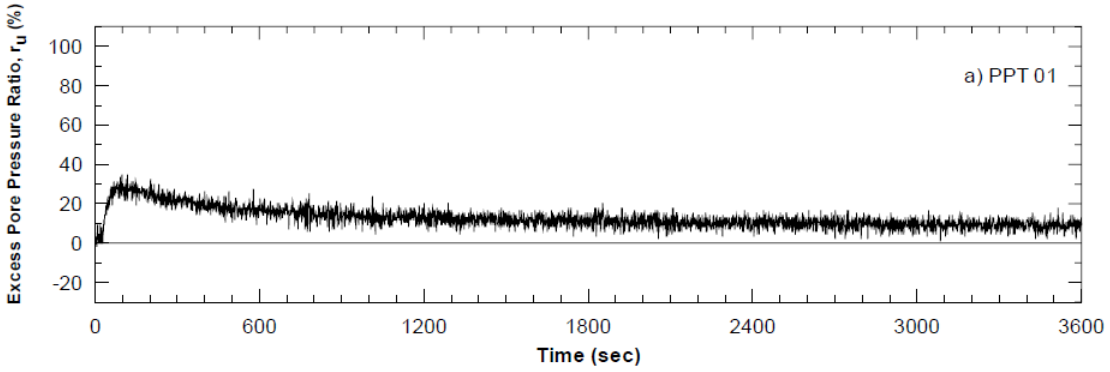
Excess Pore Pressure Ratio, r_u (%)
100
80
60
40
20
0
-20
a) PPT 01
0
600
1200
1800
2400
3000
3600
Time (sec)

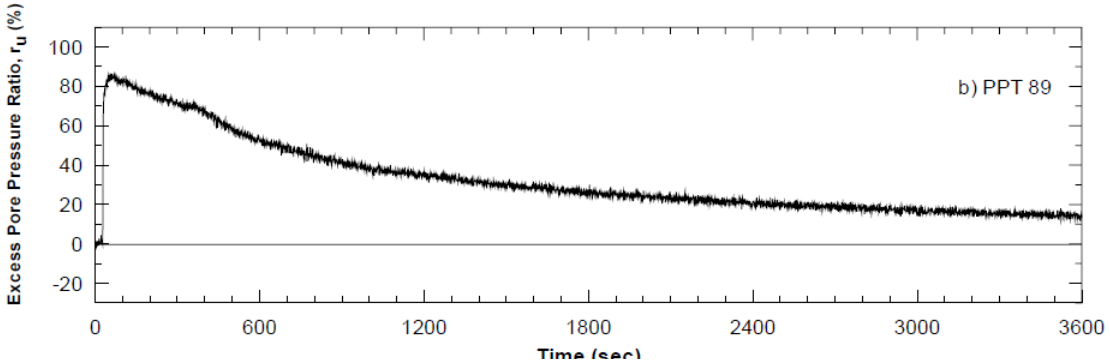
Excess Pore Pressure Ratio, r_u (%)
100
80
60
40
20
0
-20
b) PPT 89
0
600
1200
1800
2400
3000
3600

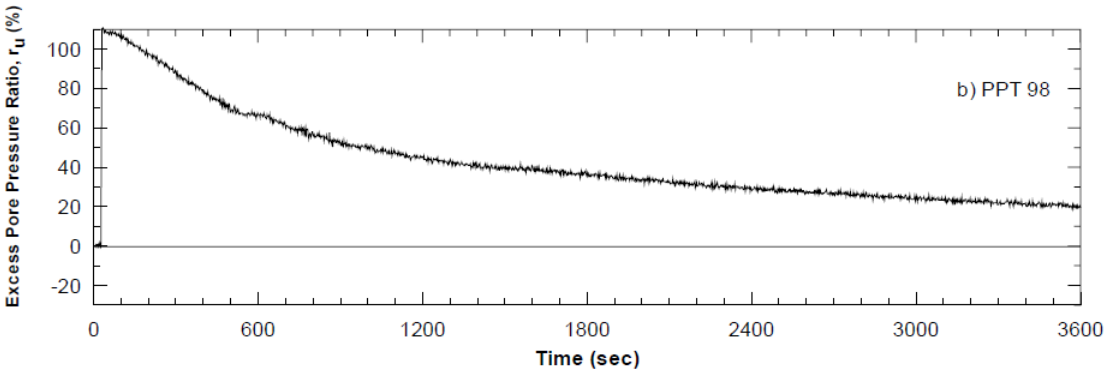
Excess Pore Pressure Ratio, r_u (%)
100
80
60
40
20
0
-20
0
600
1200
1800
2400
3000
3600
Time (sec)
b) PPT 98

APPENDIX B – BLASTING AND IN-SITU DATA

B.1 MULTIPLE BLASTS

$R/W^{0.33}$ $m/kg^{0.33}$	Ru	SPT $(N_1)_{60}$	Effective Overburden Pressure, σ'v (kPa)	Relative Density, Dr (%)	Shear Wave Velocity, Vs (m/s)	CRR (Youd et al 2001)	Fines Content %
5.82	0.16	15	13.6	70	110	0.194	5
2.37	1.00	3	39.4	50	120	0.085	5
4.24	0.98	2	47.7	40	125	0.077	5
3.77	0.98	11	30.7	50	115	0.15	5
2.64	0.18	15	13.6	70	110	0.194	5
4.82	1.00	11	30.7	50	115	0.15	5
2.53	0.72	2	47.7	40	125	0.077	5
2.64	0.76	15	13.6	70	110	0.194	5
5.71	0.82	11	30.7	50	115	0.15	5
2.45	1.00	7	22.4	58	120	0.12	5
2.55	1.00	3	56	28	125	0.077	5
2.23	0.92	11	30.7	50	115	0.15	5
2.35	0.98	11	30.7	50	115	0.15	5
4.95	0.25	15	13.6	70	110	0.194	5
4.30	0.42	15	13.6	70	110	0.194	5
4.30	1.00	11	30.7	50	115	0.15	5
4.13	1.00	11	30.7	50	115	0.15	5
2.64	0.94	2	47.7	40	125	0.077	5
3.16	1.00	11	30.7	50	115	0.15	5
5.82	0.28	15	13.6	70	110	0.194	5
2.37	1.00	3	39.4	50	120	0.085	5
4.24	0.97	2	47.7	40	125	0.077	5
3.77	0.98	11	30.7	50	115	0.15	5
2.64	0.32	15	13.6	70	110	0.194	5
4.82	1.00	11	30.7	50	115	0.15	5
2.53	0.94	2	47.7	40	125	0.077	5
2.64	0.55	15	13.6	70	110	0.194	5
5.71	0.86	11	30.7	50	115	0.15	5
2.45	1.00	7	22.4	58	120	0.12	5
2.55	1.00	3	56	28	125	0.077	5
2.23	1.00	11	30.7	50	115	0.15	5
2.35	1.00	11	30.7	50	115	0.15	5
4.95	0.28	15	13.6	70	110	0.194	5
4.30	0.31	15	13.6	70	110	0.194	5
4.30	0.95	11	30.7	50	115	0.15	5
4.13	0.99	11	30.7	50	115	0.15	5
2.64	1.00	2	47.7	40	125	0.077	5
3.16	0.98	11	30.7	50	115	0.15	5
16.89	0.27	3.4	62.6	43	127	0.061	15
10.85	0.28	3.4	62.6	43	127	0.061	15
9.99	0.30	3.4	62.6	43	127	0.061	15
8.58	0.38	3.4	62.6	43	127	0.061	15
7.94	0.46	3.4	62.6	43	127	0.061	15
7.04	0.13	3.4	62.6	43	127	0.061	15

$R/W^{0.33}$ $m/kg^{0.33}$	Ru	SPT $(N_1)_{60}$	Effective Overburden Pressure, σ'v (kPa)	Relative Density, Dr (%)	Shear Wave Velocity, Vs (m/s)	CRR (Youd et al 2001)	Fines Content %
5.35	0.24	3.4	62.6	43	127	0.061	15
4.75	0.31	3.4	62.6	43	127	0.061	15
4.46	0.88	3.4	62.6	43	127	0.061	15
2.35	0.62	7	84.4	35	160	0.152	40
7.91	0.53	7	59.3	30	210	0.124	15
7.18	0.65	7	59.3	30	210	0.124	15
6.44	0.74	7	59.3	30	210	0.124	15
6.07	0.80	7	59.3	30	210	0.124	15
5.68	0.83	7	59.3	30	210	0.124	15
5.45	0.87	7	59.3	30	210	0.124	15
5.20	0.91	7	59.3	30	210	0.124	15
4.30	0.72	7	59.3	30	210	0.124	15
3.65	0.79	7	59.3	30	210	0.124	15
3.40	0.84	7	59.3	30	210	0.124	15
3.13	0.89	7	59.3	30	210	0.124	15
3.00	0.90	7	59.3	30	210	0.124	15
2.85	0.94	7	59.3	30	210	0.124	15
2.78	0.96	7	59.3	30	210	0.124	15
6.00	0.28	4	27.1	12	90	0.065	5
5.40	0.3	4	27.1	12	90	0.065	5
4.00	0.3	4	27.1	12	90	0.065	5
4.00	0.42	4	27.1	12	90	0.065	5
9.80	0.07	4	27.1	12	90	0.065	5
5.20	0.25	4	27.1	12	90	0.065	5
3.90	0.25	4	27.1	12	90	0.065	5
3.90	0.35	4	27.1	12	90	0.065	5
11.19	0.02	10	66.8	35	165	0.13	8
8.26	0.05	10	66.8	35	165	0.13	8
6.75	0.08	10	66.8	35	165	0.13	8
6.35	0.11	10	66.8	35	165	0.13	8
5.83	0.15	10	66.8	35	165	0.13	8
5.33	0.17	10	66.8	35	165	0.13	8
5.17	0.20	10	66.8	35	165	0.13	8
4.92	0.22	10	66.8	35	165	0.13	8
4.65	0.25	10	66.8	35	165	0.13	8
4.56	0.28	10	66.8	35	165	0.13	8
4.41	0.30	10	66.8	35	165	0.13	8
4.23	0.32	10	66.8	35	165	0.13	8
4.17	0.34	10	66.8	35	165	0.13	8
4.06	0.35	10	66.8	35	165	0.13	8
3.93	0.40	10	66.8	35	165	0.13	8
3.89	0.41	10	66.8	35	165	0.13	8
3.80	0.47	10	66.8	35	165	0.13	8
3.70	0.48	10	66.8	35	165	0.13	8

$R/W^{0.33}$ $m/kg^{0.33}$	Ru	SPT $(N_1)_{60}$	Effective Overburden Pressure, σ'v (kPa)	Relative Density, Dr (%)	Shear Wave Velocity, Vs (m/s)	CRR (Youd et al 2001)	Fines Content %
3.66	0.52	10	66.8	35	165	0.13	8
3.59	0.54	10	66.8	35	165	0.13	8
3.53	0.57	10	66.8	35	165	0.13	8
3.50	0.58	10	66.8	35	165	0.13	8
3.45	0.62	10	66.8	35	165	0.13	8
3.38	0.64	10	66.8	35	165	0.13	8
8.89	0.08	10	84.4	35	160	0.13	8
6.72	0.17	10	84.4	35	160	0.13	8
5.79	0.21	10	84.4	35	160	0.13	8
5.23	0.22	10	84.4	35	160	0.13	8
4.73	0.24	10	84.4	35	160	0.13	8
4.38	0.27	10	84.4	35	160	0.13	8
4.17	0.30	10	84.4	35	160	0.13	8
3.94	0.32	10	84.4	35	160	0.13	8
3.76	0.36	10	84.4	35	160	0.13	8
3.68	0.38	10	84.4	35	160	0.13	8
3.57	0.41	10	84.4	35	160	0.13	8
3.47	0.43	10	84.4	35	160	0.13	8
3.44	0.48	10	84.4	35	160	0.13	8
3.38	0.50	10	84.4	35	160	0.13	8
3.33	0.51	10	84.4	35	160	0.13	8
3.31	0.54	10	84.4	35	160	0.13	8
3.27	0.58	10	84.4	35	160	0.13	8
3.23	0.60	10	84.4	35	160	0.13	8
3.20	0.62	10	84.4	35	160	0.13	8
3.17	0.64	10	84.4	35	160	0.13	8
3.13	0.65	10	84.4	35	160	0.13	8
3.10	0.67	10	84.4	35	160	0.13	8
3.06	0.69	10	84.4	35	160	0.13	8
3.02	0.72	10	84.4	35	160	0.13	8
8.86	0.10	10	100.3	35	175	0.13	8
7.07	0.32	10	100.3	35	175	0.13	8
6.47	0.44	10	100.3	35	175	0.13	8
5.88	0.48	10	100.3	35	175	0.13	8
5.47	0.47	10	100.3	35	175	0.13	8
5.26	0.30	10	100.3	35	175	0.13	8
4.98	0.37	10	100.3	35	175	0.13	8
4.76	0.37	10	100.3	35	175	0.13	8
4.64	0.38	10	100.3	35	175	0.13	8
4.44	0.41	10	100.3	35	175	0.13	8
4.28	0.43	10	100.3	35	175	0.13	8
4.18	0.48	10	100.3	35	175	0.13	8
4.02	0.49	10	100.3	35	175	0.13	8
3.88	0.50	10	100.3	35	175	0.13	8

$R/W^{0.33}$ $m/kg^{0.33}$	Ru	SPT $(N_1)_{60}$	Effective Overburden Pressure, σ'v (kPa)	Relative Density, Dr (%)	Shear Wave Velocity, Vs (m/s)	CRR (Youd et al 2001)	Fines Content %
3.79	0.51	10	100.3	35	175	0.13	8
3.65	0.54	10	100.3	35	175	0.13	8
3.54	0.58	10	100.3	35	175	0.13	8
3.46	0.59	10	100.3	35	175	0.13	8
3.36	0.60	10	100.3	35	175	0.13	8
3.27	0.61	10	100.3	35	175	0.13	8
3.19	0.63	10	100.3	35	175	0.13	8
3.13	0.65	10	100.3	35	175	0.13	8
3.07	0.68	10	100.3	35	175	0.13	8
3.04	0.69	10	100.3	35	175	0.13	8
7.61	0.09	10	118.8	35	180	0.124	8
6.54	0.13	10	118.8	35	180	0.124	8
6.41	0.16	10	118.8	35	180	0.124	8
5.66	0.19	10	118.8	35	180	0.124	8
5.30	0.25	10	118.8	35	180	0.124	8
5.22	0.25	10	118.8	35	180	0.124	8
4.93	0.27	10	118.8	35	180	0.124	8
4.76	0.28	10	118.8	35	180	0.124	8
4.73	0.30	10	118.8	35	180	0.124	8
4.56	0.31	10	118.8	35	180	0.124	8
4.46	0.33	10	118.8	35	180	0.124	8
4.44	0.36	10	118.8	35	180	0.124	8
4.31	0.37	10	118.8	35	180	0.124	8
4.22	0.38	10	118.8	35	180	0.124	8
4.20	0.39	10	118.8	35	180	0.124	8
4.08	0.40	10	118.8	35	180	0.124	8
3.99	0.41	10	118.8	35	180	0.124	8
3.96	0.42	10	118.8	35	180	0.124	8
3.85	0.42	10	118.8	35	180	0.124	8
3.77	0.42	10	118.8	35	180	0.124	8
3.69	0.43	10	118.8	35	180	0.124	8
3.59	0.43	10	118.8	35	180	0.124	8
3.52	0.44	10	118.8	35	180	0.124	8
3.49	0.44	10	118.8	35	180	0.124	8
11.11	0.03	10	135.6	35	185	0.12	8
9.45	0.08	10	135.6	35	185	0.12	8
9.03	0.09	10	135.6	35	185	0.12	8
7.81	0.10	10	135.6	35	185	0.12	8
7.22	0.13	10	135.6	35	185	0.12	8
7.02	0.15	10	135.6	35	185	0.12	8
6.45	0.17	10	135.6	35	185	0.12	8
6.12	0.18	10	135.6	35	185	0.12	8
5.99	0.19	10	135.6	35	185	0.12	8
5.63	0.20	10	135.6	35	185	0.12	8

$R/W^{0.33}$ $m/kg^{0.33}$	Ru	SPT $(N_1)_{60}$	Effective Overburden Pressure, σ'v (kPa)	Relative Density, Dr (%)	Shear Wave Velocity, Vs (m/s)	CRR (Youd et al 2001)	Fines Content %
5.42	0.22	10	135.6	35	185	0.12	8
5.33	0.24	10	135.6	35	185	0.12	8
5.10	0.25	10	135.6	35	185	0.12	8
4.95	0.26	10	135.6	35	185	0.12	8
4.89	0.27	10	135.6	35	185	0.12	8
4.73	0.28	10	135.6	35	185	0.12	8
4.62	0.29	10	135.6	35	185	0.12	8
6.13	0.21	10	66.8	35	165	0.13	8
4.52	0.31	10	66.8	35	165	0.13	8
3.70	0.45	10	66.8	35	165	0.13	8
3.48	0.48	10	66.8	35	165	0.13	8
3.20	0.52	10	66.8	35	165	0.13	8
2.93	0.54	10	66.8	35	165	0.13	8
2.85	0.60	10	66.8	35	165	0.13	8
2.71	0.70	10	66.8	35	165	0.13	8
2.56	0.75	10	66.8	35	165	0.13	8
2.51	0.80	10	66.8	35	165	0.13	8
2.43	0.85	10	66.8	35	165	0.13	8
2.33	0.90	10	66.8	35	165	0.13	8
2.29	0.92	10	66.8	35	165	0.13	8
2.23	0.93	10	66.8	35	165	0.13	8
2.16	0.94	10	66.8	35	165	0.13	8
2.14	0.95	10	66.8	35	165	0.13	8
5.09	0.31	10	84.4	35	160	0.13	8
3.86	0.40	10	84.4	35	160	0.13	8
3.33	0.50	10	84.4	35	160	0.13	8
3.00	0.52	10	84.4	35	160	0.13	8
2.71	0.60	10	84.4	35	160	0.13	8
2.51	0.62	10	84.4	35	160	0.13	8
2.38	0.67	10	84.4	35	160	0.13	8
2.24	0.70	10	84.4	35	160	0.13	8
2.12	0.78	10	84.4	35	160	0.13	8
2.06	0.80	10	84.4	35	160	0.13	8
1.99	0.85	10	84.4	35	160	0.13	8
1.92	0.88	10	84.4	35	160	0.13	8
1.89	0.90	10	84.4	35	160	0.13	8
1.85	0.91	10	84.4	35	160	0.13	8
1.82	0.92	10	84.4	35	160	0.13	8
1.80	0.92	10	84.4	35	160	0.13	8
1.78	0.95	10	84.4	35	160	0.13	8
4.60	0.28	10	100.3	35	175	0.13	8
3.67	0.41	10	100.3	35	175	0.13	8
3.38	0.50	10	100.3	35	175	0.13	8
3.09	0.55	10	100.3	35	175	0.13	8

$R/W^{0.33}$ $m/kg^{0.33}$	Ru	SPT $(N_1)_{60}$	Effective Overburden Pressure, σ'v (kPa)	Relative Density, Dr (%)	Shear Wave Velocity, Vs (m/s)	CRR (Youd et al 2001)	Fines Content %
2.89	0.60	10	100.3	35	175	0.13	8
2.80	0.62	10	100.3	35	175	0.13	8
2.67	0.68	10	100.3	35	175	0.13	8
2.56	0.72	10	100.3	35	175	0.13	8
2.50	0.78	10	100.3	35	175	0.13	8
2.41	0.80	10	100.3	35	175	0.13	8
2.33	0.84	10	100.3	35	175	0.13	8
2.28	0.85	10	100.3	35	175	0.13	8
2.20	0.89	10	100.3	35	175	0.13	8
2.13	0.92	10	100.3	35	175	0.13	8
4.10	0.37	10	118.8	35	180	0.124	8
3.53	0.48	10	118.8	35	180	0.124	8
3.48	0.59	10	118.8	35	180	0.124	8
3.05	0.65	10	118.8	35	180	0.124	8
2.85	0.71	10	118.8	35	180	0.124	8
2.81	0.75	10	118.8	35	180	0.124	8
2.64	0.78	10	118.8	35	180	0.124	8
2.55	0.82	10	118.8	35	180	0.124	8
2.53	0.85	10	118.8	35	180	0.124	8
2.44	0.88	10	118.8	35	180	0.124	8
2.39	0.90	10	118.8	35	180	0.124	8
2.38	0.90	10	118.8	35	180	0.124	8
2.31	0.90	10	118.8	35	180	0.124	8
2.27	0.91	10	118.8	35	180	0.124	8
2.26	0.91	10	118.8	35	180	0.124	8
2.21	0.92	10	118.8	35	180	0.124	8
2.17	0.92	10	118.8	35	180	0.124	8
6.12	0.17	10	135.6	35	185	0.12	8
5.21	0.27	10	135.6	35	185	0.12	8
4.97	0.33	10	135.6	35	185	0.12	8
4.33	0.41	10	135.6	35	185	0.12	8
4.02	0.50	10	135.6	35	185	0.12	8
3.91	0.53	10	135.6	35	185	0.12	8
3.60	0.60	10	135.6	35	185	0.12	8
3.43	0.65	10	135.6	35	185	0.12	8
3.36	0.71	10	135.6	35	185	0.12	8
3.16	0.75	10	135.6	35	185	0.12	8
3.03	0.79	10	135.6	35	185	0.12	8
2.98	0.83	10	135.6	35	185	0.12	8
2.85	0.84	10	135.6	35	185	0.12	8
2.76	0.85	10	135.6	35	185	0.12	8
5.89	0.7	4.00	45.40	50	120.00	0.09	10.00
5.67	0.62	4.00	45.40	50	120.00	0.09	10.00
5.50	0.53	4.00	45.40	50	120.00	0.09	10.00

$R/W^{0.33}$ $m/kg^{0.33}$	Ru	SPT $(N_1)_{60}$	Effective Overburden Pressure, σ'v (kPa)	Relative Density, Dr (%)	Shear Wave Velocity, Vs (m/s)	CRR (Youd et al 2001)	Fines Content %
7.78	0.31	4.00	45.40	50	120.00	0.09	10.00
9.02	0.51	4.00	45.40	50	120.00	0.09	10.00
2.69	0.93	4.00	45.40	50	120.00	0.09	10.00
2.52	0.99	4.00	45.40	50	120.00	0.09	10.00
2.34	0.99	4.00	45.40	50	120.00	0.09	10.00
2.20	0.84	4.00	45.40	50	120.00	0.09	10.00
5.07	0.79	4.00	45.40	50	120.00	0.09	10.00
7.13	0.14	4.00	45.40	50	120.00	0.09	10.00
5.97	0.07	4.00	45.40	50	120.00	0.09	10.00
4.62	0.84	4.00	45.40	50	120.00	0.09	10.00
6.90	0.12	4.00	45.40	50	120.00	0.09	10.00
4.20	0.97	4.00	45.40	50	120.00	0.09	10.00
4.37	0.33	4.00	45.40	50	120.00	0.09	10.00
4.05	0.73	4.00	45.40	50	120.00	0.09	10.00
12.18	0.18	4.00	45.40	50	120.00	0.09	10.00
8.11	0.28	4.00	45.40	50	120.00	0.09	10.00
7.20	0.32	4.00	45.40	50	120.00	0.09	10.00
6.75	0.35	4.00	45.40	50	120.00	0.09	10.00
16.69	0.09	4.00	45.40	50	120.00	0.09	10.00
11.09	0.12	4.00	45.40	50	120.00	0.09	10.00
9.76	0.14	4.00	45.40	50	120.00	0.09	10.00
8.48	0.18	4.00	45.40	50	120.00	0.09	10.00
11.31	0.09	4.00	45.40	50	120.00	0.09	10.00
10.82	0.14	4.00	45.40	50	120.00	0.09	10.00
9.81	0.21	4.00	45.40	50	120.00	0.09	10.00
9.79	0.07	11	60	50	120	0.165	10
8.26	0.11	11	60	50	120	0.165	10
7.75	0.12	11	60	50	120	0.165	10
7.67	0.14	11	60	50	120	0.165	10
7.41	0.16	11	60	50	120	0.165	10
6.86	0.3	11	67.89	50	120	0.165	10
4.17	0.6	11	67.89	50	120	0.165	10
3.67	0.99	11	67.89	50	120	0.165	10
7.14	0.24	11	67.89	50	120	0.165	10
4.34	0.72	11	67.89	50	120	0.165	10
3.80	0.99	11	67.89	50	120	0.165	10
7.13	0.1	10	75.78	50	120	0.154	10
6.89	0.2	16	83.67	50	120	0.227	10
4.19	0.8	16	83.67	50	120	0.227	10
3.69	0.99	16	83.67	50	120	0.227	10
7.16	0.25	16	83.67	50	120	0.227	10
4.36	0.6	16	83.67	50	120	0.227	10
3.82	0.99	16	83.67	50	120	0.227	10
19.35	0.05	4.00	27.10	12	90.00	0.07	5.00

$R/W^{0.33}$ $m/kg^{0.33}$	Ru	SPT $(N_1)_{60}$	Effective Overburden Pressure, σ'v (kPa)	Relative Density, Dr (%)	Shear Wave Velocity, Vs (m/s)	CRR (Youd et al 2001)	Fines Content %
14.52	0.09	4.00	27.10	12	90.00	0.07	5.00
12.21	0.12	4.00	27.10	12	90.00	0.07	5.00
10.52	0.22	4.00	27.10	12	90.00	0.07	5.00
9.18	0.31	4.00	27.10	12	90.00	0.07	5.00
8.17	0.62	4.00	27.10	12	90.00	0.07	5.00
7.27	0.7	4.00	27.10	12	90.00	0.07	5.00
6.46	0.83	4.00	27.10	12	90.00	0.07	5.00
5.82	0.91	4.00	27.10	12	90.00	0.07	5.00
19.33	0.1	4.00	61.90	12	90.00	0.07	5.00
14.50	0.18	4.00	61.90	12	90.00	0.07	5.00
12.19	0.25	4.00	61.90	12	90.00	0.07	5.00
10.51	0.3	4.00	61.90	12	90.00	0.07	5.00
9.17	0.35	4.00	61.90	12	90.00	0.07	5.00
8.15	0.45	4.00	61.90	12	90.00	0.07	5.00
7.25	0.6	4.00	61.90	12	90.00	0.07	5.00
6.44	0.65	4.00	61.90	12	90.00	0.07	5.00
5.79	0.77	4.00	61.90	12	90.00	0.07	5.00
5.26	0.88	4.00	61.90	12	90.00	0.07	5.00
20.57	0.05	4.00	27.10	12	90.00	0.07	5.00
15.51	0.09	4.00	27.10	12	90.00	0.07	5.00
13.12	0.11	4.00	27.10	12	90.00	0.07	5.00
11.38	0.15	4.00	27.10	12	90.00	0.07	5.00
10.01	0.22	4.00	27.10	12	90.00	0.07	5.00
8.99	0.37	4.00	27.10	12	90.00	0.07	5.00
8.09	0.62	4.00	27.10	12	90.00	0.07	5.00
7.30	0.73	4.00	27.10	12	90.00	0.07	5.00
6.67	0.75	4.00	27.10	12	90.00	0.07	5.00
6.14	0.77	4.00	27.10	12	90.00	0.07	5.00
20.33	0.06	1.00	45.50	12	90.00	0.05	5.00
15.32	0.12	1.00	45.50	12	90.00	0.05	5.00
12.95	0.18	1.00	45.50	12	90.00	0.05	5.00
11.23	0.29	1.00	45.50	12	90.00	0.05	5.00
9.87	0.38	1.00	45.50	12	90.00	0.05	5.00
8.86	0.53	1.00	45.50	12	90.00	0.05	5.00
7.97	0.77	1.00	45.50	12	90.00	0.05	5.00
7.19	0.88	1.00	45.50	12	90.00	0.05	5.00
6.57	1	1.00	45.50	12	90.00	0.05	5.00
20.24	0.15	4.00	66.30	12	90.00	0.05	5.00
15.25	0.21	4.00	66.30	12	90.00	0.05	5.00
12.88	0.25	4.00	66.30	12	90.00	0.05	5.00
11.16	0.33	4.00	66.30	12	90.00	0.05	5.00
9.80	0.37	4.00	66.30	12	90.00	0.05	5.00
8.79	0.48	4.00	66.30	12	90.00	0.05	5.00
7.89	0.65	4.00	66.30	12	90.00	0.05	5.00

$R/W^{0.33}$ $m/kg^{0.33}$	Ru	SPT $(N_1)_{60}$	Effective Overburden Pressure, σ'v (kPa)	Relative Density, Dr (%)	Shear Wave Velocity, Vs (m/s)	CRR (Youd et al 2001)	Fines Content %
7.10	0.87	4.00	66.30	12	90.00	0.05	5.00
6.47	0.89	4.00	66.30	12	90.00	0.05	5.00
5.95	1	4.00	66.30	12	90.00	0.05	5.00
17.81	0.07	4.00	27.10	12	90.00	0.07	5.00
13.30	0.12	4.00	27.10	12	90.00	0.07	5.00
11.13	0.18	4.00	27.10	12	90.00	0.07	5.00
9.53	0.25	4.00	27.10	12	90.00	0.07	5.00
8.27	0.37	4.00	27.10	12	90.00	0.07	5.00
7.31	0.58	4.00	27.10	12	90.00	0.07	5.00
6.46	0.86	4.00	27.10	12	90.00	0.07	5.00
5.71	0.88	4.00	27.10	12	90.00	0.07	5.00
5.16	0.9	4.00	27.10	12	90.00	0.07	5.00
17.82	0.06	1.00	45.50	12	90.00	0.05	5.00
13.30	0.1	1.00	45.50	12	90.00	0.05	5.00
11.13	0.17	1.00	45.50	12	90.00	0.05	5.00
9.54	0.3	1.00	45.50	12	90.00	0.05	5.00
8.27	0.37	1.00	45.50	12	90.00	0.05	5.00
7.31	0.6	1.00	45.50	12	90.00	0.05	5.00
6.46	0.9	1.00	45.50	12	90.00	0.05	5.00
5.71	1	1.00	45.50	12	90.00	0.05	5.00
17.86	0.12	4.00	61.80	12	90.00	0.07	5.00
13.34	0.2	4.00	61.80	12	90.00	0.07	5.00
11.17	0.29	4.00	61.80	12	90.00	0.07	5.00
9.57	0.34	4.00	61.80	12	90.00	0.07	5.00
8.30	0.42	4.00	61.80	12	90.00	0.07	5.00
7.34	0.6	4.00	61.80	12	90.00	0.07	5.00
6.50	0.9	4.00	61.80	12	90.00	0.07	5.00
5.75	1	4.00	61.80	12	90.00	0.07	5.00
20.11	0.04	4.00	27.10	12	90.00	0.07	5.00
15.13	0.09	4.00	27.10	12	90.00	0.07	5.00
12.76	0.13	4.00	27.10	12	90.00	0.07	5.00
11.03	0.19	4.00	27.10	12	90.00	0.07	5.00
9.66	0.34	4.00	27.10	12	90.00	0.07	5.00
8.62	0.54	4.00	27.10	12	90.00	0.07	5.00
7.71	0.75	4.00	27.10	12	90.00	0.07	5.00
6.89	0.78	4.00	27.10	12	90.00	0.07	5.00
6.22	0.82	4.00	27.10	12	90.00	0.07	5.00
5.65	0.86	4.00	27.10	12	90.00	0.07	5.00
20.12	0.07	1.00	45.50	12	90.00	0.05	5.00
15.13	0.12	1.00	45.50	12	90.00	0.05	5.00
12.76	0.17	1.00	45.50	12	90.00	0.05	5.00
11.03	0.23	1.00	45.50	12	90.00	0.05	5.00
9.66	0.3	1.00	45.50	12	90.00	0.05	5.00
8.63	0.45	1.00	45.50	12	90.00	0.05	5.00

$R/W^{0.33}$ $m/kg^{0.33}$	Ru	SPT $(N_1)_{60}$	Effective Overburden Pressure, σ'v (kPa)	Relative Density, Dr (%)	Shear Wave Velocity, Vs (m/s)	CRR (Youd et al 2001)	Fines Content %
7.71	0.7	1.00	45.50	12	90.00	0.05	5.00
6.89	0.88	1.00	45.50	12	90.00	0.05	5.00
6.22	1	1.00	45.50	12	90.00	0.05	5.00
20.15	0.08	4.00	61.80	12	90.00	0.05	5.00
15.16	0.12	4.00	61.80	12	90.00	0.07	5.00
12.79	0.15	4.00	61.80	12	90.00	0.07	5.00
11.06	0.26	4.00	61.80	12	90.00	0.07	5.00
9.69	0.42	4.00	61.80	12	90.00	0.07	5.00
8.66	0.54	4.00	61.80	12	90.00	0.07	5.00
7.74	0.69	4.00	61.80	12	90.00	0.07	5.00
6.92	0.75	4.00	61.80	12	90.00	0.07	5.00
6.26	0.8	4.00	61.80	12	90.00	0.07	5.00
5.69	0.95	4.00	61.80	12	90.00	0.07	5.00
14.89	0.1	1.00	45.50	12	90.00	0.05	5.00
10.98	0.2	1.00	45.50	12	90.00	0.05	5.00
9.06	0.38	1.00	45.50	12	90.00	0.05	5.00
7.64	0.52	1.00	45.50	12	90.00	0.05	5.00
6.52	0.64	1.00	45.50	12	90.00	0.05	5.00
5.66	0.94	1.00	45.50	12	90.00	0.05	5.00
4.93	1	1.00	45.50	12	90.00	0.05	5.00

B.2 SINGLE BLASTS

$R/W^{0.33}$ $m/kg^{0.33}$	Ru	Relative Density, Dr (%)	SPT $(N_1)_{60}$	Effective Overburden Pressure, σ'v (kPa)	Shear Wave Velocity, Vs (m/s)	CRR (Youd et al 2001)	Fines Content %
4.81	0.46	43	3.4	62.6	127	0.061	15
17.50	0.10	43	3.4	62.6	127	0.061	15
14	0.02	12.00	4	27.1	90	0.065	5
15	0.03	12.00	4	27.1	90	0.065	5
6.5	0.2	12.00	4	27.1	90	0.065	5
6.5	0.35	12.00	4	27.1	90	0.065	5
16	0.019	12.00	4	27.1	90	0.065	5
12	0.031	12.00	4	27.1	90	0.065	5
5	0.3	12.00	4	27.1	90	0.065	5
5	0.47	12.00	4	27.1	90	0.065	5
5.02	0.58	30	7	59.3	210	0.124	15
7.48	0.15	35	7	84.4	160	0.152	40
2.41	0.46	70	9.1	39.9	270	0.132	5
3.03	0.645	70	9.1	39.9	270	0.132	5
4.12	0.32	70	9.1	39.9	270	0.132	5
4.55	0.417	70	9.1	39.9	270	0.132	5
4.82	0.30	70	9.1	39.9	270	0.132	5
6.07	0.398	70	9.1	39.9	270	0.132	5
7.03	0.24	70	9.1	39.9	270	0.132	5
7.24	0.16	70	9.1	39.9	270	0.132	5
7.47	0.01	70	9.1	39.9	270	0.132	5
7.58	0.275	70	9.1	39.9	270	0.132	5
8.24	0.21	70	9.1	39.9	270	0.132	5
9.09	0.236	70	9.1	39.9	270	0.132	5
9.65	0.09	70	9.1	39.9	270	0.132	5
12.05	0.03	70	9.1	39.9	270	0.132	5
12.36	0.09	70	9.1	39.9	270	0.132	5
14.06	0.14	70	9.1	39.9	270	0.132	5
16.48	0.05	70	9.1	39.9	270	0.132	5
20.59	0.02	70	9.1	39.9	270	0.132	5
21.10	0.14	70	9.1	39.9	270	0.132	5
28.13	0.02	70	9.1	39.9	270	0.132	5

APPENDIX C – STATISTICAL REGRESSION ANALYSIS

C.1 MULTIPLE BLASTS: LOGARITHMIC-BASED MULTIPLE REGRESSION ANALYSIS

Test #1 – Parameter: Scaled Distance LN ($R/W^{0.33}$)

Regression Statistics	
Multiple R	0.65865314
R Square	0.43382395
Adjusted R Square	0.43245638
Standard Error	0.22444794
Observations	416

ANOVA

	df	*SS*	*MS*	*F*	*Significance F*
Regression	1	15.98062023	15.98062023	317.22133	4.30653E-53
Residual	414	20.85602764	0.050376878		
Total	415	36.83664787			

	Coefficients	*Standard Error*	*t Stat*	*P-value*	*Lower 95%*	*Upper 95%*
Intercept	1.08735736	0.033952864	32.02549752	4.24E-114	1.020615856	1.15409886
LN ($R/W^{0.33}$)	-0.34984807	0.019642569	-17.8107082	4.307E-53	-0.38845968	-0.3112365

Test #2 - Parameters: Scaled Distance LN ($R/W^{0.33}$), Relative Density D_R (%)

Regression Statistics	
Multiple R	0.70062054
R Square	0.49086914
Adjusted R Square	0.48840362
Standard Error	0.21309818
Observations	416

ANOVA

	df	*SS*	*MS*	*F*	*Significance F*
Regression	2	18.08197374	9.04098687	199.09317	2.88586E-61
Residual	413	18.75467413	0.045410833		
Total	415	36.83664787			

	Coefficients	*Standard Error*	*t Stat*	*P-value*	*Lower 95%*	*Upper 95%*
Intercept	1.38218899	0.05401523	25.5888754	3.24E-87	1.276009933	1.48836805
LN ($R/W^{0.33}$)	-0.42041648	0.021340413	-19.700485	2.144E-61	-0.46236586	-0.3784671
D_R (%)	-0.0056366	0.000828604	-6.80251996	3.622E-11	-0.00726541	-0.0040078

Test #3 - Parameters: Scaled Distance LN ($R/W^{0.33}$) , Effective Overburden Pressure *σ'vo* (kPa)

Regression Statistics	
Multiple R	0.7252181
R Square	0.52594129
Adjusted R Square	0.52364561
Standard Error	0.20562745
Observations	416

ANOVA

	df	*SS*	*MS*	*F*	*Significance F*
Regression	2	19.37391409	9.686957043	229.10005	1.1464E-67
Residual	413	17.46273378	0.042282648		
Total	415	36.83664787			

	Coefficients	*Standard Error*	*t Stat*	*P-value*	*Lower 95%*	*Upper 95%*
Intercept	1.3841185	0.045441692	30.45922045	1.17E-107	1.294792658	1.47344435
LN ($R/W^{0.33}$)	-0.40792225	0.019127538	-21.3264381	1.385E-68	-0.44552172	-0.3703228
σ'_{vo} (kPa)	-0.0028608	0.000319343	-8.95838339	1.142E-17	-0.00348854	-0.0022331

Test #4 - Parameters: Scaled Distance LN ($R/W^{0.33}$) , Corrected SPT $(N_1)_{60}$ value

Regression Statistics	
Multiple R	0.75882163
R Square	0.57581027
Adjusted R Square	0.57375608
Standard Error	0.19451142
Observations	416

ANOVA

	df	*SS*	*MS*	*F*	*Significance F*
Regression	2	21.21092003	10.60546002	280.31046	1.23359E-77
Residual	413	15.62572783	0.037834692		
Total	415	36.83664787			

	Coefficients	*Standard Error*	*t Stat*	*P-value*	*Lower 95%*	*Upper 95%*
Intercept	1.58191898	0.05133323	30.81666552	4.11E-109	1.481011991	1.68282597
LN ($R/W^{0.33}$)	-0.48495462	0.020538129	-23.6124053	1.225E-78	-0.52532693	-0.4445823
SPT $(N_1)_{60}$	-0.03651231	0.003105426	-11.7575867	9.947E-28	-0.04261672	-0.0304079

Test #5 - Parameters: Scaled Distance LN ($R/W^{0.33}$) , Cyclic Resistance Ratio CRR (determined from Youd et al. 2001)

Regression Statistics	
Multiple R	0.72758983
R Square	0.52938696
Adjusted R Square	0.52710796
Standard Error	0.20487879
Observations	416

ANOVA

	df	*SS*	*MS*	*F*	*Significance F*
Regression	2	19.500841	9.750420499	232.28937	2.5416E-68
Residual	413	17.33580687	0.041975319		
Total	415	36.83664787			

	Coefficients	*Standard Error*	*t Stat*	*P-value*	*Lower 95%*	*Upper 95%*
Intercept	1.58115865	0.062194046	25.42299063	1.68E-86	1.458902289	1.70341501
LN ($R/W^{0.33}$)	-0.46224371	0.021728277	-21.2738324	2.364E-68	-0.50495552	-0.4195319
CRR	-2.87461125	0.313899898	-9.15773235	2.487E-18	-3.49165197	-2.2575705

Test #6 - Parameters: Scaled Distance LN ($R/W^{0.33}$) , Corrected Shear Wave Velocity v_{s1} (m/s)

Regression Statistics	
Multiple R	0.7494545
R Square	0.56168204
Adjusted R Square	0.55955944
Standard Error	0.19772412
Observations	416

ANOVA

	df	*SS*	*MS*	*F*	*Significance F*
Regression	2	20.69048355	10.34524178	264.61919	1.07025E-74
Residual	413	16.14616431	0.039094829		
Total	415	36.83664787			

	Coefficients	*Standard Error*	*t Stat*	*P-value*	*Lower 95%*	*Upper 95%*
Intercept	1.76421343	0.068537773	25.74074642	7.198E-88	1.629487047	1.8989398
LN ($R/W^{0.33}$)	-0.48029514	0.020992136	-22.8797646	1.986E-75	-0.5215599	-0.4390304
v_{s1} (m/s)	-0.00334562	0.000304812	-10.97601	9.084E-25	-0.0039448	-0.0027464

Test #7 - Parameters: Scaled Distance LN ($R/W^{0.33}$) , Corrected SPT $(N_1)_{60}$ value, Effective Overburden Pressure $\sigma'vo$ (kPa)

Regression Statistics	
Multiple R	0.80314984
R Square	0.64504967
Adjusted R Square	0.6424139
Standard Error	0.17859624
Observations	408

ANOVA

	df	*SS*	*MS*	*F*	*Significance F*
Regression	3	23.41809554	7.806031847	244.72914	1.75862E-90
Residual	404	12.88623345	0.031896617		
Total	407	36.304329			

	Coefficients	*Standard Error*	*t Stat*	*P-value*	*Lower 95%*	*Upper 95%*
Intercept	1.74658213	0.050693717	34.45362123	2.57E-122	1.646925725	1.84623854
LN ($R/W^{0.33}$)	-0.51196304	0.019131973	-26.7595528	1.723E-91	-0.54957369	-0.4743524
SPT $(N_1)_{60}$	-0.03189077	0.00310311	-10.2770352	3.647E-22	-0.03799102	-0.0257905
σ'_{vo} (kPa)	-0.00207399	0.000303343	-6.8371092	2.996E-11	-0.00267031	-0.0014777

Test #8 - Parameters: Scaled Distance LN ($R/W^{0.33}$) , Corrected SPT $(N_1)_{60}$ value, Effective Overburden Pressure $\sigma'vo$ (kPa), Fines Content FC (%)

Regression Statistics	
Multiple R	0.77999816
R Square	0.60839713
Adjusted R Square	0.60458591
Standard Error	0.18734499
Observations	416

ANOVA

	df	*SS*	*MS*	*F*	*Significance F*
Regression	4	22.4113107	5.602827674	159.63316	2.6933E-82
Residual	411	14.42533717	0.035098144		
Total	415	36.83664787			

	Coefficients	*Standard Error*	*t Stat*	*P-value*	*Lower 95%*	*Upper 95%*
Intercept	1.71041169	0.056868368	30.07667986	6.91E-106	1.598622544	1.82220083
LN ($R/W^{0.33}$)	-0.49881337	0.019982627	-24.9623516	2.261E-84	-0.53809427	-0.4595325
SPT $(N_1)_{60}$	-0.02945405	0.003237444	-9.09793252	4.002E-18	-0.03581807	-0.02309
σ'_{vo} (kPa)	-0.00165486	0.000320941	-5.1562724	3.924E-07	-0.00228575	-0.001024
FC (%)	-0.00554957	0.003256674	-1.70406171	0.0891254	-0.01195139	0.00085224

Test #9 - Parameters: Scaled Distance LN ($R/W^{0.33}$) , Corrected SPT $(N_1)_{60}$ value, Effective Overburden Pressure *σ'vo* (kPa), Cyclic Resistance Ratio CRR (Youd et al. 2001)

Regression Statistics	
Multiple R	0.77915576
R Square	0.60708369
Adjusted R Square	0.60325969
Standard Error	0.1876589
Observations	416

ANOVA

	df	*SS*	*MS*	*F*	*Significance F*
Regression	4	22.36292822	5.590732054	158.75607	5.34797E-82
Residual	411	14.47371965	0.035215863		
Total	415	36.83664787			

	Coefficients	*Standard Error*	*t Stat*	*P-value*	*Lower 95%*	*Upper 95%*
Intercept	1.61629804	0.068349401	23.64758172	1.141E-78	1.481940032	1.75065606
LN ($R/W^{0.33}$)	-0.49042471	0.020259051	-24.2076845	4.178E-81	-0.53024899	-0.4506004
SPT $(N_1)_{60}$	-0.04104683	0.009835614	-4.17328611	3.666E-05	-0.06038121	-0.0217124
σ'_{vo} (kPa)	-0.00155657	0.000356349	-4.36810974	1.589E-05	-0.00225707	-0.0008561
CRR	1.09739211	0.890033369	1.232978619	0.2182885	-0.6521933	2.84697753

Test #10 - Parameters: Scaled Distance LN ($R/W^{0.33}$) , Corrected SPT $(N_1)_{60}$ value^2

Regression Statistics	
Multiple R	0.73605991
R Square	0.5417842
Adjusted R Square	0.53956523
Standard Error	0.20216225
Observations	416

ANOVA

	df	*SS*	*MS*	*F*	*Significance F*
Regression	2	19.95751367	9.978756834	244.16102	1.02558E-70
Residual	413	16.8791342	0.040869574		
Total	415	36.83664787			

	Coefficients	*Standard Error*	*t Stat*	*P-value*	*Lower 95%*	*Upper 95%*
Intercept	1.39758839	0.043866914	31.85973825	2.55E-113	1.311358125	1.48381866
LN ($R/W^{0.33}$)	-0.45147821	0.020473413	-22.0519275	8.709E-72	-0.4917233	-0.4112331
SPT $(N_1)_{60}$^2	-0.00206093	0.000208926	-9.86442829	9.456E-21	-0.00247162	-0.0016502

Test #11 - Parameters: Scaled Distance LN ($R/W^{0.33}$) , Corrected SPT $(N_1)_{60}$ value x Effective Overburden Pressure $\sigma'vo$ (kPa), Corrected SPT $(N_1)_{60}$ value, Effective Overburden Pressure $\sigma'vo$ (kPa)

Regression Statistics	
Multiple R	0.778289
R Square	0.60573377
Adjusted R Square	0.60189663
Standard Error	0.18798099
Observations	416

ANOVA

	df	*SS*	*MS*	*F*	*Significance F*
Regression	4	22.3132015	5.578300374	157.8607	1.07976E-81
Residual	411	14.52344637	0.035336852		
Total	415	36.83664787			

	Coefficients	*Standard Error*	*t Stat*	*P-value*	*Lower 95%*	*Upper 95%*
Intercept	1.64935449	0.083919072	19.65410785	4.112E-61	1.48439036	1.81431863
LN ($R/W^{0.33}$)	-0.49495324	0.019938584	-24.8238913	8.958E-84	-0.53414757	-0.4557589
σ'vo (kPa) x $(N_1)_{60}$	-4.7024E-05	0.000143215	-0.3283463	0.7428171	-0.00032855	0.0002345
σ'_{vo} (kPa)	-0.00130008	0.001439446	-0.90318404	0.3669573	-0.00412968	0.00152951
SPT $(N_1)_{60}$	-0.02739478	0.007452777	-3.67578197	0.0002686	-0.0420451	-0.0127445

Test #12 - Parameters: Scaled Distance LN ($R/W^{0.33}$) , square root of Corrected SPT $(N_1)_{60}$ value

Regression Statistics	
Multiple R	0.76143996
R Square	0.57979081
Adjusted R Square	0.5777559
Standard Error	0.19359663
Observations	416

ANOVA

	df	*SS*	*MS*	*F*	*Significance F*
Regression	2	21.35754989	10.67877495	284.9219	1.7605E-78
Residual	413	15.47909797	0.037479656		
Total	415	36.83664787			

	Coefficients	*Standard Error*	*t Stat*	*P-value*	*Lower 95%*	*Upper 95%*
Intercept	1.78762593	0.065389672	27.33804695	1.105E-94	1.659087853	1.91616401
LN ($R/W^{0.33}$)	-0.48872823	0.020530375	-23.805129	1.763E-79	-0.52908529	-0.4483712
√SPT $(N_1)_{60}$	-0.18001996	0.015029733	-11.9775882	1.4E-28	-0.20956427	-0.1504756

Test #13 - Parameters: Scaled Distance LN ($R/W^{0.33}$) , square root of Effective Overburden Pressure *σ'vo* (kPa)

Regression Statistics	
Multiple R	0.71695441
R Square	0.51402363
Adjusted R Square	0.51167023
Standard Error	0.20819611
Observations	416

ANOVA

	df	*SS*	*MS*	*F*	*Significance F*
Regression	2	18.93490747	9.467453737	218.41778	1.9321E-65
Residual	413	17.90174039	0.043345618		
Total	415	36.83664787			

	Coefficients	*Standard Error*	*t Stat*	*P-value*	*Lower 95%*	*Upper 95%*
Intercept	1.52970811	0.062151831	24.61243838	5.391E-83	1.407534738	1.65188149
LN ($R/W^{0.33}$)	-0.40308274	0.019327666	-20.8552208	1.675E-66	-0.4410756	-0.3650899
√σ'$_{vo}$ (√kPa)	-0.04362246	0.005283922	-8.25569725	2.058E-15	-0.0540092	-0.0332357

Test #14 - Parameters: Scaled Distance LN ($R/W^{0.33}$) , Effective Overburden Pressure *σ'vo* (kPa), square root of Corrected SPT $(N_1)_{60}$ value

Regression Statistics	
Multiple R	0.77866334
R Square	0.6063166
Adjusted R Square	0.60344998
Standard Error	0.18761389
Observations	416

ANOVA

	df	*SS*	*MS*	*F*	*Significance F*
Regression	3	22.33467125	7.444890416	211.50874	5.04092E-83
Residual	412	14.50197662	0.035198972		
Total	415	36.83664787			

	Coefficients	*Standard Error*	*t Stat*	*P-value*	*Lower 95%*	*Upper 95%*
Intercept	1.82970117	0.063870131	28.64721187	4.33E-100	1.704149193	1.95525314
LN ($R/W^{0.33}$)	-0.49661466	0.019952148	-24.8902852	3.946E-84	-0.53583536	-0.457394
σ'$_{vo}$ (kPa)	-0.00167866	0.000318605	-5.26877023	2.219E-07	-0.00230495	-0.0010524
√SPT $(N_1)_{60}$	-0.1460715	0.01592682	-9.17141619	2.257E-18	-0.17737946	-0.1147635

Test #15 - Parameters: Scaled Distance LN ($R/W^{0.33}$) , Effective Overburden Pressure *σ'vo* (kPa), Corrected SPT $(N_1)_{60}$ value, Corrected Shear Wave Velocity v_{s1} (m/s)

Regression Statistics	
Multiple R	0.78667982
R Square	0.61886515
Adjusted R Square	0.61515581
Standard Error	0.18482405
Observations	416

ANOVA

	df	*SS*	*MS*	*F*	*Significance F*
Regression	4	22.79691749	5.699229374	166.83962	1.04586E-84
Residual	411	14.03973037	0.034159928		
Total	415	36.83664787			

	Coefficients	*Standard Error*	*t Stat*	*P-value*	*Lower 95%*	*Upper 95%*
Intercept	1.84440754	0.068802647	26.80721756	2.876E-92	1.709158555	1.97965652
LN ($R/W^{0.33}$)	-0.52391602	0.02102763	-24.9156004	3.598E-84	-0.56525113	-0.4825809
σ'_{vo} (kPa)	-0.00062642	0.000432073	-1.44981076	0.1478739	-0.00147577	0.00022292
SPT $(N_1)_{60}$	-0.02566694	0.003358038	-7.64343512	1.508E-13	-0.03226801	-0.0190659
v_{s1} (m/s)	-0.00170237	0.000450624	-3.77781154	0.0001816	-0.00258819	-0.0008166

Test #16 - Parameters: Scaled Distance LN ($R/W^{0.33}$) , Effective Overburden Pressure *σ'vo* (kPa), Corrected SPT $(N_1)_{60}$ value, Corrected Shear Wave Velocity v_{s1} (m/s), Cyclic Resistance Ratio CRR (Youd et al. 2001), Relative Density D_R (%)

Regression Statistics	
Multiple R	0.80368953
R Square	0.64591686
Adjusted R Square	0.64072248
Standard Error	0.17857926
Observations	416

ANOVA

	df	*SS*	*MS*	*F*	*Significance F*
Regression	6	23.79341177	3.965568628	124.34932	5.51311E-89
Residual	409	13.04323609	0.031890553		
Total	415	36.83664787			

	Coefficients	*Standard Error*	*t Stat*	*P-value*	*Lower 95%*	*Upper 95%*
Intercept	1.75967564	0.074007669	23.77693639	4.16E-79	1.614192767	1.9051585
LN ($R/W^{0.33}$)	-0.53245423	0.020563982	-25.8925649	3.222E-88	-0.57287851	-0.4920299
σ'_{vo} (kPa)	-0.00014666	0.000479032	-0.30615172	0.7596449	-0.00108833	0.00079502
SPT $(N_1)_{60}$	-0.0646679	0.010113195	-6.39440859	4.406E-10	-0.08454823	-0.0447876
v_{s1} (m/s)	-0.00186494	0.00044888	-4.15465326	3.969E-05	-0.00274734	-0.0009825
CRR	5.11136914	1.064033548	4.803766896	2.189E-06	3.019712211	7.20302606
D_R (%)	-0.00538952	0.001058177	-5.09321669	5.385E-07	-0.00746967	-0.0033094

Test #17 - Parameters: Scaled Distance LN ($R/W^{0.33}$) , Corrected SPT $(N_1)_{60}$ value, Corrected Shear Wave Velocity v_{s1} (m/s), Cyclic Resistance Ratio CRR (Youd et al. 2001)

Regression Statistics	
Multiple R	0.7895766
R Square	0.62343121
Adjusted R Square	0.6197663
Standard Error	0.1837136
Observations	416

ANOVA

	df	*SS*	*MS*	*F*	*Significance F*
Regression	4	22.96511577	5.741278943	170.10851	8.85088E-86
Residual	411	13.87153209	0.033750686		
Total	415	36.83664787			

	Coefficients	*Standard Error*	*t Stat*	*P-value*	*Lower 95%*	*Upper 95%*
Intercept	1.76988579	0.076093833	23.2592541	5.649E-77	1.620304139	1.91946744
LN ($R/W^{0.33}$)	-0.51995872	0.020842263	-24.9473251	2.625E-84	-0.56092945	-0.478988
SPT $(N_1)_{60}$	-0.04686674	0.008544162	-5.48523551	7.229E-08	-0.06366245	-0.030071
v_{s1} (m/s)	-0.00200773	0.000326769	-6.1441783	1.901E-09	-0.00265008	-0.0013654
CRR	2.08679691	0.782555525	2.666643892	0.0079637	0.54848635	3.62510747

C.2 MULTIPLE BLASTS: POWER-BASED MULTIPLE REGRESSION ANALYSIS

Test #1 – Parameter: Scaled Distance LN ($R/W^{0.33}$)

Regression Statistics	
Multiple R	0.703486677
R Square	0.494893505
Adjusted R Square	0.493673441
Standard Error	0.551018413
Observations	416

ANOVA

	df	*SS*	*MS*	*F*	*Significance F*
Regression	1	123.1576417	123.15764	405.629135	2.21378E-63
Residual	414	125.6992146	0.3036213		
Total	415	248.8568563			

	Coefficients	*Standard Error*	*t Stat*	*P-value*	*Lower 95%*	*Upper 95%*
Intercept	0.688934337	0.083354087	8.2651537	1.912E-15	0.525084331	0.85278434
LN ($R/W^{0.33}$)	-0.971210455	0.048222395	-20.140237	2.2138E-63	-1.066001726	-0.8764192

Test #2 - Parameters: Scaled Distance LN ($R/W^{0.33}$), Relative Density D_R (%)

Regression Statistics	
Multiple R	0.749747089
R Square	0.562120697
Adjusted R Square	0.560000216
Standard Error	0.513661468
Observations	416

ANOVA

	df	*SS*	*MS*	*F*	*Significance F*
Regression	2	139.8875895	69.943795	265.091141	8.70337E-75
Residual	413	108.9692668	0.2638481		
Total	415	248.8568563			

	Coefficients	*Standard Error*	*t Stat*	*P-value*	*Lower 95%*	*Upper 95%*
Intercept	1.520835658	0.130200749	11.680698	1.9654E-27	1.264896856	1.77677446
LN ($R/W^{0.33}$)	-1.170327338	0.051439895	-22.751356	7.2784E-75	-1.271443998	-1.0692107
D_R (%)	-0.01590431	0.001997306	-7.9628824	1.645E-14	-0.019830463	-0.0119782

Test #3 - Parameters: Scaled Distance LN ($R/W^{0.33}$) , Effective Overburden Pressure *σ'vo* (kPa)

Regression Statistics	
Multiple R	0.74274751
R Square	0.551673863
Adjusted R Square	0.549502792
Standard Error	0.519752765
Observations	416

ANOVA

	df	*SS*	*MS*	*F*	*Significance F*
Regression	2	137.2878232	68.643912	254.102189	1.13285E-72
Residual	413	111.5690331	0.2701429		
Total	415	248.8568563			

	Coefficients	*Standard Error*	*t Stat*	*P-value*	*Lower 95%*	*Upper 95%*
Intercept	1.294512456	0.114860369	11.270314	7.1728E-26	1.068728615	1.5202963
LN ($R/W^{0.33}$)	-1.089718065	0.048347585	-22.539245	6.2289E-74	-1.184756098	-0.99468
σ'_{vo} (kPa)	-0.005837818	0.000807186	-7.2323105	2.3226E-12	-0.007424522	-0.0042511

Test #4 - Parameters: Scaled Distance LN ($R/W^{0.33}$) , Corrected SPT $(N_1)_{60}$ value

Regression Statistics	
Multiple R	0.784890633
R Square	0.616053306
Adjusted R Square	0.614194
Standard Error	0.480989112
Observations	416

ANOVA

	df	*SS*	*MS*	*F*	*Significance F*
Regression	2	153.309089	76.654545	331.335078	1.41889E-86
Residual	413	95.54776728	0.2313505		
Total	415	248.8568563			

	Coefficients	*Standard Error*	*t Stat*	*P-value*	*Lower 95%*	*Upper 95%*
Intercept	1.87637304	0.126937148	14.781906	5.4716E-40	1.62684958	2.1258965
LN ($R/W^{0.33}$)	-1.295600267	0.05078682	-25.510561	7.0436E-87	-1.395433162	-1.1957674
SPT $(N_1)_{60}$	-0.087665782	0.007679117	-11.416128	2.0129E-26	-0.10276081	-0.0725708

Test #5 - Parameters: Scaled Distance LN ($R/W^{0.33}$) , Cyclic Resistance Ratio CRR (determined from Youd et al. 2001)

Regression Statistics	
Multiple R	0.767663964
R Square	0.589307961
Adjusted R Square	0.587319138
Standard Error	0.497459721
Observations	416

ANOVA

	df	*SS*	*MS*	*F*	*Significance F*
Regression	2	146.6533266	73.326663	296.309844	1.55279E-80
Residual	413	102.2035297	0.2474662		
Total	415	248.8568563			

	Coefficients	*Standard Error*	*t Stat*	*P-value*	*Lower 95%*	*Upper 95%*
Intercept	1.964671843	0.151011398	13.01009	1.1379E-32	1.66782504	2.26151865
LN ($R/W^{0.33}$)	-1.261585027	0.052757742	-23.912794	5.975E-80	-1.365292213	-1.1578778
CRR	-7.426569069	0.762170424	-9.7439744	2.4887E-20	-8.924786137	-5.928352

Test #6 - Parameters: Scaled Distance LN ($R/W^{0.33}$) , Corrected Shear Wave Velocity v_{s1} (m/s)

Regression Statistics	
Multiple R	0.771684745
R Square	0.595497346
Adjusted R Square	0.593538495
Standard Error	0.493696976
Observations	416

ANOVA

	df	*SS*	*MS*	*F*	*Significance F*
Regression	2	148.1935974	74.096799	304.003449	6.74938E-82
Residual	413	100.6632589	0.2437367		
Total	415	248.8568563			

	Coefficients	*Standard Error*	*t Stat*	*P-value*	*Lower 95%*	*Upper 95%*
Intercept	2.249472024	0.17113183	13.144673	3.2545E-33	1.913073994	2.58587005
LN ($R/W^{0.33}$)	-1.271965043	0.052415224	-24.267091	1.7083E-81	-1.374998933	-1.1689312
v_{s1} (m/s)	-0.007713557	0.000761085	-10.13495	1.0487E-21	-0.00920964	-0.0062175

Test #7 - Parameters: Scaled Distance LN ($R/W^{0.33}$) , Corrected SPT $(N_1)_{60}$ value, Effective Overburden Pressure $\sigma'vo$ (kPa)

Regression Statistics	
Multiple R	0.808579473
R Square	0.653800765
Adjusted R Square	0.651229978
Standard Error	0.458106268
Observations	408

ANOVA

	df	*SS*	*MS*	*F*	*Significance F*
Regression	3	160.115418	53.371806	254.319365	1.14313E-92
Residual	404	84.78398651	0.2098614		
Total	407	244.8994045			

	Coefficients	*Standard Error*	*t Stat*	*P-value*	*Lower 95%*	*Upper 95%*
Intercept	2.175886276	0.130031346	16.733552	3.9545E-48	1.920263739	2.43150881
LN ($R/W^{0.33}$)	-1.343123291	0.049074251	-27.369206	4.8473E-94	-1.439596064	-1.2466505
SPT $(N_1)_{60}$	-0.080210743	0.007959596	-10.077238	1.8682E-21	-0.09585814	-0.0645633
σ'_{vo} (kPa)	-0.003672592	0.000778085	-4.7200376	3.256E-06	-0.005202194	-0.002143

Test #8 - Parameters: Scaled Distance LN ($R/W^{0.33}$) , Corrected SPT $(N_1)_{60}$ value, Effective Overburden Pressure $\sigma'vo$ (kPa), Fines Content FC (%)

Regression Statistics	
Multiple R	0.794277314
R Square	0.630876452
Adjusted R Square	0.627284009
Standard Error	0.472758962
Observations	416

ANOVA

	df	*SS*	*MS*	*F*	*Significance F*
Regression	4	156.9979305	39.249483	175.612084	1.47873E-87
Residual	411	91.85892579	0.223501		
Total	415	248.8568563			

	Coefficients	*Standard Error*	*t Stat*	*P-value*	*Lower 95%*	*Upper 95%*
Intercept	2.112543328	0.14350547	14.720995	1.0692E-39	1.830447076	2.39463958
LN ($R/W^{0.33}$)	-1.320848726	0.050425508	-26.194059	1.1685E-89	-1.4199728	-1.2217247
SPT $(N_1)_{60}$	-0.075499098	0.008169585	-9.2414847	1.3249E-18	-0.091558481	-0.0594397
σ'_{vo} (kPa)	-0.002796817	0.000809884	-3.4533529	0.00061117	-0.004388849	-0.0012048
FC (%)	-0.011732027	0.008218109	-1.4275822	0.1541715	-0.027886796	0.00442274

Test #9 - Parameters: Scaled Distance LN ($R/W^{0.33}$) , Corrected SPT $(N_1)_{60}$ value, Effective Overburden Pressure *σ'vo* (kPa), Cyclic Resistance Ratio CRR (Youd et al. 2001)

Regression Statistics	
Multiple R	0.793164786
R Square	0.629110377
Adjusted R Square	0.625500746
Standard Error	0.473888572
Observations	416

ANOVA

	df	*SS*	*MS*	*F*	*Significance F*
Regression	4	156.5584307	39.139608	174.2866	3.93249E-87
Residual	411	92.29842558	0.2245704		
Total	415	248.8568563			

	Coefficients	*Standard Error*	*t Stat*	*P-value*	*Lower 95%*	*Upper 95%*
Intercept	2.058994158	0.172600393	11.929255	2.2468E-28	1.719704486	2.39828383
LN ($R/W^{0.33}$)	-1.315605955	0.051159485	-25.715778	1.2985E-87	-1.416172845	-1.2150391
SPT $(N_1)_{60}$	-0.069544159	0.024837538	-2.7999619	0.00535188	-0.118368614	-0.0207197
σ'_{vo} (kPa)	-0.003133468	0.000899876	-3.482109	0.00055084	-0.004902402	-0.0013645
CRR	-0.599799295	2.247570678	-0.2668656	0.78970649	-5.017967207	3.81836862

Test #10 - Parameters: Scaled Distance LN ($R/W^{0.33}$) , Corrected SPT $(N_1)_{60}$ value^2

Regression Statistics	
Multiple R	0.766341003
R Square	0.587278532
Adjusted R Square	0.585279881
Standard Error	0.498687301
Observations	416

ANOVA

	df	*SS*	*MS*	*F*	*Significance F*
Regression	2	146.1482893	73.074145	293.837434	4.29717E-80
Residual	413	102.708567	0.248689		
Total	415	248.8568563			

	Coefficients	*Standard Error*	*t Stat*	*P-value*	*Lower 95%*	*Upper 95%*
Intercept	1.43484852	0.108209486	13.259914	1.1097E-33	1.222138483	1.64755856
LN ($R/W^{0.33}$)	-1.215568223	0.050503153	-24.069155	1.2432E-80	-1.314843507	-1.1162929
SPT $(N_1)_{60}$^2	-0.004955275	0.000515372	-9.6149558	6.9605E-20	-0.005968353	-0.0039422

Test #11 - Parameters: Scaled Distance LN ($R/W^{0.33}$) , Corrected SPT $(N_1)_{60}$ value x Effective Overburden Pressure $\sigma'vo$ (kPa), Corrected SPT $(N_1)_{60}$ value, Effective Overburden Pressure $\sigma'vo$ (kPa)

Regression Statistics	
Multiple R	0.794543112
R Square	0.631298757
Adjusted R Square	0.627710424
Standard Error	0.472488449
Observations	416

ANOVA

	df	*SS*	*MS*	*F*	*Significance F*
Regression	4	157.103024	39.275756	175.930916	1.16953E-87
Residual	411	91.75383228	0.2232453		
Total	415	248.8568563			

	Coefficients	*Standard Error*	*t Stat*	*P-value*	*Lower 95%*	*Upper 95%*
Intercept	1.767144426	0.210929798	8.3778795	8.6193E-16	1.352508627	2.18178023
LN ($R/W^{0.33}$)	-1.311022215	0.050115444	-26.160044	1.6323E-89	-1.409536779	-1.2125077
σ'vo (kPa) x $(N_1)_{60}$	-0.00057042	0.000359969	-1.5846383	0.11381763	-0.00127803	0.00013719
σ'_{vo} (kPa)	0.002571896	0.003618033	0.7108546	0.47757755	-0.004540263	0.00968405
SPT $(N_1)_{60}$	-0.049083864	0.018732485	-2.6202538	0.00911197	-0.085907295	-0.0122604

Test #12 - Parameters: Scaled Distance LN ($R/W^{0.33}$) , square root of Corrected SPT $(N_1)_{60}$ value

Regression Statistics	
Multiple R	0.786567398
R Square	0.618688272
Adjusted R Square	0.616841726
Standard Error	0.479335794
Observations	416

ANOVA

	df	*SS*	*MS*	*F*	*Significance F*
Regression	2	153.9648183	76.982409	335.051662	3.42258E-87
Residual	413	94.89203797	0.2297628		
Total	415	248.8568563			

	Coefficients	*Standard Error*	*t Stat*	*P-value*	*Lower 95%*	*Upper 95%*
Intercept	2.365124967	0.161901631	14.608407	2.9412E-39	2.046870966	2.68337897
LN ($R/W^{0.33}$)	-1.303639516	0.050832205	-25.645937	1.8407E-87	-1.403561627	-1.2037174
√SPT $(N_1)_{60}$	-0.430902904	0.037212884	-11.579401	4.8045E-27	-0.504053182	-0.3577526

Test #13 - Parameters: Scaled Distance LN ($R/W^{0.33}$) , square root of Effective Overburden Pressure *σ'vo* (kPa)

Regression Statistics	
Multiple R	0.736530919
R Square	0.542477795
Adjusted R Square	0.540262191
Standard Error	0.525056293
Observations	416

ANOVA

	df	*SS*	*MS*	*F*	*Significance F*
Regression	2	134.9993186	67.499659	244.844214	7.50092E-71
Residual	413	113.8575377	0.2756841		
Total	415	248.8568563			

	Coefficients	*Standard Error*	*t Stat*	*P-value*	*Lower 95%*	*Upper 95%*
Intercept	1.574553523	0.156742654	10.045469	2.1789E-21	1.26644065	1.8826664
LN ($R/W^{0.33}$)	-1.077790227	0.048743047	-22.111671	4.7498E-72	-1.173605628	-0.9819748
√σ'$_{vo}$ (√kPa)	-0.087335425	0.01332569	-6.5539139	1.6736E-10	-0.11353006	-0.0611408

Test #14 - Parameters: Scaled Distance LN ($R/W^{0.33}$) , Effective Overburden Pressure *σ'vo* (kPa), square root of Corrected SPT $(N_1)_{60}$ value

Regression Statistics	
Multiple R	0.793533268
R Square	0.629695047
Adjusted R Square	0.626998652
Standard Error	0.472939903
Observations	416

ANOVA

	df	*SS*	*MS*	*F*	*Significance F*
Regression	3	156.7039298	52.234643	233.532171	1.71246E-88
Residual	412	92.15292648	0.2236722		
Total	415	248.8568563			

	Coefficients	*Standard Error*	*t Stat*	*P-value*	*Lower 95%*	*Upper 95%*
Intercept	2.435571101	0.16100478	15.127322	1.9722E-41	2.119077803	2.7520644
LN ($R/W^{0.33}$)	-1.316843681	0.050295673	-26.182047	1.0998E-89	-1.415711823	-1.2179755
σ'$_{vo}$ (kPa)	-0.002810555	0.000803144	-3.4994428	0.00051708	-0.004389326	-0.0012318
√SPT $(N_1)_{60}$	-0.374063349	0.040148566	-9.316979	7.3107E-19	-0.452984932	-0.2951418

Test #15 - Parameters: Scaled Distance LN ($R/W^{0.33}$) , Effective Overburden Pressure *σ'vo* (kPa), Corrected SPT $(N_1)_{60}$ value, Corrected Shear Wave Velocity v_{s1} (m/s)

Regression Statistics	
Multiple R	0.803634376
R Square	0.64582821
Adjusted R Square	0.642381283
Standard Error	0.463085175
Observations	416

ANOVA

	df	*SS*	*MS*	*F*	*Significance F*
Regression	4	160.718778	40.179695	187.36345	3.08787E-91
Residual	411	88.13807825	0.2144479		
Total	415	248.8568563			

	Coefficients	*Standard Error*	*t Stat*	*P-value*	*Lower 95%*	*Upper 95%*
Intercept	2.536801339	0.172388208	14.715631	1.1262E-39	2.197928771	2.87567391
LN ($R/W^{0.33}$)	-1.397322505	0.052685696	-26.521857	4.687E-91	-1.50088955	-1.2937555
σ'_{vo} (kPa)	0.000299684	0.001082579	0.2768242	0.78205427	-0.001828399	0.00242777
SPT $(N_1)_{60}$	-0.064298346	0.008413718	-7.6420847	1.5217E-13	-0.080837635	-0.0477591
v_{s1} (m/s)	-0.004982571	0.001129058	-4.413032	1.3041E-05	-0.00720202	-0.0027631

Test #16 - Parameters: Scaled Distance LN ($R/W^{0.33}$) , Effective Overburden Pressure *σ'vo* (kPa), Corrected SPT $(N_1)_{60}$ value, Corrected Shear Wave Velocity v_{s1} (m/s), Cyclic Resistance Ratio CRR (Youd et al. 2001), Relative Density D_R (%)

Regression Statistics	
Multiple R	0.817500419
R Square	0.668306934
Adjusted R Square	0.663441021
Standard Error	0.44924303
Observations	416

ANOVA

	df	*SS*	*MS*	*F*	*Significance F*
Regression	6	166.3127627	27.718794	137.344614	9.31845E-95
Residual	409	82.54409355	0.2018193		
Total	415	248.8568563			

	Coefficients	*Standard Error*	*t Stat*	*P-value*	*Lower 95%*	*Upper 95%*
Intercept	2.442904725	0.186177438	13.121379	4.5168E-33	2.076920657	2.80888879
LN ($R/W^{0.33}$)	-1.426510005	0.051731793	-27.575112	2.4472E-95	-1.52820338	-1.3248166
σ'_{vo} (kPa)	0.000637922	0.001205076	0.5293622	0.5968414	-0.001730994	0.00300684
SPT $(N_1)_{60}$	-0.130704329	0.025441266	-5.1374931	4.3194E-07	-0.180716287	-0.0806924
v_{s1} (m/s)	-0.004989121	0.001129225	-4.4181802	1.2763E-05	-0.00720893	-0.0027693
CRR	9.799457568	2.676736647	3.6609719	0.0002842	4.537579546	15.0613356
D_R (%)	-0.013836561	0.002662003	-5.1977999	3.1911E-07	-0.019069477	-0.0086036

Test #17 - Parameters: Scaled Distance LN ($R/W^{0.33}$) , Corrected SPT $(N_1)_{60}$ value, Corrected Shear Wave Velocity v_{s1} (m/s), Cyclic Resistance Ratio CRR (Youd et al. 2001)

Regression Statistics	
Multiple R	0.803768871
R Square	0.646044398
Adjusted R Square	0.642599575
Standard Error	0.462943818
Observations	416

ANOVA

	df	*SS*	*MS*	*F*	*Significance F*
Regression	4	160.772578	40.193145	187.540645	2.72464E-91
Residual	411	88.08427826	0.214317		
Total	415	248.8568563			

	Coefficients	*Standard Error*	*t Stat*	*P-value*	*Lower 95%*	*Upper 95%*
Intercept	2.465992876	0.191750473	12.860427	4.7914E-32	2.089058885	2.84292687
LN ($R/W^{0.33}$)	-1.389254394	0.052520864	-26.451476	9.3412E-91	-1.492497419	-1.2860114
SPT $(N_1)_{60}$	-0.075540127	0.021530616	-3.5084982	0.00050042	-0.117863991	-0.0332163
v_{s1} (m/s)	-0.004684772	0.000823433	-5.6893168	2.4265E-08	-0.006303438	-0.0030661
CRR	1.128875269	1.971978367	0.5724582	0.56732457	-2.74754634	5.00529688

C.3 SINGLE BLASTS: LOGARITHMIC-BASED MULTIPLE REGRESSION ANALYSIS

Test #1 – Parameter: Scaled Distance LN ($R/W^{0.33}$)

Regression Statistics	
Multiple R	0.8326384
R Square	0.6932867
Adjusted R Square	0.6830629
Standard Error	0.1015369
Observations	32

ANOVA

	df	*SS*	*MS*	*F*	*Significance F*
Regression	1	0.699116712	0.6991167	67.811217	3.42351E-09
Residual	30	0.309292507	0.0103098		
Total	31	1.008409219			

	Coefficients	*Standard Error*	*t Stat*	*P-value*	*Lower 95%*	*Upper 95%*
Intercept	0.7547018	0.067678492	11.151279	3.409E-12	0.616483838	0.8929197
LN ($R/W^{0.33}$)	-0.2516375	0.03055797	-8.2347567	3.424E-09	-0.31404515	-0.1892297

Test #2 - Parameters: Scaled Distance LN ($R/W^{0.33}$), Relative Density D_R (%)

Regression Statistics	
Multiple R	0.8326765
R Square	0.6933502
Adjusted R Square	0.6722019
Standard Error	0.1032621
Observations	32

ANOVA

	df	*SS*	*MS*	*F*	*Significance F*
Regression	2	0.699180689	0.3495903	32.785203	3.60014E-08
Residual	29	0.30922853	0.0106631		
Total	31	1.008409219			

	Coefficients	*Standard Error*	*t Stat*	*P-value*	*Lower 95%*	*Upper 95%*
Intercept	0.7517267	0.078819839	9.5372774	1.912E-10	0.590522004	0.9129313
LN ($R/W^{0.33}$)	-0.2516006	0.031080788	-8.0950529	6.303E-09	-0.31516797	-0.1880333
D_R (%)	5.628E-05	0.000726527	0.0774587	0.9387906	-0.00142964	0.0015422

Test #3 - Parameters: Scaled Distance LN ($R/W^{0.33}$) , Effective Overburden Pressure *σ'vo* (kPa)

Regression Statistics	
Multiple R	0.8378539
R Square	0.7019991
Adjusted R Square	0.6814474
Standard Error	0.1017954
Observations	32

ANOVA

	df	*SS*	*MS*	*F*	*Significance F*
Regression	2	0.707902413	0.3539512	34.157579	2.37768E-08
Residual	29	0.300506805	0.0103623		
Total	31	1.008409219			

	Coefficients	*Standard Error*	*t Stat*	*P-value*	*Lower 95%*	*Upper 95%*
Intercept	0.69485	0.093961679	7.3950358	3.789E-08	0.502676773	0.8870232
LN ($R/W^{0.33}$)	-0.2493853	0.030733236	-8.1145154	6.002E-09	-0.31224184	-0.1865288
σ'_{vo} (kPa)	0.0013721	0.00149013	0.9207889	0.3647575	-0.00167556	0.0044198

Test #4 - Parameters: Scaled Distance LN ($R/W^{0.33}$) , Corrected SPT $(N_1)_{60}$ value

Regression Statistics	
Multiple R	0.8327977
R Square	0.693552
Adjusted R Square	0.6724177
Standard Error	0.1032281
Observations	32

ANOVA

	df	*SS*	*MS*	*F*	*Significance F*
Regression	2	0.699384226	0.3496921	32.816347	3.56594E-08
Residual	29	0.309024993	0.010656		
Total	31	1.008409219			

	Coefficients	*Standard Error*	*t Stat*	*P-value*	*Lower 95%*	*Upper 95%*
Intercept	0.764072	0.090728596	8.4215127	2.79E-09	0.578511208	0.9496328
LN ($R/W^{0.33}$)	-0.2518608	0.031098879	-8.098709	6.246E-09	-0.31546512	-0.1882564
SPT $(N_1)_{60}$	-0.001212	0.007649668	-0.158444	0.8752052	-0.01685737	0.0144333

Test #5 - Parameters: Scaled Distance LN ($R/W^{0.33}$) , Cyclic Resistance Ratio CRR (determined from Youd et al. 2001)

Regression Statistics	
Multiple R	0.8327445
R Square	0.6934635
Adjusted R Square	0.672323
Standard Error	0.103243
Observations	32

ANOVA

	df	*SS*	*MS*	*F*	*Significance F*
Regression	2	0.699294936	0.3496475	32.802679	3.58091E-08
Residual	29	0.309114282	0.0106591		
Total	31	1.008409219			

	Coefficients	*Standard Error*	*t Stat*	*P-value*	*Lower 95%*	*Upper 95%*
Intercept	0.7635485	0.097038001	7.8685512	1.119E-08	0.565083488	0.9620135
LN ($R/W^{0.33}$)	-0.2519207	0.031148516	-8.0877265	6.421E-09	-0.31562654	-0.1882148
CRR	-0.0741263	0.573256433	-0.1293074	0.8980071	-1.24656732	1.0983147

Test #6 - Parameters: Scaled Distance LN ($R/W^{0.33}$) , Corrected Shear Wave Velocity v_{s1} (m/s)

Regression Statistics	
Multiple R	0.8328586
R Square	0.6936534
Adjusted R Square	0.6725261
Standard Error	0.103211
Observations	32

ANOVA

	df	*SS*	*MS*	*F*	*Significance F*
Regression	2	0.69948653	0.3497433	32.832016	3.54886E-08
Residual	29	0.308922689	0.0106525		
Total	31	1.008409219			

	Coefficients	*Standard Error*	*t Stat*	*P-value*	*Lower 95%*	*Upper 95%*
Intercept	0.745169	0.085733674	8.6916719	1.436E-09	0.569823913	0.920514
LN ($R/W^{0.33}$)	-0.251385	0.031091324	-8.0853735	6.459E-09	-0.31497386	-0.1877961
v_{s1} (m/s)	4.267E-05	0.000229034	0.1863237	0.8534882	-0.00042575	0.0005111

C.4 SINGLE BLASTS: POWER-BASED MULTIPLE REGRESSION ANALYSIS

Test #1 – Parameter: Scaled Distance LN ($R/W^{0.33}$)

Regression Statistics	
Multiple R	0.7687546
R Square	0.5909837
Adjusted R Square	0.5773498
Standard Error	0.7825746
Observations	32

ANOVA

	df	*SS*	*MS*	*F*	*Significance F*
Regression	1	26.54652036	26.54652	43.34671	2.76136E-07
Residual	30	18.37268866	0.612423		
Total	31	44.91920902			

	Coefficients	*Standard Error*	*t Stat*	*P-value*	*Lower 95%*	*Upper 95%*
Intercept	1.2656333	0.521617714	2.4263618	0.0214725	0.200347784	2.3309188
LN ($R/W^{0.33}$)	-1.5506159	0.235519117	-6.5838219	2.761E-07	-2.031610114	-1.0696217

Test #2 - Parameters: Scaled Distance LN ($R/W^{0.33}$), Relative Density D_R (%)

Regression Statistics	
Multiple R	0.7729439
R Square	0.5974423
Adjusted R Square	0.5696797
Standard Error	0.7896436
Observations	32

ANOVA

	df	*SS*	*MS*	*F*	*Significance F*
Regression	2	26.83663536	13.418318	21.519681	1.86212E-06
Residual	29	18.08257367	0.623537		
Total	31	44.91920902			

	Coefficients	*Standard Error*	*t Stat*	*P-value*	*Lower 95%*	*Upper 95%*
Intercept	1.0652906	0.602734276	1.76743	0.0876789	-0.167439373	2.2980206
LN ($R/W^{0.33}$)	-1.5481361	0.237674379	-6.5136853	3.932E-07	-2.034234791	-1.0620374
D_R (%)	0.0037896	0.005555742	0.6821093	0.5005821	-0.007573145	0.0151524

Test #3 - Parameters: Scaled Distance LN ($R/W^{0.33}$) , Effective Overburden Pressure *σ'vo* (kPa)

Regression Statistics	
Multiple R	0.7839793
R Square	0.6146236
Adjusted R Square	0.5880459
Standard Error	0.7726087
Observations	32

ANOVA

	df	*SS*	*MS*	*F*	*Significance F*
Regression	2	27.60840492	13.804202	23.12555	9.89315E-07
Residual	29	17.3108041	0.5969243		
Total	31	44.91920902			

	Coefficients	*Standard Error*	*t Stat*	*P-value*	*Lower 95%*	*Upper 95%*
Intercept	0.6076309	0.71315221	0.8520353	0.4011763	-0.850929148	2.0661909
LN ($R/W^{0.33}$)	-1.5258563	0.233259723	-6.5414476	3.648E-07	-2.002925957	-1.0487866
σ'_{vo} (kPa)	0.0150846	0.011309822	1.3337641	0.1926625	-0.008046548	0.0382158

Test #4 - Parameters: Scaled Distance LN ($R/W^{0.33}$) , Corrected SPT $(N_1)_{60}$ value

Regression Statistics	
Multiple R	0.7697105
R Square	0.5924543
Adjusted R Square	0.5643477
Standard Error	0.7945207
Observations	32

ANOVA

	df	*SS*	*MS*	*F*	*Significance F*
Regression	2	26.61257978	13.30629	21.078834	2.22616E-06
Residual	29	18.30662924	0.6312631		
Total	31	44.91920902			

	Coefficients	*Standard Error*	*t Stat*	*P-value*	*Lower 95%*	*Upper 95%*
Intercept	1.1183866	0.698315336	1.6015495	0.1200937	-0.309828641	2.5466018
LN ($R/W^{0.33}$)	-1.5471066	0.239360303	-6.4635053	4.504E-07	-2.036653363	-1.0575598
SPT $(N_1)_{60}$	0.0190464	0.058877587	0.323491	0.7486447	-0.101371816	0.1394646

Test #5 - Parameters: Scaled Distance LN ($R/W^{0.33}$) , Cyclic Resistance Ratio CRR (determined from Youd et al. 2001)

Regression Statistics	
Multiple R	0.7704681
R Square	0.593621
Adjusted R Square	0.5655949
Standard Error	0.7933826
Observations	32

ANOVA

	df	*SS*	*MS*	*F*	*Significance F*
Regression	2	26.66498745	13.332494	21.180981	2.13552E-06
Residual	29	18.25422157	0.6294559		
Total	31	44.91920902			

	Coefficients	*Standard Error*	*t Stat*	*P-value*	*Lower 95%*	*Upper 95%*
Intercept	1.0375478	0.745699696	1.3913749	0.1746943	-0.487579251	2.5626749
LN ($R/W^{0.33}$)	-1.5433139	0.239364355	-6.4475509	4.702E-07	-2.032868938	-1.0537588
CRR	1.911117	4.405255073	0.4338266	0.6676247	-7.098641154	10.920875

Test #6 - Parameters: Scaled Distance LN ($R/W^{0.33}$) , Corrected Shear Wave Velocity v_{s1} (m/s)

Regression Statistics	
Multiple R	0.7718095
R Square	0.5956899
Adjusted R Square	0.5678065
Standard Error	0.7913604
Observations	32

ANOVA

	df	*SS*	*MS*	*F*	*Significance F*
Regression	2	26.7579212	13.378961	21.363565	1.98317E-06
Residual	29	18.16128782	0.6262513		
Total	31	44.91920902			

	Coefficients	*Standard Error*	*t Stat*	*P-value*	*Lower 95%*	*Upper 95%*
Intercept	1.0377148	0.65735482	1.578622	0.12527	-0.306726782	2.3821563
LN ($R/W^{0.33}$)	-1.5445793	0.23838978	-6.4792177	4.316E-07	-2.03214113	-1.0570175
v_{s1} (m/s)	0.0010203	0.001756094	0.5810039	0.5657264	-0.002571318	0.0046119